Mutations involving *RBP4* and *SOX3* underlie two novel forms of congenital eye malformations

by

Christopher M. Chou

A dissertation submitted in partial fulfillment
of the requirements for the degree of
Doctor of Philosophy
(Human Genetics)
in the University of Michigan
2012

Doctoral Committee:

Associate Professor Thomas M. Glaser, Chair
Professor Jeffrey W. Innis
Professor John V. Moran
Associate Professor Philip J. Gage
Associate Professor Donna M. Martin

2012

Dedicated to Mom, Dad, Tina and Jennifer for their endless love and support

ACKNOWLEDGEMENTS

First and foremost, I would like to thank my mentor Tom Glaser. His scientific acumen and dedication to good science has been a constant source of inspiration throughout my graduate studies. His unwavering support and the time he makes for his students allowed me to flourish as a young scientist, especially during the final year of my training when it mattered most. Tom has always stood for excellence in his scientific endeavors, earning him great respect amongst colleagues and students. I am forever thankful for his mentorship.

I would also like to thank my dissertation committee members for their helpful insight and time.

I am also grateful to the various family members who actively volunteered their time and effort to help push these studies forward. Without their help, my thesis would never have materialized into what it is now.

A special thank you goes to Tanya Bardakjian and Dr. Adele Schneider at the Albert Einstein Medical Center for providing DNA samples but more importantly

for their admirable work with families of the anophthalmia and microphthalmia community. Their work touches lives and instills hope upon families and serves as a great source of inspiration for me.

I also want to acknowledge various members of the University of Michigan community for their help. Dr. Christine Nelson, our clinical collaborator, was instrumental in obtaining the probands for each study, clinical information gathering and diagnostic testing. Former resident and now practicing physician Dr. Jonathan Pribila also helped with eye examinations of our research subject volunteers. Katy Downs, Kari Branham and Elizabeth Butler contributed greatly with their expertise in genetic counseling during various family meetings. Dr. Phil Gafken and Lisa Jones at the Fred Hutchinson Cancer Research Center were absolutely indispensable for our mass spectroscopy analysis. Dr. Phil Kirchhoff, provided insight with molecular modeling in Part I of the thesis. Dr. Robert Lyons, Susan Dagenais and Christine Brennan at the DNA sequencing core aided tremendously with all sequencing needs, especially during the early stages of both projects. Dr. Thom Saunders and the late Margaret Van Keuren of the UM Transgenic Core made both transgenic mouse lines. Monica Lohmier at the UM Kellogg Eye Center was always available to perform phlebotomy on our research subjects. The Life Sciences Institute (LSI) Center for Chemical Genomics and Dr. Jeanne Stuckey at the structural protein core provided details and assistance with protein-related assays. Dr. Anthony Antonellis provided many control DNA

samples that I used in Part I. Drs. Friedhelm Hildebrandt and Edgar Otto helped tremendously with genomic library construction and bioinformatics support during the early stages of Part I. Theresa Banas and Sherry Taylor provided tremendous administrative assistance throughout the duration of both projects.

C.M.C. was supported by NIH grant R01 EY19497 and NIH predoctoral training grants T32-GM07544 and T32-HD007505.

TABLE OF CONTENTS

LIST OF FIGURES

LIST OF ABBREVIATIONS

AD	Autosomal dominant
ADH	Alcohol dehydrogenase
AEMC	Albert Einstein Medical Center
ALK	Alkaline phosphatase
ALT	Alanine aminotransferase
ARES	Aromatase excess syndrome
arRP	Autosomal recessive retinitis pigmentosa
ASD	Anterior segment dysgenesis
ASD	Atrial septal defect
AST	Aspartate aminotransferase
atRA	all-*trans*-retinoic acid
BAC	Bacterial artificial chromosome
BAF	B-allele frequency
BASR	Bilateral anophthalmia and XX sex-reversal
βME	β-mercaptoethanol
BMP	Bone morphogenetic protein
BSA	Bovine serum albumin
CBCP	Complete blood count
cDNA	Complementary DNA

CGH	Comparative genomic hybridization
CGH	X-linked congenital hypertrichosis
CGHM	Center for Genetics and Health and Medicine
CM	Conditioned media
CMTC	Cutis marmorata telangiectasia congenital
CNE	Conserved non-coding element
CNS	Central nervous system
CNV	Copy number variant
CRABP	Cellular retinoic acid binding protein
CRALBP	Cellular retinaldehyde binding protein
CRBP	Cellular retinol binding protein
Cre	Cre recombinase
DAB	Dimaminobenzidene
DAPI	4’,6’-diamidino-2-phenylindole
DB	Decidua basalis
dbSNP	Database of single nucleotide polymorphisms
DMEM	Dulbecco’s modified eagle medium
DNA	Deoxyribonucleic acid
DOC	Deoxycholate
EFTF	Eye field transcription factor
EGFR	Estimated glomerular filtration rate
EOM	Extraocular muscles
ER	Endoplasmic reticulum
FGF	Fibroblast growth factor
GCL	Ganglion cell layer
GFAP	Glial fibrillary acidic protein

GFP	Green fluorescent protein
GI	Gastrointestinal
H&E	Hematoxylin and eosin
HA	Hemagglutin
HCNE	Highly conserved non-coding element
HCT	Hematocrit
HDL	High density lipoprotein
HEK293T	Human embryonic kidney 293T cell line
HGB	Hemoglobin
HMG	High mobility group
HP	Hypothalamopituitary
HPES	Holoprosencephaly spectrum
HRP	Horseradish peroxidase
HUMAR	Human androgen receptor (assay)
INL	Inner nuclear layer
IP	Immunoprecipitation
IRBP	Interphotoreceptor retinol binding protein
IT	Insertional translocation
ITS	Insulin-transferrin-selenium
IU	International units
JAK/STAT	Janus kinase / Signal transducer and activator of transcription
KDEL	Endoplasmic reticulum retention peptide
LDL	Low density lipoprotein
LOD	Log of odds score
LRR	Log *R* ratio
LSC	Liquid scintillation counting

MA	MasterAMP
MAC	Microphthalmia, anophthalmia, coloboma
MALDI-TOF	Matrix-assisted laser desorption/ionization and Time-of-flight
MCH	Mean corpuscular hemoglobin
MCHC	Mean corpuscular hemoglobin concentration
MCV	Mean corpuscular volume
MGI	Mouse Genome Informatics (Jackson Laboratories)
MOE	Minimization of energy
MPV	Mean platelet volume
MRI	Magnetic resonance imaging
MS	Mass spectrometry
NCBI	National Center for Biotechnology Information
NDS	Normal donkey serum
NHLBI	National Heart, Lung and Blood Institute
NPC	Neural progenitor cell
NR	Neuroretina
OMIM	Online mendelian inheritance in man
ONL	Outer nuclear layer
PAGE	Polyacrylamide gel electrophoresis
PBS	Phosphate buffered saline
PBST	Phosphate buffered saline with 1% Triton X-100 (v/v)
PCR	Polymerase chain reaction
PFA	Paraformaldehyde
PHPV	Persistent hyperplastic primary vitreous
PLT	Platelet
POM	Periocular mesenchyme

PRS	Pierre Robin sequence
RA	Retinoic acid
RALDH	Retinaldehyde dehydrogenase
RAR	Retinoic acid receptor
RARE	Retinoic acid response element
RBC	Red blood cell (count)
RBP	Retinol binding protein (mature gene product)
RBP4	Retinol binding protein (gene)
RBP-ROH	Retinol bound to retinol binding protein
RDH	Retinol dehydrogenase
RDW	Red blood cell distribution width
RIPA	Radio-immunoprecipitation assay
RNA	Ribonucleic acid
ROH	Retinol
RPC	Retinal progenitor cell
RPE	Retinal pigment epithelium
RT-PCR	Reverse transcriptase polymerase chain reaction
RXR	Retinoid X receptor
SAS	Saturated ammonium sulfate
SCR	Short conservative region
SDM	Site-directed mutagenesis
SDS	Sodium dodecyl sulfate
SEM	Standard error of measure
SHH	Sonic hedgehog ligand
SOX	Sry-related high mobility group box
SOXB1	Sox group B1 consisting of Sox1, Sox2 and Sox3

SS	Endoplasmic reticulum signal sequence
SSC	Saline sodium citrate
SSLP	Simple sequence length polymorphism
STRA6	Stimulated by retinoic acid 6
TBS	Tris-buffered saline
TBST	Tris-buffered saline with 1% Triton X-100 (v/v)
TES	Testis-specific enhancer of Sox9
TESCO	Testis-specific enhancer of Sox9 core
TGFβ	Transforming growth factor beta
TPE	Total protein electrophoresis
TTR	Transthyretin (formerly prealbumin)
UM	University of Michigan
UPR	Unfolded protein response
uRBP	Urine retinol binding protein
UV	Ultraviolet
VAD	Vitamin A deficiency
VSD	Ventricular septal defect
WBC	White blood cell (count)
WT	Wild-type
XCI	X-chromosome inactivation

ABSTRACT

The spectrum of congenital eye malformations including microphthalmia (small eyes), anophthalmia (absent eyes) and coloboma (ventral eye defects), or MAC, causes blindness in approximately 1 in 10,000 children. We have discovered novel *RBP4* coding and *SOX3* regulatory mutations in patients with MAC disease. *RBP4* encodes plasma retinol binding protein, a lipocalin that transports vitamin A, an essential nutrient for eye development, in the bloodstream. We show *RBP4* missense mutations p.A73T and p.A75T alter the ligand-binding pocket, causing autosomal dominant MAC with reduced penetrance and a maternal parent-of-origin effect. Both mutant alleles encode dominant-negative RBPs that bind poorly to vitamin A but strongly to the STRA6 receptor on recipient cell membranes. Consequently, a vitamin A “bottleneck” is created at the maternal-fetal interface, which is likely to reduce vitamin A delivery to the fetus, particularly when the mutation is inherited from the mother. This is the first report of such a defective interfering allele for a blood cargo protein in human disease. In a separate case, we describe a novel *SOX3* regulatory mutation in a 46,XX child with bilateral anophthalmia and SRY-negative female-to-male sex reversal. In this patient, a paternal *de novo* 9q21→ Xq27 insertional translocation

has juxtaposed *TRPM3* exons 1 and 2 downstream from *SOX3*, at the midpoint of a 180-bp pallindrome. This implicates a dominant, gain-of-function mechanism whereby ectopic *SOX3* transcription disrupts early eye and gonadal development. Transgenic mouse models test this hypothesis and reveal sensitivity of the developing eye to alterations in SoxB1 (Sox2) spatiotemporal activity. This thesis highlights genetic and environmental factors that influence eye development, and it has broad implications for other congenital disorders.

CHAPTER I

INTRODUCTION

Early patterning of the vertebrate eye

The eye is an exquisitely complex tissue that allows an organism to perceive its environment through vision. Vision, or light perception, requires the coordinated activity of multiple structures such as the cornea, lens and retina to convert light into an electrical stimulus that is interpretable by the central nervous system (CNS). Formation of these mature sub-specialized tissues depends on a highly organized process involving cells derived from three major sources: surface ectoderm, neuroepithelium and periocular mesenchyme (POM). These tissue interactions set the foundation for proper growth and maturation of tissues during later stages of eye development.

The vertebrate eye begins as part of a single eye field in the anterior neural plate comprised of multipotent retinal precursors during late gastrulation (Figure 1.1A) (Graw, 2003; Inoue et al., 2000). At approximately the third week of pregnancy in humans (embryonic day E8.5 in mice), the eye field splits into two halves giving rise to bilateral optic pits. Originally described by Spemann (Spemann, 1924), this structure represents the first morphologic event in eye development. Shortly thereafter in the placode stage, they enlarge to form optic vesicles that originate from ventral forebrain neuroepithelium (prosencephalon) and expand laterally through mesenchyme until the dorsal portion makes contact with the overlying surface pre-placodal ectoderm. This contact induces the lens placode which appears as a thickening at the point of contact with the optic vesicle. At E10, through vital tissue-tissue interactions with ectoderm (Hyer et al., 2003),

both the the optic vesicle and lens placode invaginate, forming a bilayered optic cup and lens vesicle, respectively. The optic cup inner layer develops into the presumptive neuroretina (NR) that produces cells for light sensation and innervation of the CNS. The outer layer becomes the future retinal pigment epithelium (RPE) that nourishes the retina and supports light-sensing photoreceptor cell development (Strauss, 2005). The margin between the two layers develops into the iris and ciliary bodies. The mature iris modulates retinal illumination through its control over the pupil and the ciliary body secretes aqueous humor and controls lens accommodation. Narrowing at the proximal end of the optic cup forms the optic stalk, which will later contribute to the optic nerve. Meanwhile, the lens vesicle separates and detaches completely from the ectoderm and positions itself within the optic cup to form the future lens. Along its entire inferior aspect, the optic cup is incomplete at the so-called choroid (optic) fissure. This open cleft contains the hyaloid artery and vein, which forms the hyaloid vasculature and supplies the embryonic eye with blood. As development proceeds, the patent choroid fissure fuses beginning at its base at the forebrain wall and concluding at the ventral aspect of the pupil. Eventually the fetal eye vasculature regresses, giving way to the ophthalmic artery and vein that serve as the primary blood source through the choroid vasculature. Once each major compartment is established, the histogenic phase begins where cells undergo the process of terminal differentiation until the mature eye is formed (Figure 1.1B).

The periocular mesenchyme (POM) is a loose collection of cells that contribute greatly to early eye morphogenesis through signaling pathways targeted to the optic cup and the anterior and auxiliary eye structures. Historically, the POM was thought to

derive strictly from paraxial head mesoderm, however fate mapping studies in birds using chick-quail chimeras, vital dye labeling and neural crest-specific antibodies, showed contributions from both neural crest and mesoderm (Johnston et al., 1979; Le Lievre and Le Douarin, 1975). This property extends to mammalian eye development as seen with both neural-crest specific (Wnt1-Cre) or mesoderm-specific (αGSU-Cre) lineage trace systems that show the presence of both cell types within the anterior structures of the eye (Gage et al., 2005). Classic tissue explant experiments demonstrate the POM is necessary for growth of the eye beyond the optic vesicle stage (Holtfreter, 1939). During the optic cup stage, POM plays an essential role in RPE fate specification (Fuhrmann et al., 2000) and downstream maintenance (Evans and Gage, 2005). Elsewhere, when the lens vesicle separates from the surface ectoderm, surrounding mesenchymal cells migrate into the space between the detached structures. There they form distinct layers and with additional mesenchymal infiltration eventually condense into the corneal endothelium (Haustein, 1983). The anterior surface ectoderm becomes the corneal epithelium. Corneal endothelium differentiation allows for separation of the cornea and lens (Kidson et al., 1999; Reneker et al., 2000) permitting the optic cup margins to elongate between the 15^{th} and 20^{th} week of gestation (E17 – E19 in mice). Additional mesenchymal cells migrate in and establish the iris and ciliary body stroma. Within the iridocorneal angle formed between the iris and cornea, an accumulation of mesenchymal cells condense and flatten to form the trabecular meshwork surrounding the future Canal of Schlemm, the aqueous humor outlet tract. Auxiliary structures such as extraocular muscles arise from mesenchymal condensations. They represent a mix of mesoderm-derived myofibers and neural-crest

derived connective tissue and fascia. Additionally, the fetal hyaloid vasculature consists of mesodermal endothelial cells and neural crest smooth muscle cells (Gage et al., 2005).

Molecular pathways governing early eye development

In the vertebrate anterior neural plate eye-field, a host of transcription factors (EFTFs) including *Lhx2*, *Rx*, *Pax6*, *Six3* and *Six6* prime the initiation of eye development (Zuber et al 2003). Many share common ancestry to orthologous genes in *Drosophila melanogaster* where they also function in oculogenesis. *Pax6* is the homolog of *Drosophila eyeless* and *twin of eyeless* (Quiring et al 1994) and *Six3* and *Six6* are homologs of *Drosophila sine oculis* (Oliver et al 1995). Loss of EFTFs, through targeted or spontaneous mutations in mice, leads to abnormal or no eyes (Hill et al., 1991; Lagutin et al., 2003; Li et al., 2002; Mathers et al., 1997; Porter et al., 1997). Conversely, mis-expression of *Rx*, *Pax6*, *Six3* or *Six6* can induce ectopic eye tissues (Andreazzoli et al., 1999; Bernier et al., 2000; Chow et al., 1999; Chuang and Raymond, 2001; Halder et al., 1995; Loosli et al., 1999; Oliver et al., 1996). The potent actions of EFTFs, combined with their loss-of-function eye phenotypes, unequivocally show eye development is highly conserved at the molecular level.

Formation and expansion of the optic vesicle from the forebrain requires dramatic shifts in cellular morphology and movement (Svoboda et al 1987). During neurulation, pre-specified retinal progenitor cells (RPC) within the eye field move toward the dorsal midline as the neural tube closes before turning around into the evaginating optic vesicle (Martinez-Morales et al., 2004). The retinal homeodomain transcription factor

Rx/RAX is a major gene involved in this process. First expressed prior to optic vesicle formation (Furukawa et al., 1997), null or hypomorphic alleles are associated with anophthalmia in multiple vertebrate species including mouse (*Rx*), frog (*Rx1*), zebrafish (*Rx3/chokh*) and medaka (*eyeless*) (Andreazzoli et al., 1999; Furukawa et al., 1997; Kennedy et al., 2004; Loosli et al., 2003; Mathers et al., 1997; Tucker et al., 2001; Winkler et al., 2000). In the absence of *Rx,* optic vesicle evagination completely fails. Mouse chimera experiments involving wild-type and mutant *Rx* cells show mutant cells are excluded from the evaginating optic vesicle (Medina-Martinez et al., 2009). Thus, *Rx/RAX* acts in a cell autonomous manner to specify retinal progenitor cells that will participate in the lateral expansion phase. *Rx3*, the medaka *RAX* homolog, also segregates bipotential precursors of the anterior forebrain and promotes a retinal progenitor fate over a posterior telencephalic fate (Stigloher et al., 2006). Furthermore, *Rx* down-regulates genes that promote midline convergence such as *Nlcam* (Brown et al., 2010), an adhesion molecule that governs cell migratory properties. While the role of *Rx/RAX* in retinal precursor specification and migration is well-established, many questions remain about its exact molecular function in relation to other EFTFs.

The presumptive NR and RPE are specified in the optic vesicle stage well before they become morphologically distinct. The dorsal region is fated to become the RPE and the distal/ventral portion the NR. Initial studies showed each layer has competency to differentiate into either NR or RPE (Araki and Okada, 1977; Coulombre and Coulombre, 1965; Opas et al., 2001; Reh and Pittack, 1995), but only recently have the molecular mechanisms begun to surface. Initial specification of NR is largely mediated by fibroblast growth factor (FGF) signaling from the surface ectoderm (Guillemot and

Cepko, 1992; Horsford et al., 2005; Hyer et al., 1998; Nguyen and Arnheiter, 2000). Establishment of the unique identity of both NR and RPE arises in large part from two transcription factors, Chx10 (Vsx2) and Mitf (Horsford et al., 2005), respectively. Each possesses antagonistic effects upon the other. Within the E10 optic cup, the developing NR must generate millions of cells in preparation for the histogenic phase. Proliferation in the retina is governed by a series of extrinsic and intrinsic factors. Chief among the latter is Chx10, a homeobox transcription factor that is the first known NR-specific expressed gene (Liu et al., 1994). Chx10 acts primarily as a transcriptional repressor (Clark et al., 2008; Dorval et al., 2005) and controls RPC proliferation by preventing accumulation of $p27^{Kip1}$, a cyclin-dependent kinase inhibitor that promotes cell cycle exit (Green et al., 2003). Homozygous *Chx10*$^{-/-}$ null mice (*ocular retardation, or*^{J}*/or*^{J}) develop microphthalmia with thin retinas and no optic nerves due to insufficient RPC proliferation (Burmeister et al., 1996). Knockdown of *chx10* in zebrafish yields a similar phenotype (Barabino et al., 1997). Consequently, a diminished RPC pool weakens positive feedback loops that help to maintain its proliferative capacity. For example, absence of the first-born cells that form the optic nerve (i.e. retinal ganglion cells) leads to a drastic reduction in Sonic hedgehog (Shh) signaling and RPC proliferation (Sigulinsky et al., 2008). In parallel to RPC and NR identity maintenance, Chx10 acts as a regional repressor of the RPE specification factor *Mitf* (Horsford et al., 2005).

The *Mitf* gene encodes a basic helix-loop-helix transcription factor necessary for establishing RPE cell identity and is expressed throughout the neuroectoderm of the mouse optic vesicle beginning at E9.0, but is specifically downregulated in the NR by Chx10 (Hughes et al., 1993; Nguyen and Arnheiter, 2000). *Mitf* $^{-/-}$ mutant mice (*mi/mi*)

show failure of RPE differentiation and microphthalmia with an RPE-to-NR fate switch in the dorsal region of the eye (Bumsted and Barnstable, 2000; Hodgkinson et al., 1993). The position of *Mitf* at the top of the RPE genetic hierarchy has generated interest in its upstream and downstream regulatory determinants. Pax2 and Pax6 are already present in the presumptive mouse RPE and directly activate *Mitf* expression with overlapping functionality (Baumer et al., 2003). Dorsal periocular mesenchyme signaling is also critical for *Mitf* activation possibly through a TGFβ-mediated pathway, but the exact nature of the molecular signal remains unclear (Fuhrmann et al., 2000; Kagiyama et al., 2005). Furthermore, species-differences in mouse versus chick *Mitf* expression relative to the amount of contacting RPE-POM surface area further obscures the inductive relationship between RPE and POM (Mochii et al., 1998; Muller et al., 2007; Nguyen and Arnheiter, 2000). Other studies have implicated bone morphogenetic protein (BMP), a TGFβ superfamily member, as a potent inducer of *Mitf* in chick; however, this does not extend to mammals (Hyer et al., 2003; Muller et al., 2007). Once expressed, Mitf regulates key downstream genes involved in terminal pigment differentiation (e.g. *Dct*, *Tyrp1* and *tyrosinase*) (Bentley et al., 1994; Jiao et al., 2004; Yasumoto et al., 1994; Yavuzer et al., 1995). Over 40 Mitf target genes have been discovered to-date (Cheli et al., 2010); however, the function of each target within the greater RPE transcriptional hierarchy remains largely unknown.

Extrinsic pathways also play a vital role in normal eye development and disruptions in these pathways can result in blindness. Wnt signaling is a type of signaling pathway and exists in two major forms, canonical versus non-canonical pathways that differ in specific activators. Wnt proteins act at multiple levels in non-

mammalian eye development and exhibits significant interspecies differences (Fuhrmann, 2008). All vertebrates suppress canonical Wnt signaling in the rostral CNS early in eye development to promote anterior neural ectoderm specification (Nordstrom et al., 2002; Satoh et al., 2004), mediated in part by Six3 (Lagutin et al., 2003; Liu et al., 2010). Subsequently in non-mammalian species, non-canonical Wnt signaling is activated for retinal progenitor activation of Rx and Pax6 (Maurus et al., 2005), cell migration during optic vesicle evagination (Cavodeassi et al., 2005; Lee et al., 2006), and suppression of canonical Wnt mechanisms (Westfall et al., 2003). However, the opposite is true in mouse, given the loss of analogous non-canonical Wnt ligands, Wnt4 or Wnt11, and transmembrane receptor Fzd3 mutants have no reported eye defects (Majumdar et al., 2003; Stark et al., 1994; Wang et al., 2002). In contrast, forced Wnt expression in chick retina is sufficient to promote iris and ciliary body formation, and Wnt signaling inhibition using a dominant-negative Lef-1 (a Wnt effector protein) results in iris hypoplasia (Cho and Cepko, 2006). Activation of Wnt signaling in mouse retinal explants as well as Cre-mediated *in vivo* stabilization of β-catenin in mouse retina leads to upregulation of ciliary margin markers at the expense of neuroretinal ones (Liu et al., 2007). Consistent with the previously mentioned studies, endogenous Wnt activity is detected in the optic cup ciliary margin across multiple vertebrates (Liu et al., 2003; Liu et al., 2006; Van Raay et al., 2005). In summary, Wnt signaling is important for vertebrate eye development but is used differently amongst various species. In particular mammals largely repress Wnt signaling during early eye patterning only to activate it during later stages of terminal cell differentiation.

FGF signaling emanates from the lens placode to help specify the neuroretina and initiate optic cup morphogenesis, but also functions in lens development. All four FGF receptor genes (*Fgfr1-4*) are activated in the mid-to-late embryonic lens (de Iongh et al., 1997; de Iongh et al., 1996; Kurose et al., 2005). Subsequent knock-out studies show FGF signaling is indispensable for proper lens development and fiber cell differentiation (Zhao et al., 2008). However, due to the heterogeneous expression of FGF proteins secreted in the surface ectoderm, no single essential ligand has been identified (Smith et al., 2010).

Retinoids in early eye development

Vitamin A is an essential nutrient that must be ingested through diet mainly as α/β-carotenoids or retinyl esters (e.g. retinyl palmitate). Though its existence was implied in ancient Egyptian scrolls dating back 3,500 years (Wolf, 1996), only in the early 20th century did pioneering nutritional studies by Elmer McCollum, Frederick Hopkins, and Lafayette Mendel finally lead to the discovery of “fat-soluble factor A” (Hopkins, 1912; McCollum, 1913, 1915; Osborne, 1914a, b). Vitamin A, as it was later termed, has a characteristic β-ionone ring and isoprene tail chemical structure that serves as the base form for a class of molecules known as retinoids. Collectively, retinoids have been linked to major human diseases such as cancer, type 2 diabetes and third-world childhood blindness (Mamede et al., 2011; Sommer, 2008; Yang et al., 2005). Retinoids are also indispensible for normal vision, epithelial, immune and reproductive health as well as embryonic development (Theodosiou et al., 2010). Early nutritional studies in pigs and rats showed that depriving pregnant mothers of vitamin A

consistently produced offspring with microphthalmia or anophthalmia (Hale, 1932; Warkany and Schraffenberger, 1946). Soon thereafter, Vitamin A deficiency (VAD) syndrome was defined in rats most frequently by eye defects followed by urogenital, diaphragmatic and cardiovascular malformations (Wilson et al., 1953). These studies illustrate the sensitivity of the developing eye to gestational VAD, thus establishing its imperative role in oculogenesis.

Retinoic acid (RA) signaling is a major pathway utilized throughout embryogenesis (Figure 1.2). Synthesis of RA requires vitamin A (retinol) from the diet that is solubilized and transported through the blood by retinol binding protein (RBP) (Kanai et al., 1968). At the target cell, retinol-bound RBP (RBP-ROH) interacts with the cell surface receptor STRA6 to deliver vitamin A into the cell (Kawaguchi et al., 2007). Once inside, retinol undergoes a series of oxidation reactions to form retinaldehyde and retinoic acid. To regulate local RA levels, a series of cytochrome P450 enzymes metabolize RA into water-soluble oxidized derivatives that are freely eliminated. Once generated, RA acts in a paracrine fashion, freely diffusing across cell membranes either for signaling or degradation. In the body, all-*trans*-RA (atRA) is the most abundant form; however, pharmacological induction of the 9-*cis*-RA isomer has been observed. Both RA isomers serve as ligands for a series of nuclear receptors that regulate gene transcription (Duester, 2000). Upon binding atRA, the retinoic acid receptors (RARα, β and γ) and retinoid X receptors (RXRα, β and γ) form RAR/RXR heterodimers and activate target gene expression through DNA retinoic acid response elements, or RAREs (Duester, 2009). In turn, RAR/RXR dimers can interact with a number of transcriptional co-repressor or co-activator complexes to further regulate gene

expression levels (Niederreither and Dolle, 2008). RA signaling is thought to act predominantly through the RAR moiety since RXRs can only bind 9-cis-RA (Allenby et al., 1993; Heyman et al., 1992; Levin et al., 1992). The latter form is undetectable under normal physiologic conditions, and is unable to rescue RA deficiency phenotypes when administered exogenously (Mic et al., 2003).

Mammals are equipped with three RAR receptors (α, β and γ) and three RXR receptors (α, β and γ). Each of the six subtypes is expressed as two N-terminal isoform variants (Mollard et al., 2000) that are expressed in highly overlapping tissue patterns. In the early optic cup stage (E10.5), Rarα, Rarβ and Rarγ are all expressed in periocular mesenchyme. Rarα and Rxrα are uniformly distributed in the embryonic retina and Rxrγ is exclusive to the RPE (Mori et al., 2001). RAR and RXR receptors show significant functional overlap as evidenced by relatively mild ocular phenotypes seen in a subset of single retinoid receptor mutants: persistent retrolenticular membrane (*Rarb*, *Rxra*), absent Harderian glands (*Rarg*), and truncated ventral retina with a thickened cornea (*Rxra*) (Ghyselinck et al., 1997; Kastner et al., 1994; Lohnes et al., 1993; Lufkin et al., 1993; Sucov et al., 1994). However, ocular and extraocular phenotypes are dramatically increased in compound null mutants of two receptors. For example, E18.5 *Rara;Rarg* double mutants display microphthalmia and coloboma with truncation of the ventral retina, fusion of the cornea and iris, and conjunctival defects (Lohnes et al., 1994). Anterior segment defects are also observed in *Rxra;Rarb* compound mutants, suggesting a cooperative effect between Rxrα and Rarβ/γ receptors in this region of the eye (Kastner et al., 1997). *Rarb;Rarg* neonates show a malformed ventral retina due to coloboma, mesenchymal infiltrates in the optic nerve, and persistent retrolentricular

membrane (Lohnes et al., 1994). It is worth noting that many extraocular phenotypes such as congenital heart and brain malformations, axial skeletal defects, and testicular abnormalities are also observed in both single and double RAR receptor mutants (Niederreither and Dolle, 2008). Thus, studies from mutant retinoid receptor models confirm many phenotypes seen in VAD syndrome; however, their overlapping domains and functions have made it difficult to pinpoint individual receptor contributions.

Cytosolic alcohol dehydrogenases (ADHs) and microsomal retinol dehydrogenases (RDHs) catalyze a reversible first step in RA synthesis, namely, retinol conversion to retinaldehyde (Figure 1.2). ADHs include Adh1, Adh7 (formerly *Adh3*), Adh4 and RDHs include Rdh1 and Rdh10. There is minimal tissue restriction of ADH/RDH activity since Adh3 and Rdh1 are ubiquitously expressed (Molotkov et al., 2002; Zhang et al., 2007). The ubiquitous expression of Adh3 and Rdh1 protects against loss of any single alcohol dehydrogenase gene. For example, loss of Rdh1 has no impact on embryonic development (Zhang et al., 2007), strongly supporting enzymatic compensation by other ADH or RDH members. In contrast, *Rdh10* is expressed in the presumptive RPE of the E10.5 optic cup and is the first of any ADH or RDH discovered to show an embryonic eye phenotype, albeit mild, consisting of cornea and ventral retina agenesis and a hypoplastic lens (Sandell et al., 2007). It has since been demonstrated that Rdh10 is the primary enzyme for embryonic RA synthesis *in vivo* (Farjo et al., 2011).

Retinaldehyde dehydrogenases Raldh1, Raldh2 and Raldh3 (*Aldh1a1-3*) catalyze the oxidation of retinaldehyde to retinoic acid, the second irreversible step in RA synthesis (Figure 1.2). The *Aldh1a* gene subfamily exhibits highly dynamic and

compartmentalized expression patterns. Much of our knowledge of RA signaling derives from comparisons of Raldh expression (where RA is synthesized) in conjunction with RARE-LacZ reporter transgenes on knockout backgrounds (where RA signaling occurs) (Mendelsohn et al., 1991; Rossant et al., 1991). Of the three Raldh genes, *Raldh2* is the primary eye field initiator and is later found in the surface ectoderm, optic vesicles, and transiently in the POM from E8.0 – E10.0 (Mic et al., 2002; Niederreither et al., 1999). Raldh3 is first detected in surface ectoderm shortly after and independently of Raldh2, and by E9 expands significantly throughout the surface ectoderm to cover eye regions bilaterally (Li et al., 2000). Later in development at E11, Raldh3 is detected throughout the dorsal RPE and expanding ventral retina. At E11, Raldh1 is also activated in the dorsal retina. The same Raldh1 and Raldh3 pattern is found in chick (Grun et al., 2000).

As with RAR/RXR knockout studies, functional compensation leads to relatively mild ocular phenotypes for *Raldh2*$^{-/-}$ and *Raldh3*$^{-/-}$ single knockout mice, but no phenotype for *Raldh1*$^{-/-}$ mice (Dupe et al., 2003; Fan et al., 2003; Mic et al., 2002; Niederreither et al., 1999). The eye phenotype of *Raldh2*$^{-/-}$ containing a RARE-LacZ reporter transgene shows absent RA synthesis in the E8 optic vesicle where in wild-type embryos, abundant levels of RA are produced (Mic et al., 2002). It should be noted that *Raldh2*$^{-/-}$ embryos die at E10.5 from gross cardiac, axial and neural malformations, thus prohibiting ocular analysis at later timepoints without dietary RA intervention. *Raldh3*$^{-/-}$ embryos are lethal after birth and exhibit shortening of the ventral retina, lens rotation and persistence of the primary vitreous body (PHPV) (Dupe et al., 2003). To better characterize individual and overall contributions of Raldh1-3 activity in the eye, double and triple mutant knockouts were examined (Molotkov et al., 2006). This study revealed

several previously unappreciated key facts. Contrary to previous thought, RA signaling is not necessary for dorsoventral patterning of the retina; however, it is required for invagination of the ventral optic cup. Raldh2 and Raldh3 generate adequate RA to initiate optic cup formation, and continued Raldh3 expression completes it. Raldh3 is also necessary for choroid fissure closure at E13.5. In the absence of all other retinaldehyde dehydrogenases, Raldh1 by itself is unable to initiate ventral optic cup morphogenesis which may be explained by its 10-fold lower enzymatic activity for RA synthesis than Raldh2 or Raldh3 (Grun et al., 2000). Second, RA from Raldh1 and Raldh3 activity in the retina acts upon POM in a paracrine fashion to stimulate apoptosis and control mesenchymal cell numbers (Molotkov et al., 2006). This prevents excessive infiltration of surrounding mesenchymal cells into the optic cup. During embryonic development of *Raldh2*$^{-/-}$ and *Raldh3*$^{-/-}$ embryos, maternal RA supplementation is able to rescue the phenotype demonstrating an important gene-environment interaction.

Retinoic acid gradients exist in many developing tissues such as the CNS. These gradients are important for correct anterior-posterior patterning and epithelial-to-mesenchymal transition of cranial neural crest cells (Sakai et al., 2001; Uehara et al., 2007). These gradients arise from opposing actions of Raldh and CYP26 cytochrome P450 enzymes (Cyp26a1, Cyp26b1 and Cyp26c1). The latter group of enzymes metabolizes and reduces overall RA levels (Abu-Abed et al., 2001; Uehara et al., 2007; Yashiro et al., 2004). Cyp26a1 and Cyp26c1, but not Cyp26b1, are expressed in the embryonic retina in an equatorial stripe at the Raldh1 and Raldh3 boundary, thus defining three RA-concentration zones (Li et al., 2000; Sakai et al., 2004; Wagner et al., 2000). Despite prominent expression of Cyp26a1 and Cyp26c1 in the retina, no ocular

phenotypes have been reported in any of the three single knockout models. *Cyp26a1*$^{-/-}$*;Cyp26c1*$^{-/-}$ double knockouts have reduced eye size at E9.5, but this is secondary to gross CNS malformations (Uehara et al., 2007). These abnormalities are similar to, but more severe than, the effects seen in *Cyp26a1*$^{-/-}$ single knockout embryos (Sakai et al., 2001) suggesting cooperativity in CNS patterning. It is unknown whether Cyp26 enzymatic cooperativity occurs in the embryonic retina, because no detailed analysis of the eye was reported (Sakai et al., 2004). Thus, it remains unclear if total loss of RA catabolism in the retina has any bearing on eye development. It is worth noting that excessive retinoid intake during human pregnancy is teratogenic and causes cranial neural crest defects such as cleft lip and craniosynostosis, and cardiovascular, thymic and CNS malformations (Lammer et al., 1985; Rothman et al., 1995). Microphthalmia has been noted in several animal models of gestational retinoic acid toxicity; however, this was infrequent and accompanied by severe CNS abnormalities (micro- or exencephaly) suggesting a potential bystander effect (Shenefelt, 1972).

Genetics of congenital eye malformations

Disruption or failure of initial eye patterning steps can lead to significant structural defects. Clinical microphthalmia, anophthalmia and coloboma (MAC) is a spectrum of eye diseases that result in varying degrees of ocular malformations in one or both eyes (Figure 1.3). Anophthalmia is the most severe and refers to the absence of eye globes resulting in total blindness. Children born with microphthalmia have very small eyes (< 2 standard deviations below mean axial length). The mildest form is coloboma, which appears as a notch in the inferior aspect of the iris consistent with a patent choroid

fissure. In microphthalmia or coloboma, vision may be spared or significantly impacted, depending on the structural defect. The incidence of MAC is approximately 1 in 10,000 live births (Morrison et al., 2002). MAC may appear as an isolated clinical finding or as part of a syndrome such as CHARGE syndrome (OMIM 214800), Lenz microphthalmia syndrome (OMIM 309800), Branchio-oculo-facial syndrome (OMIM 113620) and Goltz syndrome (OMIM 305600). These all have characteristic features that guide appropriate medical management and genetic testing.

For this thesis, the term “mendelian” is defined as a mutant trait with 100% penetrance and a 1:1 segregation ratio. Non-mendelian traits deviate from these criteria and various diseases with non-Mendelian inheritance patterns and associated mechanisms are reviewed elsewhere (Van Heyningen and Yeyati, 2004). Mendelian forms of congenital eye disease based on single gene mutations provide enormous insight into normal human eye development. The vast majority encode transcription factors that serve critical roles in cell proliferation, specification or differentiation. Many homeodomain transcription factor genes are associated with human eye malformations and reproduce similar phenotypes in animal models such as in autosomal recessive forms of MAC involving *RAX* (OMIM 601881) and *CHX10* (OMIM 251600). As discussed above, both are critical factors in retinal progenitor cell maintenance. Two affected individuals with *RAX* compound heterozygous mutations with unilateral anophthalmia and contralateral sclerocornea were separately reported (Lequeux et al., 2008; Voronina et al., 2004). *RAX* mutations affecting the DNA binding domain are the most severe and have been verified as null alleles (Voronina et al., 2004). Other novel *RAX* variants in regions apart from the DNA binding domain are associated with the

MAC spectrum (Gonzalez-Rodriguez et al., 2010); however, their functional effects not yet been examined. Several of these alleles are also associated with midline CNS defects and hydrocephaly, which possibly expands the *RAX* human mutation phenotype beyond the eye. Humans with homozygous *CHX10*$^{-/-}$ null mutations present with non-syndromic microphthalmia, iris coloboma, cataracts and a thickened sclera (Ferda Percin et al., 2000). Unlike mice, *CHX10*$^{-/-}$ humans develop intact optic nerves.

OTX2 is another homeodomain transcription factor of the bicoid class associated with human eye disease. It is located at human chromosome 14q22 and is related to the *Drosophila* gene orthodenticle (Simeone et al., 1993). The *OTX2* gene product functions in regional specification of RPE, anterior neuroectoderm and the pituitary gland (Martinez-Morales et al., 2003; Martinez-Morales et al., 2001; Simeone et al., 1993). Inactivating mutations, insertions, intragenic and whole-gene deletions in *OTX2* are associated with autosomal dominant microphthalmia and anophthalmia with pituitary defects (Ashkenazi-Hoffnung et al., 2010; Ragge et al., 2005a; Schilter et al., 2011; Tajima et al., 2009; Wyatt et al., 2008). Dominant-negative forms of *OTX2* also cause disease (Diaczok et al., 2008). Additional *OTX2* loss-of-function features include anterior segment defects and hypoplasia/aplasia of the optic nerve and chiasm. In mice, *Otx2*$^{+/-}$ mice have phenotypes that vary between microphthalmia/anophthalmia with agnathia to normal. Full *Otx2* knockouts are embryonic lethal by E9.5 with missing optic vesicles (Acampora et al., 1995; Matsuo et al., 1995). Thus, *Otx2/OTX2* mutations in mice and humans produce highly variable phenotypes but consistently show eye abnormalities.

Apart from homeodomain transcription factor genes, loss-of-function mutations in the SOX (SRY-related high-mobility group, or HMG, box) family member *SOX2* cause MAC (Fantes et al., 2003). Patients with *SOX2* haploinsufficiency most often suffer from bilateral anophthalmia, though less severe ocular phenotypes have been reported such as anterior segment dysgenesis, retinal dystrophy, coloboma, optic nerve hypo- or aplasia (OMIM 184429) (Schneider et al., 2009). Patients with inactivating *SOX2* mutations oftentimes show additional features including epilepsy, endocrine abnormalities from pituitary hypoplasia, sensorineural hearing loss and craniofacial abnormalities (Bardakjian and Schneider, 2011). Anophthalmia-Esophageal-Genital syndrome refers to the co-presence of anophthalmia, tracheo-esophageal fistula or esophageal atresia, and genitourinary tract findings. *SOX2* mutations are estimated to cause approximately 10% of all anophthalmia cases (Fantes et al., 2003), making them the most common known cause of MAC.

SOX2 is a single exon gene located on human chromosome 3q26. It encodes a 317-amino acid protein with an N-terminal domain of unknown function, a high-mobility group (HMG) DNA binding domain and C-terminal transcriptional activation domain (Stevanovic et al., 1994). Sox2 functions in development of the central nervous system and its derivative structures such as the eye, ear and hypothalamic-pituitary axis (Kelberman et al., 2006; Kiernan et al., 2005; Taranova et al., 2006). During embryogenesis Sox2 is most prominently expressed in the CNS along with *Sox1* and *Sox3*, two other SoxB1 members (Collignon et al., 1996; Pevny et al., 1998; Rex et al., 1997; Uwanogho et al., 1995; Wood and Episkopou, 1999). *Sox2* expression persists in the outbudding optic vesicles and in the optic cup neuroretina. In RPCs, *Sox2* functions

to maintain progenitor characteristics and is down-regulated only upon neuronal differentiation. Significant loss of Sox2 activity (> 70%) leads to RPC proliferation defects and ocular growth retardation (Taranova et al., 2006).

While mutations in transcription factor genes account for the majority of MAC-causing single gene disorders, other classes of genes have been identified as well. Given the established link between vitamin A and oculogenesis, it was hypothesized that mutations in retinoid pathway genes account for a subset of unexplained congenital eye malformations (Hornby et al., 2003). Only recently, the first human genetic link between retinoid metabolism and MAC was discovered in patients with homozygous null *STRA6* mutations (Golzio et al., 2007; Pasutto et al., 2007). Complete loss of STRA6 causes Matthew-Wood Syndrome (MWS, OMIM 610745), an autosomal recessive disease characterized by anophthalmia, congenital heart defects, lung hypoplasia, diaphragmatic hernia and mental retardation (Seller et al., 1996). *STRA6* mutations are also found in patients with isolated MAC (Casey et al., 2011). Attempts to establish a genotype-phenotype correlation between different mutations affecting various STRA6 protein domains and their associated human phenotypes have so far come up empty (Chassaing et al., 2009).

STRA6 is a 20-exon gene located on human chromosome 15q24 and encodes a novel 670-amino acid receptor with nine predicted transmembrane domains (Kawaguchi et al., 2008b). Originally discovered as a retinoic acid-responsive gene in a cancer cell line (Chazaud et al., 1996), STRA6 defines a new family of receptors and mediates cellular vitamin A uptake through its ligand RBP (Kawaguchi et al., 2007). Biochemical studies demonstrate STRA6 is not simply a passive agent, but is a “sensor” that

mediates retinol uptake based on intracellular storage levels (Kawaguchi et al., 2011). Under certain disease states, STRA6 can also act as a cytokine receptor that utilizes the JAK/STAT signaling cascade (Berry et al., 2011). Consistent with STRA6 mutation-associated human eye malformations, STRA6 RNA localizes to embryonic eye specifically in POM and presumptive RPE (Bouillet et al., 1997). However, *Stra6*$^{-/-}$ mice display only very mild retinal phenotypes (Ruiz et al., 2012). Interspecies differences in loss-of-function phenotypes are not uncommon; however, the absence of a Stra6-null developmental eye phenotype does raise questions about other related family members that may compensate for loss of Stra6, as well as alternative retinoid delivery pathways. While the nutritional requirement of vitamin A in eye development remains constant across all vertebrates, the genetics of vitamin A metabolism and potential loss-of-function congenital eye defects in homologous genes may vary across species.

Anterior segment dysgenesis (ASD) involves failure of the lens, iris, ciliary body, or cornea. *PAX6* is located on human chromosome 11p13 and was the first ASD gene discovered. Heterozygous *PAX6* mutations cause aniridia (OMIM 106200) with associated brain anomalies (Abouzeid et al., 2009; Jordan et al., 1992; Mitchell et al., 2003; Sisodiya et al., 2001). Complete loss of PAX6 leads to anophthalmia with major CNS malformations (Glaser et al., 1994). In mouse, Small-eye (*Sey*) phenotype arises from inactivating *Pax6* mutations (Hill et al., 1991). *Sey/+* mice exhibit microphthalmia with corneal defects and *Sey/Sey* mice display anophthalmia and perish at birth due to respiratory distress. Developmentally, Pax6 is critical for iris specification, optic cup morphogenesis and lens formation (Baumer et al., 2002; Davis-Silberman et al., 2005; Grindley et al., 1997; Marquardt et al., 2001; Matsushima et al., 2011; Smith et al.,

2009). Its contribution to all three structures stems from two distinct regions of Pax6 activity. In the surface ectoderm, Pax6 partners with Sox2 to activate transcription for lens formation (Kamachi et al., 2001). Selective removal of ectodermal Pax6 results in failed lens induction consistent with *Small eye* features (Davis-Silberman et al., 2005). In the distal optic cup margins, Pax6 is critical to maintaining retinal progenitor pools for iris and ciliary body formation, and its loss leads to iris hypoplasia (Davis-Silberman et al., 2005). Since the initial discovery of *PAX6* in human aniridia, additional gene mutations in *PITX2*, *PITX3*, *MAF* and *FOXC1* have been identified in human patients with ASD (Jamieson et al., 2002; Mears et al., 1998; Semina et al., 1998; Semina et al., 1996).

Regulatory mutations in eye diseases: an emerging class

Regulatory disruptions alter spatiotemporal and quantitative levels of gene expression without affecting the actual transcription units. Originally, cytogenetic analysis was the only available tool for investigating diseases at a genome-wide level, and even so with only moderate resolution. Major advances since then have uncovered multiple examples of regulatory mutations and their mechanisms in a variety of human diseases. Collectively, these are known as "*cis*-ruptions" (Kleinjan and Coutinho, 2009). The most common form is chromosomal translocation that transfers control elements from one genomic position to another. *PAX6* cytogenetic rearrangements affecting critical 3' regulatory sequences cause aniridia (Fantes et al., 1995; Kleinjan et al., 2001). Translocations proximal to *PITX2* (4q26) lead to Rieger syndrome (OMIM

180500), a disease characterized by anterior segment dysgenesis of the eye, dental and craniofacial abnormalities (Trembath et al., 2004). Chromosomal translocations involving *FOXC1* and *TGFβ2* have also been described in patients with autosomal dominant iridogoniodysgenesis and glaucoma and Peter's anomaly, respectively (David et al., 2003; Davies et al., 1999).

Many other types of regulatory mutations are associated with congenital eye diseases. For example, interstitial deletions can eliminate important regulatory elements, as seen with 3' deletions in *PAX6*-mediated aniridia (Lauderdale et al., 2000). Other disruptive mechanisms include single nucleotide changes that alter transcription factor binding motifs (De Gobbi et al., 2006; Jeong et al., 2008), promoter downregulation via read-through transcription (Ligtenberg et al., 2009; Tufarelli et al., 2003), epigenetic alteration (Ottaviani et al., 2009), regulatory duplications (Dathe et al., 2009; Kurth et al., 2009), or capture by a foreign promoter or enhancer (Demura et al., 2007). The final mechanism is illustrated by the *Odsex* mouse where disruption of regulatory sequences 1 Mb upstream of *Sox9* causes autosomal dominant microphthalmia and XX sex reversal (Bishop et al., 2000). Under normal conditions, Sox9 is transiently expressed in the RPE; however, this regulatory mutation causes persistent RPE expression that coincides with the onset of microphthalmia (Qin et al., 2004).

In general, members of the SOX gene family are targets for regulatory mutations due to vast expanses of regulatory sequences surrounding the SOX gene transcription units. Regulatory SOX mutations are associated with female-to-male sex-reversal, congenital deafness and cleft palate (Benko et al., 2009; Bishop et al., 2000; Kiernan et

al., 2005). Phylogenetically, SOX genes are divided into ten evolutionarily conserved classes of potent transcriptional regulators essential for sex determination, CNS and sensory organ formation, neural crest maturation, germ cell maintenance, and chondrocyte and immune systems development (Figure 1.4A) (Bowles et al., 2000; Epstein et al., 2008). The founding SOX member is a Y-linked male sex-determining gene *SRY* (Gubbay et al., 1990). SRY expression initiates in the XY bipotential gonad and with SF1, activates SOX9 and drives male sex determination (Figure 1.4B) (Sekido and Lovell-Badge, 2008). In keeping with the pivotal role of SRY in sex determination, SOX genes tend to control genetic hierarchies in a multitude of systems. Loss-of-function SOX gene mutations lead to a wide range of human developmental diseases. Thus, it is not surprising that gain-of-function regulatory mutations have similar consequences, especially in forming eye tissue that is highly responsive to SOX-mediated regulation. As our comprehension of the gene regulatory code improves, additional regulatory mechanisms and new disease loci will undoubtedly be discovered.

Novel mechanistic insights into congenital eye malformations

Retinoids and SOX genes are absolutely essential for normal embryogenesis. Thus, the mechanisms by which they function remain an important area of research, not only for development, but also for possible disease pathogenesis. In this dissertation, I have focused my analysis on two genes implicated in different forms of congenital eye malformations, *RBP4* and *SOX3*.

In Chapter II, I describe two novel *RBP4* missense mutations (p.A73T and p.A75T) in three independent families with autosomal dominant non-syndromic MAC.

This disease trait shows incomplete penetrance and a significant maternal parent-of-origin effect in all three families. *RBP4* encodes plasma retinol binding protein and is the major source of retinoids for vitamin A dependent tissues. Using a variety of functional assays, I describe how both mutations negatively impact vitamin A (retinol) binding, but in all other regards, functionally mimic the wild-type protein. Consequently, the two mutant RBP forms create a molecular “bottleneck” at the STRA6 receptor thus depleting vitamin A delivery into cells. Furthermore, this “bottleneck” phenomenon explains the maternal-origin effect of MAC in all three families, because the maternal-fetal interface (visceral yolk sac and placenta) is a major target site of vitamin A delivery during pregnancy. This work uncovers a novel dominant-negative disease mechanism involving a blood cargo protein and establishes *RBP4* as the second retinoid pathway gene mutated in MAC.

In Chapter III, I explore a novel regulatory mutation involving *SOX3* in a child with bilateral clinical anophthalmia and XX sex-reversal. A large 640 kb autosomal insertion translocation involving 9q21 sequences was found inserted into Xq27 in a 180 bp palindrome previously associated with another X-linked dominant disease (Zhu et al., 2011). The insertion occurred approximately 83 kb downstream of *SOX3*, a gene with no appreciable role in eye development. I find this translocation does not disrupt normal X-chromosome inactivation. I test the hypothesis that ectopic SOX3 activity in the early eye can lead to severe malformations. Based on *in vitro* functional assays, I find SOX3 and SOX2 have similar overlapping transcriptional activation properties. By targeting Sox2 or Sox3 overexpression to the developing neuroretina using a Chx10 bacterial artificial transgene, I find Sox overexpression can result in microphthalmia with profound

defects in retinal lamination and retinal ganglion cell differentiation. This study identifies a human-specific X-linked palindrome that is prone to disease-causing rearrangements and also implicates *SOX3* gain-of-function regulatory mutations in bilateral anophthalmia, XX sex-reversal and potentially a wider host of human diseases.

Figure 1.1. Development and maturation of the vertebrate eye. (**A**) Schematic of early eye patterning beginning in late gastrulation through the optic cup stage. The single eye field splits into two lateral optic vesicles that expand to contact the lens placode (cross-section view). At the lens pit stage, invagination of optic vesicle causes the lens placode to form the lens pit. In the optic cup, the inner and outer layers represent the future NR and RPE, respectively. The margins develop into the iris and ciliary body. The proximal portion of the optic cup narrows to form the optic stalk. Surface ectoderm forms the cornea with POM contributions. (**B**) Structure of the mature human eye. Anterior and posterior segments are divided by the vertical line. Light enters through the cornea and is focused by the lens through the vitreous humor onto the retina (inset). Within the retina, light passes through all layers down to the rod and cone photoreceptors. These cells convert light into an electrical stimulus that traverses back through the retina to the retinal ganglion cells whose axons relay visual information to the brain via the optic nerve. The retinal pigment epithelium sits adjacent to the retina and provides nutrients and support. Note, the optical axis (dotted line) does not coincide with the optic nerve or the fovea which is the area of highest resolution in the retina. Both images adapted from (Graw, 2003).

A

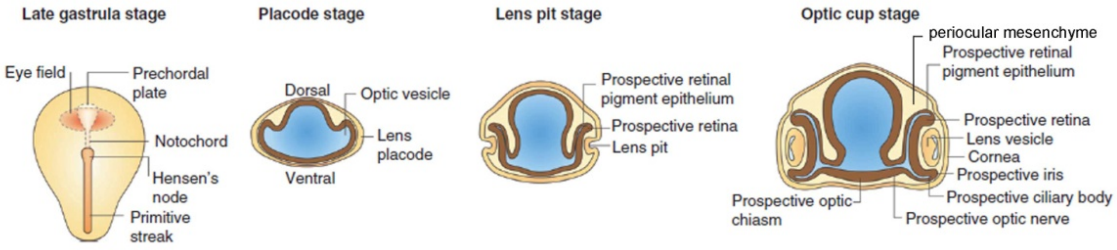
Late gastrula stage
Eye field
Prechordal plate
Notochord
Hensen's node
Primitive streak
Placode stage
Dorsal
Optic vesicle
Lens placode
Ventral
Lens pit stage
Prospective retinal pigment epithelium
Prospective retina
Lens pit
Optic cup stage
periocular mesenchyme
Prospective retinal pigment epithelium
Prospective retina
Lens vesicle
Cornea
Prospective iris
Prospective ciliary body
Prospective optic chiasm
Prospective optic nerve

B

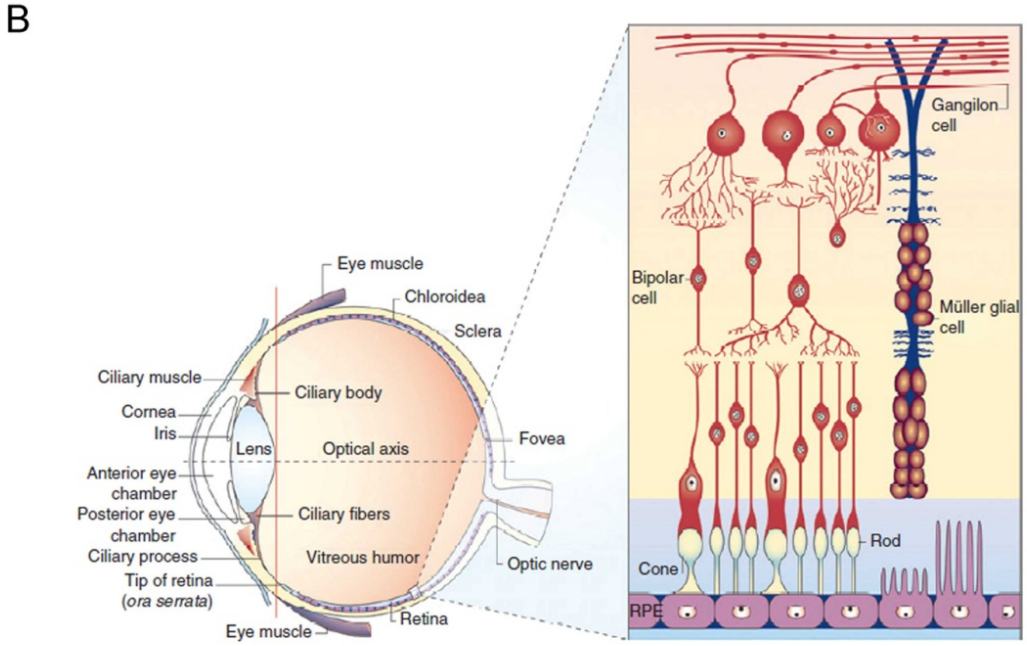
Eye muscle
Chloroidea
Sclera
Ciliary muscle
Ciliary body
Cornea
Iris
Lens
Optical axis
Fovea
Anterior eye chamber
Posterior eye chamber
Ciliary fibers
Ciliary process
Vitreous humor
Optic nerve
Tip of retina (ora serrata)
Retina
Eye muscle
Gangilon cell
Bipolar cell
Müller glial cell
Rod
Cone
RPE

Figure 1.2. Retinoic acid signaling. Cells generate retinoic acid by first taking up vitamin A (retinol) from circulating retinol binding protein (RBP) using the STRA6 transmembrane receptor. Internalized retinol associates with cellular retinol binding proteins (CRBP) and is immediately shuttled to alcohol dehydrogenases (ADH or RDH) for conversion to retinaldehyde. Next, retinaldehyde dehydrogenases (RALDH1-3) oxidize retinaldehyde to retinoic acid (RA). This is secreted and acts in paracrine fashion on target tissues. RA freely diffuses across membranes, associates with intracellular retinoic acid binding proteins (CRABP) and is shuttled to nuclear receptors RAR and RXR. Upon RA ligand docking with RAR, RAR-RXR heterodimers bind DNA retinoic acid response elements (RARE) and modulate target gene expression. Nearby cells fine tune overall retinoic acid levels through CYP26A1,B1 or C1-mediated RA metabolism. These enzymes convert RA into polar metabolites that are readily eliminated from the body. Image adapted from (Duester, 2008).

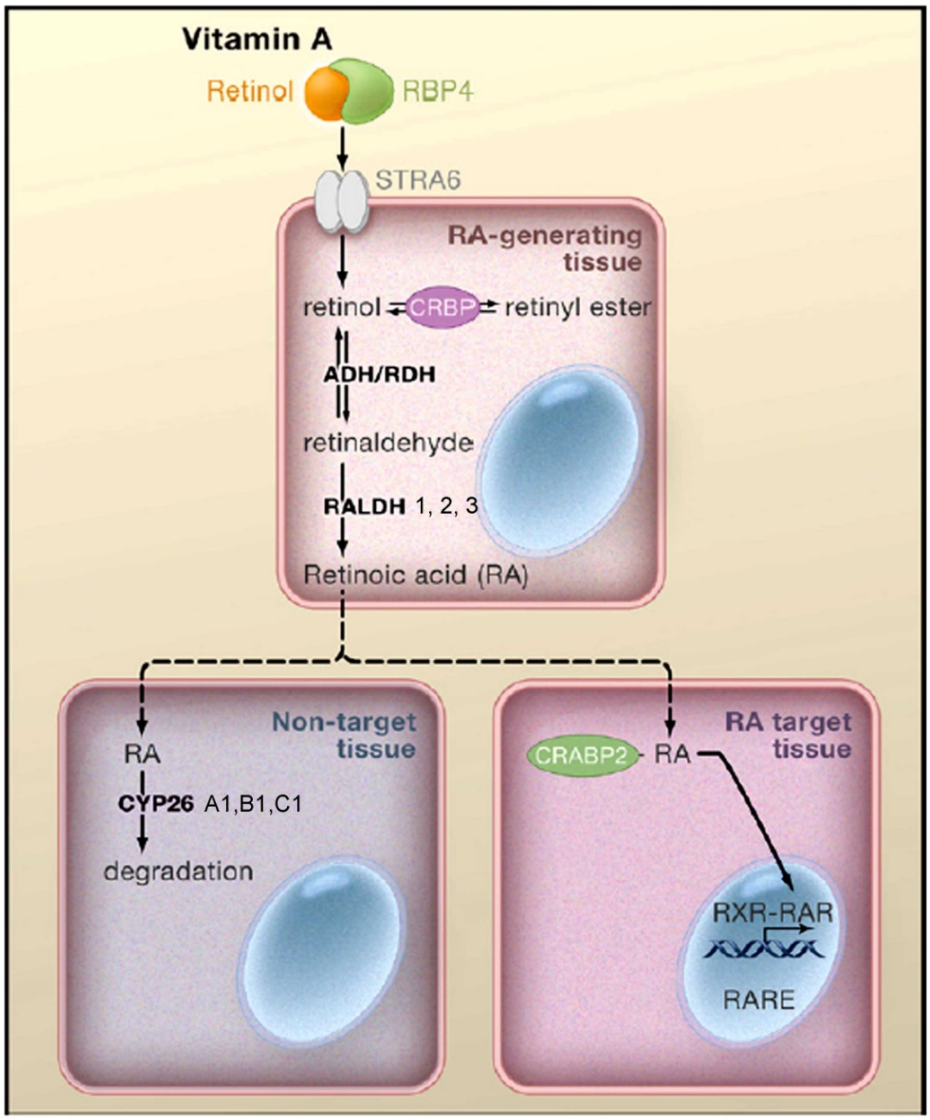
Vitamin A
Retinol
RBP4
STRA6
RA-generating tissue
retinol
CRBP
retinyl ester
ADH/RDH
retinaldehyde
RALDH 1, 2, 3
Retinoic acid (RA)
Non-target tissue
RA
CYP26 A1,B1,C1
degradation
RA target tissue
CRABP2
RA
RXR-RAR
RARE

Figure 1.3. Clinical presentation of microphthalmia, anophthalmia and coloboma (MAC). (**A**) Female child with severe left microphthalmia and normal right eye. (**B**) A male child with left microphthalmia. (**C**) Newborn with bilateral clinical anophthalmia. (**D**) Anterior eye photograph shows a nasoinferior pupillary notch, or iris coloboma (arrowhead). (**E**) Fundus photography of individual presenting with iris coloboma reveals coloboma (col) extension into the retina and optic nerve head (onh) consistent with a patent choroid fissure. Scleral tissue becomes visible due to missing ventral retina. Eye fundus image of an unaffected eye (**F**). Patient images A – C adapted from (Bakrania et al., 2007; Prasad et al., 2009; Ragge et al., 2007). Panel D adapted from http://www.nei.nih.gov/eyeonnei/insight/archive/0110.asp. Panels E - F adapted from http://webeye.ophth.uiowa.edu/eyeforum/cases/53-retina-choroidal-coloboma-visual-field.htm.

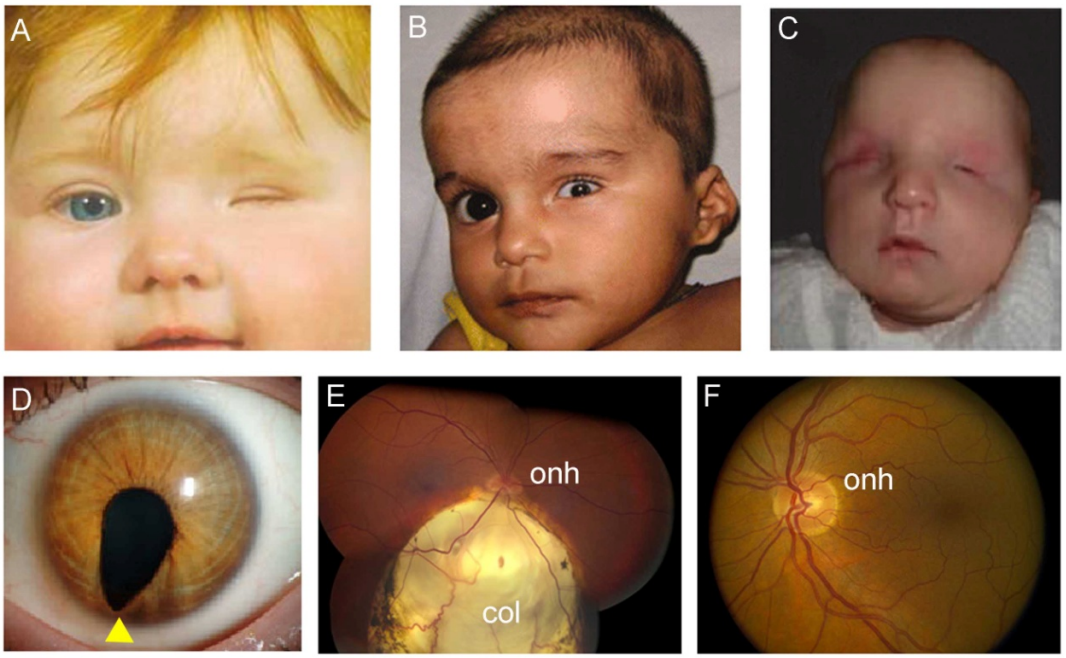
A
B
C
D
E
onh
col
F
onh

Figure 1.4. SOX phylogeny and SRY male sex determination. (**A**) Unrooted phylogenetic tree for all vertebrate and invertebrate (underlined) SOX HMG DNA binding domain protein sequences. Branch lengths denote extent of divergence. Ten classes of SOX genes are denoted by color and representative member is shown for orthologous mammalian groups. Inset, enlarged group B1 and B2 SOX members. dr, *Drosophila melanogaster* (fruit fly); ce, *Caenorhabditis elegans* (worm); se, *Strongylocentrotus purpuratus* (sea urchin); zf, *Danio rerio* (zebrafish); tr, *Oncorhynchus mykiss* (rainbow trout), xe, *Xenopus laevis* (frog); ch, *Gallus gallus* (chicken); pi, *Sus scrofa* (pig); mo, *Mus musculus* (mouse); tw, *Macropus eugenii* (tamar wallaby); or, *Pongo pygmaeus* (orangutan); hu, *Homo sapiens* (human). Image adadpted from (Bowles et al., 2000). (**B**) Male sex determination by Sry in the XY gonad. Sf1 binds to sites (green) in TES (testis specific enhancer of Sox9) through its zinc-finger binding domain and sensitizes Sox9 transcription in the genital ridge. Sry is transiently expressed and binds to HMG binding motifs (yellow). Synergistic action between Sry and Sf1 significantly upregulates Sox9 expression (orange). Sox9 maintains its own expression independent of Sry and drives testis differentiation. Image adapted and modified from (Sekido and Lovell-Badge, 2009).

A

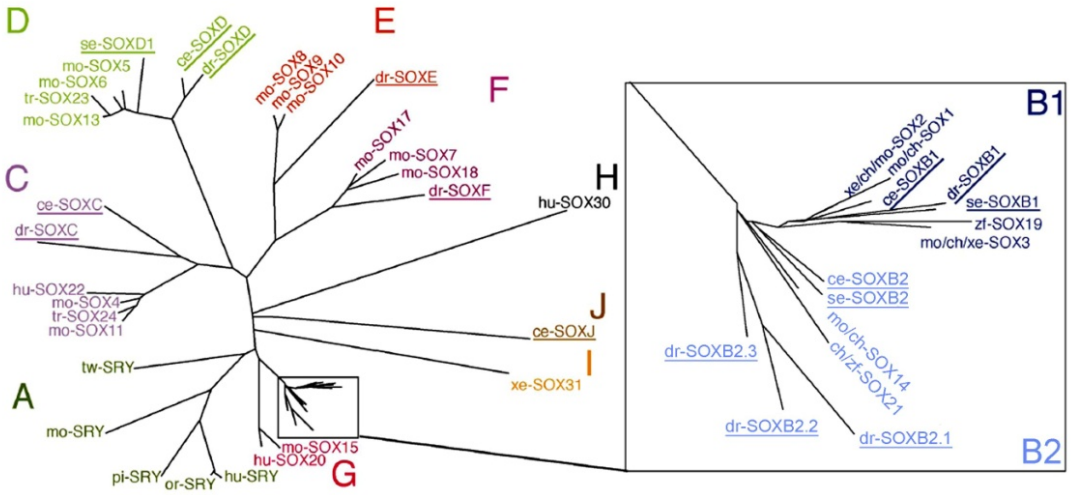
D
se-SOXD1
ce-SOXD
dr-SOXD
mo-SOX5
mo-SOX6
tr-SOX23
mo-SOX13
E
mo-SOX8
mo-SOX9
mo-SOX10
dr-SOXE
F
mo-SOX17
mo-SOX7
mo-SOX18
dr-SOXF
C
ce-SOXC
dr-SOXC
hu-SOX22
mo-SOX4
tr-SOX24
mo-SOX11
H
hu-SOX30
J
ce-SOXJ
I
xe-SOX31
tw-SRY
A
mo-SRY
mo-SOX15
hu-SOX20
pi-SRY
or-SRY
hu-SRY
G
B1
xe/ch/mo-SOX2
mo/ch-SOX1
ce-SOXB1
dr-SOXB1
se-SOXB1
zf-SOX19
mo/ch/xe-SOX3
ce-SOXB2
se-SOXB2
mo/ch-SOX14
ch/zf-SOX21
dr-SOXB2.3
dr-SOXB2.2
dr-SOXB2.1
B2

B

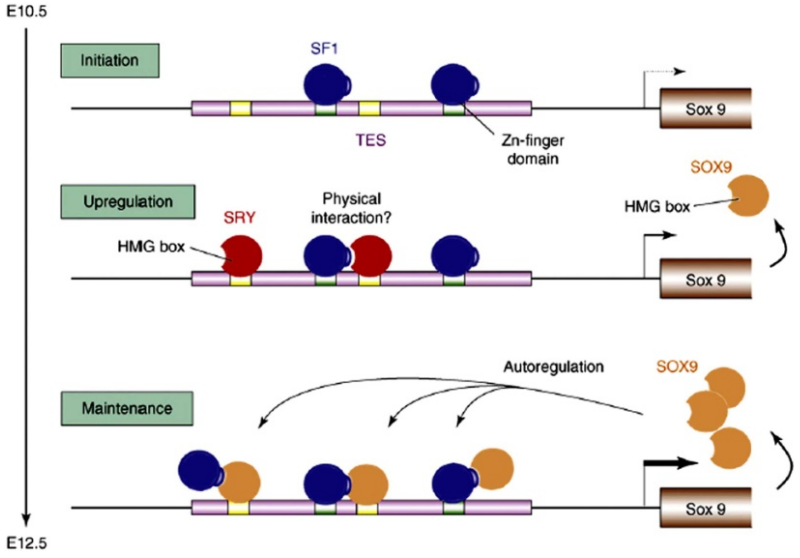
E10.5
Initiation
SF1
Sox 9
TES
Zn-finger
domain
Upregulation
SRY
Physical
interaction?
SOX9
HMG box
HMG box
Sox 9
Autoregulation
SOX9
Maintenance
Sox 9
E12.5

CHAPTER II

DOMINANT-NEGATIVE *RBP4* MUTATIONS CAUSE CONGENITAL EYE MALFORMATIONS THROUGH A MATERNAL-FETAL NUTRITIONAL INTERACTION

Vitamin A (retinol) is an essential nutrient important for early eye morphogenesis. Gestational vitamin A deficiency poses a serious risk factor for ocular malformations and congenital blindness. Through genetic mapping, we have identified two novel missense mutations in *RBP4* (p.A73T and p.A75T) in three unrelated families showing autosomal dominant transmission of microphthalmia, anophthalmia and coloboma (MAC). MAC in these families exhibits low penetrance and a significant maternal parent-of-origin effect. In one of the three families, two blind males also present with severe neurological deficits (epilepsy, motor retardation and autistic features). *RBP4* encodes plasma retinol binding protein, a circulating cargo protein responsible for mobilization of liver vitamin A stores and overall retinoid homeostasis. Our study demonstrates both *RBP4* mutant alleles encode dominant-negative forms that structurally and functionally resemble wild-type protein except they bind retinol poorly. Despite this, both mutant forms retain high-affinity STRA6 receptor binding. This mimicry effect generates sequential vitamin A “bottlenecks” at sites of STRA6 expression occurring first at the maternal-fetal interface and then again in the fetal eye. Consequently, vitamin A delivery to the fetal eye through the RBP system may be compromised leading to structural eye defects. Thus, we define a novel disease mechanism involving a plasma cargo protein and discuss the potential impact of dietary vitamin A on disease penetrance and the maternal origin effect. This study provides novel insights into congenital diseases governed by maternal-fetal and gene-environment interactions.

CONTRIBUTIONS

Chapter II will be submitted for publication as:

Chou CM, Tarle S, Pribila J, Bardakjian T, Schneider A, Nelson C, Glaser T. Dominant-negative *RBP4* mutations cause congenital eye malformations through a maternal-fetal nutritional interaction.

The clinical studies in this chapter were performed by Christine Nelson, MD and Jonathan Pribila, MD (Family 1). Clinical data from Families 2 and 3 were collected by Adele Schneider, MD and Tanya Bardakjian MS GC. Processing of DNA samples including transformation and culturing of Epstein-Barr Virus (EBV) transformed peripheral blood lymphocytes and a subset of SSLP genotyping and analysis were performed by Sue Tarle. Mass spectrometry (RBP trypsinization and MALDI-TOF) was performed by Dr. Phil Gafken, PhD and Lisa Jones. RBP molecular modeling was done by Dr. Paul Kirchhoff, PhD. All clinical diagnostic tests, except plasma RBP, were performed by University of Michigan Hospitals (Ann Arbor, MI). Retinol binding protein tests were performed by Quest Laboratories (San Juan Capistrano, CA).

INTRODUCTION

Human eye development initiates between the 3rd and 6th week of gestation. Originally described by Spemann (Spemann, 1924), this begins with a single eye field in the anterior neural plate during late gastrulation. From this, the optic vesicles expand outward to make contact with the overlying surface ectoderm. Through a series of reciprocal inductions, the optic vesicles invaginate to form two bilayered optic cups (Graw, 2010). The inner and outer layers represent the future retina and retinal pigment epithelium, respectively. The iris and ciliary bodies develop from the optic cup margins and the lens from the surface ectoderm. As a whole, the optic cup is incomplete along its entire inferior aspect at the so-called optic (choroid) fissure. This embryonic structure fuses beginning from its base at the forebrain wall and terminates at the iris. Finally, the surrounding periocular mesenchyme, a mix of mesoderm and neural crest cells, helps to pattern the eye and contributes to formation of anterior and auxiliary structures including the cornea, iris and extraocular muscles (Davis-Silberman and Ashery-Padan, 2008; Gage et al., 2005). Disruption of early eye patterning leads to structural defects of the globe.

Congenital microphthalmia, anophthalmia and coloboma (MAC) is a spectrum of eye diseases that affects 1 in 10,000 live births (Morrison et al., 2002). Anophthalmia is defined as the absence of the eye globes. Microphthalmia is a milder form of MAC characterized by small eyes. Coloboma is a ventral pupillary defect caused by incomplete fusion of the choroid fissure, possibly affecting the retina and optic nerve. Disease severity is a reflection of timing with earlier disruptions producing more severe phenotypes. One or both eyes may be involved and vision loss is total in anophthalmia

but may be spared in milder forms. Most cases occur in isolation but approximately one-third manifest as a component of a syndrome (Morrison et al., 2002). A number of genetic causes of MAC have been identified such as loss-of-function *SOX2* mutations that account for approximately 10% of all known MAC cases (Fantes et al., 2003). Other monogenic forms exist due to inactivating mutations in *RX* and *CHX10* (Ferda Percin et al., 2000; Voronina et al., 2004), *BCOR* in Oculofaciocardiodental syndrome and Lenz microphthalmia (Ng et al., 2004), *HCCS* in Microphthalmia with Linear Skin defects syndrome (Prakash et al., 2002), and in rare cases *PAX6* (Glaser et al., 1994). Several signaling pathways in the developing eye may also be disrupted such as TGFβ signaling factors *BMP4* and *GDF6* and Sonic hedgehog *SHH* (Asai-Coakwell et al., 2007; Reis et al., 2011). Environmental factors such as infectious diseases and toxin exposure have been investigated as well. In particular, poor maternal nutrition has been implicated as a major risk factor for congenital eye abnormalities (Hornby et al., 2000).

Vitamin A is an essential nutrient that is indispensible for survival and must be consumed through diet. Its most widely recognized function is maintenance of the visual cycle by use of 11-*cis*-retinal (vitamin A aldehyde form) to generate rhodopsin, a light sensitive visual pigment (Wald, 1968). Consequently, vitamin A deficiency (VAD) first manifests as night blindness, a reversible disease of visual adaptation to dark environments (Dowling and Wald, 1958). Apart from vision, vitamin A is also essential for epithelial, reproductive and immune health (Sporn et al., 1994). Nutritional studies have implicated maternal vitamin A deficiency in the generation of newborn eye malformations along with urogenital, diaphragmatic, cardiovascular and pulmonary defects, or so-called VAD syndrome (Hale, 1935; Wilson et al., 1953). More recently,

the molecular role of vitamin A in retinoic acid signaling has been well characterized. Vitamin A is mobilized from the liver but because of its lipophilic nature it must be transported in blood by retinol binding protein (RBP) (Kanai et al., 1968). At the target cell, RBP binds the transmembrane receptor STRA6 and delivers retinol into the cell (Kawaguchi et al., 2007). Within the cytoplasm, retinol undergoes two oxidation reactions catalyzed first by retinol dehydrogenase to form retinal, then by retinal dehydrogenase to synthesize retinoic acid. This potent signaling molecule is active throughout embryogenesis and is required for normal development. Recently, the first genetic links between human retinoid metabolism and MAC were established. Loss-of-function mutations in *STRA6* lead to autosomal recessive non-syndromic MAC or Matthew-Wood syndrome (OMIM 601186) characterized by structural eye defects, diaphragmatic hernia, cardiac malformations, and pulmonary hypoplasia/aplasia (Golzio et al., 2007; Pasutto et al., 2007). In comparison, inactivating mutations in *RBP4*, which encodes RBP, lead to a much milder phenotype in autosomal recessive night blindness with coloboma (Biesalski et al., 1999).

Here we identify a set of hereditary defects in *RBP4* which disrupt vitamin A transport and lead to severe structural eye defects. These mutations are dominant with a maternal parent-of-origin effect, but are weakly penetrant. We present evidence that the encoded gene products structurally and functionally mimic wild-type RBP, but fail to bind vitamin A. Furthermore, we show these defective proteins retain high affinity binding for the STRA6 receptor, which out-compete wild-type RBP, and potentially reduces vitamin A delivery across tissues. This molecular mechanism exposes a maternal-fetal nutritional interaction with increased vulnerability to vitamin A deficiency

and consequently newborn eye malformations. Previous biochemical and nutritional studies indicate penetrance of structural eye defects can vary depending on the amount and type of maternal vitamin A consumption. Our findings have broad implications in the etiology of other congenital diseases experienced through gene-environment interactions.

RESULTS

Autosomal dominant MAC with reduced penetrance and maternal-origin-effect

A large seven-generation pedigree (Family 1), was identified through second cousin probands with anophthalmia (Figure 2.1A). Extensive genealogical records document a family history of congenital eye disease dating back to the early 19th century, with an autosomal dominant inheritance pattern. The overall penetrance of the disease trait is relatively low (P = 0.4), based on 54 informative meioses (Figure 2.S1). The phenotypes of mutation carriers range from normal (VI-3, VI-7) to uni- or bilateral microphthalmia (small eyes) to complete absence of both eye globes (Figure 2.1B and Table 2.1). In addition, several individuals have ventronasal colobomas, notch-like defects of the iris and/or retina, arising from incomplete closure of the embryonic choroid fissure (Onwochei et al., 2000). There is a marked skewing in the Mendelian transmission pattern, suggesting a parent-of-origin effect. Nearly all affected individuals (10 of 11) inherited the trait from their mothers, such that maternal penetrance is seven-fold greater than paternal penetrance (P_{mat} = 0.7, P_{pat} = 0.1) (Figure 2.S1B). There is a single instance of paternal disease transmission, in a monozygous twin pregnancy

where only one twin (VI-2) was affected. The discordant twins highlight the contribution of genetic and non-genetic factors in this disease.

A new autosomal dominant MAC locus on chromosome 10q23

As a first step to map the disease mutation, we excluded 30 gene loci previously associated with MAC in humans or animal models (Table 2.3) by comparing haplotypes of the two probands. We then examined and collected DNA samples from all available family members, and performed genome-wide multipoint linkage analysis (Figure 2.S1C,D). We initially applied a simple autosomal dominant (AD) model, scoring only affecteds and obligate carriers. This analysis suggested three candidate regions 1q41, 10q23 and 19p13, with peak LOD scores >2 (Figure 2.1C). To distinguish between regions, we included unaffected, at-risk family members and applied AD models with uniform (P_{global} = 0.4) or sex-specific (P_{mat} = 0.7, P_{pat} = 0.1) reduced penetrance. This analysis indicated a chromosome 10q23 localization with a peak LOD score of 3.01 (Figure 2.1C). The 10q23 nonrecombinant interval spans 8.2 Mb and contains 81 genes (Figure 2.S2). Given the general importance of vitamin A in vertebrate eye development (Warkany and Schraffenberger, 1946), we tested three genes in the 10q23 interval: *RBP4*, *CYP26A1* and *CYP26C1* all of which have roles in vitamin A transport and retinoic acid metabolism.

Dominant *RBP4* mutations found in three independent MAC families

RBP4, or retinol binding protein 4, is a six-exon gene spanning 9.4 kb of genomic DNA (Figure 2.2A). We screened proband DNA exon-by-exon and discovered a novel

missense mutation (c.223G>A, p.A75T) that co-segregates with disease (Figure 2.2B, left panel). This mutation is not found in over 5,358 normal controls distributed among various public databases (dbSNP135, 1000 Genomes, HapMap, Exome Variant Server) nor in 307 neurologically normal controls we screened by PCR (data not shown). In total, 11,330 control chromosomes were examined.

We sought to verify if mutations in *RBP4* are overrepresented in the MAC population. Therefore we investigated a cohort of 75 additional unrelated MAC trios. We identified two additional probands, one male with bilateral anophthalmia (Family 2) and one female with left microphthalmia and coloboma (Family 2.2). Both affecteds share a novel identical missense mutation (c.217G>A, p.A73T), but haplotype analysis revealed two distinct haplotypes indicating a recurrent mutation (Figure 2.S3). Much like in Family 1, both p.A73T probands inherited the mutation from their mothers (Figure 2.2B, center and right panels). The Family 2 proband has a second nephew (IV-1) on the maternal side with severe microphthalmia who in turn has an obligate carrier mother (III-7). As in Family 1, the obligate carrier male II-3 in Family 2 did not have any affected children. In Family 3, the mother (II-2) has a unilateral optic disc pit. These observations extend what is seen in Family 1 and bring the total maternal disease transmission count to 13 versus only one inherited paternally.

RBP4 **p.A73T and p.A75T alter amino acid residues critical for retinol binding**

RBP4 encodes plasma retinol binding protein (RBP), a lipocalin superfamily shuttle protein for mobilizing the all-*trans*-retinol (ROH) from the liver to target tissues such as the eye, skin and placenta (D'Ambrosio et al., 2011). The domains and crystal structure

of this protein are known (Figure 2.2D and 2.S4) (Cowan et al., 1993; Zanotti et al., 1993). Both missense mutations involve alanine-to-threonine substitutions at codons 55 (A55T) or 57 (A57T) in β-strand C of the mature RBP polypeptide (codons 73 and 75 in the primary translation product prior to signal sequence cleavage; Figure 2.2C) (Soprano et al., 1981). Phylogenetic comparison of RBP across vertebrates shows complete conservation suggesting a critical role for these two residues (Figure 2.2E). X-ray crystallographic studies demonstrate that wild-type A55 and A57 form stabilizing hydrophobic interactions with C4 and C3 of the retinol β-ionone ring, respectively (Figure 2.S4) (Cowan et al., 1990). There also exists two previously reported *RBP4* mutations p.G93D and p.I59N (G75D and I41N in the mature sequence) in two compound heterozygous sisters with autosomal recessive night blindness (Biesalski et al., 1999). I41 and G75 are located in β-strands B and D, respectively (Figure 2.2D), and both interact with β-ionone ring side groups (Cowan et al., 1990). Biochemical studies show RBP G75D and I41N bind retinol poorly (Folli et al., 2005). Based on molecular modeling, A55T and A57T are both able to accommodate retinol; however, there is increased strain due to steric and hydrophilic effects introduced by the threonine side chain (Figure 2.S4B).

RBP A55T and A57T are secreted as stable 21 kD monomers

If A55T and A57T are pathogenic, we sought to understand how they differed from both recessive forms. To further investigate, we compared molecular properties of wild-type and all dominant and recessive mutants at multiple points along the RBP lifecycle. RBP is constitutively expressed in liver cells, binds retinol and is secreted as holo-RBP (Muto

et al., 1972; Peterson et al., 1973; Soprano et al., 1982; Soprano et al., 1986b). To test the secretion properties of wild-type, A55T, A57T, G75D and I41N RBP mutant proteins, we employed an *in vivo* cell-culture system based on a previous study (Melhus et al., 1992) (Figure 2.3A). An N-terminus hemagglutin epitope tag (RBP^{HA}) was added to each form for tracking purposes. As a retention control, we used wild-type with KDEL appended to the C-terminus (Munro and Pelham, 1987). Looking at 48 hr conditioned media (CM), we found both threonine forms were present at equal steady-state levels compared to wild-type and migrated at the expected size of 21 kD (Figure 2.3B). This agrees with a timecourse study of ^{35}S metabolically-labeled RBP in CM from 0 – 18 hr post-transfection showing equivalent accumulation levels of wild-type RBP as well as A55T and A57T mutant forms (data not shown). However, we noticed RBP G75D and I41N consistently appeared less abundant than wild-type protein. To probe further, we ran samples under non-denaturing conditions and discovered G75D and I41N forms are secreted primarily as 42 kD homodimers linked by inter-molecular disulfide bonds (Figure 2.3B and Figure 2.S5). We confirmed this finding by cross-linking CM prior to denaturing electrophoresis (Figure 2.3B). This result suggests that RBP G75D and I41N are highly unstable in the monomeric form. Next, we examined intracellular RBP levels and found equivalent protein amounts for wild-type, A55T and A57T as expected (Figure 2.3C). On the other hand, we typically observed slightly elevated levels for G75D and even higher retention for I41N indicating a possible secretion defect. This is consistent with non-immunodetectable plasma RBP in both p.G93D;p.I59N compound heterozygous sisters (Biesalski et al., 1999). In all cases, we do not detect the unfolded protein response (UPR) that would indicate ER stress (Figure 2.S4B), nor is there

evidence of cellular localization defects (data not shown). Altogether, our results show RBP A55T and A57T are secreted as stable 21 kD monomers whereas G75D and I41N show aberrant homodimerization associated with increased cellular retention.

Our studies predict that p.A73T/+ and p.A75T/+ heterozygous individuals should exhibit normal circulating RBP levels. We tested this prediction in three p.A75T/+ obligate carriers (Family 1: VI-2, VI-3 and VI-7) and found all to be within normal limits (Table 2.2). Thus, it appears that neither threonine substitution leads to significant reductions in circulating plasma RBP which is consistent with the secretion data. In sharp contrast, RBP G75D or I41N are undetectable in circulation, possibly due to increased cellular retention and atypical homodimerization.

RBP A55T and A57T complex normally with transthyretin

Transthyretin (TTR) is a 55 kD homotetrameric liver-secreted protein that directly interacts with holo-RBP in a 1-to-1 molar ratio (Heller and Horwitz, 1974), thus creating a circulating 76 kD macromolecular complex (Kanai et al., 1968). This complex prevents RBP from undergoing kidney filtration, allowing it to remain in circulation for vitamin A delivery to target tissues (Soprano, 1994). To examine whether RBP A55T, A57T, G75D and I41N can partner with TTR, we used a co-immunoprecipitation assay combining RBP^{HA} and wild-type human transthyretin (Figure 2.3D) (Melhus et al., 1991). Our results show that after HA normalization, TTR interacts equally well with RBP wild-type, A55T and A57T but not G75D or I41N (Figure 2.3E). This holds true even after adjusting for amount of TTR bound per mole of RBP (i.e. to fairly compare monomeric versus homodimeric forms). We also observe human wild-type RBP and bovine TTR

interaction (Figure 2.3E). This is expected given that both evolutionary conserved proteins show cross-species interchangeability with one another (Berni et al., 1992; Kopelman et al., 1976). Our results indicate that RBP A55T and A57T mutants can form TTR-RBP complexes, but G75D and I41N cannot. Despite this partnership, TTR secretion does not depend on vitamin A status (Navab et al., 1977) nor does RBP secretion depend on TTR (van Bennekum et al., 2001), therefore both are subject to independent regulatory mechanisms. In agreement with this, we observe no TTR deficiency in the serum of three p.A75T/+ obligate carrier females (Table 2.2). Normal circulating TTR levels are also observed for p.I59N and p.I59N/p.G93D heterozygous individuals (Biesalski et al., 1999).

Mass spectrometry of p.A75T/+ carrier serum identifies wild-type and A57T forms

Thus far, our experimental data suggests RBP A55T and A57T should be present in the circulation at an equal fraction to wild-type. To test this, we purified RBP A57T from serum of an obligate carrier (VI-2, Figure 2.S6) and performed mass spectrometry to measure relative quantities of RBP wild-type versus A57T. We included purified HA-recombinant RBP wild-type, A57T and 1:1 pre-mixed controls. The predicted size difference between tryptic peptides encompassing amino acid position 57 is 30 Da (m/z = 3,170 for A57T and 3,140 for wild-type; Figure 2.4A). Of the resulting MALDI-TOF mass spectrum (Figure 2.4B), we identified m/z peaks in the 3,100 to 3,220 range corresponding to both wild-type and A57T in a 2-to-1 ratio, respectively (Figure 2.4C). Peptide sequencing confirms analysis of the correct targets (data not shown). Based on controls, the observed m/z peaks are specific to RBP and the different relative

intensities are not due to differences in ionization potentials (Figure 2.4C). This result demonstrates A57T constitutes approximately one-third of all circulating RBP in p.A75T/+ carriers.

To determine the underlying reason(s) for the asymmetric ratio of A57T-to-WT RBP we first tested for imprinting at the *Rbp4* locus. We performed RNA analysis in a F1 cross of two divergent inbred mouse strains (DBA/2J x C57BL/6) with several expressed single nucleotide polymorphisms within the 3' UTR of the *Rbp4* mRNA transcript. We examined F1 adult liver and E14.5 embryonic liver, placenta and whole embryo (minus liver) and found bi-allelic expression in all tissues (Figure 2.S5). Ruling out imprinting, we next hypothesized possible unequal rates of kidney filtration secondary to an as-yet unknown cause. In such a case, we would expect to see an inverted urine ratio (i.e. 1-to-2 WT-to-mutant). Thus, we quantified relative levels of purified urine RBP using the same mass spectrometry protocol (Figure 2.S7A-C). However, we again found the ratio to be at least 2-to-1 WT-to-mutant, mirroring the serum RBP ratio (Figure 2.S7D). This result indicates no difference in glomerular filtration rate and urine output of wild-type and A57T mutant RBP.

RBP A55T and A57T bind retinol poorly

Given the strong link between vitamin A deficiency and congenital eye defects, it is essential to establish whether the two threonine-substituted RBP forms are capable of binding retinol. To this end, we developed two independent vitamin A binding assays. First, we metabolically labeled HeLa cells expressing wild-type or mutant RBP with ^{35}S methionine and cysteine (Figure 2.5A). RBP G75D and I41N were included as negative

controls (Folli et al., 2005). We then exposed cells to ^{3}H all-*trans*-retinol and allowed binding to occur for 1.5 hr. After ^{35}S-RBP^{HA} HA immunopurification, we compared ^{3}H/^{35}S normalized ratios. Our results show that RBP A55T had negligible retinol binding whereas A57T retained roughly 16% of wild-type levels (Figure 2.5B). Our result indicates position 57 can better tolerate structural and chemical modifications than position 55. This is consistent with X-ray crystallographic data that places the A57 single methyl R-group at a distance of 4Å from C3 of retinol (Cowan et al., 1990). The A55 R-group resides only 3.7Å and 3.6Å from C3 and C4, respectively. As a second independent measure of vitamin A binding, we chose to exploit the up to 15-fold increase in fluorescence intensity exhibited by retinol when bound as holo-RBP versus alone in solution (Goodman and Leslie, 1972). Using purified recombinant RBP^{HA}, we measured fluorescence emission intensity (excitation 330 nm, emission 460 nm) using various retinol concentrations from 1 – 5,000 nM in PBS alone (Figure 2.5C). We also included blanking controls containing no RBP and no retinol. Our results led to two critical observations. First, both RBP A55T and A57T accommodate retinol well under ideal (saline only) conditions as predicted by our molecular modeling study. Furthermore, relative fluorescence intensities of both forms are consistent with the metabolic double-labeling experiment. Second, RBP A57T and wild-type binding curves are essentially identical. Faced with this discrepancy, we recalled previous studies demonstrating the holo-WT complex exhibits remarkable stability in the face of environmental stressors including extreme non-physiologic temperatures, pH conditions and apolar solutions (Cogan et al., 1976; Raz et al., 1970). Hypothesizing that both threonine substitutions may weaken overall retinol binding, we subjected RBP-ROH

complexes to increasingly apolar or amphipathic environments using ethanol and Triton X-100, respectively (Figure 2.5D and E). Indeed, both treatments unmasked inherent binding deficiencies in RBP A55T and A57T as measured by relative fluorescence. These data indicate exposure to hydrophobic agents exploits inherent weaknesses in retinol binding due to the threonine substitution.

Our retinol binding data combined with the presence of RBP A57T in serum together predict that p.A73T/+ and p.A75T/+ heterozygous carriers should exhibit reduced circulating retinol levels. We tested total fasting serum retinol levels in the same three p.A75T/+ carriers as before (p.A73T/+ carriers were unavailable for testing), and found all three to have fasting levels below the lower normal limit (Table 2.2). Individuals VI-2 and VI-3 each had roughly 50% average levels, which is in general agreement with the fraction of mutant RBP in p.A75T/+ carrier serum. On the other hand, VI-7 was just below normal, which is likely attributable to her daily vitamin A supplementation at the time of testing. As a second independent measure, when we purified serum RBP from individual VI-2, we noticed approximately 50% fluorescence intensity decrease compared to control after total protein normalization. Altogether, our study highlights *RBP4* p.A73T and p.A75T as an allelic series, each with significantly reduced retinol binding capacity with the former being most severe. The overall reduction in retinol binding in our experiments correlates with lowered *in vivo* circulating retinol levels in p.A75T/+ carriers.

RBP A55T and A57T bind STRA6 at higher steady-state levels than wild-type

STRA6, or stimulated by retinoic acid 6 (Bouillet et al., 1997), is the first-identified RBP receptor that mediates cellular uptake of vitamin A (Kawaguchi et al., 2007). Its importance in cellular retinoid processing is illustrated by patients with homozygous inactivating *STRA6* mutations born with microphthalmia or anophthalmia (Casey et al., 2011; Chassaing et al., 2009; Golzio et al., 2007; Pasutto et al., 2007). In addition, affected individuals may also have congenital heart defects, diaphragmatic hernia and pulmonary hypoplasia/aplasia, features consistent with VAD syndrome. At target tissue membranes, STRA6 binds holo-RBP with high affinity (Kawaguchi et al., 2007). Upon translocation of vitamin A into the cell, apo-RBP dissociates allowing the next holo-RBP molecule to bind the unoccupied receptor. To examine RBP A55T and A57T binding strength, we employed a modified cell-culture system based on a previously described protocol (Kawaguchi and Sun, 2010). We generated ^{35}S-labeled apo-WT, holo-WT, A55T and A57T RBP and applied equivalent amounts to HEK293T cells expressing STRA6^{myc} or control (Figure 2.6A). We confirmed expression and cell surface localization of STRA6^{myc} by anti-Stra6 Western blot and myc immunocytofluorescence (Figure 2.6B). After one hour, we measured steady-state binding by radioactive counts. After correcting for background, we discovered RBP A57T and A55T bound with 4- and 7-fold higher levels than holo-WT, respectively (Figure 2.6C). Consistent with its diminished role upon vitamin A delivery, apo-WT showed lowered steady-state binding levels compared to holo-WT. Given the heterozygous state of affected individuals in all three families, we investigated the effects of adding “cold” unlabeled holo-WT competitor with each ^{35}S RBP^{HA} form. By adding increasing molar amounts of competitor (5X and 150X molar ratio), we observed a similar displacement for RBP

A57T and holo-WT (Figure 2.6C). Conversely, twice as much relative A55T remained bound at this intermediate level of competitor. As expected, at higher molar amounts of cold RBP, we observe near complete dissociation of all ^{35}S-labeled forms. Our results reveal that both RBP A57T and A55T have strong STRA6 receptor affinity despite poor ligand binding.

DISCUSSION

In this study, we identify two hereditary defects in human *RBP4* that cause autosomal dominant MAC with low penetrance and a maternal parent-of-origin effect. At the molecular level, this disease arises from dominant-negative forms of RBP that structurally and functionally mimic holo-WT RBP, except for a paradoxical combination of poor retinol binding and higher apparent STRA6 receptor affinity. To our knowledge, this is the first example of a blood cargo protein with this unique property that underlies a human disease. Our overall conclusion is supported by multiple independent observations: 1) it is the most parsimonious interpretation of our *in vivo* functional results, mass spectrometry and clinical diagnostic testing in conjunction with previously known data, 2) linkage mapping in a large family favors 10q23 by at least 11-times more than other candidate regions, 3) *RBP4* mutations are overrepresented in the MAC population and are absent in controls, 4) RBP is involved in vitamin A transport and specific ablation of the RBP pathway predisposes to structural eye defects (Quadro et al., 2005), further reinforcing the link between VAD and congenital eye malformations, and 5) the parent-of-origin effect is explained by deficient maternal-fetal exchange of

vitamin A at the visceral yolk sac and placenta, two sites of STRA6 and RBP expression (Johansson et al., 1999; Sapin et al., 1997; Soprano et al., 1986a) .

A unified molecular and physiologic disease model

Based on the unique molecular properties of RBP A55T and A57T, we hypothesize a novel dominant-negative disease mechanism (Figure. 2.7A). In heterozygous carriers, both *RBP4* alleles are expressed in the liver and co-localize to the endoplasmic reticulum (Rask et al., 1983; Smith et al., 1998). There they co-exist as apo-WT and a structural mimic of holo-WT (i.e. mutant). Only apo-WT is able to bind vitamin A. Regardless, both forms partner with TTR and are secreted into circulation as stable pentameric complexes. At target cell membranes, both RBP mutants bind STRA6. Holo-WT rapidly delivers vitamin A and promptly dissociates. However, mutant RBP binding persists because of altered RBP-STRA6 structural properties. At steady-state levels, more STRA6 receptors are occupied by mutant RBP than are available for holo-WT. This phenomenon results in a molecular “bottleneck” that prevents normal delivery of vitamin A.

At a physiologic level, the maternal parent-of-origin effect is a reflection of two sequential vitamin A “bottlenecks” at the maternal-fetal interface (i.e. yolk sac and mature placenta) and then at cells of the developing fetal eye (Figure 2.7B). In mammals, the yolk sac performs the earliest placental functions (when eye development begins) while the chorio-allantoic placenta develops. If a pregnant mother is a p.A73T/+ or p.A75T/+ carrier, she will co-express and secrete wild-type and mutant RBP from her liver. If she transmits the mutant *RBP4* allele to her fetus, a series of

potential vitamin A “bottlenecks” arise. The first occurs at the fetal-derived placental syncytiotrophoblast layer where maternal RBP first interacts with fetal STRA6 (Johansson et al., 1999). Maternal RBP does not cross into fetal circulation (Quadro et al., 2004b), indicating that retinol transfer from maternal to fetal RBP must occur. This most likely happens at the visceral endoderm of the yolk sac, a tissue known to synthesize RBP *de novo* in human, sheep, rat and mouse (Harney et al., 1994; Johansson et al., 1999; Liu et al., 1991; Sapin et al., 1997; Soprano et al., 1986a), and accumulate retinoids throughout rodent gestation (Johansson et al., 1997). Expression of components necessary for retinol uptake and RBP loading (STRA6, TTR and cellular retinol binding proteins CRBP-I or CRBP-II) have yet to be confirmed in first trimester human yolk sac tissue. Their presence is likely given many studies in non-human mammals demonstrate, in addition to RBP, yolk sac visceral endoderm also expresses STRA6, TTR, and cellular retinol binding proteins CRBP-I and CRBP-II (Bouillet et al., 1997; Johansson et al., 1997; Sapin et al., 2000a). In mouse, complete loss of CRBP-II, coupled with maternal vitamin A deficiency, leads to features consistent with VAD syndrome including eye defects (Xueping et al., 2002). Since the human yolk sac disappears one-third the way through pregnancy (unlike in rodents), its relative contribution to retinoid delivery over time may decline as the chorio-allantoic placenta matures by the second trimester. The final “bottleneck” occurs at fetal eye tissues where STRA6 is expressed (Bouillet et al., 1997) where fetal RBP interacts with fetal STRA6.

Given that all potential “bottleneck” sites are fetal-derived tissues may explain why disease risk is highest when both mother and fetus are carriers, as seen in all three families in Chapter II (13 of 14 cases). Notably, an individual from a twin-pregnancy

developed unilateral iris and chorioretinal coloboma (IV-2, Figure 2.1B) despite having a genotypically normal mother. This is likely explained by the presence of a twin which created a nutritional competition and global physiologic vitamin A deficiency *in utero*, producing a threshold effect in one twin but not the other. Twin pregnancies are considered high risk in part due to potential uneven nutrient distribution (e.g. twin-twin transfusion syndrome) (Lopriore et al., 2011). Indeed, the affected twin weighed less at birth than her unaffected sister (IV-3) (Table 2.S1). We predict that any entity capable of altering maternal retinoid levels in a carrier whose vitamin A status is already tenuous could amplify risk of eye abnormalities in offspring relative to non-carriers. Among all the potential genetic or environmental factors, dietary vitamin A status is paramount (Figure 2.7B), and adequate consumption is likely the major reason for low penetrance. Additional environmental factors may include infectious diseases and toxin exposure (Hornby et al., 2000) or liver disease (Smith and Goodman, 1971). This form of MAC highlights a gene-environment interaction centered on maternal and fetal *RBP4* genotypes and maternal vitamin A status during the first two months of pregnancy.

Structural basis for RBP molecular mimicry

RBP is the prototypical member of the ancient lipocalin protein family, which is part of the calycin superfamily. Lipocalins have been described in all branches of life including mammals, crustaceans, insects and bacteria (Flower, 1996). These small globular proteins function in transport of principally small hydrophobic molecules in processes such as nutrient transport, coloration, olfaction, pheromone transport, immune function and cell homeostasis (Grzyb et al., 2006). Lipocalins are subgrouped into kernel or

outlier classes by tertiary structure and the presence of one to three short conservative regions (SCRs) (Flower et al., 1993). The ligand binding portion, or calyx, is formed by a folded β-sheet comprised of six to eight antiparallel strands (A-H) with an open and closed end. At the open end is a loop scaffold that seals and protects the ligand, most notably the A-B loop. A C-terminal α-helix exists as well. Ligand selectivity is conferred by amino acid residues lining the binding pocket.

The paradoxical abolishment of RBP ligand binding with high affinity receptor binding argues strongly for a structural mimicry effect. Based on known crystal structures of human holo- and apo-WT RBP, the major structural difference is observed in the A-B loop defined by amino acids 34 through 37 (Cowan et al., 1990; Newcomer et al., 1984; Zanotti et al., 1993). In the holo form, F36 points toward the interior of the cavity but in the apo form, it folds out and is positioned in space previously occupied by the retinol hydroxyl group (Zanotti et al., 1993). Given the size and position deep within the cavity, it is unlikely the threonine side chain mimics retinol itself. Instead, the substitution likely produces an allosteric effect that stabilizes the critical A-B loop in the holo position. Molecular modeling suggests a network of hydrogen bonds anchored by the threonine hydroxyl group may mediate this stabilization (Figure 2.S4D). Moreover, this thermodynamically favorable state confers a more static nature to the altered protein reflected in all tested properties.

Under vitamin A sufficient conditions, ingested retinoids are taken up by hepatocytes and either stored as retinyl esters in hepatic stellate (Ito) cells (Blomhoff et al., 1982; Yamada et al., 1987) or re-directed to the hepatocyte ER for holo-RBP secretion (Muto et al., 1972; Sporn et al., 1994). Within individuals, RBP concentration

is highly regulated and remains constant except in certain disease states (Soprano, 1994). In chronic vitamin A deficiency, increased hepatic RBP accumulation leads to a decline in serum RBP (Muto et al., 1972), because RBP secretion depends on retinol binding (Marinari et al., 1987; Melhus et al., 1992; Muto et al., 1972; Smith et al., 1978). Therefore, the presence of RBP A57T at a significant fraction in carrier serum was quite surprising given poor ligand binding. We first considered the possibility of extrahepatic sources of RBP. Quantitative RNA studies of *de novo* extrahepatic synthesis estimate 10-20% contribution to overall circulating RBP-ROH (Soprano et al., 1986b). If true in humans, each *RBP4* allele expressed in non-liver tissues accounts for at most 10% of total serum RBP, far less than our measurement of ~33% (Figure 2.4). This rules out extrahepatic tissues as the primary source of circulating mutant RBP in p.A75T/+ carriers. How then does mutant RBP secrete from the liver despite impaired retinol binding? The simplest explanation is an allosteric effect that allows mutant RBP to bypass the vitamin A requirement by appearing as “holo-WT” on its external surface. This is bolstered by our data indicating no significant differences in gene transcription levels, secretion rates or gross tertiary structure alterations between mutant and wild-type forms. Thus, we favor a bypass model, and relative reduction of mutant RBP in circulation most likely stems from a post-secretion phenomenon.

It is known that holo-RBP exhibits approximately 5-fold greater TTR affinity than apo-RBP (Fex et al., 1979; Smith and Goodman, 1971). Furthermore, the A-B loop is a critical participant in the TTR-RBP docking interface, specifically L35 on holo-RBP (Monaco et al., 1995; Naylor and Newcomer, 1999; Sivaprasadarao and Findlay, 1994). In contrast, the position of the A-B loop in apo-RBP is not favorable for TTR-RBP

interaction (Heller and Horwitz, 1973). The equal steady-state levels of macromolecular complex suggest TTR is largely oblivious to the threonine substitutions deep inside the retinol binding pocket. The absence of overt mutant RBP urinary excretion further supports this notion. Preservation of the TTR-RBP docking interface requires proper holo configuration of multiple external loops (including A-B) but no direct involvement of binding pocket residues (Naylor and Newcomer, 1999). For this reason, we believe the nature of the TTR interaction is largely unaltered for both A55T and A57T forms.

Our data and previous studies indicate holo-RBP binds STRA6 with greater affinity than apo-RBP (Redondo et al., 2008). Upon release of retinol into the cell, it is unclear what additional molecular modifications on RBP, if any, drive its dissociation from STRA6. In other words, what accounts for increased A55T and A57T receptor binding? One possibility is that under normal circumstances, the A-B loop simply folds back into the apo position, signaling to the receptor that retinol has been unloaded. STRA6 would then confirm delivery based on feedback from cellular retinol binding protein (CRBP) and lecithin-retinol acyltransferase (LRAT) (Amengual et al., 2012; Kawaguchi et al., 2011) and undergo a final conformational shift that releases apo-RBP. However, if the A-B loop is fixed in the holo position, STRA6 may continuously attempt to “unlock” the RBP molecule without success, thus prolonging the interaction. A second possibility is that RBP docking allows the A-B loop to swing open and prime STRA6 for delivery. However, without vitamin A exchange, the receptor awaits but never receives necessary feedback signals from CRBP and LRAT to promote apo-RBP dissociation. Regardless of the true dissociation mechanism, our experimental observation may explain the asymmetric distribution of RBP forms in carrier blood. In the adult, STRA6 is

broadly expressed in multiple tissues including RPE, choroid plexus, brain meninges and capillaries, kidney, spleen, bronchus, testis and female genital tracts (Bouillet et al., 1997) providing ample target membranes for mutant RBP attachment.

At this time, we cannot rule out other major allosteric changes or altered ligand specificities for RBP A55T or A57T. Both changes are unlikely given all reported *RBP4* mutations to-date yield forms that accommodate retinol under ideal conditions suggesting relatively intact tertiary structures (our study and (Folli et al., 2005)). Also, changes in retinoid specificity are predicted to abolish TTR binding and promote glomerular filtration (Horwitz and Heller, 1973) thus arguing against a dominant phenotype. Nevertheless, X-ray crystallographic studies would prove highly insightful into the structural basis for mimicry. Both RBP A55T and A57T may represent novel separation-of-function mutants that uncouple vitamin A binding with secretion, TTR and STRA6 binding. In general, the mimicry effect parallels viral defective interfering particles that inhibit the replication of non-defective viruses in the same cell (Huang and Baltimore, 1970). Less strictly, this is similar to dominant mutations of cellular receptor proteins that encode constitutively active forms independent of ligand binding such as *FGFR3* mutations in achondroplasia (Webster and Donoghue, 1996).

RBP4 **mutations at the threshold of VAD syndrome**

Empirically, the eye is most frequently affected in VAD syndrome (Hale, 1935; Warkany and Schraffenberger, 1946; Wilson et al., 1953). In Family 1 (p.A75T/+), the disease appears to be restricted to the developing eye, suggesting vitamin A level drops below a critical threshold to produce ocular defects. The more severe p.A73T allele correlates

slightly with worsened eye and neurological phenotypes (Family 2). However, an affected child with the same genotype has only unilateral microphthalmia with no other findings (Family 3). This may reflect additional unknown genetic modifiers and/or variations in maternal vitamin A status during the respective pregnancies. Indeed, *Rbp4*-null mouse pups born from *Rbp4*-null dams are normal under vitamin A sufficient conditions (Quadro et al., 1999), but develop VAD syndrome features with insufficient maternal dietary retinoids (Quadro et al., 2005). Variations in maternal vitamin A status would predict graded developmental phenotypes and low penetrance as seen in this study. While this may lead to misdiagnosis of “sporadic” cases, affected individuals and carriers can be potentially easily screened for potential *RBP4* mutations through fasting retinol blood tests.

As with fetal development, VAD in adults first manifests in the eye beginning with night blindness and progresses to dry eye (xerophthalmia) with conjunctival Bitot’s spots (deposits of bacterial overgrowth and dead epithelial cells) (Sommer, 2008). If untreated, this can lead to corneal ulcerations, keratomalacia, permanent blindness and death from immune failure. The absence of any such signs among all known carriers in our study may at first seem paradoxical. However, this can be explained by two reasons: 1) the dominant-negative mechanism does not necessitate total vitamin A loss through the RBP pathway, and 2) all three families experience normal Western diets abundant in retinol, retinyl esters, and α/β-carotenoids. Intestinal enterocytes convert all forms into retinyl esters and package them into chylomicrons (Agadir et al., 1999; Huang and Goodman, 1965). A significant fraction of post-prandial chylomicron retinoids (25%) are directly taken up by extrahepatic tissues without RBP involvement

(Goodman et al., 1965). This allows *Rbp4*$^{-/-}$ mice maintained on vitamin A sufficient diets to develop normally and remain healthy and viable (Quadro et al., 1999). Furthermore, there may be additional retinoid stores (e.g. lung) that are activated via alternative pathways in the absence of circulating RBP-ROH (Quadro et al., 2004a). In humans, complete loss of *RBP4* in two compound heterozygous sisters on a normal eastern European diet suffer from mild night blindness with dermatologic issues, but no life-threatening complications (Biesalski et al., 1999). Their carrier mother shows 50% normal circulating RBP and retinol levels but is clinically normal. From these nutritional studies, it is clear the demand for vitamin A in embryonic and adult eye is highest, but under normal circumstances, supply far exceeds demand. Despite the fact that RBP-ROH accounts for 95-99% of total circulating retinoid in the fasting state (Soprano, 1994), these studies demonstrate the presence of alternative retinoid pathways that can significantly compensate for an impaired RBP delivery system. In this regard, retinyl ester supplementation may prove an effective prophylactic measure for female *RBP4* mutation carriers of child-bearing age.

Gene-environment interactions in maternal parent-of-origin diseases

The existence of hereditary defects in maternal vitamin A metabolism with predisposition to structural eye defects has been hypothesized (Hornby et al., 2003) but never verified. Based on our observations, dominant *RBP4* mutations may represent the missing link. This mechanism is distinct from other known maternal-specific developmental pathways including mitochondrial or ooplasmic RNA inheritance and imprinting. The maternal effect has been described classically in patients with

congenital heart disease (Burn et al., 1998; Connolly and Warnes, 1994; Nora and Nora, 1987) and pyloric stenosis (Dodge, 1970; Kidd and Spence, 1976; Krogh et al., 2010). However, due to the complexity of gene-environment interactions, no convincing disease mechanism has been put forth. One exception is a recent study on congenital scoliosis that identified transient gestational hypoxia as an environmental component leading to altered FGF signaling and disrupted somitogenesis (Sparrow et al., 2012). Likewise, our study adds a new dimension in the form of molecular mimicry that interferes with maternal-fetal nutrient transport, causing vitamin A deficiency at the cellular level and structural eye malformations. This gene-environment interaction mirrors mutations in *MTHFR,* folic acid deficiency and spina bifida (Rozen, 1996).

EXPERIMENTAL PROCEDURES

Clinical data

All human studies were approved by the University of Michigan (UM) and Albert Einstein Medical Center (AEMC) Institutional Review Boards, and informed consent was obtained from all subjects. Families were ascertained through the UM oculoplastic service or AEMC anophthalmia registry. Eye exams, fundus photography and magnetic resonance imaging (MRI) studies were performed at UM Kellogg Eye Center (Table 2.1). Routine blood tests for retinol, RBP and transthyretin (prealbumin) were performed on obligate carrier samples collected after a 12 hr fast (Table 2.2). See Extended Clinical Description for details.

Genetic Analysis

In index Family 1, genotypes were determined for 51 simple sequence length polymorphism (SSLP, Table 2.3) and 6070 single nucleotide polymorphism (SNP) loci using blood, saliva or buccal DNA. Biallelic SNPs were assessed using the HL12 BeadChip platform and Beadstudio software (Illumina, San Diego, CA). Genetic analysis was performed in three steps. Exclusion tests were performed by comparing the two probands using SSLP markers flanking 30 genes previously associated with MAC phenotypes (Table S2). MERLIN v1.1.2 (Abecasis et al., 2002) multipoint linkage analysis was performed on a core pedigree consisting of all living affected individuals, obligate carriers and their spouses (n = 20). The linkage analysis was then extended to include all collected (n = 33, Figure 2.S1C and D) and nodal family members. Linkage scores were calculated by summing LOD values from two subpedigrees (Figure 2.S1D), discarding duplicate phenotypic information (Bellenguez et al., 2009) and applying an autosomal dominant inheritance model with uniform or sex-specific reduced penetrance estimated from the pedigree.

We screened 75 unrelated MAC probands and 307 neurologically normal control samples for variants in *RBP4* exons by Sanger sequencing PCR products (Table 2.4). As a further control, we queried the exome variant server (EVS) database of 5,358 normal individuals for variations in *RBP4* exon 3 at the pertinent genomic positions. Chromosome 10q haplotypes of Families 2 and 3 were compared using the Human Omni1-Quad SNP platform (Illumina). All genomic analysis was performed in the University of Michigan DNA core.

Molecular protein modeling

Minimization of Energy software (MOE, (Chemical Computing Group, 2012)) was used to calculate surface plots and hydrogen bond networks based on the trigonal X-ray crystal structure of human holo RBP (protein data bank structure 1BRP for holo-RBP and 1BRQ for apo-RBP, (Zanotti et al., 1993)). The MMFF94x parameters were used for all energy minimizations. In the case of the holo structure, bond orders for the retinol were corrected. Hydrogen atoms were added and relaxed with energy minimization. To generate the mutants, alanine was mutated to threonine. The side chain of threonine was then relaxed with energy minimization along with further refinement of the hydrogen atom positions. In the case of the holo structure, retinol and sides chains of any residue with one or more atoms within 4.5 A of retinol were then relaxed with energy minimization along with further refinement of the hydrogen atom positions. In the case of the apo structure for the A57T mutant the positions of the binding site water molecules were relaxed with energy minimization but not in the wild-type or A55T mutant. Displayed surfaces represent the molecular surface between retinol and residues 55-57 (and F36) of the protein. Hydrophilic regions of the surfaces are shown in purple, hydrophobic regions in green, and neutral in white. All images were generated using PyMol version 1.5.0 (Schrodinger, LLC, Portland, OR).

RBP secretion and TTR coimmunoprecipitation assays

HeLa cell cultures were transfected in parallel with pUS2-RBP^{HA} plasmid vectors expressing wild-type (WT), mutant (A55T, A57T, G73D, I41N) or ER retention (WT^{KDEL}) human RBP proteins with an N-terminal hemagglutinin (HA) epitope, or empty vector control (for cloning primers see Table 2.5). After 48 hrs, conditioned media (CM) and

RIPA cell lysates were electrophoresed through native or denaturing polyacrylamide gels and compared by HA Western blot analysis. To evaluate RBP multimerization, CM was crosslinked in 0.5% glutaraldehyde for 30 min prior to denaturing electrophoresis, with or without 2 mM βME (2-mercaptoethanol). To assess TTR binding, HeLa cells were cotransfected with pUS2-TTR^{myc} and wild-type or mutant pUS2-RBP^{HA} plasmids. Secreted RBP^{HA} complexes were immunopurified from CM with anti-HA agarose beads (Sigma, St Louis, MO), washed in PBS, and tested for TTR content by Western blot analysis. See Extended Experimental Procedures for molecular cloning, cell culture, immunostaining, protein electrophoresis and Western blot details.

Retinol binding assays

To assess retinol ligand binding to RBP *in vivo*, HeLa cells were transfected with WT or mutant pUS2-RBP^{HA} plasmids in delipidated media, metabolically labeled with ^{35}S-methionine and -cysteine in serum-free media for 1.5 hrs, and exposed to ^{3}H-retinol (Perkin Elmer, Waltham, MA) for an additional 1.5 hrs. RBP was HA-immunopurified from CM after 48 hrs, washed three times in PBS containing 1% Triton X-100, 0.5% Na deoxycholate (DOC), and eluted in 2% SDS. The ^{3}H/^{35}S ratio was measured by liquid scintillation counting and normalized to WT.

For *in vitro* assays, native recombinant *apo* RBP^{HA} was immunopurified from transfected HeLa CM, eluted from anti-HA agarose beads using HA peptide (Anaspec, Fremont, CA), and dialyzed into PBS. Homogeneity was verified by syproruby PAGE analysis. Equal amounts of WT, A55T or A57T rRBP^{HA} protein were loaded with 0 to 10 μM fresh all-*trans* retinol for 1 hr in PBS. Binding was quantified by retinol fluorescence

(330 nm excitation, 460 nm emission) (Cogan et al., 1976) using a Flexstation-3 microplate reader (Molecular Devices, Sunnyvale, CA). To assess binding in nonpolar or amphipathic conditions, parallel assays were performed in the presence of 0 to 50% ethanol or in 1% Triton X-100, 0.5% DOC for 0 to 75 min, respectively.

RBP purification from clinical samples and mass spectrometry

We enriched RBP from 20 ml human plasma by differential ammonium sulfate precipitation and Sephadex G-100 gel exclusion chromatography in PBS ± 6 M Urea as described (Raghu et al., 2003) (Figure 2.S6). Pooled fractions were dialyzed into 50 mM ammonium bicarbonate and electrophoresed through polyacrylamide gels. In parallel, we purified HA-recombinant RBP (WT, A55T and A57T) from cell conditioned media (HA-IP Kit, Sigma). Samples were subjected to PAGE under denaturing conditions and Coomassie stained (GelCode Blue, Thermo) and gel-excised for mass spectrometry. All mass spectrometry was run at the Fred Hutchinson Cancer Research Center Proteomics Facility. Clinical samples and HA-purified recombinant RBP^{HA} controls were proteolytically digested in-gel as described (Shevchenko et al., 1996). Extracted peptides were taken to dryness via vacuum centrifugation and then desalted using Zip-Tips (Millipore, Billerica, MA) per the manufacturer's instructions. One-tenth of the desalted material (1 uL in 50% acetonitrile and 0.1% trifluoroacetic acid) was mixed with 2 uL of 5 mg/mL α-cyano-4-hydroxycinammic acid (suspended in 50% acetonitrile and 0.1% trifluoroacetic acid) and spotted on a stainless steel MALDI target. MALDI TOF/TOF was performed with a 4800 MALDI TOF-TOF mass spectrometer (AB Sciex, Foster City, CA). Both MS and MS/MS data were analyzed through the instrument's

Data Explorer software and with the assistance of GPMAW software v. 9.1 (Lighthouse Data, Denmark). For urine RBP mass spectroscopic analysis, we purified RBP from first morning urine (8 ml) by overnight dialysis versus PBS and immunoprecipitation with anti-RBP4 antibody (DAKO, Carpinteria, CA). Following elution in 2% SDS, RBP was isolated on a denaturing gel without βME and submitted for mass spectrometry as described above.

RBP binding to STRA6 membrane receptor

Equal amounts of immunopurified ^{35}S-labeled *apo* WT, *holo* WT, A55T and A57T recombinant RBP^{HA} (6 x 10^8 cpm/μg specific activity) ± excess unlabeled *holo* WT competitor were added to paired sets of HEK293T cells transfected with pUS2-STRA6^{myc} or vector control. After 1 hr incubation at 37^{o}C, the cells were gently washed with prewarmed PBS (Kawaguchi and Sun, 2010) and bound ^{35}S was counted by liquid scintillation. For each mutant, receptor-specific binding was calculated by subtracting the corresponding vector control. STRA6^{myc} expression was verified by myc immunofluorescence and STRA6 Western analysis.

EXTENDED EXPERIMENTAL PROCEDURES

Genomic and DNA analysis

Targeted sequence capture was done on a pooled sample of eight affecteds and obligate carriers in family 1 to enrich for the desired chromosome 1 haplotype. We used a dual custom oligonucleotide capture array (Nimblegen) specific to human chromosome 1q32-41 (hg18, chr1:208,589,440-219,941,307). We converted the captured DNA into an Illumina paired-end genomic library using a Paired End Library Kit (Illumina, San Diego, CA). Reads were sequenced on a Illumina GenomeAnalyzer sequencer at the University of Michigan DNA Sequencing Core. Validated read data was viewed and analyzed using GenomeStudio software. We achieved an average coverage of 18X across the 11.4 Mb interval. Heterozygous variants were filtered for presence in known databases (dbSNP 131, 1000 genomes, HapMap) with priority given to coding or UTR variants. Novel intronic variants were screened using Spliceport (Dogan et al., 2007) and intergenic variants were screened using JASPAR (Bryne et al., 2008). In parallel, we screened 34 positional candidate genes by PCR across all three candidate regions defined by linkage. To do so, we used custom designed oligonucleotide primers on proband lymphoblastoid cell line DNA to look for inherited heterozygous changes within exons or splice donor or acceptor sites. PCR products were agarose gel purified (Wizard SV gel system, Promega) and both strands were Sanger sequenced at the University of Michigan DNA core. For a comprehensive *RBP4* primer list see Supplemental Table 3. For control genotypes, 307 individuals were

genotyped by hand and approximately 5,358 controls were screened *in silico* using the NHLBI Exome Variant Server v.0.0.13.

Rbp4 RNA analysis

To test bi-allelic expression of mouse *Rbp4*, we performed a test cross between C57BL/6 and DBA/2J (Jackson Laboratory, Bar Harbor, ME), two inbred strains with different alleles at the expressed SNP (eSNP) locus rs30796132. Multiple crosses produced F1 adults and E14.5 embryos (Figure 2.S5). We dissected adult liver and embryonic placentae and whole embryo tissue and additionally removed the embryonic liver. Multiple littermates were tested for each tissue. Tissues were homogenized into Trizol (Invitrogen, Carslbad, CA) and RNA was extracted according to manufacturer's protocol. First-strand cDNA synthesis (Transcriptor, Roche, Indianapolis, IN) was performed and subsequent PCR reactions (25 µl) were performed using primers mRbp4_F (5'-GCA GAC AGC TAC TCC TTT GTG TT) and Rbp4_R (5'-AGG AAG ATG GTG ACT ATA TGT TTA AT). PCR products were agarose gel purified (Wizard SV gel system, Promega) and sequenced. Animals were housed in accordance with UCUCA guidelines.

RBP4, TTR and STRA6 expression vectors

We generated three cDNA expression vectors encoding human RBP4, TTR and STRA6. Full length WT cDNA clones were ordered (OpenBiosystems, Lafayette, CO) and PCR amplified then subcloned into pUS2 (generous gift of D. Turner) using EcoRI and XhoI restriction sites. For RBP4, we generated native and mature N-terminal

hemagglutinin (HA) epitope tagged versions. For TTR and STRA6, we engineered native and C-terminal myc epitope tagged versions. Mutant RBP4 expression plasmids were created using site directed mutagenesis, or SDM (Liu and Naismith, 2008) with mismatch oligonucleotides specific to each mutant (see Table 2.5 for a comprehensive list of cloning and SDM oligonucleotides). Vectors were raised in DH5α bacteria grown in ampicillin (100 µg/ml) liquid cultures and harvested for maxi prep DNA (Qiagen, Valencia, CA) for transfection.

Tissue culture and cell transfection

HeLa and HEK-293T cells (ATCC, Manassas, VA) were grown in Dulbecco's Modified Eagle Medium supplemented with 10% heat-inactivated fetal bovine serum, L-glutamine (2 mM), penicillin (50 U/ml) and streptomycin (50 µg/ml) hereafter referred to as "rich media". Cells were incubated in 37^{o}C humidified tissue culture incubators with 5% $CO_{2.}$ Typically, cells were plated at 1 x 10^{6} per 60 mm dish and grown until cells reached a confluency of approximately 50%. Transfection (FuGene6, Promega) was carried out using a 3:1 F6:DNA ratio for HeLa cells and 4:1 ratio for HEK-293T cells per the manufacturer's protocol. In most cases, at 24 hours post-transfection, fresh culture media (± serum) was given depending on the experiment.

Immunostaining

Cells plated on glass chamber slides (LabTek-II, Nunc, Rochester, NY) were fixed at room temperature for 5 minutes in 4% paraformaldehyde. Cells were blocked and permeabilized in 5% NDS, PBST for 1 hour at room temperature. HeLa cells were

stained with rat-anti-HA 1:500 (Roche 3F10) primary antibody overnight and donkey-anti-rat DyLite 488 1:1000 (Molecular Probes) for 2 hours. Cells were then washed and nuclear counterstained with 4',6'-diamidino-2-phenylindole (DAPI) for 5 minutes. Slides were mounted with Fluorsave reagent (Millipore) and visualized on an Olympus BX51 fluorescence microscope. HEK-293T cells were similarly processed except with rabbit-anti-c-myc 1:100 (Santa Cruz Biotechnology) primary antibody and donkey-anti-rabbit DyLite 488 1:1000 (Jackson Laboratory, Bar Harbor, ME).

PAGE and Western blot

Denaturing PAGE was initiated by mixing samples with equal volume 2X Laemmli buffer (125 mM Tris, 4% SDS, 10% β-mercaptoethanol) at 100^{o}C for 5 minutes. Loaded samples were run on 4-12% Bis-Tris polyacrylamide mini gels (Invitrogen, Carlsbad, CA) at 200V for 40 minutes in 1X MES-SDS running buffer (Invitrogen). For native PAGE, protein samples were mixed with equal volume 2X Tris-glycine running buffer (Invitrogen) without SDS and βME and immediately run on 4-20% Tris-Glycine mini gels (Invitrogen) at 125V for 6 hours at 4^{o}C. All PAGE was done using an XCell SureLock^{TM} Mini-Cell Electrophoresis system (Invitrogen).

For Syproruby staining, PAGE gels were pre-fixed in 50% methanol, 10% glacial acetic acid for 30 minutes at room temperature then incubated overnight protected from light with 1X Syproruby solution (Biorad, Hercules, CA). Gels were washed with fix solution for 30 minutes, rinsed with Milli-Q water and imaged using a Typhoon Phosphorimager (GE Healthcare) with Excitation/Emission at 280 nm and 610 nm, respectively.

For western blots, transfer proceeded at 200 mA, 120V for two hours at 4^{o}C using 1X MES transfer buffer, 5% βME onto Hybond ECL nitrocellulose membranes (GE Healthcare). For Tris-Glycine gels a pre-soak step in 1X MES-SDS running buffer twice for 30 minutes was done prior to transfer for denaturing proteins *in situ*. Membranes were washed with TBS and blocked for 1 hour at room temperature in TBS 5% BSA, 1% milk and incubated with primary antibody from 2 hours to overnight. Primary antibodies for western blots consist of rat-anti-HA 1:5,000 cell lysates and 1:50,000 for conditioned media (High Affinity 3F10, Roche), rabbit-anti-RBP4 1:5,000 (DAKO), rabbit-anti-TTR 1:5,000 (DAKO), mouse anti-BiP 1:1,000 (BD Transduction Labs, Franklin Lakes, NJ), mouse-anti-αTubulin 1:100 (Abcam) and mouse-anti-STRA6 1:1,000 (B01P, Abnova). Next, membranes were washed with TBST three times for 5 minutes and incubated for 1 hour with a horseradish peroxidase (HRP) conjugated secondary antibody. Membranes were washed with TBS then bathed in chemiluminescent detection solution (ECL Plus, Amersham), exposed to film for 1 to 60 minutes (Biomax MS, Kodak) and developed on a Kodak A2000 developer.

RBP biochemical analysis

Mature RBP^{HA} (WT and mutants) was harvested from HeLa cells 48 hours post-transfection from conditioned media. Briefly, CM was HA immunoprecipitated using a mouse anti-HA monoclonal antibody covalently linked to agarose beads (HA IP Kit, Sigma Aldrich). In some cases, RBP^{HA} was eluted under denaturing conditions according to the manufacturer's protocol using 1X Laemmli buffer (Sigma, St. Louis, MO). In other instances, RBP^{HA} was eluted under non-denaturing conditions using HA

peptide in 100 µg/ml PBS (Anaspec, Fremont, CA) three times for 15 minutes rotating at room temperature. To remove HA peptide, eluates were pooled, spin concentrated in 3,000 MWCO columns (EMD Millipore, Bilerica, MA), dialyzed against PBS pH 7.4 overnight at 4^{o}C then once again for 3 hours at room temperature. Protein concentration was assessed by absorbance at 280 nm (A280) on a Flexstation3 microplate reader (Molecular Devices, Sunnyvale, CA), Syproruby-staining solution on gels containing protein standards or RBP4 WB with standard.

Crosslinking

Conditioned media was treated with 0.5% glutaraldehyde vol/vol (Fisher Scientific) for 30 minutes at room temperature. Reactions were quenched in 250 mM Tris.

Figure 2.1. Family 1 with anophthalmia, microphthalmia and coloboma (MAC) disease. (**A**) Seven-generation pedigree segregating the disease trait in an autosomal dominant pattern with reduced penetrance. Eleven family members have uni- or bilateral microphthalmia or coloboma (gray symbols), or clinical anophthalmia (black symbols). The probands are indicated in generation VII (arrows). Nine obligate carriers (dotted symbols) transmitted the disease mutation but are clinically normal. A global penetrance of 0.4 was estimated from 54 informative meioses (11 cases vs. 27 expected). The penetrance values for maternal (0.7 from 29 meioses) and paternal (0.1 from 17 meioses) transmission are significantly different (P = 0.036, Fisher's exact test), suggesting a parent-of-origin effect (Figure 2.S1B). (**B**) Anterior eye and fundus montage photographs of affected family members demonstrate a wide range of phenotypes, including iris and chorioretinal colobomas (ventronasal wedge-like defects in VI-2, VII-2 and VII-3), microphthalmia (III-12 and VII-2), and bilateral clinical anophthalmia (VII-5). VII-5, T2-weighted coronal image with extraocular muscles (red arrows) but absence of eye globes. VII-5 axial T2 image with fat-suppression shows hyperintense orbital cysts, bilaterally (yellow arrows). The left orbit contains two cysts measuring 1 cm x 4 mm and 4 x 6 mm. The right orbit contains a 1.4 x 1 cm cyst. Proband VII-2 has contralateral anophthalmia. The coloboma in VI-2 involves the entire uveal and neuroretinal axis of the left eye, from the pupillary margin to the optic nerve head (onh), and corresponds anatomically to a patent choroid fissure. Bright scleral connective tissue is visible through the ventral chorioretinal defect. crc, chorioretinal coloboma. (**C**) Genetic mapping of MAC disease locus to chromosome 10q23. Multipoint LOD score plot of autosomes, derived by MERLIN linkage analysis of Family 1, using only affected individuals and obligate carriers. Among four positive regions, three have LOD scores >2, suggestive of linkage (1q41, 10q23 and 19p13). To refine the map position, an expanded linkage analysis was performed using all available family members, and autosomal dominant (AD) models with uniformly reduced or sex-specific penetrance values. The results favor chromosome 10 localization with an odds ratio >11 and a genome-wide LOD score >3.

A

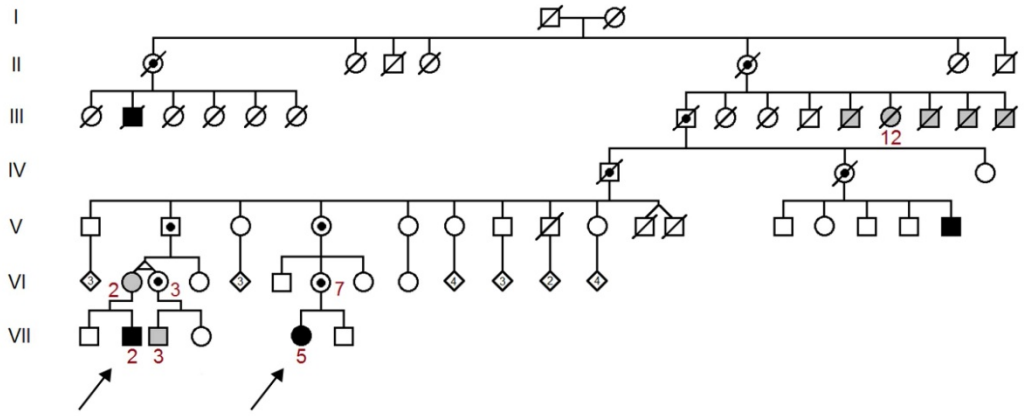

B

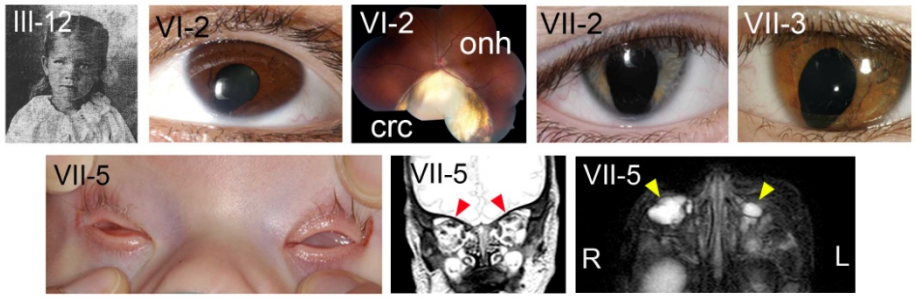

C

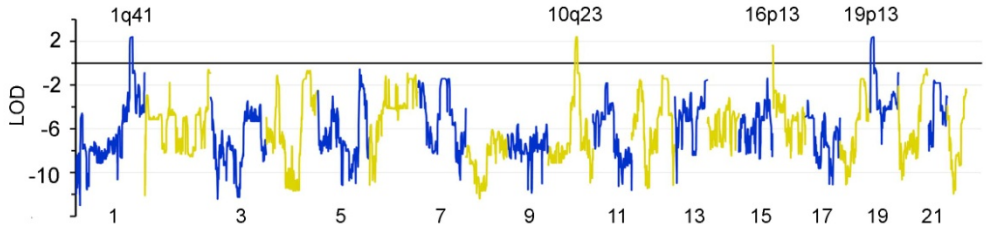

Model	peak LOD score 1q41	10q23	16p13	19p13	odds favoring chr 10 versus chr 1	chr 16	chr 19
AD (affecteds only)	2.39	2.40	1.64	2.39	1.02	5.75	1.02
AD with reduced penetrance (all)	2.38	2.86	-0.05	2.41	3.02	8.1E2	2.81
AD with sex-specific penetrance (all)	1.86	**3.01**	-0.92	1.94	14.12	8.5E3	11.75

Figure 2.2. *RBP4* mutations in three independent families with congenital eye malformations. (**A**) The *RBP4* gene has six exons and spans 9.4 kb. The map shows UTRs (white), coding DNA for the signal sequence (gray) and mature protein (black), and position of the mutations in exon 3 (red box). (**B**). Sequence chromatograms from probands and parents show novel heterozygous missense mutations in index Family 1 (c.223G>A, p.A75T) and unrelated Families 2 and 3 (c.217G>A, p.A73T). In each pedigree, the disease trait and mutation are maternally transmitted. The mother in Family 2 (II-1) is an obligate carrier with a family history of anophthalmia. The mother in Family 3 (II-2) has a unilateral optic pit. The p.A73T mutations in Families 2 and 3 occur on different chr 10q haplotypes (Figure 2.S3). (**C**) Primary structure of translated RBP showing the two alanine-to-threonine substitutions (red) in β-strand C in the mature polypeptide (yellow bar). Two previously reported RBP alleles associated with autosomal recessive nyctalopia (night blindness), I41N and G75D (gray), are located in β-strands B and D, respectively. Note that A73T and A75T in the primary translation product correspond to A55T and A57T in mature RBP, following cleavage of the 18-amino acid N-terminal signal sequence (SS). Symbols: gray bar, endoplasmic reticulum SS peptide; cyan coils, α-helical regions; blue arrows A-H, eight β-strands comprising the β-barrel fold. (**D**) Ribbon diagrams showing the three-dimensional X-ray crystal structure of RBP and positions of dominant A55T and A57T (red) and recessive I41N and G75D (gray) substitutions. In the wild-type structure (1BRP), these four amino acids are oriented with side chains facing the hydrophobic retinol-binding pocket. The RBP lipocalin has a β-barrel structure, with eight anti-parallel strands (dark blue) forming the ligand pocket, and a C-terminal α-helix (cyan). Three loops (green) surrounding the calyx opening interface with transthyretin (TTR) homotetramer. The N-terminus, where an HA epitope tag was introduced, is relatively unconstrained. (**E**) Local amino acid alignment showing complete evolutionary conservation of alanines 55 and 57 among vertebrates.

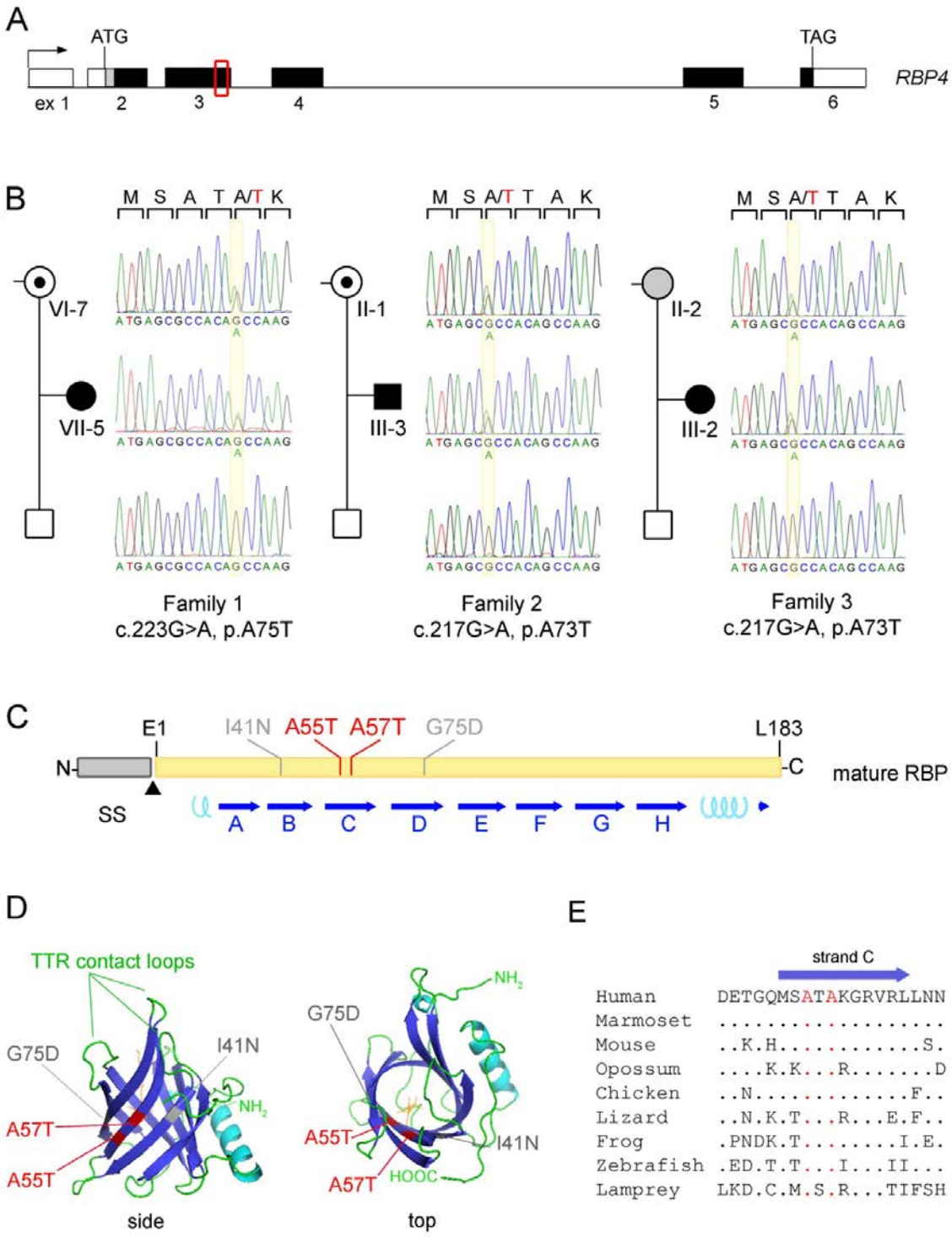
A
ATG
TAG
RBP4
ex 1
2
3
4
5
6
B
M S A T A/T K
M S A/T T A K
M S A/T T A K
VI-7
VII-5
II-1
III-3
II-2
III-2
ATGAGCGCCACAGCCAAG
Family 1
c.223G>A, p.A75T
Family 2
c.217G>A, p.A73T
Family 3
c.217G>A, p.A73T
C
E1
I41N
A55T
A57T
G75D
L183
N
C
mature RBP
SS
A
B
C
D
E
F
G
H
D
TTR contact loops
G75D
I41N
NH2
A57T
A55T
side
NH2
G75D
A55T
I41N
A57T
HOOC
top
E
strand C
Human DETGQMSATAKGRVRLLNN
Marmoset ....
Mouse ..K.H..........S.
Opossum ....K.K...R.......D
Chicken ..N.............F..
Lizard ..N.K.T...R...E.F..
Frog .PNDK.T........I.E.
Zebrafish .ED.T.T...I...II...
Lamprey LKD.C.M.S.R...TIFSH

Figure 2.3. A55T and A57T proteins are secreted as stable RBP monomers and interact with transthyretin *in vivo*. (**A**) Experimental design. Conditioned media (CM) and lysates of transfected HeLa cells were compared to assess the production, secretion and structural integrity of RBP^{HA} proteins. (**B**) HA (hemagglutinin) Western blot analysis of CM electrophoresed under native or denaturing conditions. WT, A55T and A57T proteins are abundantly secreted as 21 kD monomers (top). In contrast, I41N and G75D proteins appear to aggregate intracellularly, as 42 kD homodimers covalently linked by disulfide bonds (Figure. 2.S5A). This observation was confirmed by crosslinking in 0.5% glutaraldehyde prior to electrophoresis (bottom). In standard denaturing gels loaded with equivalent volumes of CM (middle), the abundance of G75D and I41N mutant proteins is slightly decreased compared to WT, A55T and A57T. (**C**) Western analysis of corresponding cell lysates shows increased cellular retention of I41N compared to other forms (top) and the α-tubulin loading control (bottom). However, I41N is secreted more efficiently than WT^{KDEL}, which has an endoplasmic reticulum (ER) retention signal at the C-terminus. (**D**) Experimental design for TTR binding. HeLa cells were cotransfected with RBP^{HA} and TTR^{myc} cDNA expression plasmids, and the resulting RBP^{HA} was purified from conditioned media with anti-HA agarose beads. TTR binding was evaluated by Western blot (WB) analysis of the immunoprecipitate (IP). Under normal conditions, TTR monomers form stable homotetramers (four brown circles), which bind single RBP protein molecules (black bar) prior to secretion. (**E**) Western blots showing A55T and A57T proteins complex stably with TTR, similar to wild-type RBP, but G75D and I41N interact poorly with TTR. The same membrane was sequentially probed with antibodies to TTR (top) and HA (bottom). Equivalent amounts of RBP were loaded in each lane. Human WT RBP can partner with fetal bovine TTR (13.5 kD) in the culture media, as well as human TTR^{myc} (15.1 kD).

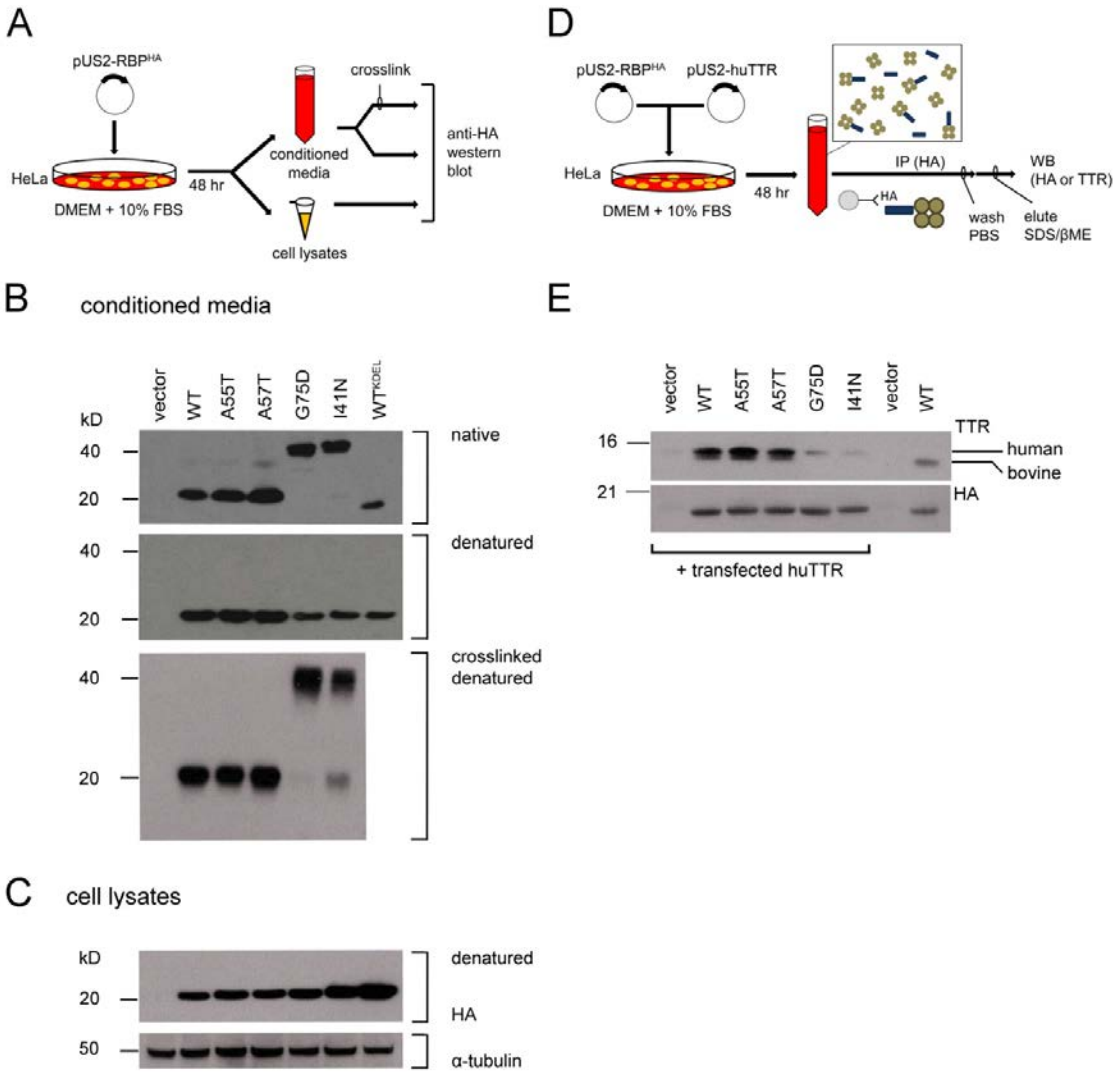
A
pUS2-RBP^HA
HeLa
DMEM + 10% FBS
48 hr
conditioned media
crosslink
cell lysates
anti-HA western blot
D
pUS2-RBP^HA
pUS2-huTTR
HeLa
DMEM + 10% FBS
48 hr
IP (HA)
HA
wash PBS
elute SDS/βME
WB (HA or TTR)
B
conditioned media
vector
WT
A55T
A57T
G75D
I41N
WT^KDEL
kD
40
20
native
denatured
crosslinked denatured
E
vector
WT
A55T
A57T
G75D
I41N
vector
WT
16
21
TTR
human
bovine
HA
+ transfected huTTR
C
cell lysates
kD
20
50
denatured
HA
α-tubulin

Figure 2.4. Mass spectrometric analysis of RBP proteotypes in p.A75T/+ carrier plasma. (**A**) Primary sequence and sizes of informative tryptic peptides encompassing RBP residue 57. The WT (3,140 Da) and A57T mutant (3,170 Da) forms differ by 30 mass units. In addition to these species, modified peptides are expected for each allele, due to iodoacetamide alkylation of methionine 53 (♦) during sample preparation, including sulfoxide (+16 Da, single asterisk) and alkylation-decomposition (-48 Da, double asterisk) derivatives. (**B**) MALDI-TOF spectrum of RBP purified from control human plasma (800 to 4,000 m/z). The critical region (red box) is indicated. Y-axis represents relative intensity (**C**) Expanded view of control (top) and carrier subject (bottom) spectra from 3,100 to 3,250 m/z. In the control sample, two single-ionization peaks corresponding to WT RBP (red lines) are detected in this range. In the carrier subject, both WT peaks are detected, along with peaks corresponding to the A57T mutant protein (green lines). The identity of peptide ions was verified by tandem MS/MS analysis. Judging from peak signal intensities, the ratio of WT to A57T proteins in the subject plasma is approximately 2 to 1. (**D**) Comparable MALDI-TOF spectra for recombinant RBP^{HA} proteins, purified from HeLa-conditioned media. The 50:50 mix spectrum demonstrates equivalent ionization efficiency for WT and A57T tryptic peptides. The invariant 3,223.3 m/z peak represents human keratin (a common contaminant) and serves as an internal standard.

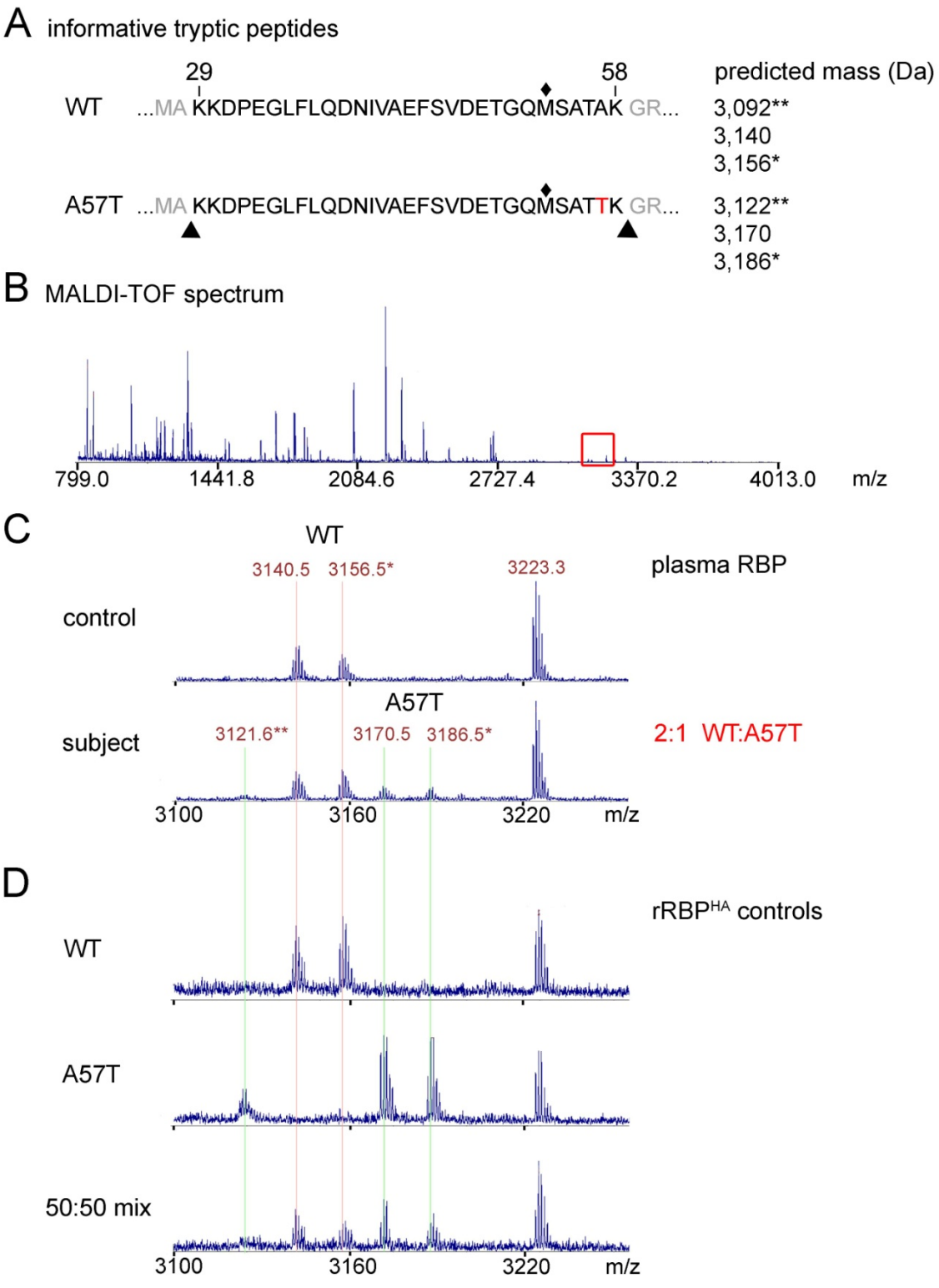
A informative tryptic peptides
29
58
predicted mass (Da)
WT ...MA KKDPEGLFLQDNIVAEFSVDETGQMSATAK GR...
3,092**
3,140
3,156*
A57T ...MA KKDPEGLFLQDNIVAEFSVDETGQMSATTK GR...
3,122**
3,170
3,186*
B MALDI-TOF spectrum
799.0
1441.8
2084.6
2727.4
3370.2
4013.0
m/z
C
WT
3140.5
3156.5*
3223.3
plasma RBP
control
A57T
3121.6**
3170.5
3186.5*
subject
2:1 WT:A57T
3100
3160
3220
m/z
D
rRBP^HA controls
WT
A57T
50:50 mix
3100
3160
3220
m/z

Figure 2.5. A55T and A57T proteins bind retinol poorly. (**A**) *in vivo* ^{3}H-retinol-binding assay. RBP^{HA} proteins, synthesized by transfected HeLa cells, were metabolically labeled with ^{35}S-methionine and -cysteine, and loaded with ^{3}H-retinol. Following HA immunopurification from conditioned media, and washing in PBS with 1% Triton X-100 and 0.5% deoxycholate (DOC), the ^{3}H/^{35}S ratio of RBP^{HA} was determined by liquid scintillation counting (LSC). (**B**) Histogram showing ^{3}H-retinol binding data normalized to WT (left). Error bars give the SEM for three parallel assays. The A55T and A57T proteins retain significantly less ^{3}H-retinol than wild-type, with A55T being most severely affected. The misfolded G75D and I41N proteins also bind retinol poorly, as expected. Autoradiogram of denaturing polyacrylamide gel showing equivalent levels of ^{35}S-RBP^{HA} in whole conditioned media (right). RBP is the major secreted protein. (**C**) *in vitro* retinol binding profiles for pure recombinant WT and mutant RBP^{HA}, measured by retinol fluorescence in PBS, with 1 μM protein (left). The A55T mutant exhibits significantly less retinol binding, whereas A57T and WT profiles are similar in this highly polar solvent. The homogeneity and concentration of rRBPs was assessed by A_{280} and syproruby gels (right). (**D**) Normalized retinol binding curves in PBS with 0 to 50% ethanol. As the polarity of the environment decreases, the affnity of mutant rRBPs is differentially reduced compared to WT. Binding was assessed by 460 nm fluorescence after 1 hr in 10 μM retinol. (**E**) Sensitivity of mutant RBPs in an amphipathic environment. Retinol fluorescence of purified rRBPs was measured after exposure to weak nonionic detergents (1% Triton X-100 and 0.5% deoxycholate in PBS) for 0 to 75 min. In each assay, A55T is more severely affected than the A57T allele.

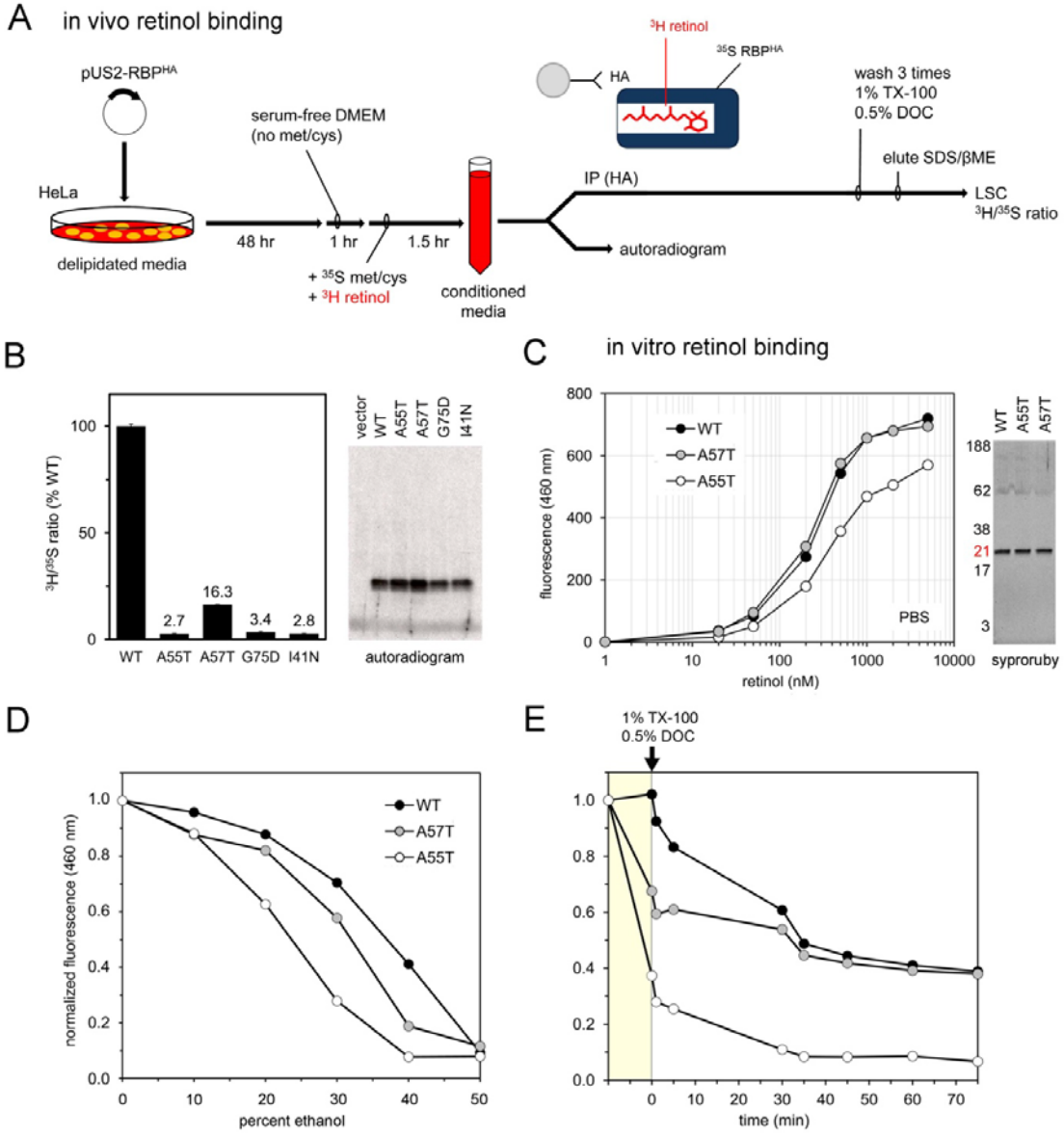
A
in vivo retinol binding
pUS2-RBP^HA
HeLa
delipidated media
serum-free DMEM
(no met/cys)
48 hr
1 hr
1.5 hr
+ 35S met/cys
+ 3H retinol
conditioned
media
3H retinol
35S RBP^HA
HA
IP (HA)
autoradiogram
wash 3 times
1% TX-100
0.5% DOC
elute SDS/βME
LSC
3H/35S ratio
B
3H/35S ratio (% WT)
100
50
0
2.7
16.3
3.4
2.8
WT A55T A57T G75D I41N
vector
WT
A55T
A57T
G75D
I41N
autoradiogram
C
in vitro retinol binding
fluorescence (460 nm)
800
600
400
200
0
WT
A57T
A55T
PBS
1 10 100 1000 10000
retinol (nM)
WT
A55T
A57T
188
62
38
21
17
3
syproruby
D
normalized fluorescence (460 nm)
1.0
0.8
0.6
0.4
0.2
0.0
WT
A57T
A55T
0 10 20 30 40 50
percent ethanol
E
1% TX-100
0.5% DOC
1.0
0.8
0.6
0.4
0.2
0.0
0 10 20 30 40 50 60 70
time (min)

Figure 2.6. A55T and A57T proteins bind the STRA6 membrane receptor more strongly than WT. (**A**) Binding assay. HEK293T cells were transfected with pUS2-STRA6^{myc} expression plasmid DNA and exposed to 60,000 cpm WT or mutant ^{35}S-RBP^{HA} ± unlabeled holo WT RBP competitor. After 1 hr, bound cellular radioactivity was measured by LSC. (**B**) STRA6^{myc} expression in HEK293T cultures. *left*, Fluorescence micrographs of transfected cells immunostained with anti-myc antibody (green) and counterstained with DAPI (blue). The STRA6 receptor is localized to cell membranes. *right*, Western blot simultaneously probed with antibodies to human STRA6 (72 kD) and α-tubulin (50 kD). The human embryonic kidney (HEK) cell line contains little or no endogenous STRA6 antigen. (**C**) Histogram showing equilibrium binding of ^{35}S-labeled WT, A55T and A57T proteins in the absence (black bars) or presence (gray bars) of unlabeled (cold) holo WT competitor. Error bars give the SEM for three parallel assays. In this assay, wild-type holo RBP binds STRA6 with 3X higher affinity than the apo form. A57T and A55T mutants bind with approximately 4X and 8X higher affinity than holo WT, respectively. These effects may arise from thermodynamic or kinetic differences in RBP docking and/or dissociation. Scale bars in B, 40 μm.

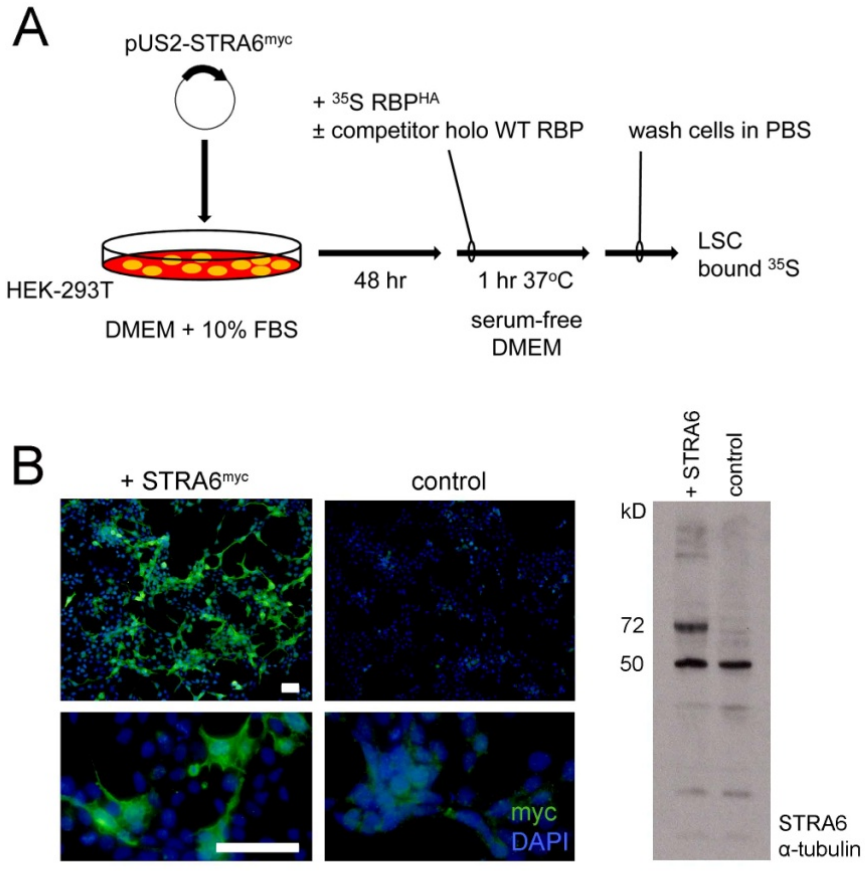
A
pUS2-STRA6myc
+ 35S RBPHA
± competitor holo WT RBP
wash cells in PBS
HEK-293T
48 hr
1 hr 37oC
LSC
bound 35S
DMEM + 10% FBS
serum-free
DMEM
B
+ STRA6myc
control
myc
DAPI
+ STRA6
control
kD
72
50
STRA6
α-tubulin
C
35S RBP cpm
2500
2000
1500
1000
500
0
apo WT
holo WT
A57T
A55T
cold competitor

Figure 2.7. Model for disease pathogenesis, dominant inheritance and maternal effects. (**A**) RBP life cycle in wild-type individuals (top) and heterozygotes (bottom). In mutation carriers, A55T or A57T proteins are co-expressed with WT proteins in hepatocytes and maternal fetal barrier (placenta or visceral yolk sac). Upon secretion, the A55T and A57T mutant proteins circulate in the maternal or fetal bloodstream bound to TTR, as stable entities with little to no retinol. The mutant RBPs dissociate from TTR at target tissues and bind STRA6 with higher affinity than WT proteins. At the molecular level, the mutant RBPs thus act as defective interfering particles. This molecular mimicry blocks holo WT binding, disrupts cellular retinol delivery, and provides a mechanism for the dominant inheritance pattern. (**B**) At the physiological level, phenotypic expression of the anophthalmia trait depends jointly on the maternal and fetal genotypes (left columns), which control retinol transport to the maternal-fetal barrier and developing fetal eyes, respectively. Dominant-negative *RBP4* alleles may impair vitamin A delivery at both steps during pregnancy, creating two sequential “bottlenecks” (vertical gray lines) – but only when the mutation is maternally transmitted. This unique maternal-fetal interaction thus provides a novel nutritional mechanism for the skewed inheritance pattern. The developing eye is highly sensitive to retinoid levels, and has a relatively low phenotypic threshold. The *RBP4* mutations are susceptibility alleles for vitamin A deficiency (VAD). As such, the penetrance and expressivity depend on dietary vitamin A levels (colored lines), suggesting a simple approach for prenatal therapeutic intervention. NOTE: vitamin A reduction amounts depicted across the placenta and fetal eye tissues are for illustrative purposes only. The exact relative reductions across both tissues is unknown.

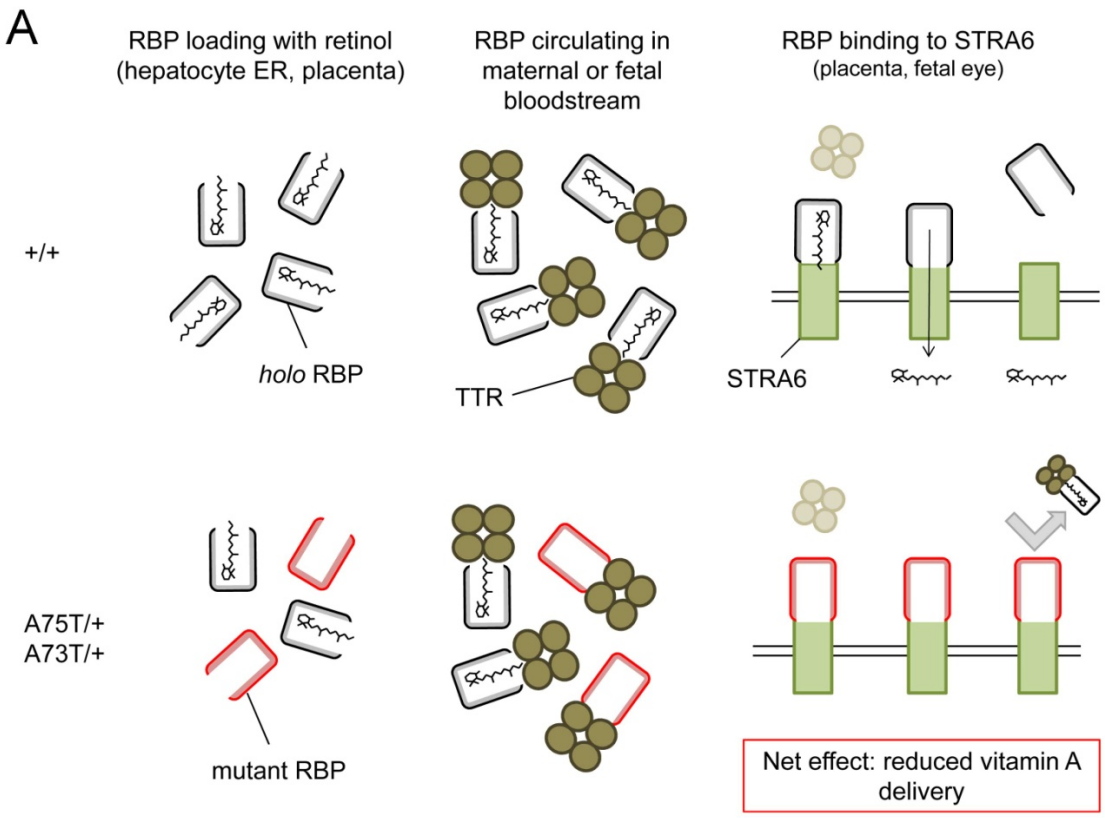
A
RBP loading with retinol
(hepatocyte ER, placenta)
RBP circulating in
maternal or fetal
bloodstream
RBP binding to STRA6
(placenta, fetal eye)
+/+
holo RBP
TTR
STRA6
A75T/+
A73T/+
mutant RBP
Net effect: reduced vitamin A
delivery

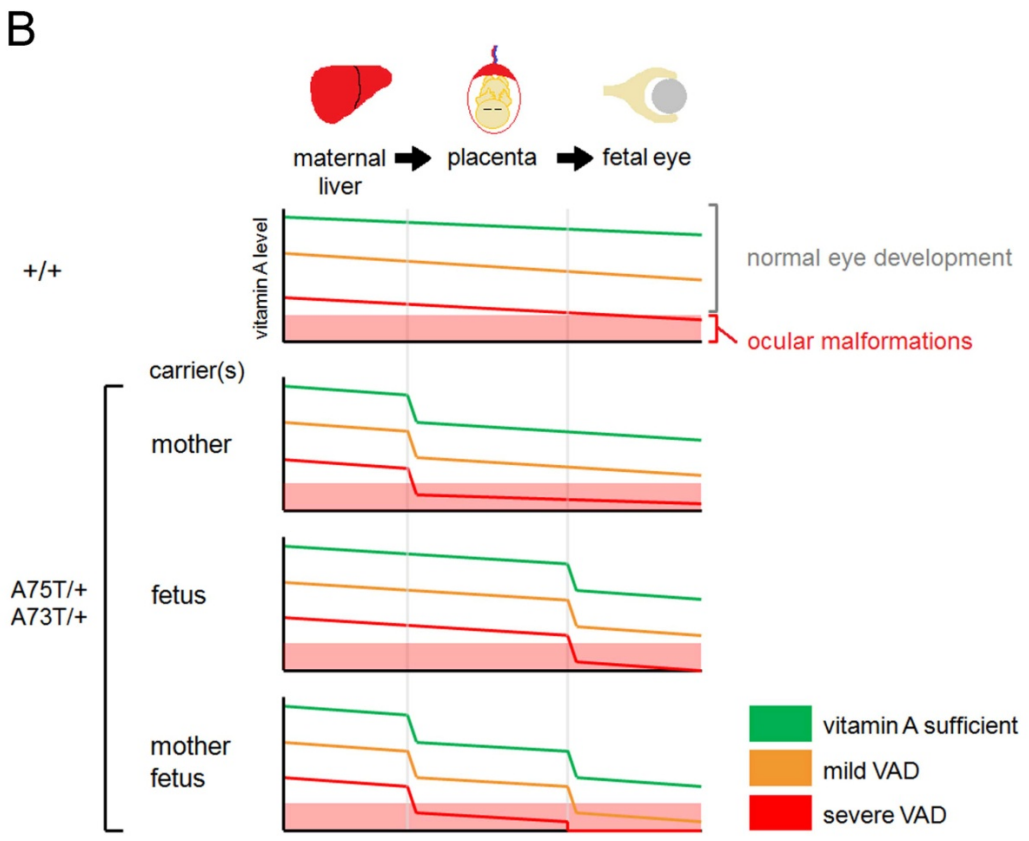
B
maternal
liver
placenta
fetal eye
+/+
vitamin A level
normal eye development
ocular malformations
carrier(s)
mother
A75T/+
A73T/+
fetus
mother
fetus
vitamin A sufficient
mild VAD
severe VAD

Figure 2.S1. Detailed segregation and linkage analysis of Family 1. (**A**) Pedigree diagram showing the at-risk sibships used to estimate penetrance in black. Penetrance values were calculated from segregation data, either including (P = 0.41) or excluding (P = 0.36) two probands (arrows) to correct for ascertainment bias. Noncontributing individuals are shown in light gray. (**B**) Pedigree diagram highlighting the parent transmitting the causative mutation to affected individuals and obligate carriers. Among 11 family members with eye malformations, 10 inherited the disease trait from their mother (dark red), and only one (VI-2) inherited it from her father (dark blue). This individual is notable as a discordant monozygous twin with unilateral coloboma, who was clinically underweight at birth. Normal obligate carriers are similarly marked to indicate maternal (pink) or paternal (light blue) transmission. The sex-specific penetrance values differ significantly, suggesting a parent-of-origin effect. (**C**) Collection of genotype and phenotype data. Pedigree diagram showing individuals who provided DNA samples (red) and/or were evaluated clinically. Phenotypes were assessed by ophthalmic exams at UM Kellogg Eye Center (asterisks) or were documented by report and family photographs (double dagger). (**D**) Pedigree splitting strategy for MERLIN linkage analysis. Multipoint calculations were performed separately on subpedigrees 1 (red) and 2 (green), and the LOD scores were summed. Two nodal individuals (yellow) were included in both subpedigrees, but their phenotypic data (carrier status) were only used once.

A penetrance

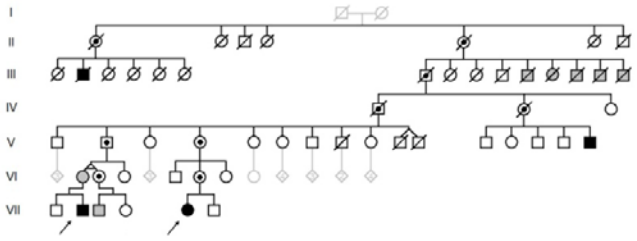

◆ anophthalmia
◇ microhthalmia or coloboma
◈ obligate carrier

54 at-risk individuals
54 ÷ 2 = 27 expected cases
11 observed cases
P = 11 ÷ 27 = 0.41
P_{corr} = 9 ÷ 25 = 0.36 (omitting probands)

B parent-of-origin effect

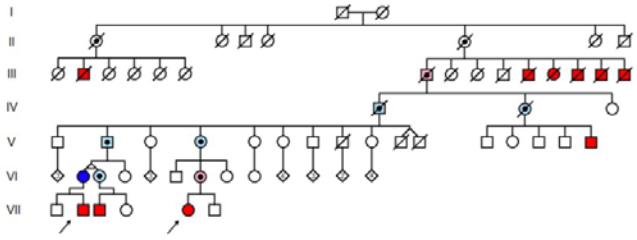

◆ affected, inherited from mother
◇ unaffected, inherited from mother
◆ affected, inherited from father
◇ unaffected, inherited from father

29 at-risk offspring maternal transmission
P_{mat} = (10 ÷ 29) x 2 = 0.69

17 at-risk offspring paternal transmission
P_{pat} = (1 ÷ 17) x 2 = 0.12

P = 0.036 (Fisher's exact test)

C DNA collection and phenotype assessment

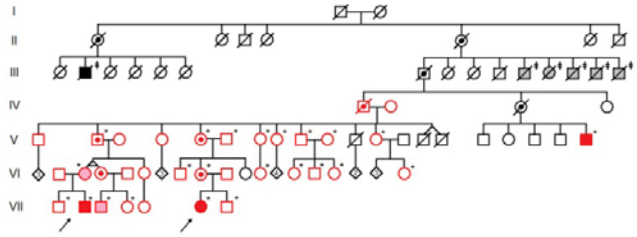

◇ collected DNA
* examined at Univ. Michigan
‡ disease phenotype by report & family photographs

D linkage

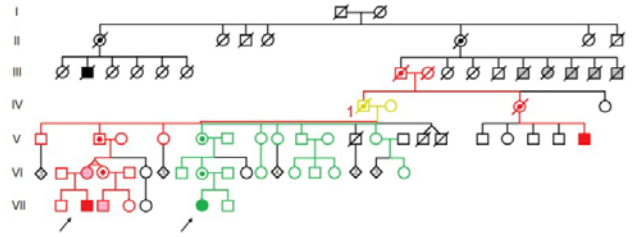

◇ subpedigree 1
◇ subpedigree 2
◇ overlap

Figure 2.S2. Genetic mapping of MAC disease locus to chromosome 10q23. (**A**) Expanded view of chromosome 10 linkage data showing a single LOD peak at 10q23-24 for all three models: AD with complete penetrance, calculated using only affecteds and obligate carriers (red), and AD with uniformly reduced (blue, P_{global} = 0.4) or sex-specific (green, P_{mat} = 0.7 and P_{pat} = 0.1) penetrance, calculated using all family members. The inset shows the 10 cM interval with LOD >0 delimited by markers rs2039305 (centromeric) and rs713251 (telomeric). (**B**) Gene view of the 8.2 Mb critical region on chromosome 10 with 81 candidate genes (GRCh37/hg19, Feb 2009 assembly). *RBP4* (serum retinol binding protein, red) is encoded on the (–) strand.

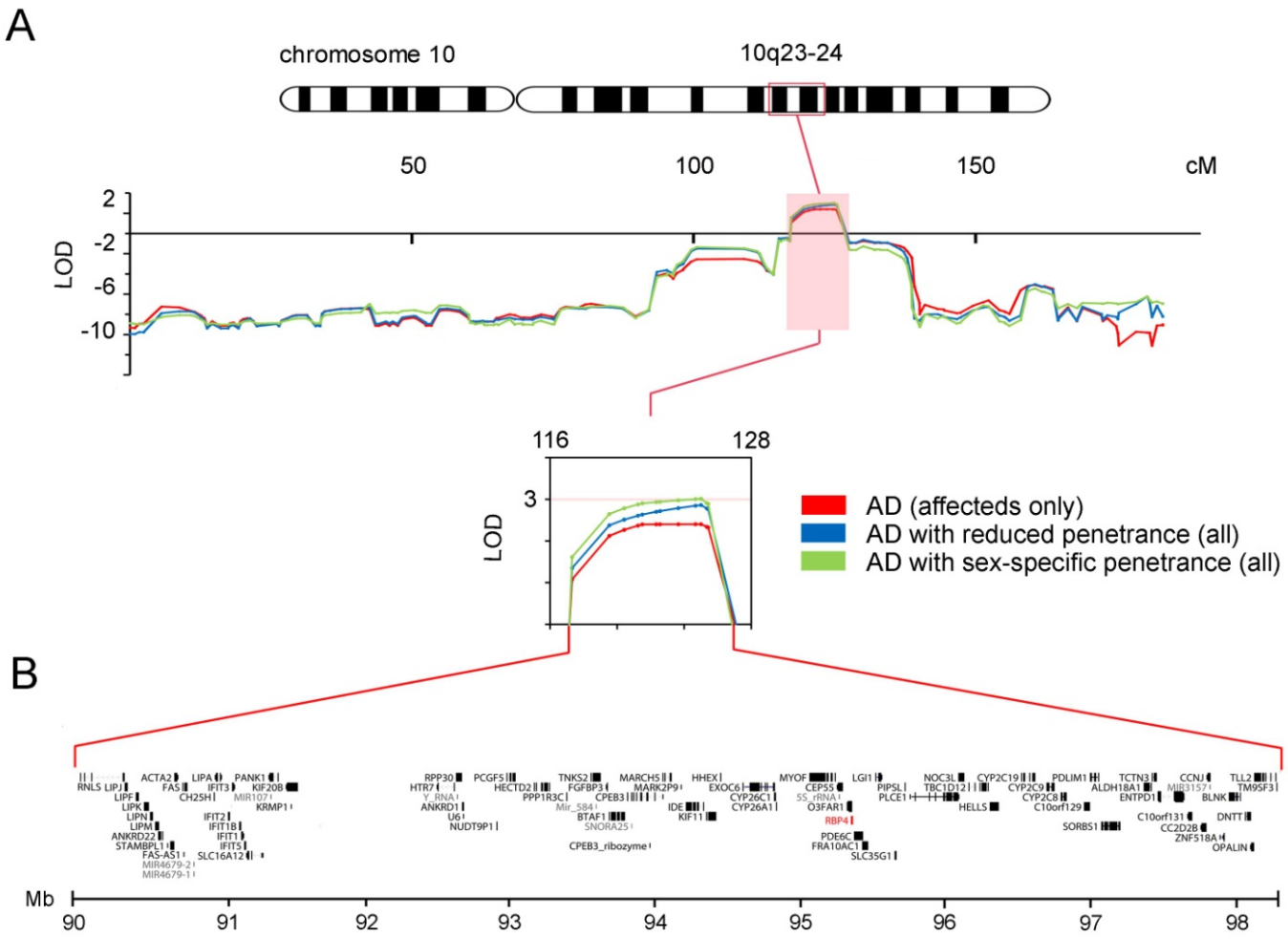
A
chromosome 10
10q23-24
50
100
150
cM
LOD
2
-2
-6
-10
116
128
3
AD (affecteds only)
AD with reduced penetrance (all)
AD with sex-specific penetrance (all)
B
Mb
90
91
92
93
94
95
96
97
98

Figure 2.S3. Maternal transmission of autosomal dominant MAC disease in Families 2 and 3. (**A**) Five-generation pedigree with anophthalmia and developmental delay in the proband (III-3, arrow) and a maternal cousin (IV-1). Both affected males inherited the disease trait from an unaffected female (II-2 and III-7). (**B**) Three-generation pedigree with unilateral microphthalmia in the proband (III-2, arrow) and a unilateral optic pit in her mother (II-2). No further history of congenital eye disease is available. Clinical details are provided in Extended Clinical Description and Table 2.1. Black or gray symbols, affected; dotted symbol, obligate carrier. (**C**) *RBP4* p.A73T mutations in Families 2 and 3 occur on independent chromosome 10q haplotypes. Trios were genotyped for 1.2×10^6 biallelic SNP markers using the Illumina Human Omni1-quad platform. Haplotype analysis was performed for chromosome 10q23 markers located in a 30 kb interval encompassing *RBP4* exon 3. Map positions relative to A73 were determined using hg18 coordinates (NCBI36, Mar 2006 assembly). Phase was assigned using parental genotypes. Major (A) and minor (B) alleles and disease haplotypes (red box) are indicated. Among 18 SNP markers examined, nine were informative in the families (red hashes), including three within the *RBP4* transcription unit (red arrow).

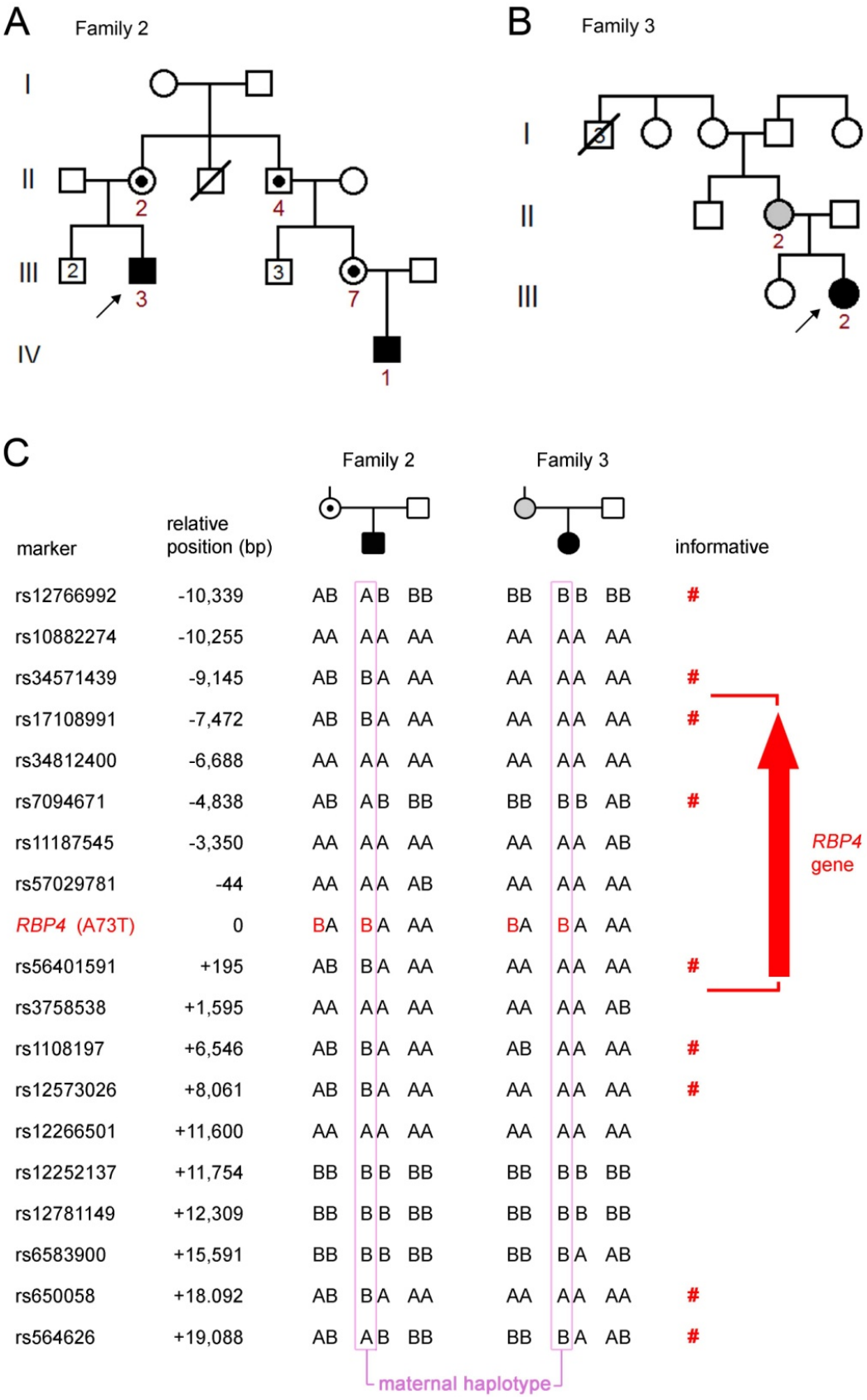
A
Family 2
I
II
III
IV
2
4
2
3
3
7
1
B
Family 3
I
II
III
2
2
C
Family 2
Family 3
marker
relative position (bp)
informative
rs12766992 -10,339 AB AB BB BB BB BB #
rs10882274 -10,255 AA AA AA AA AA AA
rs34571439 -9,145 AB BA AA AA AA AA #
rs17108991 -7,472 AB BA AA AA AA AA #
rs34812400 -6,688 AA AA AA AA AA AA
rs7094671 -4,838 AB AB BB BB BB AB #
rs11187545 -3,350 AA AA AA AA AA AB
rs57029781 -44 AA AA AB AA AA AA
RBP4 (A73T) 0 BA BA AA BA BA AA
rs56401591 +195 AB BA AA AA AA AA #
rs3758538 +1,595 AA AA AA AA AA AB
rs1108197 +6,546 AB BA AA AB AA AA #
rs12573026 +8,061 AB BA AA AA AA AA #
rs12266501 +11,600 AA AA AA AA AA AA
rs12252137 +11,754 BB BB BB BB BB BB
rs12781149 +12,309 BB BB BB BB BB BB
rs6583900 +15,591 BB BB BB BB BA AB
rs650058 +18.092 AB BA AA AA AA AA #
rs564626 +19,088 AB AB BB BB BA AB #
RBP4 gene
maternal haplotype

Figure 2.S4. A55T and A57T detailed structural characterization. (**A**) Three-dimensional view of the ligand-binding surface in wild-type holo RBP. The retinol pocket is predominantly hydrophobic (Hϕ, green), including the Ala55 and Ala57 side chains, which contact the retinol β-ionone ring. The paucity of hydrophilic surfaces (Hψ, magenta) is consistent with the lipophilic nature of retinol. (**B**) Molecular models comparing holo wild-type (WT) and mutant (A55T and A57T) proteins, generated by energy minimization (MOE) and visualized by PyMOL. The mutant RBPs are predicted to accommodate retinol within the binding pocket, despite steric effects of the larger threonine side chain. However, the increased hydrophilicity of the local environment (magenta surface) and additional protein-solvent hydrogen bonding within the lumen are unfavorable for retinol binding. (**C**) Stick diagram of wild-type (WT) holo RBP showing retinol (green) and Ala55 and Ala57. Water molecules are displaced from the ligand pocket upon retinol binding. (**D**) Molecular models suggest potential structural mimicry. *left*. In apo RBP, water molecules filling the lipocalin cavity form a network of hydrogen bonds, which are linked to F36 but do not involve A55 or A57. *middle*. In A57T mutant RBP, the chain of hydrogen bonds connects F36 to the hydroxyl group of T57. *right*. In the A55T mutant protein, a similar chain of hydrogen bonds links F36 and T55. These additional bonds may stabilize the *apo* form and have allosteric effects. In wild-type RBP, the F36 residue undergoes a discrete conformational shift upon retinol binding (Zanotti et al., 1993). In principle, the A57T and A55T substitutions may partially displace F36 in the absence of ligand, such that the mutant proteins resemble *holo* RBP in their interactions with STRA6. The models were derived from the trigonal structure of human *holo* RBP (1BRP) by energy minimzation (MOE), allowing T55 and T57 side chains to move freely while fixing the positions of other heavy atoms. Carbon (gray), hydrogen (white), oxygen (red) and nitrogen (blue) atoms, and hydrogen bonds (dotted lines) are indicated.

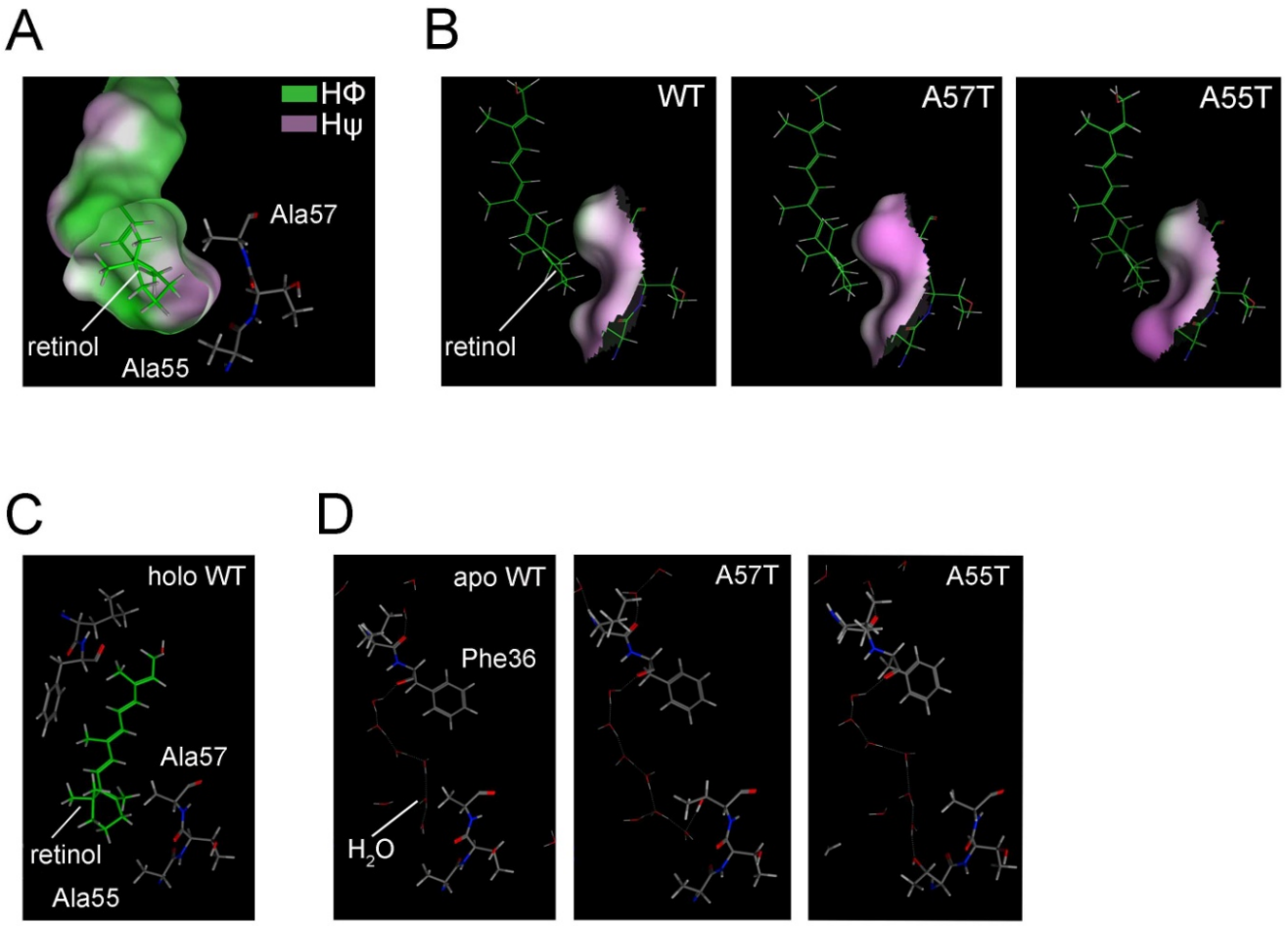
A
HΦ
Hψ
Ala57
retinol
Ala55
B
WT
A57T
A55T
retinol
C
holo WT
Ala57
retinol
Ala55
D
apo WT
Phe36
H2O
A57T
A55T

Figure 2.S5. Further characterization of RBP^{HA} expression in transfected HeLa cells and *Rbp4* in mouse tissues. (**A**) HA Western blot of conditioned media. Samples were boiled in 2% SDS prior to electrophoresis, with or without 5% β-mercaptoethanol (βME). The G75D and I41N mutant proteins exist predominantly as homodimers, which are linked by disulfide bonds. In addition, the I41N protein forms large aggregates, which migrate as tetramers or higher-order species. These aberrant multimers are completely reduced by βME (right lanes). Similar results were obtained using cell lysates (not shown), suggesting the abnormal intermolecular S-S bonds form prior to secretion, and result from misfolding of nascent G75D and I41N polypeptides in the endoplasmic reticulum (ER) during synthesis. In contrast, WT, A55T and A57T RBP proteins exist primarily as monomers. (**B**) Western blot of cell lysates probed with anti-BiP (GPR78) shows no evidence that transient expression of RBP^{HA} mutants causes ER stress or induces an unfolded protein response. (**C**) Biallelic expression of mouse *Rbp4* in fetal tissues and adult liver. RT-PCR analysis of F1 RNA samples ± reverse transcriptase (RT). The 415 bp *Rbp4* amplicon spans an informative single nucelotide variant (eSNP rs30796132) in the 3' UTR (asterisk). Sequence chromatograms of PCR products show equivalent expression of maternal and paternal alleles (yellow) in all four tissues.

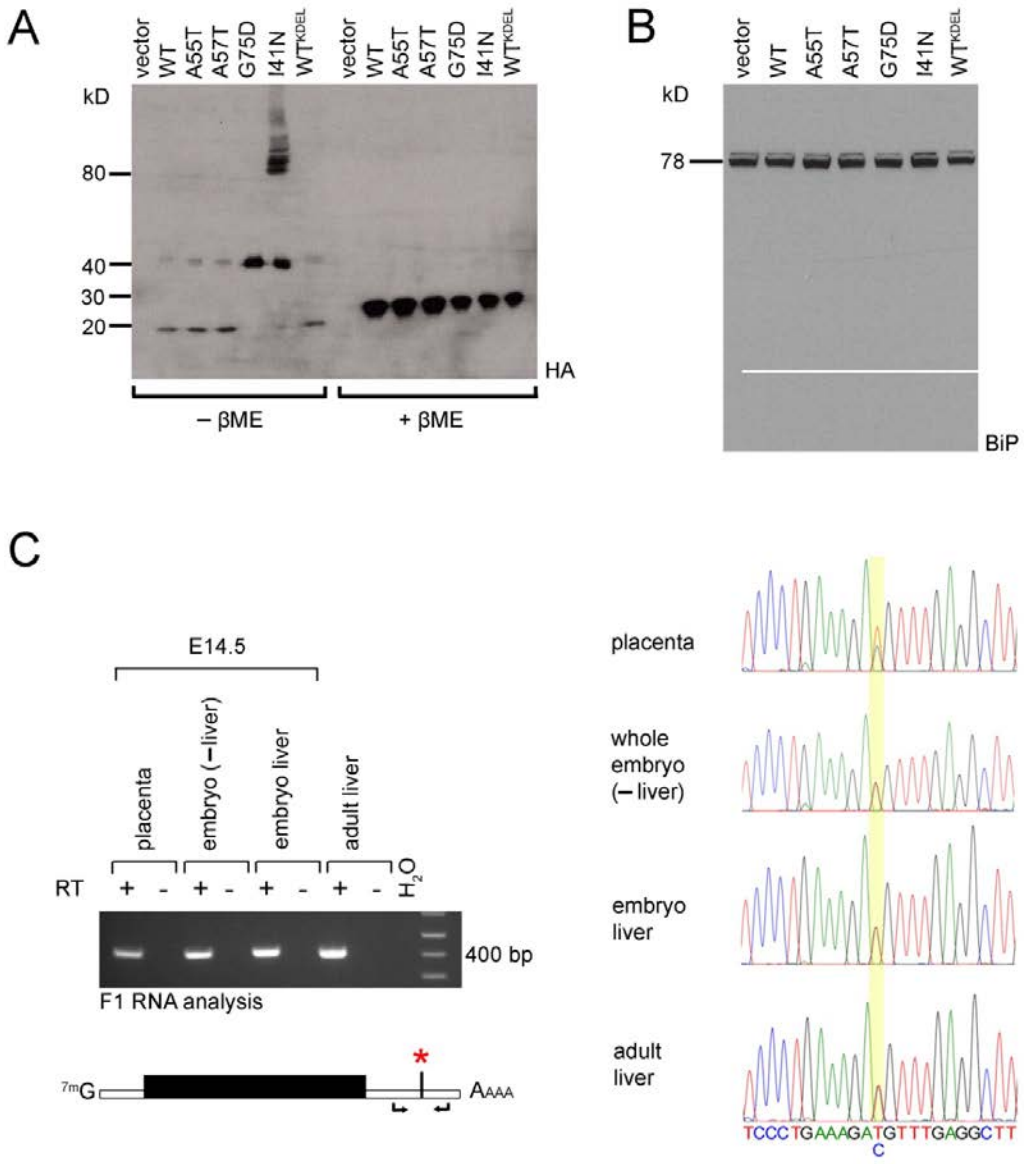
A
vector
WT
A55T
A57T
G75D
I41N
WTKDEL
kD
80
40
30
20
HA
– βME
+ βME
B
78
BiP
C
E14.5
placenta
embryo (–liver)
embryo liver
adult liver
RT
H2O
400 bp
F1 RNA analysis
7mG
AAAA
placenta
whole embryo (–liver)
embryo liver
adult liver
TCCCTGAAAGATGTTTGAGGCTT
C

Figure 2.S6. Isolation of RBP from human plasma. (**A**) Purification protocol based on Raghu *et al*, 2003. RBP was isolated from fresh blood plasma by differential precipitation in 30-60% (v/v) saturated ammonium sulfate (SAS), G-100 size exclusion chromatography in PBS (column 1) and 6M Urea PBS (column 2), and polyacrylamide gel electrophoresis (PAGE). The interaction between RBP and TTR_4 is disrupted in 6M Urea, but retinol remains bound. (**B**) Column 1 fractions (0.25 ml) from control (top) and p.A75T/+ subject (middle) plasma were monitored for protein (A_{280}) and retinol (A_{330}) absorbance, and retinol fluorescence (E_{460}). Fractions were pooled using E_{460} measurements (red shading). Note that the subject has approximately 50% retinol fluorescence compared to control, in relation to bulk plasma proteins (A_{280}). (**C**) Control column 2 fractions showing separation of RBP monomers and residual TTR_4-RBP complexes. (**D**) Denaturing polyacrylamide gel of column 2 pools showing marked enrichment of RBP. The 21 kD proteins (arrowheads) were excised for mass spectrometry. Conditioned media from HeLa cells co-transfected with RBP and TTR vectors was included as a positive control.

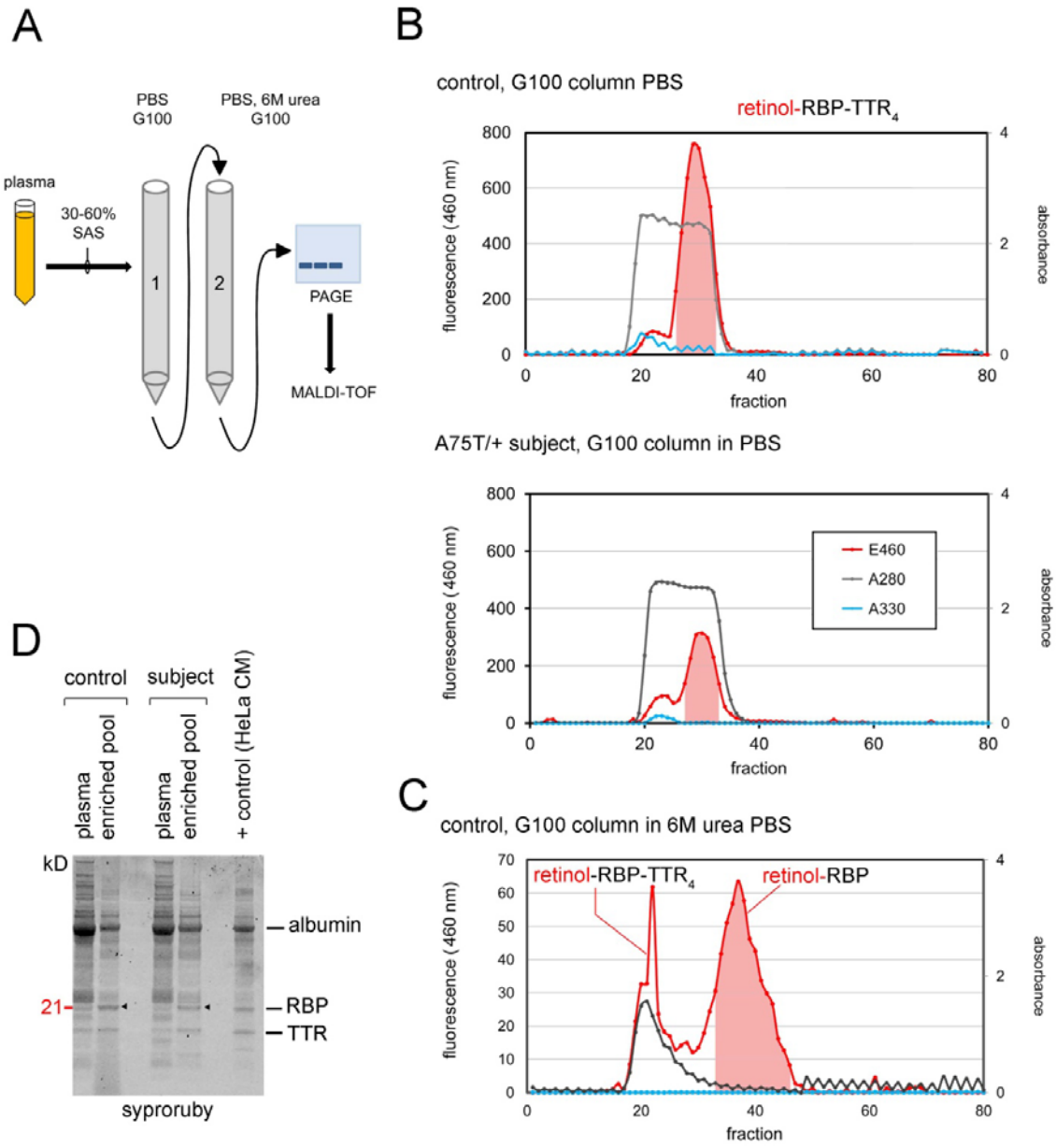
A
PBS
G100
PBS, 6M urea
G100
plasma
30-60%
SAS
1
2
PAGE
MALDI-TOF
B
control, G100 column PBS
retinol-RBP-TTR4
fluorescence (460 nm)
absorbance
fraction
A75T/+ subject, G100 column in PBS
E460
A280
A330
C
control, G100 column in 6M urea PBS
retinol-RBP-TTR4
retinol-RBP
D
control
subject
plasma
enriched pool
plasma
enriched pool
+ control (HeLa CM)
kD
21
albumin
RBP
TTR
syproruby

Figure 2.S7. MALDI-TOF spectroscopic analysis of urine RBP. (**A**) Schema for uRBP immunoprecipitation. (**B**) Western blot (WB) of whole urine from control and p.A75T/+ subject demonstrating specificity of the primary RBP antibody used for immunoprecipitation. The uRBP concentration is approximately 1% of plasma RBP. (**C**) Native coomassie gel of immunoprecipitates showing the 21 kD proteins excised for mass spectroscopy and control HeLa-conditioned media (CM). (**D**) MALDI-TOF spectra (3,100 – 3,250 m/z) of urine RBP tryptic peptides from the control and p.A75T/+ subject. The identity of peaks was verified by tandem MS/MS analysis. Wild-type RBP peptides corresponding to amino acids 29-58 were observed in both samples (3,140 and 3,156 m/z), but no A57T peptides were detected in the subject. The ratio of WT to A57T urine proteins is thus >2.

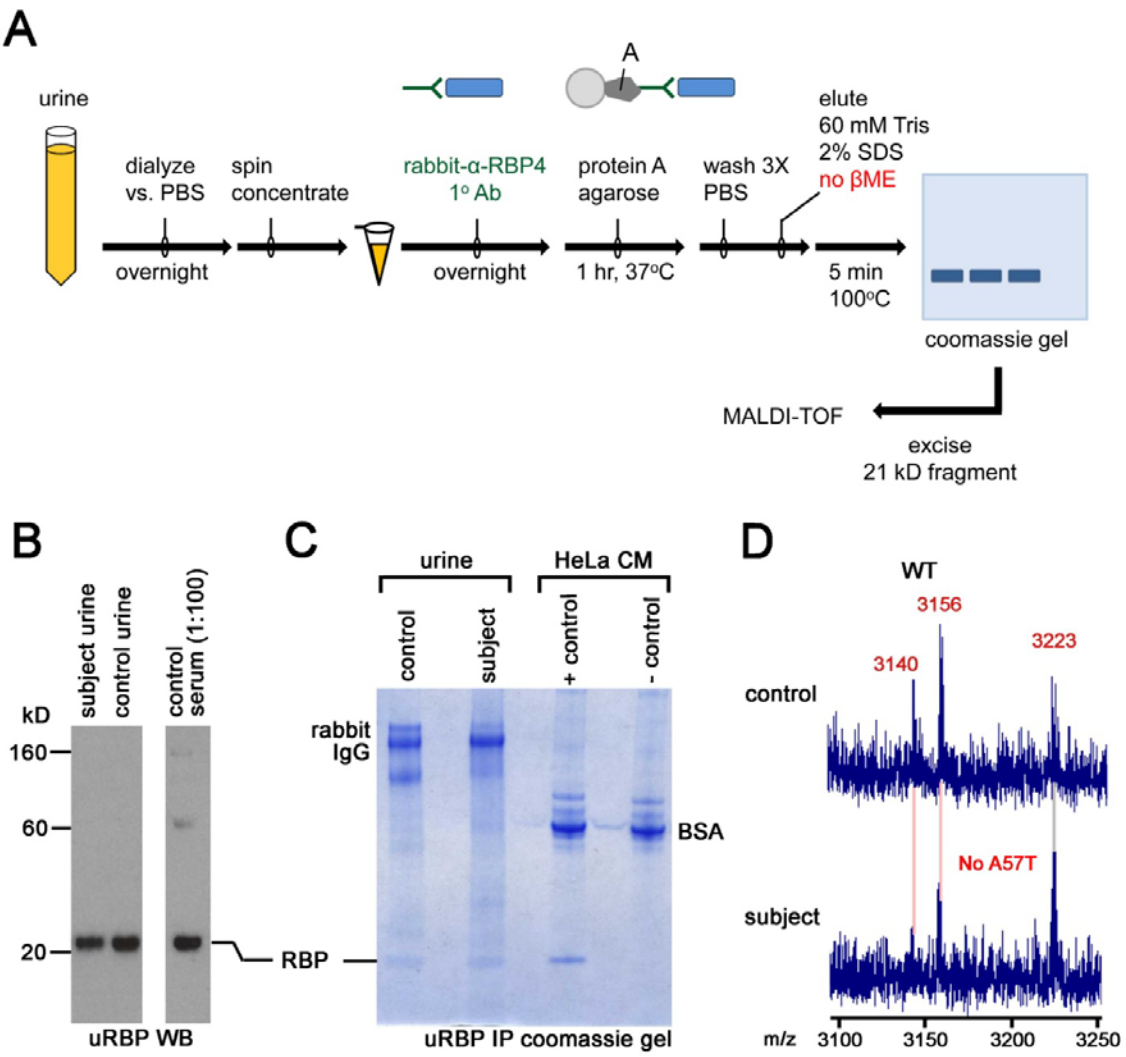
A
urine
dialyze
vs. PBS
overnight
spin
concentrate
rabbit-α-RBP4
1° Ab
overnight
A
protein A
agarose
1 hr, 37°C
wash 3X
PBS
elute
60 mM Tris
2% SDS
no βME
5 min
100°C
coomassie gel
MALDI-TOF
excise
21 kD fragment
B
subject urine
control urine
control
serum (1:100)
kD
160
60
20
RBP
uRBP WB
C
urine
HeLa CM
control
subject
+ control
- control
rabbit
IgG
BSA
uRBP IP coomassie gel
D
WT
3156
3140
3223
control
No A57T
subject
m/z
3100
3150
3200
3250

Table 2.1. Summary of clinical phenotypes

Individual	Ocular findings	Other significant findings
Family 1		
III-2	microphthalmia	
III-11	bilateral microphthalmia and coloboma	
III-12	microphthalmia and microcoria	
III-13	microphthalmia and coloboma	
III-14	microphthalmia and coloboma	
III-15	coloboma	
IV-16	bilateral anophthalmia	
VI-2	iris and chorioretinal coloboma	Birthweight = 4 lbs, 3 oz. Unaffected twin sister birthweight = 5 lbs, 1 oz.
VII-2	anophthalmia with contralateral microphthalmia and coloboma	ventricular septal defect (VSD)
VII-3	iris and retinal coloboma	atrial septal defect (ASD)
VII-5	bilateral anophthalmia	underdeveloped extraocular muscles cystic rudimentary eye removed at birth.
Family 2		
III-3	bilateral anophthalmia	mild developmental delay (motor, speech, communication) epilepsy (generalized seizures of the temporal lobe)
IV-1	bilateral microphthalmia	
Family 3		
II-2	optic pit	
III-2	microphthalmia and coloboma	

Table 2.2. Diagnostic clinical testing of p.A75T obligate carriers

	VI-2	VI-3	VI-7	Reference
Retinol	23.1	22.9	32.1*	32.5 - 78.0 mcg/dL
Retinol Binding Protein	2.2	1.9	2.8	1.5 - 6.7 mg/dL
Transthyretin	20.8	22.8	30.8	17.0 - 42.0 mg/dL

All tests were performed on 12-hour fasting blood samples.

* VI-7 was taking a steady daily course of vitamin A supplementation or retinyl palmitate, 5000 IU) plus One-A-Day prenatal vitamin (4000 IU).

All other tests were within normal limits. They include:

1. Hemoglobin A1c and fasting glucose
2. Renal panel: EGFR, sodium, potassium, chloride, CO2, urea nitrogen, creatinine, calcium, phosphorus and albumin
3. Liver panel: protein, albumin, AST, ALT, alkaline phosphatase, bilirubin (total + direct)
4. Lipid panel: cholesterol, triglycerides, HDL, LDL
5. CBCP: WBC count, RBC count, HGB, HCT, PLT, MCV, MCH, MCHC, RDW, MPV, differential and absolute counts of neutrophils, lymphocytes,
6. TPE: albumin, alpha-1, alpha-2 and beta-globulin, gamma-globulin, albumin/globulin ratio and protein electrophoresis interpretation
7. Total Vitamin D (25-Hydroxyvitamin D)

Table 2.3. Family 1 probands linkage exclusion test SSLP list

Gene	Chr	SSLP markers
VAX2	2	D2S2368, D2S286
SIX3	2	D2S391
TCF7L1	2	D2S2333, D2S388
SOX2	3	D3S1565, D3S1262
HESX1	3	D3S1289, D3S1300
FRAS1	4	D4S392, D4S2964
MSX2	5	D5S400, D5S408
SHH	7	D7S798, D7S2465
GDF6	8	D8S270, D8S1784
CHD7	8	D8S285, D8S260
VAX1	10	D10S597, D10S1693
DKK1	10	D10S196, DS101652
PAX2	10	D10S192
PAX6	11	D11S914, D11S935
FRS2	12	D12S83, D12S351
FREM2	13	D13S218, D13S263
BMP4	14	D14S276
OTX2	14	see above and below
SIX6	14	D14S63
CHX10	14	D14S258, D14S74
MCOPCB2	15	D15S1002, D15S1040
STRA6	15	D15S131, D15S205
RX/RAX	18	D18S1127, D18S64
BMP7	20	D20S100, D20S171

Other genotyped SSLP markers based on Family 1 MERLIN linkage analysis: D1S425, D1S227, D1S213, D10S1686, D10S1765, D10S185, D10S1709, D19S209, D19S894

TABLE 2.4. PCR PRIMERS FOR RBP4 MUTATION SCREENING

SDM	Size [bp]	forward primer [5'-]	Reverse primer [5'-]	MA
5'flank	801	ACTTCATCTTGCCCAGGAATC	CGCTTTTAAAGATGTTGAAACTAAA	3X
Exons 1-3*	758	GTGCTCCCTTCCCTTCACAAT	CTCCCCTTCGGTCTTTCAC	3X
Exon 4	266	GAGAAGAAACCCAGCGATTTG	TTGTGAAGGGAAGGGAGCAC	1X
Exon 5	757	CCCCTTAGTCCAAACCCACT	CGTGAGTTTCTCCGACATCTG	1X
Exon 6	600	CTCTTTTGGCACCAGTGCTT	GCATTTGAATGAAGCCAGCTC	1X

PCRs were performed using either Platinum Taq (Invitrogen) or EXPAND High Fidelity PCR [Roche] (asterisk) with 100 nM each primer, 1.5 mM $MgCl_2$ and 200 μM dNTPs. MA, Masteramp concentration [Epicentre].

Cycling conditions were 95°C x 2 min, followed by 40 cycles of [95°C x 30sec denaturation, 55°C x 60 sec annealing, 68°C x 60 sec extension], followed by 68°C x 7 min.

TABLE 2.5. RBP4, TTR AND STRA6 CLONING AND SITE-DIRECTED-MUTAGENESIS PRIMERS

cDNA PCR	Size [bp]	F/R	Primers [5'-]	MA
RBP4 WT (native)	624	F	GAATTCATGAAGTGGGTGTGGGCGCT	3X
		R	GATCATCTCGAGCTACAAAAGGTTTCTTTCTGATCTGCCATC	
RBP4 WT (HA)	651	F	GAATTCATGAAGTGGGTGTGGGCGCTCTTGCTGTTGGCGGCGCTGGGCA GCGGCCGC GCGTACCCATACGATGTTCCAGATTACGCCGAGCGCGACTGCC	3X
		R	GATCATCTCGAGCTACAAAAGGTTTCTTTCTGATCTGCCATC	
RBP4 WT (HA-KDEL)	663	F	GAATTCATGAAGTGGGTGTGGGCGCTCTTGCTGTTGGCGGCGCTGGGCA GCGGCCGC GCGTACCCATACGATGTTCCAGATTACGCCGAGCGCGACTGCC	3X
		R	GATCATCTCGAGCTAGAGCTCGTCCTTCAAAAGGTTTCTTTCTGATC	
TTR WT (myc)	495	F	GAATTCATGGCTTCTCATCGTCTGCTCCT	1X
		R	GATCATCTCGAGTCAATTCAGATCCTCTTCTGAGATGAGTTTTTGTTCT TCCTTGGG ATTGGTGACGA	
STRA6 WT (myc)	2,055	F	GATCATGGATCCATGTCGTCCCAGCCAGCAGG	3X
		R	GATCATCTCGAGTCAATTCAGATCCTCTTCTGAGATGAGTTTTTGTTCG GGCTGGGC ACCATTGGCA	

sequencing primer	Primer [5'-]
STRA6_seq1	CTGGCCACACAGCTGCAC
STRA6_seq2	GCTACATCTCAGCCTTGGTCTT
STRA6_seq3	TACACGTACCGAAACTTCTTGA

For RBP and TTR cDNA amplification, PCRs were performed using EXPAND High Fidelity PCR [Roche] with 100 nM each primer, 1.5 mM $MgCl_2$ and 200 µM dNTPs. Cycling conditions were 95°C x 2 min, followed by 30 cycles of [95°C x 30sec denaturation, 55°C x 30 sec annealing, 72°C x 60 sec extension], followed by 72°C x 7 min.

For STRA6, Pfu Ultra Taq and 1X Pfu Ultra PCR Buffer was used [Agilent]. Cycling conditions were 95°C x 5 min, followed by 30 cycles of [95°C x 30sec denaturation, 55°C x 30 sec annealing, 72°C x 120 sec extension], followed by 72°C x 7 min.

STRA6 sequencing primers were used to verify internal coding sequence post-amplification.

MA, Masteramp concentration [Epicentre]. Blue, restriction sites. Red, HA tag. Orange, myc tag.

SDM	Size [bp]	F/R	Primers [5'-]	MA
RBP4 A73T	4973	F	ACCGGCCAGATGAGCACCACAGCCAAGGGCCGAGTC	3X

		R	GGCCCTTGGCTGTGG**T**GCTCATCTGGCCGGTCTCGT	
RBP4 A75T	4973	F	AGATGAGCGCCACA**A**CCAAGGGCCGAGTCCGTCTTT	3X
		R	GACTCGGCCCTTGG**T**TGTGGCGCTCATCTGGCCGGT	
RBP4 G93D	4973	F	GCGCAGACATGGTGG**A**CACCTTCACAGACACCGAGGA	3X
		R	GTGTCTGTGAAGGTG**T**CCACCATGTCTGCGCACACGT	
RBP4 I59N	4973	F	TTCTGCAGGACAACA**A**CGTCGCGGAGTTCTCCGTGGA	3X
		R	GAGAACTCCGCGACG**T**TGTTGTCCTGCAGAACCTCT	
STRA6 WT*	12,178	F	CTCCTACCTGCTGGCC**G**GCTTTGGAATCGTGCTCTCC	3X
		R	CACGATTCCAAAGC**C**GGCCAGCAGGTAGGAGACATCC	

---

*pOTB7-STRA6 cDNA vector sold by OpenBiosystems (Cat#: MHS1011-7509230) represents STRA6 G339S. Preparation of pUS2-STRA6 WT proceeded in three steps: 1) G339S cDNA PCR amplification, 2) cloning into pUS2 and 3) site-directed mutagenesis (SDM) on pUS2-STRA6 G339S to generate the wild-type version.

All SDM reactions were performed using Pfu Ultra Taq and 1X PCR Buffer [Agilent]. Cycling conditions were 95°C x 5 min, followed by 20 cycles of [95°C x 60sec denaturation, 57°C x 60 sec annealing, 68°C x 360 sec extension], followed by 68°C x 10 min.

EXTENDED CLINICAL DESCRIPTION

Family 1. Proband VII-5 is a 6-year old female with bilateral clinical anophthalmia. Poor eye development had been suggested by prenatal ultrasound exams. She was born prematurely at 34 weeks gestation. The eyelids, palpebral conjunctivae and external ocular structures were normal, and no other birth defects were noted. Moderate hyperbilirubinemia at birth resolved with phototherapy. Magnetic resonance imaging (MRI) at 1 day revealed bilateral absence of the eye globes. The orbits contained small, cystic remnants (Right = 1.4 x 1 cm, Left = 1 cm x 4 mm and 4 x 6 mm) with thin optic nerves and a small chiasm. Extraocular muscles (EOM) were identified in coronal views, with a grossly distorted configuration on the right. No brain abnormalities were seen. At eight months, the right orbital cyst was surgically removed. Pathology showed rudimentary eye structures with calcified lentoid elements, retinal rosettes, and pigmented cells. EOM were identified histologically but were not attached to the cyst. The pregnancy was otherwise normal with no known intrauterine exposures or infections. The mother was well nourished and consumed a normal diet with standard prenatal vitamins and folate supplementation. She had a history of four miscarriages and Graves hyperthyroidism. Proband VII-5 is totally blind, but otherwise healthy.

Proband VII-2 is a 7-year old male with left anophthalmia and right microphthalmia with a ventronasal iris and chorioretinal coloboma. He was born full term by Caesarian section. Prenatal ultrasound and newborn physical exams showed no additional findings. The pregnancy was complicated by persistent nausea from weeks 5 to 14 of gestation, but there were no intrauterine exposures or infections. Brain MRI and

echocardiographic exams at age seven were normal. He has good functional vision in the right eye.

Affected male VII-3 is a 12-year old boy with a left iris and chorioretinal coloboma He also had a cardiac atrial septal defect (ASD) that was surgically repaired.

Affected female VI-2, age 42 years, is the mother of proband VII-2 and a monozygous twin. She has an inferior iris and chorioretinal coloboma in the left eye, but otherwise has good vision. Her health is otherwise excellent, with no signs of dermatological, reproductive, cardiopulmonary or immune dysfunction. Her identical twin sister (VI-3) has normal eyes. Their birth weights were 2.1 and 2.3 kgs, respectively (5th percentile for twin births).

Affected male V-16 is a 60-year old man with bilateral clinical anophthalmia, who is otherwise healthy. Six individuals in generation III, born between 1896 and 1906, were classified as affected based on family records and photographs. Their phenotypes include unilateral anophthalmia (III-2) and severe unilateral (III-12, III-14, III-15) or bilateral (III-11, III-13) microphthalmia with coloboma, variously described as ‘oblong pupils’, ‘heavy lids’, or ‘pupils at the bottom of the irises’.

Clinical laboratory data were collected from three female carriers with affected children: VI-2 (unilateral coloboma), VI-3 (normal) and VI-7 (normal). None has clinical evidence of night blindness or dry eye syndrome. Schirmer tests showed normal or mildly reduced (9-14 mm) tear production in each eye. In addition to fasting vitamin A (retinol), RBP and transthyretin (prealbumin) levels, we tested serum vitamin D, HbA1c and fasting glucose levels; renal (Na, K, Cl, HCO_3, Ca, PO_4, urea, creatinine), lipid (cholesterol, triglycerides, HDL, LDL), liver (protein, albumin, AST, ALT, ALK, total and

direct bilirubin) panels; and complete blood hematology. Apart from reduced vitamin A, the results were within normal limits.

Family 2. The proband (III-3) is a 41-year old man with bilateral clinical anophthalmia. He was born full term following an uncomplicated pregnancy, and his birth weight was normal (3.5 kg). An exam under anesthesia during infancy revealed small remnant eyes, and a right orbital encephalocele, which was surgically removed. The pathology specimen showed a cyst with loose fibrocollagenous walls, and well developed cerebral tissue interspersed with smooth and striated muscle cells. No other birth defects were noted. As a child, he exhibited mild motor developmental delay and mental retardation, characterized by delayed walking, tremors, echolalia until age seven, learning disabilities, and poor eating and sleep behavior. He also suffered from epilepsy (grand mal type), confirmed by electroencephalography, with spontaneous resolution at age 20. An MRI exam revealed no brain abnormalities.

Affected male IV-1(maternal cousin of the proband) is a 21-year old man with severe bilateral microphthalmia. In addition to congenital blindness, he experienced developmental delay similar to the proband, involving motor, learning and language impairments. Obligate carriers in the pedigree (II-2, II-3 and III-7) have normal eyes and good vision.

Family 3. Proband III-2 is a 12-year old female with left microphthalmia and a ventronasal iris coloboma. She also had capillary hemangiomas above each eyelid and on the left portion of her chest and back, consistent with cutis marmorata telangiectasia

congenita (CMTC). She was born full term following an uncomplicated pregnancy, and her birth weight was normal (4.2 kg). The mother was well nourished and consumed a normal diet with standard prenatal vitamins. The proband developed normally and has good functional vision. She is otherwise healthy. The mother reports having a unilateral optic pit.

CHAPTER III

A NOVEL INSERTIONAL TRANSLOCATION DYSREGULATING *SOX3* IN HUMAN BILATERAL ANOPHTHALMIA AND XX SEX-REVERSAL

The SOX gene family plays critical and diverse roles during vertebrate embryogenesis including CNS, skeletal, eye and sexual development. In humans, there exists a precise spatiotemporal requirement for SOX genes that often initiate vast networks of transcription factors. In this study, we present a 46,XX anatomically male child with bilateral clinical anophthalmia and female-to-male sex-reversal. Genetic analysis uncovered a 640 kb *de novo* autosomal insertion translocation of chromosome 9q21 into a genomic region proximal to *SOX3* at Xq27. The autosomal insertion contains portions of the *TRPM3* gene. The insertion site is a human-specific X-linked palindrome previously implicated in a separate congenital disorder. Our analysis shows that this insertion does not disrupt normal X chromosome silencing. In agreement with previous studies, we show that SOX3 and SOX2 have significant overlapping function in certain contexts. Furthermore, we demonstrate that elevated or ectopic SoxB1 expression in the developing eye leads to microphthalmia, poor retinal lamination and optic nerve hypoplasia/aplasia. This work is the first to test forced SoxB1 overexpression in the developing mammalian eye, and adds to the overall emerging field of regulatory mutations in complex human congenital disorders.

CONTRIBUTIONS

Chapter III will be submitted for publication as:

Chou CM, Rudolph D, Butler E, Nelson C, Glaser T. An Xq27 autosomal insertion translocation is associated with bilateral anophthalmia and XX sex-reversal.

All clinical data was collected by Dr. Christine Nelson, MD and Elizabeth Butler MS, GC. All transgenic mice were generated by the the (late) Margaret Van Keuren and Dr. Thom Saunders of the UM transgenic core. Transformation and culturing of EBV-transformed peripheral blood lymphocytes of the proband and both parents was performed by Sue Tarle. Array CGH (aCGH) was performed by Todd Ackley of the Center for Genetics in Health and Medicine (CGHM). The pd51-DC5-Luciferase construct was a generous gift of Dr. Yusuke Kamachi and Dr. Hisato Kondoh (Osaka University).

INTRODUCTION

Human congenital microphthalmia (small eyes), anophthalmia (absent eye globes) and coloboma (failure of choroid fissure closure) is a spectrum of eye diseases collectively known as MAC. In milder forms, visual impairment ranges from none to moderate, but in anophthalmia vision loss is total. The incidence of MAC is approximately 1 in 10,000 live births (Morrison et al., 2002). The phenotype can involve one or both eyes, and one-third of all cases present as part of a well-defined syndrome (Verma and Fitzpatrick, 2007). Examples include Matthew-Wood syndrome (OMIM 610745), CHARGE syndrome (OMIM 214800), Lenz microphthalmia syndrome (OMIM 309800), Branchio-oculo-facial syndrome (OMIM 113620) and Goltz syndrome (OMIM 305600).

The vertebrate eye is derived from neuroectoderm, surface ectoderm and periocular mesenchyme, and begins development around 3-6 weeks gestation in humans or embryonic day E8.5 in mice (Fuhrmann, 2010; Graw, 2003). Two optic vesicles extend bilaterally from the ventral forebrain and contact the overlying surface ectoderm. This initiates lens placode formation and subsequent optic vesicle invagination to form a bilayered optic cup. The outer layer consists of the nascent retinal pigmented epithelium (RPE) and an inner presumptive neuroretina (NR) layer. After early patterning is complete, cells in all eye compartments (lens, NR, RPE, iris, ciliary body, cornea) undergo terminal differentiation until the mature eye is formed. This entire process involves a complex interplay of cell autonomous factors and extracellular signaling pathways. FGF, BMP, Wnt and retinoic acid (RA) all play essential roles during early eye morphogenesis (Fuhrmann, 2010). Likewise, many cell intrinsic factors,

some of which are mutated in human MAC syndromes, act at the DNA level by modulating target gene expression and cell fate specification.

Advances in genetic screening techniques have revealed chromosomal disorders in an estimated 25-30% of MAC patients (Slavotinek, 2011), most often involving transcription factor or signaling pathway genes. For example, *BMP4* chromosomal interstitial deletions involving bone morphogenetic protein 4 (*BMP4*) on human chromosome 14, del(14)(q22-q23), are associated with microphthalmia and pituitary defects (Bennett et al., 1991; Elliott et al., 1993; Lemyre et al., 1998). *SOX2* is a member of the group B1 SOX (SRY-related HMG box) family that functions in CNS neural progenitor maintenance, inner ear, and eye development (Fantes et al., 2003; Graham et al., 2003; Kiernan et al., 2005). A patient with bilateral anophthalmia had a *de novo* translocation t(3;11)(q26.3;p11.2) and concomitant 740 kb deletion encompassing the entire *SOX2* gene (Fantes et al., 2003). Subsequent analysis of the coding region in other patients identified *SOX2* haploinsufficiency in approximately 10% of all MAC cases (Fantes et al., 2003; Ragge et al., 2005b). Heterozygous loss of SOX2 is the most common cause of MAC. Mutations in single genes have also been identified by candidate screening in MAC patients, and include *OTX2* (Ragge et al., 2005a), *BCOR* (Ng et al., 2004), *GDF6* (Asai-Coakwell et al., 2007; Asai-Coakwell et al., 2009; Gonzalez-Rodriguez et al., 2010), *SHH* (Schimmenti et al., 2003), *PAX6* (Glaser et al., 1994), *RAX* (Voronina et al., 2004), *CHX10* (*VSX2*) (Ferda Percin et al., 2000), *SMOC1* (Abouzeid et al., 2011; Okada et al., 2011; Rainger et al., 2011), *STRA6* (Golzio et al., 2007; Pasutto et al., 2007) and *HCCS* (Wimplinger et al., 2007).

Mammalian male sex determination is governed by the Y-linked gene *SRY* (sex-determining region Y), also known as the founding member of the SOX gene family (Koopman et al., 1991; Sekido and Lovell-Badge, 2009). In coelomic epithelial cells of the XY bipotential gonad, SRY is transiently expressed, and in conjunction with steroidogenic factor 1 (SF1), activates *SOX9*, initiating a cascade of events that specify Sertoli cell differentiation and testis formation (Sekido and Lovell-Badge, 2008). Absence of SRY in females allows for Wnt signaling to specify the female sex. Contrary to the notion that female is the "default" sex, recent evidence suggests female differentiation is an active process requiring factors like FOXL2 to inhibit the testicular pathway (i.e. *SOX9*) after birth (Uhlenhaut et al., 2009). Female-to-male XX sex-reversal is very rare, estimated to be less than 0.02% of live births (Sax, 2002). Approximately 90% of such cases are due to *SRY* translocations (Keagle, 2005). Studies indicate *SOX3*, *SOX9* or *SOX10* activation in the XX bipotential gonad (Foster et al., 1994; Polanco et al., 2010; Sutton et al., 2011) as well as homozygous loss of R-spondin 1, or *RSPO1* (Parma et al., 2006), all lead to female-to-male sex reversal in humans or mice.

In this report, we describe for the first time a *de novo* autosomal insertion translocation near *SOX3* in a child with bilateral anophthalmia and XX sex-reversal (BASR). Chromosome 9q21 genomic material, including a fraction of the *TRPM3* gene, is inserted into an Xq27 palindrome that appears to frequently mediate X-autosomal translocation events. This study not only identifies a recombination-prone disease "hotspot", but implicates *SOX3* gain-of-function regulatory mutations in bilateral anophthalmia, XX sex-reversal.

RESULTS

Bilateral anophthalmia and XX sex-reversal

The proband was born with sporadic bilateral clinical anophthalmia and a large left protruding cystic mass diagnosed as an orbital teratoma (Figure 3.1A). There was also unilateral right cryptorchidism. Radiological studies confirmed the left orbital tumor but also revealed a right retro-orbital mass coursing along the optic nerve canal up to the optic chiasm (Figure 3.1B). Extraocular muscles were present. Additional findings included agenesis of the posterior corpus callosum, inferior cerebellar vermis with prominent cistern magna and non-enchancing nodules along the ependymal border in the peritrigonal regions consistent with focal gray matter (Figure 3.1C). Clinical genetic studies displayed a 46,XX karyotype, thus defining a case of female-to-male XX sex-reversal. We confirmed the absence of SRY sequences by PCR (data not shown). There is no family history of any of the above findings.

Characterization of the left orbital tumor

The left cystic mass was surgically removed at 6 months of age and pathologically contained a rudimentary eye with ciliary body, retinal pigmented epithelium and retinal rosettes surrounded by gray matter, or neuropil (Figure 3.2A). Interspersed cartilagenous deposits and connective tissue is also observed (Figure 3.2B). The tumor as a whole is encapsulated by a thick scleral layer. We stained for axonal projections using TuJ1 and neurofilament-160 and found abundant projections throughout the tumor (Figure 3.2C). SOX9-positive glial cells appear in pockets throughout the tumor

(Figure 3.2C) but expression of other neural markers such as SOX2 or SOX3 is not detected (Figure 3.2C and 3.S1A, B). GFAP-positive glial cells are noted within the primitive eye and surrounding tumor (Figure 3.SC).

Identification of a *de novo* 9q21 duplication

We initially screened this child for the presence of *SRY* by PCR but the gene was not detected. We also looked for mutations in two other genes known to cause female-to-male sex reversal: *RSPO1* (Parma et al., 2006) and *SOX9* (Foster et al., 1994) but found no variants (data not shown). We broadened our search for *de novo* copy number variants (CNV) using genome-wide high-density SNP genotyping and discovered a 640 kb duplication of chromosome 9q21 (Figure 3,3A). The tri-allelic genotypes and signal intensities of all single nucleotide polymorphisms (SNP) in this interval were consistent with a single copy gain, or three 9q21 haplotypes. The rearrangement originated in the paternal germline based on informative genotypes (Figure 3.3B). The duplication encompasses the 5' portion of *TRPM3*, a calcium ion channel gene involved in heat nociception (Vriens et al., 2011) (Figure 3.3C) and was deleted from the paternally-inherited chromosome in a patient with autism (Pagnamenta et al., 2011). Its developmental role has not been well characterized; therefore, we screened for mouse *Trpm3* expression in embryonic eye and found transcripts at E10.5, E12.5, E14.5, E16.5, E18.6 and P1.5 (Figure 3.S3).

Breakpoint localization reveals an autosomal insertion translocation at Xq27

To further refine the breakpoints we focused on the 1.86 kb breakpoint region defined by SNPs rs1891295 and rs2309968. We designed ^{32}P-radiolabeled DNA probes targeted to single copy sequence within (probe 1) and immediately external (probe 2) to the predicted duplication breakpoint (Figure 3.3D). Based on the relative BamHI hybridization intensities of probe 2 in both blots, we narrowed our search to sequence overlying that probe. We designed inverse PCR primers on HindIII-digested genomic DNA to clone the 3.9 kb novel fragment. Inverse PCR sequencing data revealed the 9q21 duplication is an autosomal insertion translocation at Xq27 approximately 83 kb from the 3' end of the single *SOX3* exon (Figure 3.4A). The next nearest gene, *CXorf66*, is 450 kb away. We confirmed the breakpoints with forward junctional PCRs (Figure 3.4B). The insertion site is an 180 bp Xq27 palindrome (Figure 3.4B and C) previously associated with X-linked congenital hypertrichosis (Zhu et al., 2011) (Figure 3.4D). Compared to the reference genome, there is an inversion of a central 4 bp spacer sequence (TATC → GATA). Immediately telomeric is a concomitant 4 bp del(TAGC) deletion at the edge of one palindrome arm. The exact breakpoints are ambiguous due to identical overlapping sequences at each end (Figure 3.4C). No other large deletions in the *SOX3* intervening sequence or at 9q21 are detected by CNV analysis (data not shown). The proximity to *SOX3* raises its status as a top candidate gene for the pleiotropic effects seen in the proband. We hypothesized the translocation imposed a gain-of-function *SOX3* effect, causing ectopic expression in both the early developing eye and bipotential gonad. Elevated levels of ectopic SOX3 plus endogenous SOX2 protein in the embryonic eye may be detrimental to eye formation. Indeed, a gain-of-function model is strongly supported by the facts that *Sox3*$^{-/-}$ mice and humans with

SOX3 deletions have normal eyes (Rizzoti et al., 2004; Stevanovic et al., 1993). In addition, structural homology of SOX3 and SRY and their evolutionary relationship as X Y gametologs (Foster and Graves, 1994; Stevanovic et al., 1993) their shared ability to cause XX sex-reversal in mice when overexpressed (Koopman et al., 1991; Sutton et al., 2011) further supports a gain-of-function hypothesis.

Given the X-linked nature of the translocation, we wondered if the autosomal segment and surrounding regions on der(X) were subject to normal silencing by X chromosome inactivation (XCI). Previous studies have shown X-autosomal translocations are variable in their degree of autosomal inactivation (Popova et al., 2006; Sharp et al., 2002; White et al., 1998b). To our knowledge, no study has investigated XCI in the context of an autosomal insert with chromosome X sequences flanking both sides. We measured CpG island methylation status centromeric, within, and telomeric to the autosomal segment using bisulfite PCR and sequencing on peripheral blood lymphocyte DNA. We hypothesized there might be extensive hypomethylation in CpG islands within and distal to the insertion (i.e. at *SOX3*-associated CpG islands) that would permit aberrant biallelic expression and elevated SOX3 protein synthesis within individual cells. Seven Xq27 CpG islands flanking the insertion site, a single 9q21 element within the duplicated segment, and one distal Xq28 site were chosen for analysis (Figure 3.S2). Across all nine loci, we found no evidence of skewed methylation. Therefore we conclude X-chromosome inactivation proceeds normally through the autosomal segment. Standard human androgen receptor (HUMAR) assays also showed no evidence of skewed inactivation (data not shown).

Human SOX3 and SOX2 exhibit functional redundancy

SOX gene products often form heterodimeric complexes with other proteins to regulate target genes (Kondoh and Kamachi, 2010). In the lens, SOX2 is co-expressed with PAX6, and together they form a complex at the chick DC5 delta-crystallin enhancer (Kamachi et al., 2001). Both are also co-expressed in the NR as well. SOX2 and SOX3 are very closely related paralogs, sharing 92% amino acid identity (98% similarity) in the high mobility group (HMG) DNA binding domain. However, this similarity drops in the C-terminal protein interaction domain (44% identity, 60% similarity). Given the high degree of structural homology between SOX2 and SOX3, we tested SOX3-PAX6 partnering and transcriptional activation relative to SOX2-PAX6, employing a previously described DC5 luciferase assay (Figure 3.5A) (Kamachi et al., 2001). When equal amounts of SOX2- and SOX3-encoding plasmid are introduced into cells, we observe transcriptional activation levels consistent with an additive effect of both SOX proteins in their interactions with PAX6. This suggests a cooperative, and not an antagonistic effect between SOX2 and SOX3. We estimate SOX3 has approximately 50% partially overlapping cooperative transcriptional activation function with SOX2 (Figure 3.5B).

Alteration of spatiotemporal SoxB1 activity leads to structural eye defects

Given the structural and functional similarities between SOX2 and SOX3, we next tested if SoxB1 overexpression in the early mouse eye can lead to ocular malformations. Previous studies indicate overexpression of sox3 in developing zebrafish or medaka can lead to small or absent eyes (Dee et al., 2008; Koster et al., 2000). Therefore, we specifically targeted the developing neuroretina based on *SOX3* CNS

function and multiple neurologic phenotypes in the proband (brain anomalies and orbital cyst with abundant neural tissues). We modified a *Chx10* (*Vsx2*) BAC by inserting $Sox2^{HA}$-ires-Cre-pA or $Sox3^{HA}$-ires-Cre-pA cassettes into *Chx10* exon 1 (Figure 3.6A). One Chx10>Sox3 line (868) and two Chx10>Sox2 lines (217 and 317) genetically transmitted and expressed the transgene (Figure 3.6B) as confirmed by anti-HA western blot (Figure 3.6D) and GFP lineage trace (by crossing to R26*flox*GFP reporter strains). These three lines were chosen for further analysis. We mated Chx10>Sox2 founders with R26*flox*GFP homozygous mice and observed fully penetrant microphthalmia with varying severity in F1 transgenic offspring of both lines 217 and 317 (Figure 3.6C). On tissue section, we observed $Sox2^{HA}$ and $Sox3^{HA}$ expression throughout the embryonic retina of both Sox2 lines 217 and 317 as well as Sox3 line 868 (Figure 3.7A). In the adult stage for all three lines, this expression became restricted to adult bipolar cells of the inner nuclear layer (Figure 3.7D). This demonstrates apparent faithful recapitulation of the endogenous Chx10 expression pattern. Notably, the single Sox3 transgenic line (868) appeared to have completely normal eye development at all analyzed timepoints when compared to non-transgenic littermates (data not shown). We compared average eye sizes, retinal morphology and presence of cell types by immunofluorescence staining but found no significant differences between wild-type and Sox3 line 868. In contrast, lines 217 and 317 frequently had an anomalous cluster of TuJ1-positive cells posterior to the central retina at E14.5 (Figure 3.7B). This cellular aggregate also weakly expressed Brn3a, a retinal ganglion cell marker (data not shown). Another common embryonic finding was an abnormally thickened retina (Figure 3.7C). Adult retinal morphology was severely

disrupted showing poor lamination and thinning (Figure 3.7D). The ganglion cell layer was almost completely absent (Figure 3.7D, DAPI panels) explaining why the optic nerves were often missing upon enucleation. On immunofluorescence, we detected very few Brn3a-positive cells in the ganglion cell layer suggesting retinal ganglion cells were eliminated (data not shown). We tested for apoptosis during gestation using cleaved caspase-3 as a marker, but found no significantly elevated activity (data not shown).

DISCUSSION

In this report, we describe for the first time a paternally-derived *de novo* autosomal insertion translocation proximal to the X-linked gene *SOX3* (Xq27) in a 46,XX male patient with sporadic bilateral clinical anophthalmia with an orbital teratoma and XX sex-reversal (BASR). The X-linked dominance and constellation of phenotypes described herein is unlike any other known X-linked syndrome with microphthalmia or anophthalmia as a cardinal feature. Lenz microphthalmia syndrome (OMIM 309800) is an X-linked recessive trait characterized by eye, neurologic, skeletal, urogenital, dental, and cardiac malformations. Three families with Lenz-like features including anophthalmia show linkage to Xq27-28 (*ANOP1* locus); however, no individuals with female-to-male sex reversal have been reported (Forrester et al., 2001; Graham et al., 1991; Slavotinek et al., 2005). Due to its unique clinical profile, BASR likely represents a novel syndrome. The BASR translocation involves 640 kb of 9q21 autosomal sequences including portions of *TRPM3*, a gene that functions in heat nociception (Vriens et al., 2011) with no obvious role in structural development of the eye or sex

determination. We show the insertion occurred in a 180 bp near-perfect Xq27 human-specific palindrome. Collectively, the location of the 9q21 autosomal insertion, *in vitro* functional assays and transgenic mouse model analysis all suggest the developing eye may be sensitive to altered spatiotemporal activity and elevated levels of SOX transcription factor proteins. In humans, *SOX3* regulatory activating mutations may lead to a new syndrome defined by congenital eye disease and female-to-male sex reversal.

A 180-bp *SOX3* palindrome undergoes recurrent autosomal rearrangements

Inverted repeats are a class of human genomic duplications that consist of two arms of near identical DNA sequence but are inverted and complementary to one another. Analysis of chromosomal sequences shows inverted repeats are disproportionately enriched on the X chromosome relative to autosomes (Warburton et al., 2004). Palindromes are a special type of inverted repeat that form DNA secondary structures involving one (hairpin) or both (cruciform) strands. These represent weak points in the genome that often mediate sporadic translocations (Gotter et al., 2004; Kurahashi and Emanuel, 2001) and frequently cause rearrangements in cancer (Tanaka et al., 2005). The 180-bp *SOX3* palindrome contains 88 bp identical arms with a 4 bp central spacer sequence containing one mismatch. This configuration is human-specific. Chimpanzees also share both arms but are orientated in the same direction and separated by 0.6 kb of genomic sequence. Non-human primates only possess a single arm. Recently it was shown this palindrome was a target of distinct autosomal insertion translocations in X-linked congenital hypertrichosis (CGH) (Zhu et al., 2011). Here, two unrelated families with excessive hair growth over the entire body each have unique autosomal insertions

of significant size from two different chromosomes (4q31 and 5q35). There is no report of structural eye malformations or XX sex-reversal in any of the affected individuals. Thus, the phenotypic outcome in CGH and BASR is likely dictated almost exclusively by the nature of the autosomal sequences. This strongly argues against the existence of putative gonadal and eye repressors that theoretically may have been uncoupled from the *SOX3* transcription unit by the respective insertions. From these case studies, it is clear this 180 bp palindrome represents a rearrangement "hotspot" associated with multiple congenital disorders. Our genotype data demonstrate the BASR rearrangement originated in the paternal germline, consistent with an unpaired chromosome Xq during male meiosis that can serve as a substrate for aberrant recombination. This is exemplified by frequent inversions within the Factor VIII (F8) gene that cause Hemophilia A (Lakich et al., 1993).

SoxB1 knockout and overexpression in developing vertebrate tissues

The SoxB1 gene sub-family consists of *Sox1*, *Sox2* and *Sox3* and is found in many vertebrate species including humans, mice, birds and frogs (Bowles et al., 2000; Uwanogho et al., 1995; Wegner and Stolt, 2005). Based on experiments involving SoxB1 knockout and overexpression animal models along with gene profiling studies, SoxB1 factors play critical overlapping roles in central nervous system development (Bylund et al., 2003; Graham et al., 2003; Pevny et al., 1998; Wood and Episkopou, 1999; Zhao et al., 2004). *SOX3* specifically functions in CNS neural progenitor maintenance, hypothalamo-pituitary (HP) axis development and gametogenesis (Bylund et al., 2003; Laronda and Jameson, 2011; Rizzoti et al., 2004; Weiss et al., 2003).

Knockout studies and human gene deletions (Stevanovic et al., 1993) show no impact of loss of *Sox3*/*SOX3* on eye structure and function; thus, *SOX3* is considered to have a very minimal role in eye development. Instead, loss of transcriptional activity or genomic duplications encompassing *SOX3* in humans causes profound growth hormone deficiency and other endocrine issues due to pituitary defects (Burkitt Wright et al., 2009; Hol et al., 2000; Lagerstrom-Fermer et al., 1997; Laumonnier et al., 2002; Woods et al., 2005). Our proband was examined for pituitary defects but no abnormalities were found. In some instances, *SOX3* mutations are also associated with mental retardation (Hamel et al., 1996). *Sox3*$^{-/-}$ mice show severe HP axis defects consistent with human findings (Rizzoti et al., 2004), craniofacial abnormalities (Rizzoti and Lovell-Badge, 2007) and reduced fertility (Raverot et al., 2005; Weiss et al., 2003) but no ocular phenotype. Conversely, forced overexpression of sox3 in medaka and zebrafish embryos leads to small or absent eyes with additional sensory placode defects and structural CNS duplications (Dee et al., 2008; Koster et al., 2000). This finding may grossly reflect the ocular disease process in our proband. Also, the orbital cyst removed from our proband may have originated from an analogous dominant *SOX3* regulatory mechanism. This is suggested by histological evidence showing the vast majority of cyst tissue is neural in origin. We found no evidence of SOX3 expression in the cyst at birth, but this does not rule out developmental expression.

SoxB1 functional redundancy in development

Previous studies of SoxB1 factors indicate overlapping pro-neural functions (Archer et al., 2011; Collignon et al., 1996; Wegner and Stolt, 2005). Overexpression of any SoxB1

factor in chick spinal cord NPCs maintains the neural progenitor state and prohibits terminal differentiation (Bylund et al., 2003; Graham et al., 2003). Likewise, loss of one SoxB1 factor is compensated by the other two, leading to little if any phenotypic consequence later in development. In chick lens induction, Sox1, 2 and 3 have been shown to have overlapping structural and functional activities (Kamachi et al., 1998). For example, Sox2 synergizes with Pax6 in the surface ectoderm to initiate δ-crystallin lens placode formation (Kamachi et al., 2001), and this holds true for Sox1 and moderately so for Sox3. To exert their effects, SoxB1 factors form protein-protein interactions by means of their C-terminal transactivation domains (Kamachi et al., 2000). We tested the ability of human SOX3 to synergistically interact with PAX6, and found significant transactivation redundancy with SOX2 (Figure 3.5). Given the near perfect conservation of SoxB1 HMG DNA binding domains, sub-specialization of each factor arises from structural differences in the C-terminal domains, but also possibly from simple expression of one factor and inactivation of the other two (i.e. unique spatiotemporal expression patterns).

Sox2 is the only member expressed in mouse surface ectoderm for lens induction (Kamachi et al., 1998) and is the primary Sox factor in the optic cup for retinal progenitor cell (RPC) maintenance (Taranova et al., 2006). We observed extremely low levels of Sox3 neuroretinal co-localization with Sox2, but based on knockout mouse models, Sox3 contribution to retinal development is negligible. Therefore, we targeted overexpression of Sox3 or Sox2 to the early neuroretina to determine if both were capable of producing structural eye defects. Of the lines we tested, a single Sox3 line (868) revealed no ocular malformations whereas the analogous Sox2 lines showed fully

penetrant microphthalmia with abnormal retinal morphology in two of three independent lines (217 and 317). This raised the question as to whether the absence of a Sox3 overexpression phenotype is due to an inherent difference between the two paralogs or a technical limitation of the Sox3 BAC transgene. This is further complicated by the fact that only one Sox3 line (versus three Sox2 lines) passed quality control regarding genetic transmission and expression profile. While Sox2 and Sox3 exhibit high amino acid conservation within the DNA binding domain (95% identity), the C-terminal domains have significantly diverged due to the presence of Sox3 polyalanine tracts (Collignon et al., 1996). For this reason, we cannot completely rule out an inherent difference between Sox2 and Sox3 protein structure as the major cause of phenotypic discrepancy. However, the above SoxB1 studies during tissue induction all support a model of functional redundancy. Therefore, we believe the Sox2 lines (217 and 317) reflect the true phenotype of SoxB1 overexpression in the developing neuroretina. Additional Sox3 transgenic lines will need to be generated and analyzed to confirm our hypothesis.

SoxB1 downregulation in RPE is necessary for proper eye formation

Our finding necessitates the identification of ocular subcompartment(s) that are sensitive to increased SoxB1 activity; therefore, possibly leading to structural eye defects. A recent study showed that persistent expression of Sox1, 2 or 3 in the early chick RPE causes an epithelial-to-neuroretinal fate switch that severely compromises eye morphology and development (Ishii et al., 2009). Also, RPE genetic ablation using a melanocyte-specific diphtheria toxin-A “suicide” cassette leads to severe eye defects,

ranging from anophthalmia to microphthalmia with poor retinal lamination and growth (Raymond and Jackson, 1995). Loss of essential RPE signaling factors like β-catenin or its downstream targets *Mitf* and *Otx2* also produce colobomatous microphthalmia in mice (Beby et al., 2010; Hodgkinson et al., 1993; Westenskow et al., 2009). *OTX2* mutations are also associated with human congenital microphthalmia and anophthalmia (OMIM 610125) (Ragge et al., 2005a; Wyatt et al., 2008). Our findings strongly mirror those discovered in RPE genetic ablation studies, implicating the RPE as a potential target for eye malformations. It is clear that normal eye growth and morphology depends on intact RPE; therefore, studies are underway to look for potential leaky transgene expression in the early RPE of both Sox2 lines 217 and 317. The location of the anomalous cellular aggregation posterior to the central retina at E14.5 may be a clue as to RPE involvement (Figure 3.7B). These may represent retinal ganglion cell axons that failed to exit the eye due to RPE epithelial-to-neuroretinal transdifferentiation mediated by leaky Sox2 expression.

Further suggestion of RPE involvement in the pathology of our proband comes from sequences contained within the 9q21 translocation, which includes the 5' portions of *TRPM3*, specifically exons 1 and 2 and 60 kb of upstream regulatory genomic sequence. TRPM3 is a member of the human transient receptor melastatin family that functions as a selective divalent cation (Ca^{2+} and Mg^{2+}) channel (Grimm et al., 2003; Oberwinkler et al., 2005). TRPM3 is highly expressed in the kidney proximal convoluted tubule and is important for calcium homeostasis (Lee et al., 2003). Eye expression profiling shows TRPM3 and its embedded micro-RNA, miR-204, are co-expressed in fetal and adult NR and RPE (Deo et al., 2006; Karali et al., 2007). It is conceivable that

a cryptic *TRPM3* enhancer causes *SOX3* dysregulation in the RPE. The ensuing epithelial-to-neural transdifferentiation was not total, given normal XX mosaicism and presence of RPE in the rudimentary eye. However, the remaining RPE tissue was unable to support the growing neuroretina as a result of a grossly disturbed macro-environment. Likewise, the choroid plexus also expresses *TRPM3* (Deo et al., 2006) which may pinpoint the sub-ependymal gray matter nodules as additional ectopic SOX3 sites of epithelial-to-neural fate switching (Figure 3.1C). Consistent with brain malformations observed on radiological imaging (e.g. agenesis of the posterior corpus callosum, cerebellar vermis hypoplasia and enlarged 3rd and 4th ventricles), Sox3 overexpression in mouse fetal brain can produce anatomical defects leading to congenital hydrocephalus (Lee et al., 2012).

Ectopic SOX3 expression in the bipotential gonad causes XX sex-reversal

The male sex determination gene *SRY* is normally expressed in the XY bipotential gonad, binds and activates *SOX9* and initiates testis development. Of all SOX family members, SOX3 shows the highest degree of amino acid conservation with SRY in the high-mobility group (HMG) DNA binding domain (Bergstrom et al., 2000; Collignon et al., 1996). Structural similarities between SOX3 and SRY forms the basis for an original proposal of *SOX3* as a candidate XX sex-reversal gene (Graves, 1998). Transgenic studies have since shown Sox3 to cause female-to-male sex reversal when activated in the XX embryonic gonad (Sutton et al., 2011). In fact, the Sox3 HMG DNA binding domain is sufficient for testis initiation (Bergstrom et al., 2000). This is consistent with poor conservation of mammalian Sry orthologs outside of the DNA binding domain

(Bowles et al., 2000). SOX3 is also able to bind steroidogenic factor 1 and activate *SOX9* enhancer sequences in a fashion similar to SRY (Sekido and Lovell-Badge, 2008; Sutton et al., 2011). Consistent with these observations, rearrangements involving *SOX3* regulatory regions have also been reported in humans with *SRY*-negative female-to-male sex reversal (Sutton et al., 2011). In contrast, humans and mice with loss-of-function SOX3 mutations do not exhibit XX sex reversal. An increasing body of evidence continues to implicate other SOX genes in disorders of sexual development including SRY, SOX3, SOX9 and SOX10 (Bishop et al., 2000; Foster et al., 1994; Polanco et al., 2010; Sutton et al., 2011). Among them, the *Odsex* mouse is born with cataractous microphthalmia and female-to-male sex reversal, paralleling the features seen in this study. Both phenotypes are due to a long-range *cis*-acting melanocyte-specific transgene promoter inserted 1 Mb upstream of *Sox9* (Bishop et al., 2000; Qin et al., 2004). Given the strong evidence linking SOX genes to XX sex reversal, most likely SOX3 overexpression in the XX bipotential gonad of this child is the cause for this phenotype. This phenomenon only needs to occur in a small fraction of cells to trigger male sex differentiation based on XX <> XY chimera studies (Burgoyne et al., 1988). It is unknown if TRPM3 or miR-204 are expressed in the XX bipotential gonad.

SOX genes are prone to regulatory mutations

Members of the SOX gene family encode a potent class of transcription factors that are well known for evolutionarily conserved regulatory arrays capable of acting over long distances. For example, human and mouse *SOX2* are surrounded by 1.7 Mb of

genomic sequence with multiple well-characterized enhancers conserved from chicken (N1 – N4 and others) (Inoue et al., 2007; Miyagi et al., 2006; Miyagi et al., 2004; Saigou et al., 2010; Uchikawa et al., 2003). Consequently, these large regulatory regions serve as sizeable targets for rearrangements that cause disease in mice and humans. In two mouse models of deafness, *light coat and circling* (*Lcc*) and *yellow submarine* (*Ysb*), chromosomal rearrangements disrupt *Sox2* regulatory elements leading to inner ear malformations (Kiernan et al., 2005). *SOX9* illustrates the complexity underlying regulatory mutations and the disease heterogeneity that different changes at one locus can produce. In humans, mutation or deletion of *SOX9* enhancers approximately 1-2 Mb upstream cause Pierre Robin sequence (PRS, OMIM 261800), a condition defined by an underdeveloped jaw, retropositioned tongue, and cleft palate malformations (Benko et al., 2009). On the other hand, duplications within the same PRS critical region leads to a form of Cooks Syndrome (OMIM 106995) characterized by shortened digits and the absence of nails (Kurth et al., 2009). *SOX3* has been implicated in X-linked hypoparathyroidism stemming from an interstitial deletion-insertion involving 2p25 sequences near *SOX3* (Bowl et al., 2005). Within the approximate 0.8 Mb gene desert surrounding *SOX3*, there are eight highly conserved non-coding elements (HCNE) shared amongst humans to zebrafish (Navratilova et al., 2009). Five of these HCNEs are further separated in distance from the *SOX3* transcription unit by the 9q21 autosomal insertion in our proband. In isolation, many of the eight HCNEs recapitulate endogenous *Sox3* CNS expression to varying degrees (Brunelli et al., 2003; Navratilova et al., 2009; Visel et al., 2007). One ultra-conserved element (uc482) with moderate forebrain activity was deleted from the mouse genome but showed no phenotype

suggesting redundancy in the *SOX3* regulatory code (Ahituv et al., 2007). Given what has been described before and our study, regulatory SOX mutations may account for more congenital disorders than previously anticipated.

Transcriptional dysregulation by capture of a foreign promoter or enhancer is a familiar concept in human genetics and is one type of "*cis*-ruption" event (Kleinjan and Coutinho, 2009). Inversions, interstitial deletions and insertional mutagenesis, or complex combinations thereof, produce diseases that fall under this category. Aromatase excess syndrome (ARES) is characterized by high circulating estrogen levels, short stature and pre-pubertal gynecomastia (Demura et al., 2007). Aromatase is encoded by the *CYP19* gene and catalyzes a critical step in estrogen synthesis, but ARES arises when deletions or inversions juxtapose 5' regulatory enhancers next to ubiquitously expressed genes. Likewise, a *de novo* 7q inversion places Sonic hedgehog (*SHH*) under the control of an HCNE associated with another gene (*EMID2*) leading to holoprosencephaly spectrum (HPES) disorder with digital and limb anomalies (Lettice et al., 2011). Insertional translocations (IT) are a rare class due to the minimum requirement of three double-stranded DNA breaks. ITs have been described in patients with mental retardation, microcephaly, motor developmental delay and cardiac defects (Van Hemel and Eussen, 2000). Approximately 2.1% of all *de novo* cases are due to inheritance of an unbalanced rearranged chromosome from a carrier parent (Nowakowska et al., 2012); however, this is likely an underestimate when considering germline rearrangements. In BASR, a balanced rearrangement occurred in the paternal germline between chromosomes 9 and X, and of the resulting derivatives, only der(X) was transmitted to the proband. Thus, BASR and CGH are two distinct examples of

insertional translocations of autosomal sequences into a specific palindrome on Xq27 that activate a highly potent *SOX3* gene. It is evident that rearrangements mediated by this palindrome can cause a wide range of phenotypes that until now were considered etiologically distinct. Therefore, this palindrome warrants investigation for any X-linked congenital disorder with no known genetic cause. We propose the term “SOXopathy” to describe this phenomenon for all SOX family genes and associated diseases.

EXPERIMENTAL PROCEDURES

Clinical details

The proband presents as anatomically male with bilateral clinical anophthalmia. Upon further evaluation, he has a karyotype of 46,XX consistent with complete XX-sex (female-to-male) sex reversal. At birth, the left orbit contained a cystic mass that was surgically removed. Axial, coronal and sagittal orbital and brain magnetic resonance imaging confirmed the diagnosis of anophthalmos. A heterogeneously enchancing mass was seen in the left orbit consistent with the orbital teratoma. Additionally, an abnormal enhancing mass was found along the right optic nerve leading up to the chiasm. No calcifications were observed. On pathology, the left orbital cyst contained a rudimentary malformed eye with dysplastic rosettes, nervous tissue including ganglion type cells and cartilagenous deposits most prominent along the scleral wall. A diagnosis of orbital teratoma was made based on the presence of tissue derived from >2 cell lineages. The brain showed partial dysgenesis of the posterior body and splenium of the corpus callosum and inferior cerebellar vermis with a prominent cistern magna. Possible supependymal heterotopic gray matter was non-enchancing and noted bilaterally along

the peritrigonal locations. Potential septal dysplasia was noted due to an abnormally thickened anterior septum pellucidum and non-visualized posterior portion. The male genitalia were noted to have unilateral chryptorchidism. Both biological parents are normal, healthy individuals with no family history for any of these clinical findings.

Clinical studies

The proband was obtained through the University of Michigan (UM) Kellogg Eye Center Oculoplastics service. Axial, sagittal and coronal T1- and T2-weighted orbital and brain magnetic resonance imaging (echo time = 1 sec, TR = 4.7 sec, TE = 1.2 sec) was performed with gadolinium contrast or the PROPELLER technique, respectively (Forbes et al., 2001). Radiographs were interpreted by Sparrow Hospital Department of Radiology (East Lansing, MI) and UM Department of Neuro-Ophthalmology. All pathological specimens were interpreted by the UM Department of Pathology. For DNA, blood was drawn from the proband and both parents. Lymphocytes were also used to generate Epstein-Barr virus transformed lymphoblastoid cell lines. Approval was obtained from the University of Michigan institutional review board in accordance with accepted guidelines.

Orbital teratoma immunohistochemistry

We employed diaminobenzidine (DAB) staining on paraffin-embedded specimens to assess the presence of various markers associated with different cell types. Briefly, we deparaffinized tissues using Histoclear (National Diagnostics, Atlanta, GA) with brief washes in ethanol and Milli-Q water. For antigen unmasking, we boiled for 3-7 minutes

in TBS pH 9.5, allowed samples to cool for 1 hour at room temperature then blocked for 4 hours in 10% normal donkey serum (NDS) and 1% bovine serum albumin (BSA). We applied the primary antibody overnight at 4^{o}C, washed briefly then added biotin-conjugated secondary antibody for 2 hours at room temperature. For chromogenic detection, we used the avidin-biotin complex method (Vector, Burlingame, CA) with HRP (horseradish peroxidase)-conjugated streptavidin and DAB. Images were captured on an Olympus BX-51 light microscope (Olympus, Center Valley, PA). All hematoxylin and eosin (H&E) and Masson's trichrome stains were performed by the UM Department of Pathology.

Primary antibodies were rabbit-anti-Sox3 (polyclonal, 1:1000, gift from Dr. Michael Klymkowsky), rabbit-anti-Tuj1 (MRB-435P, 1:500, Covance, Princeton, NJ), rabbit-anti-Sox9 (polyclonal, 1:500, Millipore, Billerica, MA), mouse-anti-neurofilament 160 (monoclonal NN18, 1:500, Sigma Aldrich) rabbit-anti-Sox2 (polyclonal, 1:500, Abcam – discontinued), mouse-anti-GFAP (monoclonal clone G-A-5, 1:250, Sigma Aldrich).

Genetic and genomic analysis

Blood lymphocyte DNA was screened by PCR and Sanger sequencing for coding and HCNE variants. For copy number variants (CNV) analysis, we subjected whole blood genomic DNA to two microarray platforms: 1) Agilent CGH 244K and 2) Illumina 1M-Duo Beadchip arrays. Bioinformatic analysis was performed at the UM Center for Genetics and Health and Medicine (CGHM) and UM DNA sequencing core, respectively. For CNV breakpoint identification, we used inverse PCR on genomic DNA

digested with BamHI, EcoRI or HindIII (New England Biolabs, Ipswich, MA) and re-ligated overnight. We confirmed all breakpoint junctions with forward PCRs (Table S1). All reference human genome coordinates and sequences are based on the GRCh36/hg18 (March 2006) release.

Southern blot analysis

Local structural rearrangements were interrogated by Southern analysis using PCR amplicons (exons or CNEs) as substrate for probes. Briefly, genomic DNA was digested overnight using BamHI, EcoRI or HindIII, and run out 14 hrs on a 1% LE-agarose gel at 60V. Gels were denatured in 0.5 M NaOH, 1.5 M NaCl then neutralized in 8X SSC before undergoing capillary transfer overnight. Membranes were UV crosslinked and prehybridized in 50% formamide. For probe synthesis, PCR products were agarose gel-excised and ^{32}P-labeled using a random primed labeling method (Roche, Indianapolis, IN). Isotope incorporation was confirmed using a Tricarb 2000 liquid scintillation counter (Packard). Approximately 1 x 10^7 counts were added per membrane at 42^{o}C overnight. The next day, membranes were washed in 2X SSC at 55^{o}C to minimize non-specific hybridization and exposed to film at -80^{o}C from 3 – 24 hrs and developed on a Kodak A2000 developer (Kodak, Rochester, NY).

RNA analysis

Eye tissue from E10.5 and E12.5 (whole eye), E14.5, E16.5, E18.5 and P1.5 (retina) were dissected from CD-1 embryos and pups. RNA was isolated using the phenol-chloroform-isoamyl extraction method (Trizol, Invitrogen, Carlsbad, CA). Total RNA was

DNase-treated and RT-PCR was performed (SuperScript II, Invitrogen). First-strand cDNA was used for PCR using Trpm3 forward (5'- ATC CTG GAT TGA AAG AGC ATT TTA T) and reverse (5'- ATA GGA TTG GAC ATG GTC TGG TAT) primers specific to exons 4 and 8, respectively. Reactions (50 µl) were performed using Platinum Taq (Invitrogen) with 100 nM each primer, 1.5 mM $MgCl_2$ 200 µM dNTPs and 1X Masteramp concentration (Epicentre, Madison, WI). PCR products were verified by Sanger sequencing.

Bisulfite treatment and analysis

Peripheral blood lymphocyte genomic DNA was treated with sodium bisulfite (Epitect Bisulfite Kit, Qiagen). MethPrimer (Li and Dahiya, 2002; Warnecke et al., 2002) was used to design bisulfite-specific primers. Bisulfite PCRs (25 µl) used JumpStart Taq polymerase (Sigma-Adrich, St. Louis, MO) with 100 nM each primer, 1.5 mM $MgCl_2$ 200 µM dNTPs and 1X Masteramp concentration (Epicentre). For primers see Table S1. PCR products were gel-excised and TA-cloned into pCR4 (Invitrogen) and grown in chemically-competent DH5α bacterial cells (Invitrogen). At least 20 clones from each PCR were recovered, sequenced and analyzed using BiQ analyzer (Bock et al., 2005). We achieved 95% or greater conversion in all instances.

For every PCR, we created an *m* x *n* matrix where *m* = number of CpG sites and *n* = clones. To assess whether a given clone derived from X active (X_a) or inactive (X_i) we counted total number of methylated sites per clone in the mother (46, XX) and assigned the top 50^{th} percentile as X_i-derived. The lowest number of methylated sites was used as the cutoff to designate X_i if it exceeded the maximum number seen in any

clone from the father (46, XY). If not, the next lowest value in the group was chosen until this requirement was met. For the single 9q21 CpG island analyzed, the cutoff was modified to x + 1 where x = the maximum number of methylated sites in any clone from mother and father. Using these cutoffs, we counted the number of X_i- and X_a-derived clones in the child (46, XX) and assessed statistically significant deviation from the theoretical ratio using Fisher's exact test.

Expression vector cloning

We cloned the human SOX2 and SOX3 with C-terminal hemagglutin (HA) epitope tags into pUS2 (gift from D. Turner). For *SOX2* and *SOX3*, we PCR amplified both single exon genes from control genomic DNA (Table S1) and inserted them into pUS2 EcoRI and XhoI restriction sites. pCMV-PAX6 is described previously (Epstein et al., 1994). pδ51-LucII was a generous gift from Dr. Yusuke Kamachi and Dr. Hisato Kondoh (Kamachi et al., 2001). pDM-pol2-Renilla was used as a transfection control.

Tissue culture

HeLa S3 cells (ATCC, Manassas, VA) were grown in 60 mm plastic tissue culture dishes (Corning, Corning, NY) in Dulbecco's Modified Eagle Medium (DMEM) supplemented with 10% fetal bovine serum, L-glutamine (2 mM), penicillin (50 U/ml) and streptomycin (50 µg/ml). All cells were incubated at 37^{o}C, 5% CO_2 in water-jacketed tissue culture incubators.

Luciferase assay

Cells were plated at 1 x 10^6 per dish and grown until cells reached a confluency of 50%. We co-transfected cells with FuGene6 (Promega, Madison, WI) per the manufacturer protocol using a 3:1 F6:DNA ratio. Cultures grew for 48 h and harvested using the Dual Luciferase Kit (Promega) according to manufacturer instructions. Cell lysates were counted for luminescence derived from luciferase, quenched then renilla in a VICTOR^3 1420 Multilabel Counter (Perkin Elmer, Waltham, MA). Luciferase-to-renilla ratios were calculated. All datapoints were collected in triplicate.

PAGE and Western blot

Both eyes from P1 pups were pooled and solubilized in RIPA buffer. Samples were run on a 4-12% bis-tris precast minigel (Invitrogen) at 200 V, 40 minutes in 2% SDS, 5% βME boiled for 5 min. Gels were transferred overnight at 30 V then blocked in 5% bovine serum albumin, 1% non-fat milk for one hour. Primary rat-anti-HA antibody (3F10, 1:5,000, Roche) was applied for 3 hours at room temperature. Membranes were washed, incubated with horseradish peroxidase (HRP)-conjugated secondary antibody. Chemiluminescent detection was performed (ECL, GE Healthcare) and membranes exposed to film.

Transgenic mice

To faithfully express Sox2 or Sox3 in the Chx10 pattern, we generated bacterial artificial chromosome (BAC) transgenes by λRED recombineering (Lee et al., 2001). The targeting constructs were assembled with short 5' (A, 514 bp) and 3' (B, 380 bp) homology arms flanking 3.5 kb Sox^{HA}-nlsCre-FRT-amp-FRT cassette (Gene Bridges,

Heidelberg). The 5' homology arm extends from upstream genomic sequence to the exon 1 initiation codon (ATG). We also included 10 bp of endogenous Sox2 or Sox3 5' UTR sequence immediately upstream of their respective initiation (ATG) codons to promote faithful translation. The 3' homology arm is contained within intron 1. *Sox2* and *Sox3* solitary exons were engineered with a C-terminus HA epitope tag (Table S1).

Linearized targeting plasmids were used in parallel to target mouse BAC clone RP23-127O21 by λRED-mediated homologous recombination in strain SW105 (Warming et al., 2005) after heat induction. This 223 kb BAC contains 123 kb 5' and 110 kb 3' DNA flanking the *Chx10* gene. Targeted BAC clones were selected on ampicillin and chloramphenicol plates at 30^{o}C, and verified by junctional PCR and DNA sequencing. The *amp* selection cassette was then deleted by arabinose induction of *Flpe* recombinase, leaving a solitary FRT site (Andrews et al., 1985). Homogeneity and integrity of recovered Chx10>Sox2-Cre and Chx10>Sox3-Cre clones was verified by ampicillin sensitivity, junctional PCRs, restriction mapping, and pulse field gel electrophoresis.

Purified BAC transgene circular DNA was injected into fertilized (C57BL/6J x SJL/2) F2 oocytes by the UM Transgenic Animal Core. Founders were identified by transgene-specific PCR genotyping (Table S1) and lines were maintained by crossing to C57BL/6 or R26*flox*GFP reporter strains. We identified 11 founders for each transgene. We chose to analyze and maintain lines based on transmission and expression profile. The most extensively characterized transgenes in this report were Chx10>Sox2-Cre Tg 217 and 317 and Chx10>Sox3-Cre Tg 868.

Histology

Embryonic and adult eyes were fixed overnight in 4% paraformaldehyde (PFA) at 4^{o}C, cryoprotected in phosphate-buffered saline (PBS) with 10 to 30% sucrose, frozen in OCT compound (Tissue-Tek, Torrance, CA) and cryosectioned at 10 µm. For immunodetection, cryosections were blocked for 4 h at room temperature in PBTx (0.1 M $NaPO_4$ pH 7.3 0.5% Triton X-100) with 10% NDS and 1% BSA. Sections were incubated overnight with primary antibody at 4^{o}C. For fluorescence detection, sections were incubated at 2 h room temperature with appropriate secondary antibody. Nuclei were identified using 100 ng/ml 4',6-diamidino-2-phenylindole (DAPI).

Primary antibodies were rat-anti-HA (monoclonal 3F10, 1:500, Roche, Indianapolis, IN), chicken-anti-GFP (1:2000, Abcam), mouse-anti-Brn3a (monoclonal 14A6, 1:50, Santa Cruz Biotechnology), rabbit-anti-Sox2 (1:200, Abcam), rabbit-anti-Tuj1 (1:200, Covance), sheep-anti-Chx10 (1:500, Exalpha), rabbit-anti-Sox3 (polyclonal, 1:500, gift from Dr. Michael Klymkowsky) and rabbit-anti-cleaved-caspase 3 (1:100, Cell Signaling Technology).

Figure 3.1. Anterior and radiological images of a proband with bilateral anophthalmia, XX sex reversal and brain abnormalities. (**A**) Anterior photography of the proband at birth without eye globes (left) and a left orbital cystic mass (center) that was surgically removed. Pedigree illustrates a sporadic case of bilateral anophthalmia with female-to-male sex reversal (right). (**B**) Magnetic resonance imaging (MRI) performed at 1 day confirms diagnosis of bilateral anophthalmia. T1-weighted axial image reveals a heterogeneously-enhancing cystic mass (green arrow) within the left orbit. A similar appearing mass also appears along the course of the right optic tracts up to the optic chiasm (yellow arrow). T1-coronal view (center) shows both left and right orbital masses (green and yellow arrows, respectively) and the presence of extraocular muscles bilaterally (arrowheads). T1-sagittal image (right) shows agenesis of the posterior corpus callosum at birth (asterisk). (**C**) Post-surgical removal of the left orbital cyst T1- and T2-weighted MR studies performed at 1.5 years (top row) and 2.5 years (bottom row). T1-weighted axial image (top left) shows prosthetic ocular implant in both orbits (Pr). The right soft tissue lesion (arrow) remains unchanged. Coronal T2-weighted image (top center) demonstrates peritrigonal sup-ependymal nodules isotopic to gray matter (arrowheads). T1-weighted sagittal section (top right) shows no changes with the corpus callosum (asterisk). Axial T1-weighted image at 2.5 years (bottom left) reveals little change with right orbital mass (arrow), but absence of a prosthetic globe in the left orbit replaced by significantly irregular tissue consistent with previous surgical scar tissue. Axial T2-weighted PROPELLER image (bottom center) shows gray matter foci along the lateral ventricles (arrowheads). Sagittal T1-FLAIR image again shows truncation of the posterior corpus callosum with minimal change on brain morphology. Myelination pattern is normal for this child. R, right; L, left; A, anterior; P, posterior.

A

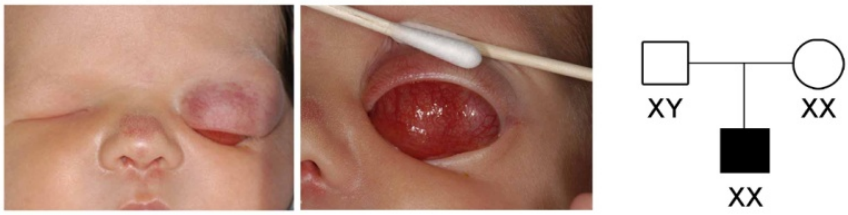

B

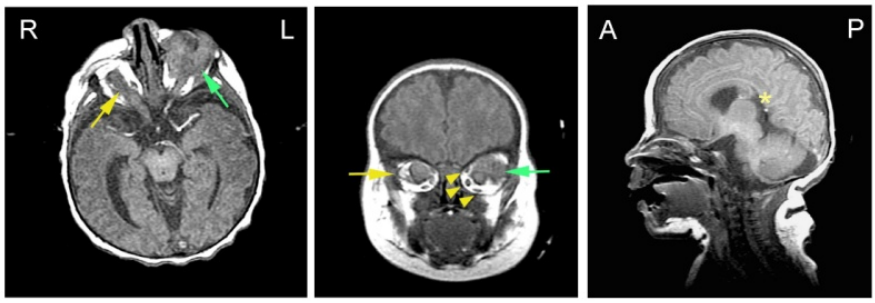

C

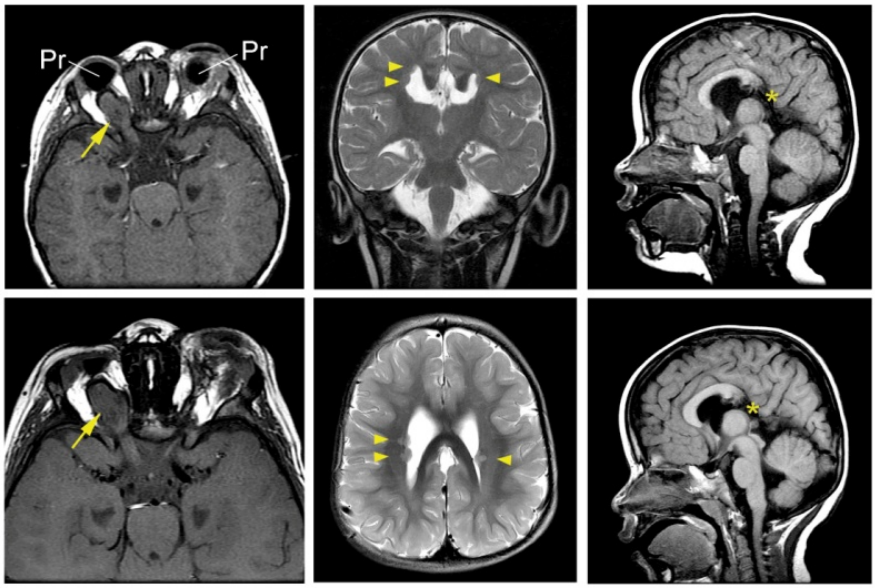

Figure 3.2. The left orbital cyst is predominantly neural and contains a rudimentary eye. (**A**) Hemotoxylin and eosin staining shows presence of a rudimentary eye containing retinal rosettes (rr) and possible ciliary body and retinal pigmented epithelium. Inset (red box) shows high magnification retinal rosette and presence of all retinal layers. A, anterior; P, posterior; Scale bar, 1 mm. (**B**) Masson's trichrome stain reveals pockets of cartilaginous tissue (c) and connective tissue (ct) throughout the primitive eye (left). Histology in a representative section elsewhere in the orbital mass (right) shows mostly neuropil tissue (n). (**C**) Diaminobenzidine (DAB) stain using anti-TuJ1primary antibody reveals tracts of axonal projections (a) amidst neuropil (n). Anti-Neurofilament 160 staining confirms the presence of neural axons (top right). Anti-Sox9 stain demonstrates pockets of Sox9 expressing cells, possibly glial or chondrocytic in origin (bottom left). Anti-Sox2 stain reveals extremely sparse and weak expression throughout the mass (bottom right). Insets show higher magnification. Scale bar, 1 mm.

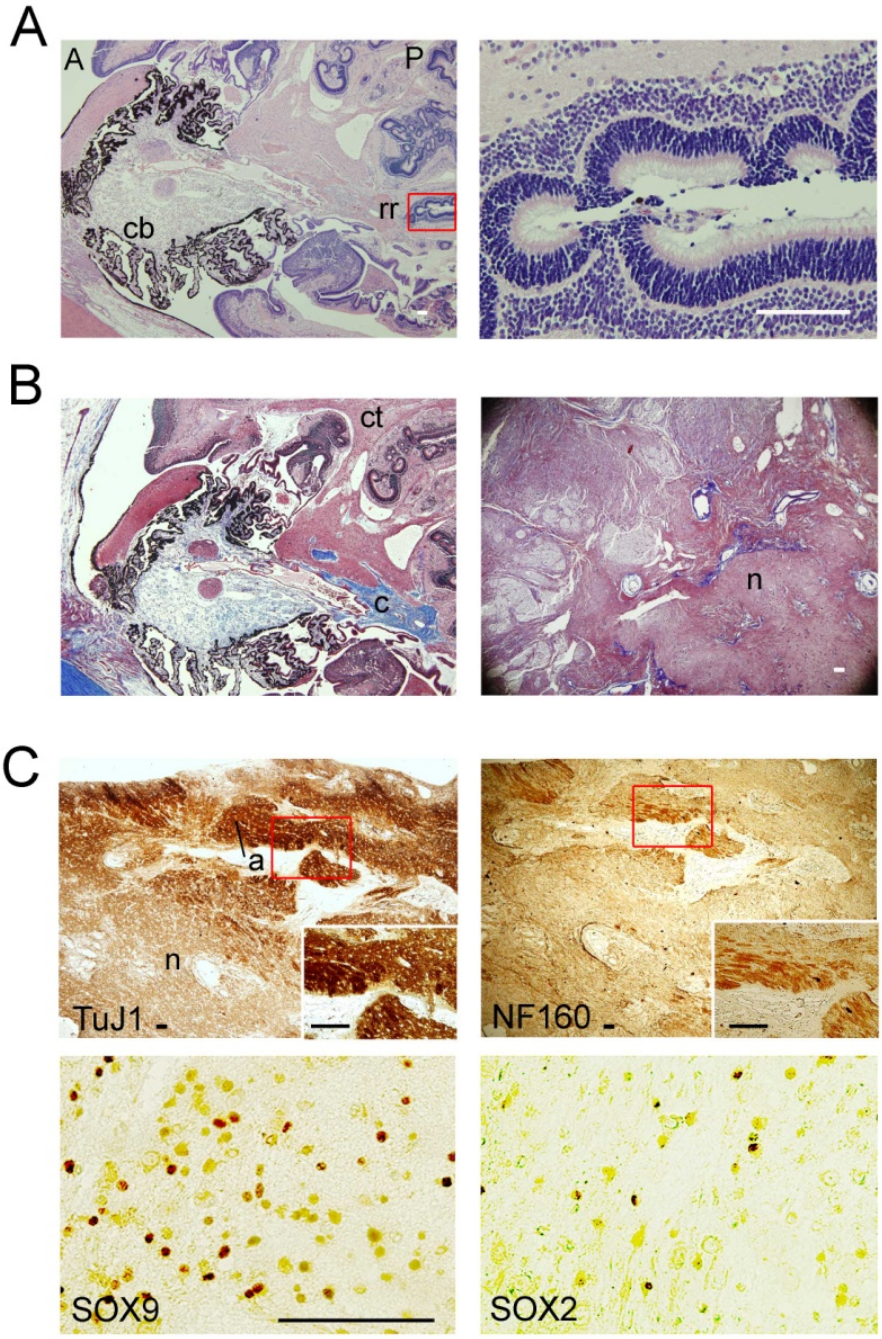
A
A
P
cb
rr
B
ct
c
n
C
a
n
TuJ1
NF160
SOX9
SOX2

Figure 3.3. Copy number variation analysis reveals a *de novo* 9q21 duplication. (A) High-density SNP genotyping in the proband and both parents reveals a *de novo* 9q21 duplication approximately 640 kb in size (yellow box). B-allele frequency (BAF) plot shows genotypes consistent with three alleles at each SNP locus (left panels). SNPs rs1891295 and rs2309968 were used for breakpoint analysis (red circles). Log *R* ratio (LRR) plots show increased signal intensity within this interval for only the child. Red line, moving average plot (window = 50 SNPs). BAF and LRR values are consistent with a single copy gain. (**B**) Genotypic analysis at multiple informative SNPs reveals three haplotypes consistent with a paternal origin (red). (**C**) Physical map of 9q21 showing the duplication contains the 5' portion of *TRPM3*, a calcium ion channel gene, and is delimited by rs3812530 and rs1891295. The true telomeric breakpoint lies in a 1.8 kb stretch between rs1891295 and rs2309968 and was chosen for further analysis. (**D**) Southern analysis at the 9q21 telomeric end using internal and flanking probes (1 and 2, respectively) relative to the predicted duplication (yellow bar) reveals novel fragments (arrowheads). Comparing novel fragment sizes to the expected size and relative signal intensities of the BamHI fragments for both probes, probe 2 was predicted to overlie the true breakpoint. To clone the 3.9 kb HindIII fragment (red arrowhead) we designed inverse PCR primers (red arrows). Restriction map is included (E, EcoRI; H, HindIII; B, BamHI).

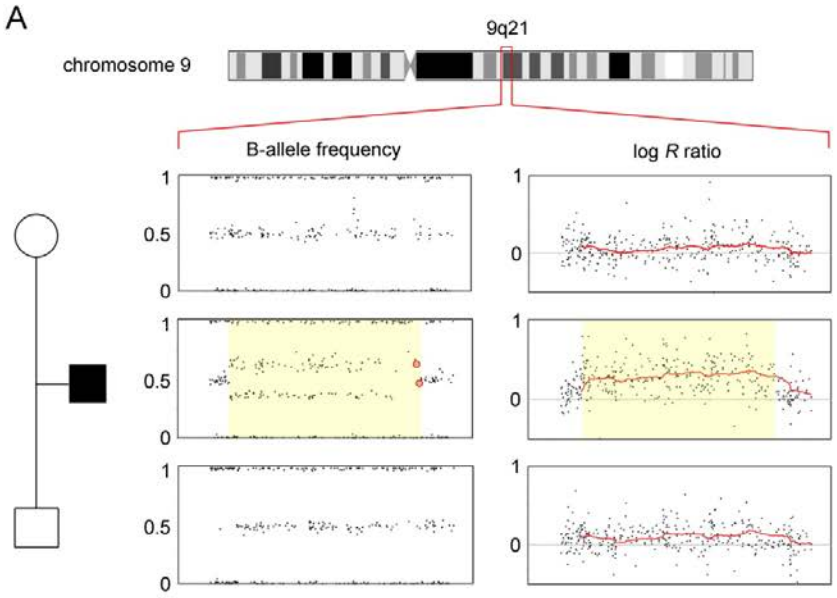
A
chromosome 9
9q21
B-allele frequency
log R ratio
1
0.5
0
1
0
B
mother child father
rs11142636 AA ABB BB
rs1337033 BB BAA AA
rs7046928 AA AAB AB
rs1742220 BB BBA BA
C
72.3 72.5 72.7 72.9 73.1 73.3 73.5 Mb
9q21.11 9q21.12 9q21.13
ex2
ex1
rs3812530 rs1891295 rs2309968

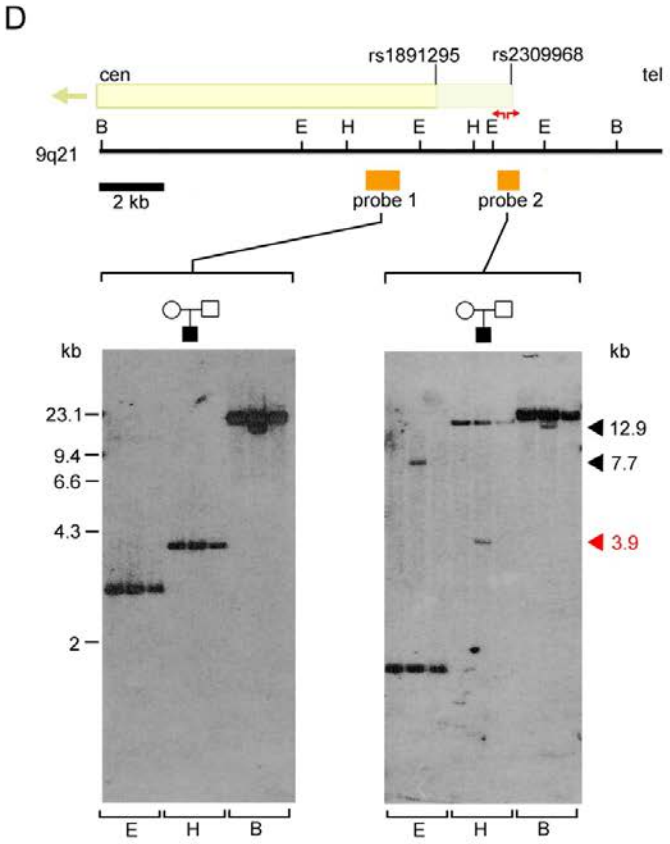
D
cen
tel
rs1891295 rs2309968
B E H E H E E B
9q21
2 kb
probe 1
probe 2
kb
23.1
9.4
6.6
4.3
2
12.9
7.7
3.9
E H B
E H B

Figure 3.4. Inverse PCR reveals a 9q21 autosomal insertion translocation at Xq27 near *SOX3*. (**A**) Inverse PCR sequence data shows the 640 kb duplicated segment (green) inserted into Xq27 downstream of *SOX3*. Neighboring genes are shown. On der(X), the orientation of the two alternate *TRPM3* promoters is opposite to that of *SOX3*. (**B**) Local view of the Xq27 insertion site located 83 kb on the 3' end of *SOX3*. A human-specific 190 bp near-perfect palindrome with two identical 88 bp arms (blue) and a 4 bp TATC central spacer sequence is flanked by repeat elements (gray bars). The 9q21 autosomal segment (green) is inserted at the palindrome center coinciding with a 4 bp del(TAGC) of the telomeric arm. Forward X centromeric and telomeric junction PCRs show this is unique to the proband. Junction chromatograms are shown. (**C**) Expanded sequence view comparing both centromeric (Xq-9q) and telomeric (9q-Xq) junctions. Chromosome 9 (red) and X (black) sequences reveal a central inversion (marked by 'X') and an adjacent 4 bp deletion. The telomeric breakpoint is ambiguous (green) due to a TTA trinucleotide match. Blue lines, identical palindrome arms. (**D**) Comparison of possible BASR breakpoints relative to two previously described insertions in familial X-linked congenital hypertrichosis in Chinese (CGHcn) and Mexican (CGHmx) families (Zhu et al., 2011).

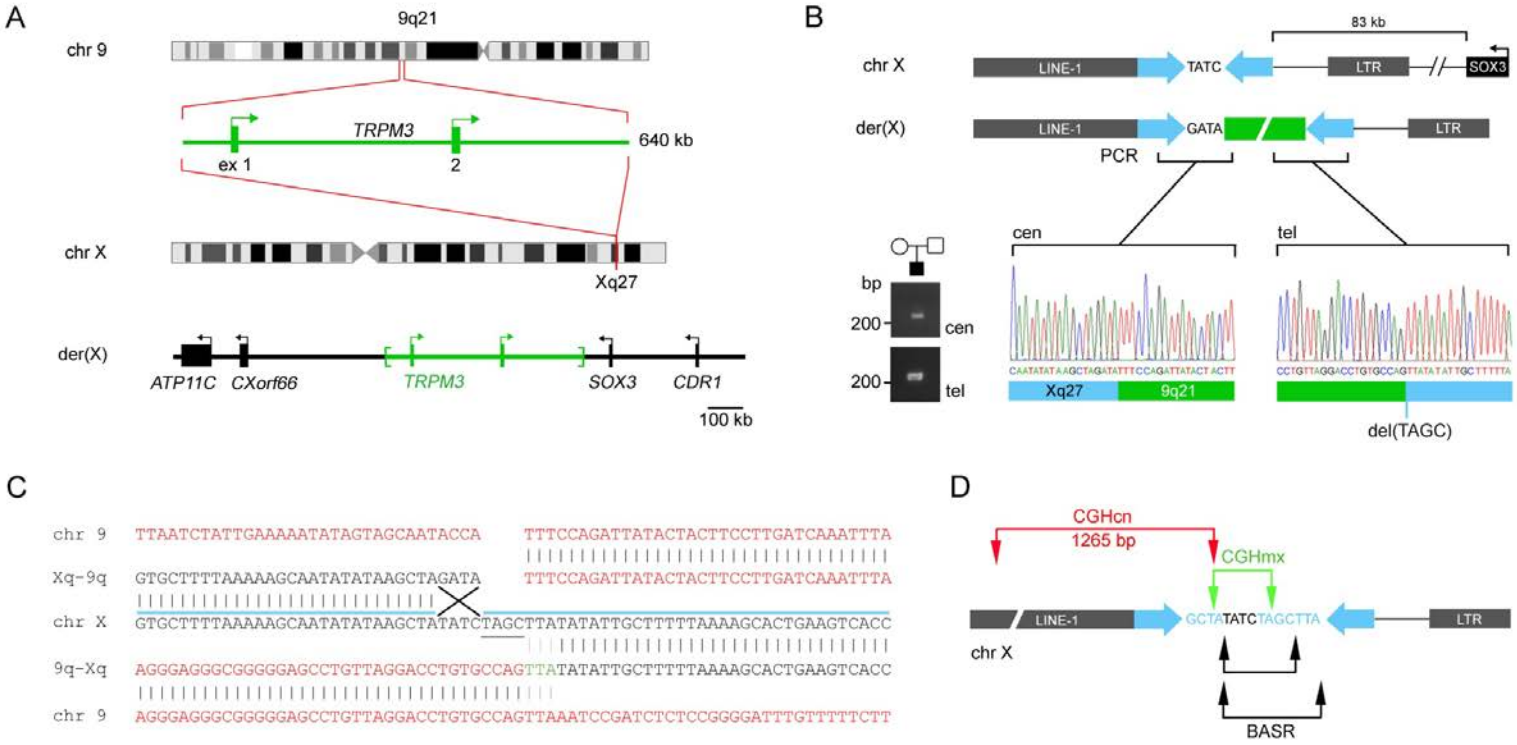
A
9q21
chr 9
TRPM3
640 kb
ex 1
2
chr X
Xq27
der(X)
ATP11C
CXorf66
TRPM3
SOX3
CDR1
100 kb
B
83 kb
chr X
LINE-1
TATC
LTR
SOX3
der(X)
LINE-1
GATA
LTR
PCR
cen
tel
bp
200
cen
200
tel
Xq27
9q21
del(TAGC)
C
chr 9 TTAATCTATTGAAAAATATAGTAGCAATACCA TTTCCAGATTATACTACTTCCTTGATCAAATTTA
Xq-9q GTGCTTTTAAAAAGCAATATATAAGCTAGATA TTTCCAGATTATACTACTTCCTTGATCAAATTTA
chr X GTGCTTTTAAAAAGCAATATATAAGCTATATCTAGCTTATATATTGCTTTTTAAAAGCACTGAAGTCACC
9q-Xq AGGGAGGGCGGGGGAGCCTGTTAGGACCTGTGCCAGTTATATATTGCTTTTTAAAAGCACTGAAGTCACC
chr 9 AGGGAGGGCGGGGGAGCCTGTTAGGACCTGTGCCAGTTAAATCCGATCTCTCCGGGGATTTGTTTTTCTT
D
CGHcn
1265 bp
CGHmx
LINE-1
GCTATATCTAGCTTA
LTR
chr X
BASR

Figure 3.5. Human SOX3 and SOX2 have overlapping functions. (**A**) Schematic of the SOX luciferase assay with a DC5-Luciferase reporter and all possible combinations of SOX2, SOX3 or PAX6 cDNA expression plasmids. (**B**) Normalized luminescence values show SOX3, in addition to SOX2, can interact with PAX6 at a known SOX2 enhancer and activate gene transcription, demonstrating functional overlap (red bar). Error bars denote standard deviation.

A

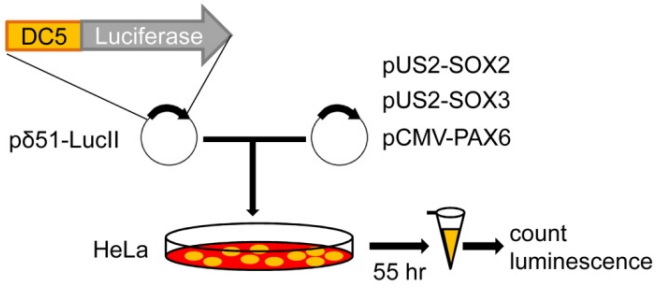
DC5
Luciferase
pδ51-LucII
pUS2-SOX2
pUS2-SOX3
pCMV-PAX6
HeLa
55 hr
count
luminescence

B

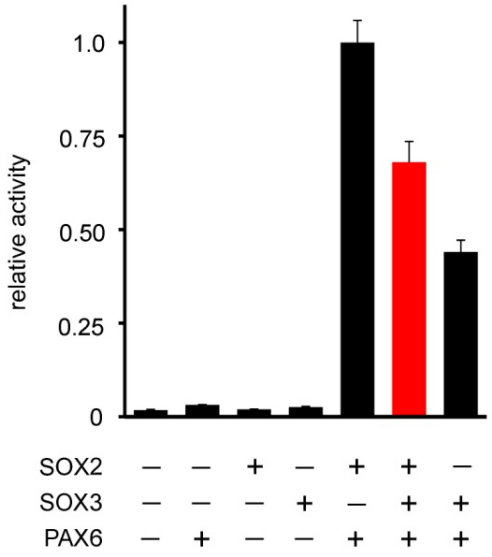
relative activity
1.0
0.75
0.50
0.25
0
SOX2 – – + – + + –
SOX3 – – – + – + +
PAX6 – + – – + + +

Figure 3.6. SoxB1 transgenic mouse models exhibit ocular malformations. (**A**) λRED recombineering strategy utilizing a Chx10 (Vsx2) bacterial artificial chromosome (BAC). A $Sox2^{HA}$ or $Sox3^{HA}$ (red bars) ires-Cre cassette (yellow and green bars, respectively) was engineered to replace Chx10 exon 1 using flanking homology arms (grey and light blue bars). Positive insertion was selected by ampicillin resistance conferred by frt-AMP-frt (purple), and was subsequently removed by FLP recombination leaving a single frt site. Final BAC transgenes are shown (bottom). (**B**) Table enumerating number of founders, successful offspring transmission, neonatal expression pattern, and ocular phenotype (if any). Neonatal expression was determined by crossing founders to R26*flox*GFP homozygotes and analyzing F1 GFP expression at birth. Both Chx10>Sox2 lines with small eyes (217 and 317) exhibited full expression. A single full expressing Chx10>Sox3 line (868) showed no phenotype. (**C**) Gross eye photographs in adults and embryonic day E14.5 embryos for lines 217 and 317 demonstrate microphthalmia. In some cases severities differed even among littermates (left panel). (**D**) Confirmation of post-natal day 1 transgene expression in lines 217, 317 and 868 by anti-hemagglutin (HA) western blot shows a major form at 45 kD corresponding to the expected sizes of $Sox2^{HA}$ and $Sox3^{HA}$. A slightly larger form at 47-48 kD is observed but does not correspond to any known post-translational modification. Anti-Sox2 or anti-Sox3 primary antibodies detect endogenous protein but do not detect the HA-tagged species based on band intensities. This most likely stems from C-terminus epitope sites that are modified beyond recognition by the HA-tag. Cre genotyping PCRs confirm transgene specificity.

A

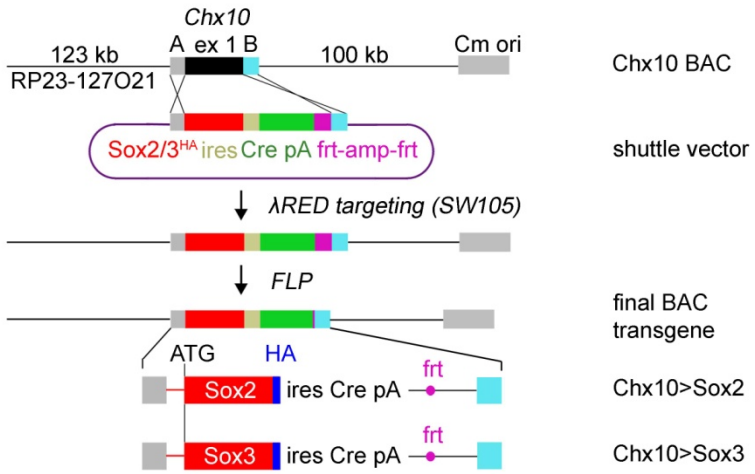

B

	# founders	transmit	neonatal expression: full	neonatal expression: mosaic	neonatal expression: none	small eyes
Chx10>Sox2	11	8 / 10	3	1	0	2 / 8
Chx10>Sox3	11	7 / 10	1	1	2	0 / 7

C

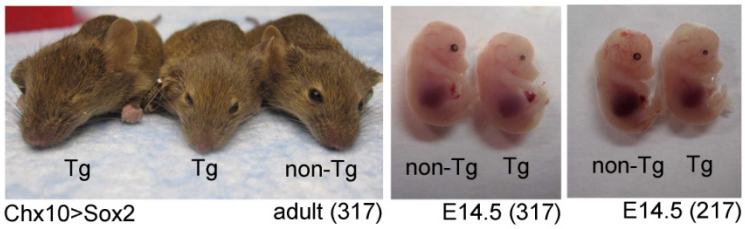

Chx10>Sox2 adult (317) E14.5 (317) E14.5 (217)

D

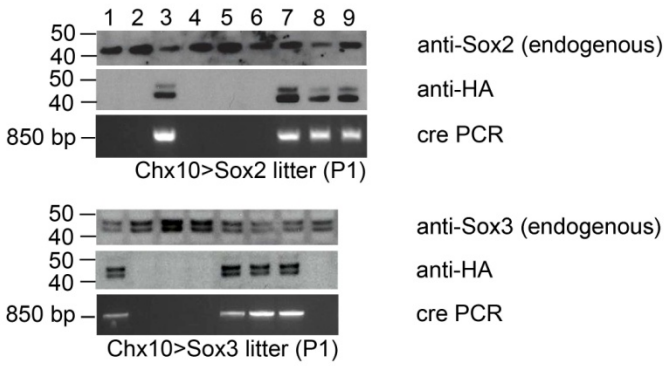

Figure 3.7. Sox2 overexpression causes small eyes with poor retinal lamination and cellular aggregates. (**A**) E14.5 embryonic eye tissue section immunostaining shows faithful and robust transgene expression in the retinoblast layer of the retina (left panels). Line 317 is representative for both Sox2 lines. Lineage tracing reveals GFP expression throughout the retina (center panels). Merge (right panels). All patterns are consistent with Chx10 endogenous expression beginning at E10 in the optic cup inner retinal layer. (**B**) Abnormal cellular aggregates posterior to the central E14.5 retina are positive for neural marker TuJ1 and GFP (top row). A non-penetrant transgenic littermate is shown for comparison at lower magnification (bottom row). (**C**) In other cases, the E14.5 retina appears thickened and dysmorphic (top row versus bottom row). This often accompanies the cellular aggregates seen in (B). A non-penetrant littermate is provided for comparison at lower magnification (bottom row). (**D**) Confocal microscopy shows adult retinal morphology is compromised in both Sox2 lines 317 and 217 (latter not shown; see third column). $Sox2^{HA}$ is limited to the bipolar cells of the inner nuclear layer (INL) and all mature cells of the retina express GFP as predicted (first and second columns). Merged images (fourth column). ONL, outer nuclear layer; INL, inner nuclear layer, GCL, ganglion cell layer. Scale bar, 200 μm.

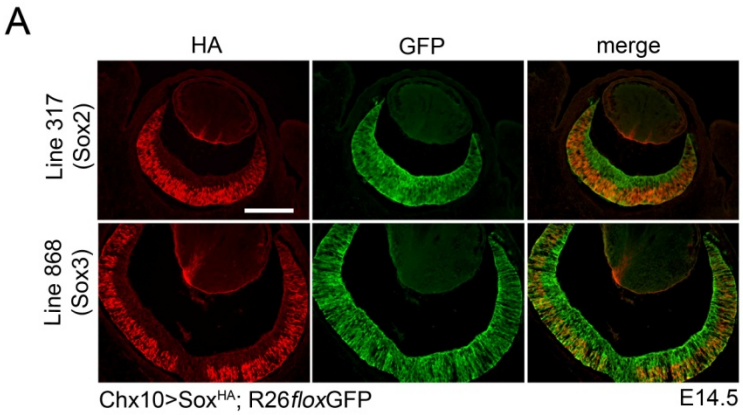
A
HA
GFP
merge
Line 317 (Sox2)
Line 868 (Sox3)
Chx10>Sox^HA; R26floxGFP
E14.5

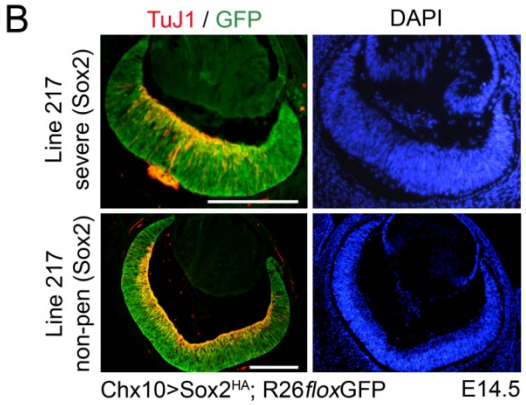
B
TuJ1 / GFP
DAPI
Line 217 severe (Sox2)
Line 217 non-pen (Sox2)
Chx10>Sox2^HA; R26floxGFP
E14.5

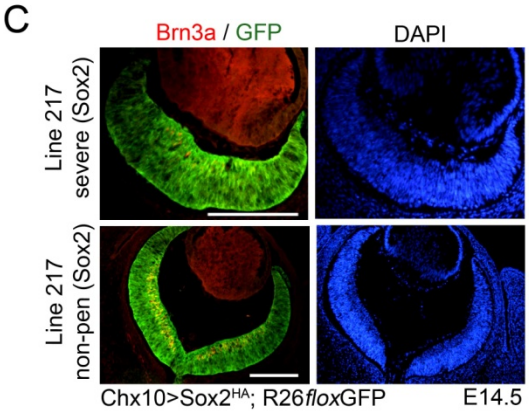
C
Brn3a / GFP
DAPI
Line 217 severe (Sox2)
Line 217 non-pen (Sox2)
Chx10>Sox2^HA; R26floxGFP
E14.5

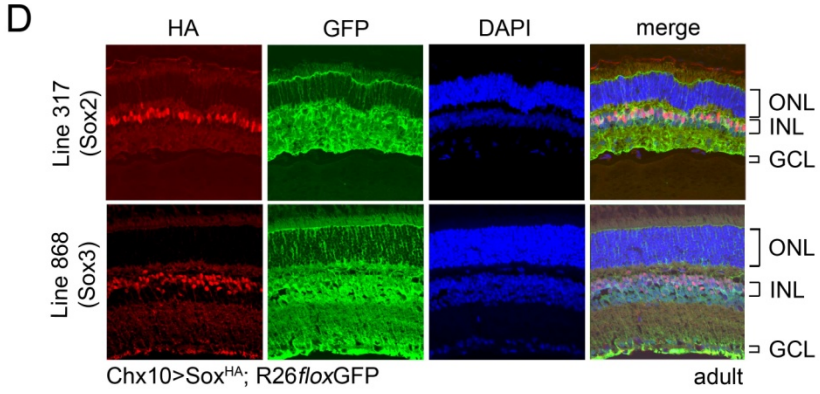
D
HA
GFP
DAPI
merge
Line 317 (Sox2)
Line 868 (Sox3)
ONL
INL
GCL
ONL
INL
GCL
Chx10>Sox^HA; R26floxGFP
adult

Figure 3.S1. Additional left orbital tumor characterization. (**A**) The cystic mass is completely SOX3 negative. Shown are three representative slides sampling different regions of the tumor, none of which have appreciable SOX3 detection. (**B**) Anti-SOX2 immunostain reveals sparse and weakly expressing pockets of cells in the aborted eye tissue (left) specifcally within retinal rosettes (center). Collections of SOX2-positive cells are found in the surrounding neuropil (right). (**C**) Abundant deposits of GFAP-expressing glial cells can be found within the remnant eye (left). Inset shows magnified image (center). Elsewhere in the tumor, morphologically-appearing glial cells are observed expressing GFAP (right panel). Scale bar, 250 μm.

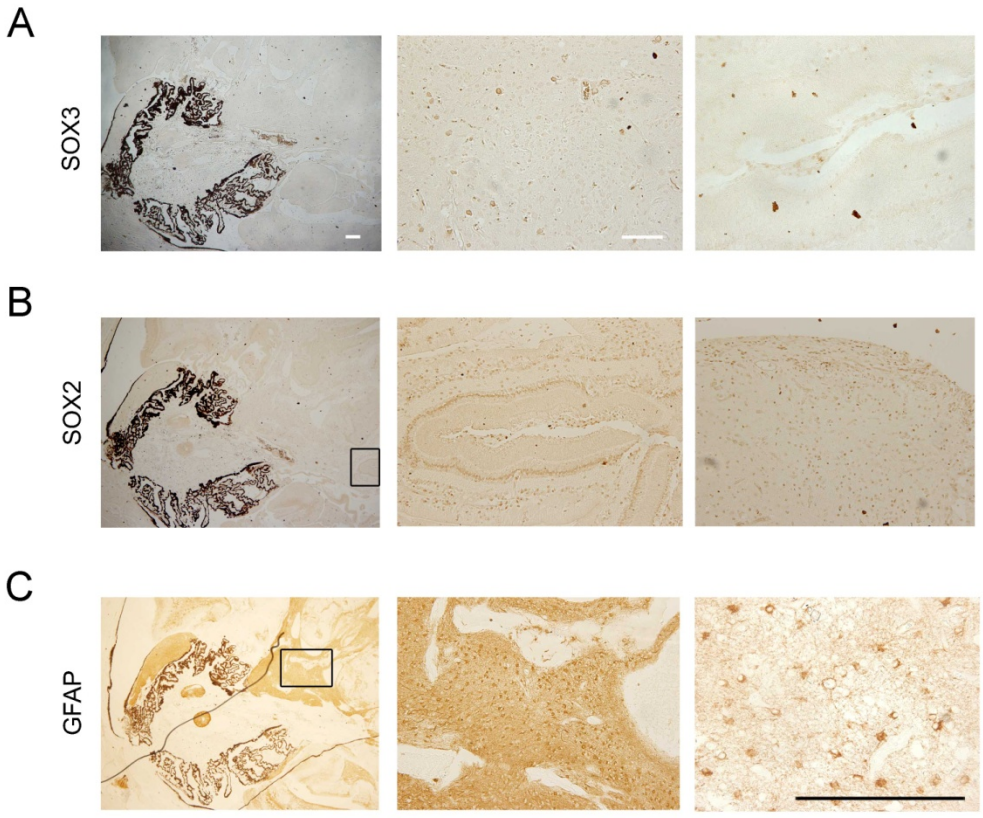
A
SOX3
B
SOX2
C
GFAP

Figure 3.S2. X-chromosome inactivation is not disrupted in the proband. (A) Physical map of der(X) shows all nine CpG islands tested for methylation status (green boxes; see UCSC genome browser hg18). These are positioned within and flanking both sides of the 9q21 insertion translocation at Xq27. One Xq28 CpG island was chosen to assay for X-chromosome inactivation (XCI) at further distances beyond Xq27. Relative positions of known genes are shown. (B) An example of CpG methylation analysis for CpG 65, the sole island within the autosomal insertion. Assuming normal XCI, the expected fraction of clones derived from $X_{inactive}$ is one-sixth. Of 29 random clones, six are designated as Xi (see Methods) in the proband consistent with normal XCI. Open circle, unmethylated, filled circle, methylated. Statistical significance is measured using Fisher's Exact Test. Numbers denote CpG islands relative to the transcriptional start site (defined as +1).

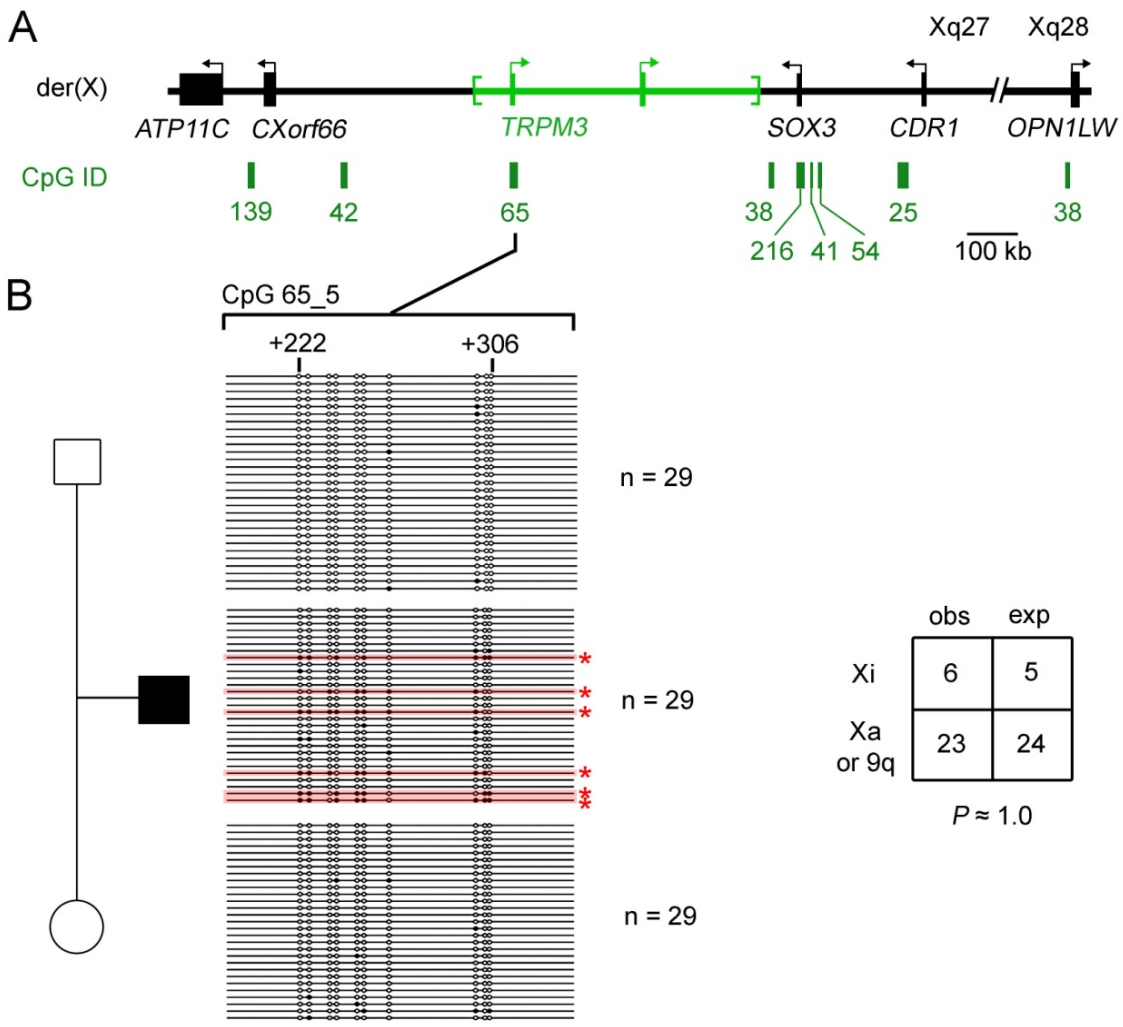
A
Xq27
Xq28
der(X)
ATP11C
CXorf66
TRPM3
SOX3
CDR1
OPN1LW
CpG ID
139
42
65
38
216
41
54
25
38
100 kb
B
CpG 65_5
+222
+306
n = 29
n = 29
n = 29
obs
exp
Xi
6
5
Xa
or 9q
23
24
P ≈ 1.0

Figure 3.S3. Trpm3 is expressed in the embryonic eye throughout gestation. (A) Physical map showing all mouse Trpm3 isoforms (mouse genome build mm9, July 2007). We designed RT-PCR primers spanning exons 4 through 8 that are contained in nearly all isoforms. (B) PCR gel showing Trpm3 transcripts detected in embryonic eye tissues at all gestational timepoints (E10.5, E12.5, E14.5, E16.5, E18.5 and P1; top panel). β-actin control (bottom panel).

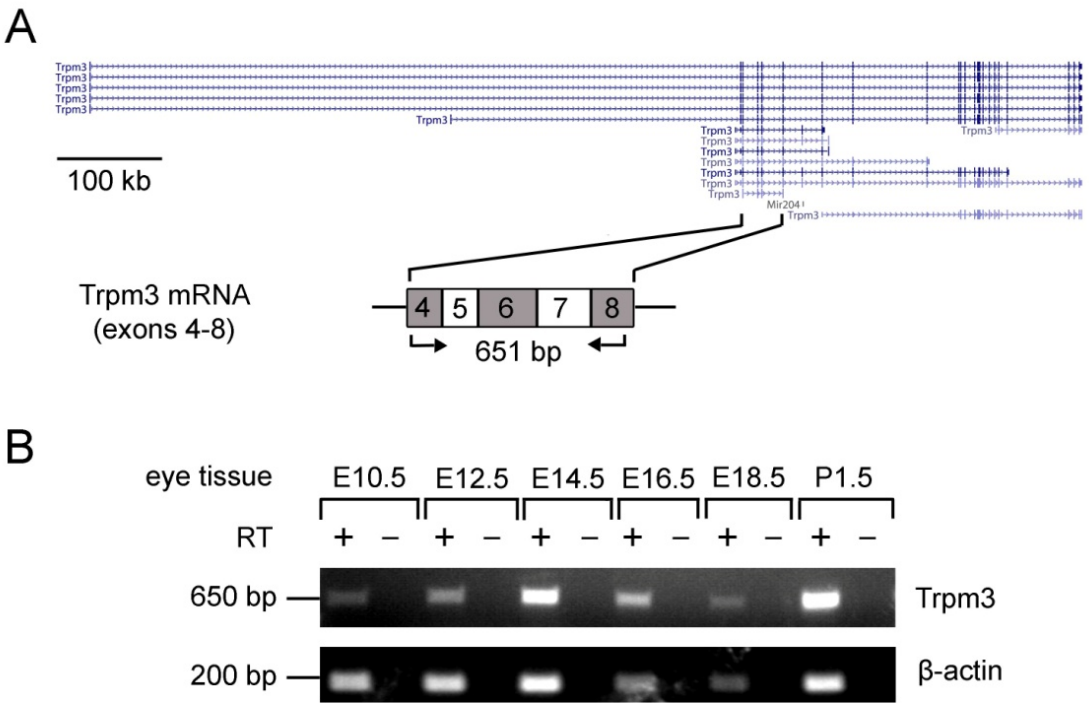
A
Trpm3
100 kb
Mir204
Trpm3 mRNA
(exons 4-8)
4
5
6
7
8
651 bp
B
eye tissue
E10.5
E12.5
E14.5
E16.5
E18.5
P1.5
RT
+ – + – + – + – + – + –
650 bp
Trpm3
200 bp
β-actin

TABLE 3.1. PCR, CLONING AND SOUTHERN PROBE PRIMERS

9q21 SOUTHERN BLOT PROBES

Region	Size [bp]	forward primer [5'-]	Reverse primer [5'-]	MA
Probe 1	1005	ATGTCCTAGACAAAAGCTAAAGCAA	CTTCATTACACTCTGTTGCTTCGTA	1X
Probe 2	700	AAATAGCAGTAGCACATGTGAATGA	TTAAAGATGACTAATGGGTTTTGCT	1X

Both PCRs were performed using Platinum Taq (Invitrogen) with 100 nM each primer, 1.5 mM $MgCl_2$ and 200 µM dNTPs. MA, Masteramp concentration [Epicentre]. Cycling conditions were 95°C x 5 min, followed by 40 cycles of [95°C x 30sec denaturation, 55°C x 30 sec annealing, 72°C x 60 sec extension], followed by 72°C x 7 min.

Xq27-9q21 BREAKPOINT IDENTIFICATION AND CONFIRMATION

Region	Size [bp]	forward primer [5'-]	Reverse primer [5'-]	MA
inverse PCR* (telomeric junction)	3,917	CTGGTCTTTCGTATACCTTGTCTCA	GATGATTCAGGACAACAACAAAAAT	1X
telomeric junction	244	CTAAGCCCCTAACATGTTTGTTCTA	TTTTTCTCTTGTTTAGGTTGTGCTT	1X
centromeric junction	319	CAGGGACCAAAATATTCTACTGAAA	GTTTATTTCTGGTGACTTCAGTGCT	1X

*PCRs were performed using EXPAND Long Template PCR [Roche] with 100 nM each primer, 1.5 mM $MgCl_2$ and 200 µM dNTPs. MA, Masteramp concentration [Epicentre]. DNA template = HindIII-digested and blood genomic DNA religated overnight. Cycling conditions were 95°C x 4 min, followed by 40 cycles of [95°C x 30sec denaturation, 48°C x 30 sec annealing, 68°C x 480 sec extension], followed by 68°C x 7 min.

All other forward PCRs were performed using Platinum Taq (Invitrogen) with 100 nM each primer, 1.5 mM $MgCl_2$ and 200 µM dNTPs. MA, Masteramp concentration [Epicentre]. Cycling conditions were 95°C x 5 min, followed by 40 cycles of [95°C x 30sec denaturation, 55°C x 30 sec annealing, 72°C x 60 sec extension], followed by 72°C x 7 min.

LUCIFERASE ASSAY CLONING PCR PRIMERS

Region	Size [bp]	forward primer [5'-]	Reverse primer [5'-]	MA
huSOX2-HA	1005	GATCATGAATTCATGTAC AACATGATGGAGACGGAG CTGAAG	GATCATGTCGACTCAGGCGTAA TCTGGAACATCGTATGGGTACA TGTGTGAGAGGGGCAGTGTGCC GTTAAT	3X
huSOX3-HA	1392	GATCATGAATTCATGCGA CCTGTTCGAGAGAACTCA TCAGGT	GATCATGTCGACTCAGGCGTAA TCTGGAACATCGTATGGGTAGA TGTGGGTCAGCGGCACCGTTCC GTTGACT	3X

Both PCRs were performed using EXPAND High Fidelity Taq (Roche) with 100 nM each primer, 1.5 mM $MgCl_2$ and 200 µM dNTPs. MA, Masteramp concentration [Epicentre]. Cycling conditions were 95°C x 5 min, followed by 40 cycles of [95°C x 60sec denaturation, 63°C x 30 sec annealing, 72°C x 180 sec extension], followed by 72°C x 7 min.

BAC TARGETING VECTOR CLONING PCR PRIMERS

Region	Size [bp]	forward primer [5'-]	Reverse primer [5'-]	MA
Sox2-HA*	1024	GATCATGTCGACCAGCGCCC GCATGTATAACATGATGGAG ACG	GATCATGTCGACTCAGGCGTA ATCTGGAACATCGTATGGGTA CATGTGCGACAGGGGCAGTGT GCCGTTA	3X
Sox3-HA*	1375	GATCATGTCGACCAAGCTGC GAATGCGACCAGCTCGAGAG AACGCATCAGGAGAGAGAA	GATCATGTCGACTCAGGCGTA ATCTGGAACATCGTATGGGTA GATGTGGGTCAGCGGCACCGT T	3X
Chx10 homology arm (A)	532	GATCATGTCGACAGATCTGTCT GAGTCTATTTGAGGCTGCTT	GATCATCTCGAGCTCCCGGTTCT TTGGAGGGGCTGA	1X
Chx10 homology arm (B)	409	GATCATCTCGAGCTACACTGCT TGGGAAAGTCACA	GATCATCTCGAGAGATCTGACAC AGGGACAAGTAGGAACAG	1X

*Both Sox2 and Sox3 PCRs were performed using EXPAND High Fidelity Taq (Roche) with 100 nM each primer, 1.5 mM $MgCl_2$ and 200 µM dNTPs. MA, Masteramp concentration [Epicentre]. Cycling conditions were 95°C x 5 min, followed by 40 cycles of [95°C x

60sec denaturation, 63°C x 30 sec annealing, 72°C x 180 sec extension], followed by 72°C x 7 min.

All PCRs were performed using Platinum Taq (Invitrogen) with 100 nM each primer, 1.5 mM $MgCl_2$ and 200 µM dNTPs. MA, Masteramp concentration [Epicentre]. Cycling conditions were 95°C x 5 min, followed by 40 cycles of [95°C x 30sec denaturation, 55°C x 30 sec annealing, 72°C x 60 sec extension], followed by 72°C x 7 min. Red = initiator methionine, Orange = HA tag, Green = restriction site, Underline = endogenous Sox2 or Sox3 5' UTR.

BISULFITE SEQUENCING PCR PRIMERS

CpG Island	Size [bp]	forward primer [5'-]	Reverse primer [5'-]	MA
CpG 65				
65_1	242	ATGGAGGTATATTGTTTGTTGTTT	CTAACTTCATTTTTATTCCCTTTTAC	1X
65_5	140	TTTAGTATTATGGAAAGGGTTTAAGT	AATTAAATTCCAAACAAAAATCCAC	1X
65_6	152	AAAATTAAATTCCAAACAAAAATCC	GGGAGGTAAGTTTAGTATTATGGAAAG	1X
65_7	100	GAAAAGAAAGTAAAGATTGGGGTTT	See 65_5 reverse primer	1X
65_8	120	ATTGGTTTAATTGTGGGTTGG	TAAACCCTACACTCTCCAAAAAAAA	1X
65_9	118	GATTGGTTTAATTGTGGGTTG	ACCCTACACTCTCCAAAAAAAAC	1X
65_10	352	GGATTTTTGTTTGGAATTTAATTTTT	CCAACCCACAATTAAACCAAT	1X
CpG 38				
38_12	340	GGTTATTTAAAATATAAAGGTAAGG	ATACTTTATTTAACAAACACAAAAC	1X
CpG 216				
216_0	192	TTTGTTTGTTGGGTTATTTGTTAAAG	AAACACCTTATTTTAATTTCTACCAAATCT	1X
216_1	258	GGAGTTTTTTAGAGTGAAAGAAAAGTTT	TAACCCAACAAACAAATAAATATCC	1X
216_2	226	GTATGGGAGATAGGTTTTAGGATTG	TAACCACAAAACAAAAACAAAAAAA	1X
216_3	177	AATTTTGTAATTTTGTTAAGGTAGAT	ACCAAAAACACTTCCAATAAACCTA	1X
216_4	156	GGGATTTTAGGTTTATTGGAAGTGT	ATCCTAAAACCTATCTCCCATACC	1X
216_5	164	GTTTATTTAGAGGTTATTAATTAGGGTTTT	TCTACCTTAACAAAATTACAAAATTATTTT	1X
216_6	276	TAGTTGGGTTTTTTATATATTTGTT	AACTTTTTAAAACCCTAATTAATAACCTCT	1X
216_7	280	TTAGTTTTTAGAAGGTTGTATATTGT	AAAAACCCAACTAAAACCCAAAC	1X
216_8	273	GTGTATTTTGGGGTTTTTTAGGG	ACAATATACAACCTTCTAAAAACTAAACTC	1X
216_9	197	AGGGAGTATTTATTTTTTTTGAGTAG	AAAAACCCCAAAATACACAATTCTA	1X
216_10	285	GGTATTATTGGGTTGTATTGTAGGT	AAAAAATAAATACTCCCTACCCAAC	1X
216_11	101	TGGTAGGTATATGTTGATTATGT	TAATAAAATCTAAACCCAACTC	1X

CpG 41				
41_16	177	TTAGTTTTGGGGTTTTTAGAATTTAG	TAAAAATAAACATCACATCTACTCC	1X
CpG 54				
54_17	297	GTAATATTTTGGATAAGGATTTGG	TAAACATCCTCCATACCTAACAAAC	1X
CpG 25				
25_1	294	TTTTTTTTAGGGAGTGGGGTAAG	CCAAAAAAACAAACTTAATTAAAAC	1X
CpG 139				
139_1	277	GATTAATTGGTAAATTGAGGGGTTT	AATCCCTCACAACAATTTTCTAAAA	1X
139_2	312	GGGTTAGGGAGTTTGGGTATAGTTA	TTTACAACCTCAAAAAAAATAAAAATAAAA	1X
139_3	220	GGTAGTTTGGGAGTTGTAGTTTAAT	ACTTTACCTAATTTAACCTTCTCACATATC	1X
CpG 38 (Xq28)				
38_1_Xq28	258	ATTTTTTTAGGATATGGTTTAGGTT	GGTGGGTATTTATAGTTGTTTTTGG	1X

All PCRs were performed using JumpStart Taq (Sigma) with 100 nM each primer, 1.5 mM $MgCl_2$ and 200 μM dNTPs. MA, Masteramp concentration [Epicentre]. Cycling conditions were 94°C x 2min, followed by 40 cycles of [94°C x 30sec denaturation, 55°C x 30 sec annealing, 72°C x 30 sec extension], followed by 72°C x 7 min.

CHAPTER IV

DISCUSSION AND FUTURE DIRECTIONS

The results in this thesis provide insights into novel disease mechanisms involving *RBP4* and *SOX3* in human congenital eye malformations. This work opens new avenues for exploration in retinoid and SOX gene biology. Chapter II describes a novel genetic form of vitamin A deficiency with two dominant-negative *RBP4* missense mutations. This is an example of a non-Mendelian disease trait with incomplete penetrance and a maternal parent-of-origin effect that is likely attributable to a gene-environment interaction. Chapter III discusses a new *SOX3* regulatory mutation involving a rearrangement-prone X-linked human-specific palindrome. The growing field of regulatory diseases is a challenging but exciting new realm in human genetics. My work has provided two new candidate genes to the list of genetic loci associated with microphthalmia, anophthalmia and coloboma (MAC). As with all new discoveries, there are many future directions that can strengthen and build upon the conclusions presented in this thesis.

Structural properties of RBP A55T and A57T

In Chapter II, we systematically examined the molecular properties of both RBP A55T and A57T mutants. Apart from the reduced ability to bind and retain retinol, both mutants function similarly to wild-type in secretion stability, TTR complex formation, yet both appear to have greater STRA6 binding affinity than wild-type. These results were unexpected given previous studies showing *apo*-RBP has 5-fold lower affinity for TTR than holo-WT (Fex et al., 1979). Furthermore, transfer of vitamin A into the cell from holo-RBP must allow for apo-RBP dissociation to enable binding of the next RBP (Kawaguchi et al., 2011) . The functional similarities observed between A55T, A57T and holo-WT implies structural mimicry through an allosteric effect mediated by the threonine substitution. Human apo- and holo-WT crystal structures are known, with the only significant difference occurring in an extracellular loop at the cavity entrance (amino acids 34 – 36) (Cowan et al., 1990; Zanotti et al., 1993). Molecular modeling suggests stabilization of this loop in the holo position may be mediated by an altered network of hydrogen bonds directly linking F36 to either T55 or T57 in the mutants. Therefore, obtaining the crystal structures of both forms is the most direct way to test the mimicry hypothesis. Performing a three-dimensional overlay of mutant, apo- and holo-WT would provide enormous structural insight at atomic resolution. One could also use this data to explore the structural interaction between RBP and STRA6. A large-scale STRA6 mutagenesis study by Kawaguchi and colleagues has defined its points of contact with RBP (Kawaguchi et al., 2008a). However, dynamic structural changes that may occur during binding and/or dissociation with STRA6 are completely unknown. My work provides a new tool that uncouples vitamin A loading from high affinity receptor

binding. Armed with the crystal structures, these two mutants may help to reveal a molecular “switch” on RBP that normally allows it to remain receptor-bound until retinol delivery is complete.

To evaluate the detrimental effects that steric hinderance and hydrophilicity of the threonine side chain has on vitamin A binding, I propose an expanded retinol binding experiment with more RBP mutants. First, one could substitute a serine at positions 55 or 57 (A55S and A57S) to reduce the size of the side chain while preserving overall hydrophilicity. Second, placement of valines at both positions (A55V and A57V) could eliminate hydrophilicity without significantly altering side chain size. Comparison of RBP A55T and A57T to both holo-WT would allow examination of each component individually in terms of overall negative impact on retinol binding.

Dominant-negative RBP in developmental eye disease

The data presented in Chapter II strongly supports a dominant-negative disease mechanism for RBP A55T and A57T. Although circumstantial, our findings are wholly consistent with an *in vivo* dominant disease model based on multiple independent observations: 1) the mutant RBP (A57T) is present at a significant fraction in blood of known carriers, 2) both mutants are significantly impaired in binding vitamin A, thus reducing circulating retinol, 3) both mutant proteins bind STRA6 at higher steady-state levels compared to holo-WT, 4) the placenta expresses both STRA6 and fetal RBP (Johansson et al., 1999; Sapin et al., 2000a), thus providing a straightforward, logical hypothesis for the maternal parent-of-origin effect of MAC, and 5) common alternative forms of vitamin A can bypass and compensate for a deficient RBP system (Quadro et

al., 2005) providing a potential explanation for incomplete penetrance. Altogether, these findings reinforce the link between vitamin A deficiency and eye malformations. To demonstrate this *in vivo*, I propose an extensive follow-up study involving delivery of purified recombinant RBP A55T, A57T, *apo*-WT, holo-WT or vehicle into pregnant wild-type mice on graded vitamin A diets. This would require injection of variable RBP doses immediately prior to conception with additional scheduled administrations through E10.5 (optic cup stage), when retinoic acid signaling is known to be active in the eye. The endpoint of this experiment is the presence or absence of eye malformations in newborn pups (P0). Measurements include eye globe axial length and gross as well as histological morphology. If a developmental eye phenotype is present, an embryonic timecourse will follow using the highest non-lethal dose to establish when eye abnormalities begin to manifest using morphology and immunohistochemistry studies on embryonic eye tissues. Alternatively, the RBP injection experiment can be performed on a *Rbp4*$^{-/-}$ background (Quadro et al., 1999) to eliminate endogenous RBP thus ensuring a pre-determined WT-to-mutant ratio upon injection.

One potential shortcoming of the transient RBP injection model is that it does not reproduce the double heterozygous carrier status of both mother and fetus. The proposed experimental protocol only alters vitamin A delivery in the maternal compartment. Given that 14 of 15 affected children across all three families in Chapter II were born from a carrier mother, this suggests both child and mother may need to carry the mutation for disease manifestation. As a follow-up, I propose to create a *Rbp4*^{A73T} knock-in mouse model (p.A73T chosen for its degree of severity). Crossing *Rbp4*$^{A73T/+}$ carrier females with wild-type males would produce 50% heterozygous and 50% wild-

type embryos. Pregnancies could occur, on average, under different maternal dietary vitamin A conditions beginning prior to conception and ranging from sufficient to none. If my hypothesis that *RBP4* p.A73T causes MAC is true, we expect a level of vitamin A deficiency that consistently produces congenital eye malformations in heterozygous but not wild-type embryos. This mating set-up also allows for complementary ^{3}H-retinol tracer experiments to quantify the cumulative depletion across both RBP "bottlenecks" (i.e. placenta and fetal eye membranes). Here, a bolus injection of ^{3}H-retinol into maternal circulation would be administered at E11.5 (the earliest timepoint at which a fetal eye can be dissected). After several hours, all embryonic eyes could be dissected and pooled (based on genotypes) then counted for ^{3}H radioactivity. Replicate experiments are performed and average percentage of input is calculated for each embryonic genotype (+/+ versus +/-). The final values represent total depletion across placenta and fetal eye, whereas the difference is depletion experienced specifically at the fetal eye.

Returning to the transient RBP injection experimental system, one additional benefit is it also allows us to investigate compartment localization of mutant RBP. Our mass spectrometry results indicate a 2-to-1 WT-to-mutant ratio in carrier blood and a similar or greater ratio in urine. This relative reduction of the mutant form *in vivo* might be attributed to several non-mutually exclusive reasons: 1) differential secretion by the liver, 2) different binding affinities for transthyretin, 3) decreased half-life in circulation or 4) mutant RBP trapping in tissue interstitium due to increased STRA6 steady state binding. Our *in vitro* data supports high STRA6 receptor binding as a major contributor. This could be tested *in vivo* through injections of equal amounts of purified mutant or

holo-WT ^{35}S-RBP prepared as transthyretin-associated pentamers. After various amounts of elapsed time post-injection, tissues known to express Stra6 (e.g. eye, testis, bone marrow) can be harvested and assayed for overall ^{35}S radioactivity as a percentage of input. We can also collect blood and urine samples during this time period to determine half-life in blood and rate of renal elimination.

Qualitatively, mutant and wild-type RBP show similar steady state binding with TTR (Chapter II). However, the resolution of our method may not capture moderate differences in binding affinities. To test the relative affinities *in vivo*, one could perform a TTR immunoprecipitation (IP) on carrier serum, isolate RBP via electrophoresis which is known to dissociate the pentameric complex (Kanai et al., 1968), and perform MALDI-TOF mass spectrometry to gauge relative levels of mutant and wild-type RBP. Unfortunately, this may be complicated by the molar excess of serum TTR to RBP, estimated at 2.5 to 1 (Peterson, 1971; Smith and Goodman, 1971). Therefore, this approach may require scaling up or utilization of other *in vitro* techniques such as two-phase partitioning (Fex et al., 1979). To best assess secretion rates of both forms *in vivo* ideally requires access to primary hepatic tissues from heterozygous carriers (e.g. liver biopsy) for primary cultures and subsequent hepatoma transformation *in vitro* (Borek, 1972). Our transfection-based system does not replicate endogenous hepatocyte *RBP4* expression levels or vitamin A-dependent RBP secretion. Unfortunately, current access to human liver tissue is not feasible; therefore, a more practical source is hepatocytes derived from a mouse knock-in line of the p.A73T allele (as discussed above). Cultured rat and human hepatoma cell lines as well as mouse primary hepatocytes routinely preserve expression of RBP and vitamin A-dependent

secretion (Bellovino et al., 1999; Borek et al., 1980; Marinari et al., 1987; Smith et al., 1978; Tosetti et al., 1992). Under serum-free vitamin A-rich conditions, a timecourse accumulation study could be used to examine secretion rates. After several hours of exposure to vitamin A, we could purify RBP from conditioned media as we did from human serum in Chapter II (Figure 2.S6) and analyze relative abundance by mass spectrometry. This method eliminates the potential confounding effect of glomerular filtration, and therefore does not rely on TTR binding for accurate measurement in CM. Furthermore, there is no evidence that RBP is internalized by liver cells from circulation; thus, CM should reflect total secretion output. Relative intracellular RBP levels should inversely correlate with the secreted ratio. We could purify RBP via immunoprecipitation of microsomal fractions and analyze purified protein using the same approach as above. Altogether, the above *in vivo* studies can further solidify the work presented in Chapter II and enhance our overall understanding of the dominant-negative disease mechanism.

Maternal-fetal transfer of retinol during pregnancy

Placental transfer of retinoids is a highly regulated process that limits the amount of teratogenic vitamin A that can reach the fetus (Bates, 1983; Moore, 1971). Vitamin A delivery across the placenta has been demonstrated in various mammalian species (Collins et al., 1994; Creech Kraft et al., 1989; Kochhar et al., 1988; Lorente and Miller, 1977; Ross and Gardner, 1994; Satre et al., 1992). Retinol transfer is mediated by two major pathways: 1) RBP (Takahashi et al., 1977) and its receptor (Sivaprasadarao et al., 1994), and 2) lipoprotein-associated (chylomicron) retinyl esters that are taken up by placental cells (Quadro et al., 2004b). In humans, placental villous mesenchymal cells

are also capable of retinyl ester synthesis and storage (Sapin et al., 2000b). A number of other species can contribute to placental retinoid transfer (e.g. retinoic acid bound to albumin, carotenoids, and water-soluble glucoronides), but these are minor in comparison to the two major forms (Spiegler et al., 2012). Despite the universal requirement for vitamin A during embryogenesis, maternal-fetal retinoid transport differs across mammals at both anatomical and molecular levels.

In mouse, the E8 – E10 yolk sac visceral endoderm, a fetal-derived primitive "liver", expresses STRA6 receptor (Bouillet et al., 1997; Johansson et al., 1997; Sapin et al., 2000a), cellular retinol binding protein 1 (CRBPI), and fetal RBP (Johansson et al., 1997). Furthermore, inhibition of fetal RBP translation in cultured mouse yolk sacs produces a phenotype consistent with VAD syndrome (including eye defects), indicating the importance of yolk sac retinoids in early organogenesis (Bavik et al., 1996). By mid-gestation, the mature fetal-derived chorio-allantoic placenta develops into a major maternal-fetal interface. Starting at E8.5, STRA6 transcripts are abundant in the placental labyrinth zone and yolk sac; however, by mid-gestation (~E12.5) only placental expression persists (Bouillet et al., 1997). In mid-late gestation (~E17), immunoreactive STRA6 and RBP are absent in the labyrinth zone of the chorio-allantoic placenta, but now present abundantly in the visceral endoderm of the yolk sac (Johansson et al., 1997). Northern blot analysis confirms the absence of RBP mRNA transcripts in E17 chorio-allantoic placenta; however, *Rbp4* transcripts are detected in the yolk sac at the same age (Johansson et al., 1997; Soprano et al., 1986a). Transthyretin (TTR) is also expressed in the mouse yolk sac during late gestation and secreted with RBP (Soprano et al., 1986a). In rat, RBP and TTR mRNA and protein co-

localize in mid-late gestational (day 14-22) yolk sac, whereby TTR protein levels initially exceeding that in fetal rat liver (Sklan and Ross, 1987; Thomas et al., 1990). The absence of STRA6 mRNA transcripts, but presence of protein in late gestation (~E17) mouse yolk sac raises a number of potential scenarios for RBP-retinol uptake: 1) STRA6 receptor perdurance, 2) a switch to another as-yet uncharacterized Stra receptor (Sapin et al., 2000a), or 3) STRA6 transcription below the threshold of RNA detection. In contrast, abundant CRBPI is found in both placental trophectoderm lining the fetal vasculature and visceral endoderm of the yolk sac at E18 (Johansson et al., 1997), indicating two locations of CRBPI retinol processing. The co-localization of STRA6, RBP, TTR and CRBPI in late-gestation mouse yolk sac strongly suggests the primary CRBPI function is to shuttle retinol to RBP for secretion into fetal circulation. Meanwhile, CRBPI co-localization with likely maternal RBP in placental trophoblasts implies an RBP-independent function of CRBPI in the placenta. Despite the abundant expression data, the relative contributions and exact molecular function(s) of trophoblast- and yolk sac-derived CRBPI and CRBPII in fetal retinoid transport remain poorly defined.

Together, the cumulative expression data suggests maternal RBP-retinol may cross into trophotblastic blood sinuses obtaining direct access to the yolk sac visceral endoderm where fetal STRA6 is expressed. A recent study shows maternal RBP does not cross the mouse maternal-fetal interface (Quadro et al., 2004b), most likely blocked at the yolk sac. Once inside the cell, retinol can bind fetal RBP for secretion into the vitelline circulation destined for the embryo proper. Furthermore, *de novo* RBP synthesis and secretion in the yolk sac behaves similarly to adult liver under conditions

of vitamin A deficiency (Soprano et al., 1988). Therefore, persistent yolk sac expression of RBP, TTR, CRBPI, CRBPII and STRA6 as well as this the resemblance to adult liver regarding RBP secretion, all suggest the yolk sac, and not chorio-allantoic placenta, acts as the primary mediator of maternal-fetal retinol transfer throughout rodent gestation.

In contrast to rodents, human placentation exhibits a different gene expression profile and relative functions of the placenta and yolk sac. In fact, the human yolk sac degenerates by week 12 of gestation, but during its existence, evidence indicates it functions as a critical site of placental exchange (Freyer and Renfree, 2009). For example, folic acid delivery to the early human conceptus depends on uterine vessels and the yolk sac (Jauniaux et al., 2007). This overall early function is especially important since blood flow through the placental intervillous space is only fully established at week 12 (Burton et al., 2002). During the first trimester, much organogenesis (including the eye) occurs, reflected by abundant *de novo* synthesis of fetal RBP protein in the yolk sac (Johansson et al., 1999). RBP is also expressed in early sheep and pig yolk sac tissues (Harney et al., 1994; Liu et al., 1991). No study has examined STRA6, TTR, CRBP-I or CRBP-II expression in the human yolk sac.

During the first trimester, human placental syncytiotrophoblasts express STRA6 receptor and contain vesicles of immunoreactive RBP. RBP is also seen in the lumen of villous vessels of the placenta (fetal) vasculature. This immunoreactive RBP is likely maternal in origin deduced by the observation that no RBP mRNA is detected in placental villi at any point during human gestation (Johansson et al., 1999). It remains unclear what molecular role STRA6 receptor plays, if any, in RBP internalization apart

from its known role in retinol uptake (Kawaguchi et al., 2007). Nevertheless, ^{125}I-radiolabeled RBP transfer studies in pregnant rhesus monkey show circulating fetal RBP is a mix of maternal and fetal-derived RBP (Vahlquist and Nilsson, 1984). These findings demonstrate maternal RBP crosses the syncytiotrophoblast layer, and a fraction may enter the general fetal circulation. This observation does not exclude the blockage of the majority of maternal RBP by the yolk sac in favor of fetal-derived RBP. Analysis of 6-13 week human fetuses show high all-*trans*-retinol tissue levels indicating successful fetal retinoid transfer (Kraft et al., 1993). Also, the majority of circulating human fetal RBP-retinol delivered through the umbilical vein is complexed to TTR (Sklan et al., 1985), indicating either re-formation of the TTR-RBP-retinol complex for fetal circulation or intact transfer across the placenta. Therefore, in first trimester pregnant human females with *RBP4* mutations, eye development may be compromised by two fetal sites of vitamin A "bottlenecks": the placental syncytiotrophoblast layer and yolk sac visceral endoderm. Much insight can be gained into human RBP placental crossing from term pregnancies of known *RBP4* p.A73T/+ or p.A75T/+ carrier mothers with genotypically normal babies. The opposite genotypic situation would also be informative regarding fetal-to-maternal transfer of RBP.

At term, immunoreactive RBP is no longer present in the villous stroma or syncytium, though RBP is still detected in the lumen of villous vessels (Johansson et al., 1999). This implies an interruption of transplacental movement of maternal RBP (but not retinol), despite evidence for RBP-retinol absorption of cultured human term syncytiotrophoblasts (Torma and Vahlquist, 1986). This discrepancy may be explained by a study of perfused term human placentae that showed uptake of maternal RBP-

retinol and subsequent degradation of the protein component (Dancis et al., 1992). The RBP fragments were secreted into fetal circulation. Retinol crossed into fetal circulation intact, though it was no longer bound to RBP upon exiting the placenta. This suggests the route between the placenta and fetal liver consists of retinol bound transiently to an as-yet unidentified carrier. Upon reaching fetal liver, retinol is then quickly transferred to fetal RBP. Indeed, greater than 90% of human newborn circulating retinol is associated with RBP (Ismadi and Olson, 1975). The phenomenon of RBP degradation and secretion into fetal circulation in first trimester placenta requires further exploration.

The decidua basalis (DB) is a maternal-derived placental structure that lines the uterine wall and participates in nutrient exchange with the fetus. Early in mouse gestation (E8 – E10), DB accumulates retinoids and expresses CRBPI, STRA6 but not RBP (Johansson et al., 1997; Sapin et al., 2000a; Sapin et al., 1997). At mid-gestation E13.5, *Rbp4* transcription initiates in the DB which coincides with a major shift in retinoid accumulation to the visceral endoderm of the yolk sac and fetal liver by E18.5 (Johansson et al., 1997; Sapin et al., 1997). Therefore, DB may represent an additional maternal site of retinol processing or storage could compromise vitamin A mobilization in *RBP4* p.A73T/+ and p.A75T/+ human carriers depending on the exact function of DB early in human development. Consistent with this hypothesis, we observe biallelic expression of *Rbp4* in mouse whole placental tissue at term (Figure 2.S5). However, based on the timing of *Rbp4* transcriptional initiation at ~E13.5, loss of retinol in the DB at this stage would have little consequence on eye initiation which begins at E8.5. This does not exclude the possibility of negative effects later in eye development such as fusion of the choroid fissure, which is a vitamin A-dependent mid-gestational event.

More work involving retinoid pathway gene expression in first trimester human DB must be completed to address many unanswered questions.

Retinoid transport and metabolism genes in congenital eye disease

RBP4 is only one of many genes directly or indirectly involved in retinoid transport or metabolism. Based on seminal work by Wilson and colleagues (Wilson et al., 1953) and two genes implicated in retinol delivery (*RBP4* and *STRA6*), it is clear the route vitamin A takes from its arrival in the intestinal lumen to the point of cellular uptake is critical in ensuring vitamin A homeostasis in pregnant mothers. Genetic deficiencies in these pathways could increase risk of maternal vitamin A deficiency during pregnancy with MAC inheritance patterns similar to the three families in Chapter II. For this reason, I hypothesize additional MAC mutations exist in genes involved directly or indirectly with retinoid metabolism, storage or transport both up- and downstream of RBP. To test this, I propose a comprehensive screen of genes that fit this criteria using exon PCR and sequencing to identify pathogenic variants.

Retinoid metabolism starts in the intestinal lumen where it arrives mostly as preformed retinoids (retinol or retinyl ester) or as proretinoid α/β carotenoids. Intestinal enzymes perform the bulk of proretinoid-to-retinoid conversion to facilitate absorption. One important lumenal enzyme and its essential co-factor are pancreatic triglyceride lipase (*PNLIP,* 10q25) and co-lipase (*CLPS,* 6p21), respectively. This complex is the major lumenal triglyceride lipase and retinyl ester hydrolase in rodents and exhibits similar enzymatic activity in humans (van Bennekum et al., 2000). Beta-carotene monooxygenase 1 (*BCMO1*, 16q23) is another lumenal enzyme for cleavage of β-

carotene into two retinaldehyde molecules. Several *BCMO1* polymorphisms and one severe hypomorphic allele lead to variable levels of hypercarotenemia and poor retinoid conversion (Leung et al., 2009; Lietz et al., 2012; Lindqvist et al., 2007) which contributes to variability in retinoid metabolism. Uptake of procarotenoids into the enterocyte relies heavily on scavenger receptor class B, type 1 (*SCARB1,* 12q24) (During and Harrison, 2007; Lobo et al., 2010; van Bennekum et al., 2005). Intestine-specific homeobox (*ISX*, 2q12) is a retinoic acid-sensitive repressor of *BCMO1* and *SCARB1* (Lobo et al., 2010; Seino et al., 2008). Constitutively active dominant mutations could simultaneously impact two vitamin A-metabolism genes.

Within the enterocyte, most retinol and carotenoids are converted into retinyl esters and packaged into chylomicrons for release into general circulation via the lymphatic system (i.e. no first-pass metabolism). Within the enterocyte, preformed retinol is transferred to CRBPII (*RBP2*, 3q23) and channeled to lecithin:retinol acyltransferase (*LRAT,* 4q32) and diacylglycerol acyltransferase 1 (*DGAT1,* 8q24) for esterification into retinyl esters (O'Byrne et al., 2005; Wongsiriroj et al., 2008). Once chylomicron remnants are taken up by the hepatocyte, retinyl esters are converted to retinol which is transferred to CRBPI (*RBP1*, 3q23) and conveyed to hepatic stellate (Ito) cells for LRAT esterification and storage (Blomhoff et al., 1982; Ghyselinck et al., 1999; Ross, 1982). There is an ongoing debate as to the exact mechanism by which retinyl esters are transferred from hepatocytes to stellate cells.

Once RBP delivers all-*trans*-retinol to target cells via STRA6, the chromophore is transferred to cellular retinol binding protein 1, or CRBP1 (*RBP1*, 3q23), and is oxidized by RDH10 (*RDH10*, 8q21) to form all-*trans*-retinaldehyde (Sandell et al., 2012). This is

further oxidized by RALDH1, 2, and 3 (*ALDH1A1-3*, 9q21,15q21, 15q26, respectively) to form all-*trans*-retinoic acid. In fact, an ongoing study in our lab has identified homozygous loss of *ALDH1A3* in non-syndromic anophthalmia (see Addendum Part I). This binds to cellular retinoic acid binding proteins 1 and 2 (*CRABP1*, 15q25 and *CRABP2,* 1q23) for transfer to various retinoic acid receptors encoded by three genes: *RARA*, *RARB* and *RARG* (17q21, 3p24 and 12q13). Upon binding retinoic acid, RARs heterodimerize with other nuclear receptors, retinoid X receptors (RXRs), encoded by genes *RXRA*, *RXRB* and *RXRG* (9q34, 6p21, 1q23).

The discovery of *RBP4* mutations in MAC patients suggests there may be other mutations in genes that specifically encode retinoid binding proteins. Therefore, special attention may be given to these genes for screening purposes. Similar to plasma RBP, shuttling retinoids between different cellular compartments also requires retinoid binding proteins that can solubilize the highly lipophilic/hydrophobic retinoid molecule in aqueous environments. As of the writing of this thesis, there are seven known mammalian retinoid binding proteins according to Mouse Genome Informatics (MGI): *Rbp1*, *Rbp2*, *Rbp3*, *Rbp4*, *Rlbp1*, *Crabp1* and *Crabp2* (see Table 4.1).

Rbp1 and *Rbp2* genes encode cellular retinol binding proteins (CRBPs) 1 and 2, respectively, that show 91-96% protein sequence identity among human, rat, mouse, pig and chick (Demmer et al., 1987; Li and Norris, 1996; Rocchi et al., 1989). CRBPI and CRBPII bind retinol upon entry into the cell and retinaldehyde after ADH/RDH-catalyzed oxidation. Biochemical studies show that CRBPI exhibits 100-fold greater binding affinity for all-*trans*-retinol than does CRBPII (MacDonald and Ong, 1987). Although both CRBPs have similar functions in retinoid processing, they show very

different expression profiles *in vivo*. CRBP1 is highly expressed in liver stellate (Ito) cells, kidney, RPE, and gonads (De Leeuw et al., 1990; Eriksson et al., 1984; Kato et al., 1984; Wardlaw et al., 1997; Zetterstrom et al., 1994). Within hepatic stellate cells, CRBPI is important for build-up of long-term retinyl ester storage and maintenance of overall vitamin A homeostasis (Ghyselinck et al., 1999). This CRBP1 storage function is tightly coupled to STRA6 receptor –mediated vitamin A uptake and LRAT-catalyzed retinyl esterification (Jiang and Napoli, 2012; Kawaguchi et al., 2011). Developmental expression of *rbp1* in zebrafish shows widespread presence of mRNA transcripts in the CNS, liver, gonads and small intestines (Liu et al., 2004). *Crbp1*-null mouse fetuses develop normally under vitamin A sufficient dietary conditions; however, fetal stores of retinyl ester, circulating retinol and steady-state RA levels are all decreased during gestation (Matt et al., 2005). *Rbp2* encodes CRBPII and is exclusively expressed in mature rat, human, chick and zebrafish intestinal enterocytes from the proximal duodenum to the ileum, except in zebrafish which show high adult liver expression (Cameron et al., 2002; Crow and Ong, 1985; Ong and Page, 1987). High levels of CRBPII in adult small intestines, with little to no expression elsewhere, suggest this protein functions primarily in retinoid intestinal absorption. CRBPII binds all-*trans*-retinol converted from dietary pro-carotenoids and retinyl esters (MacDonald and Ong, 1987), and exhibits largely identical apo- and holo-CRBPII tertiary structures (Winter et al., 1993) similar to plasma RBP. CRBPII-retinol undergoes acyl-CoA-independent esterification (Ong et al., 1987) through LRAT and to a lesser extent DGAT1 (MacDonald and Ong, 1988; Wongsiriroj et al., 2008) for chylomicron packaging. This enzymatic reaction produces predominantly retinyl palmitate and retinyl stearate in a 2:1

ratio, independent of lipid composition in the diet (Huang and Goodman, 1965). Developmental expression in zebrafish is restricted to the intestines, gall bladder and liver (Liu et al., 2004; Liu et al., 2005), suggesting a developmental role in gastrointestinal (GI) retinoid metabolism. *Crbp2* knockout mice have reduced (40%) hepatic retinyl ester stores compared to wild-type mice but grow normally and are viable (Xueping et al., 2002). However, when maternal dietary retinoid levels are reduced there is 100% mortality in *Rbp2*$^{-/-}$ pups 24 hours after birth. Furthermore, there is increased mortality among *Rbp2*$^{+/-}$ offspring if carried by *Rbp2*$^{-/-}$ dams versus wild-type dams (79% versus 30%, respectively). This may be explained by the presence of CRBPII at the maternal fetal barrier. At E18, CRBPII is detected in mouse yolk sac (fetal origin) and deciduas basalis and endometrium (maternal origin).

The *Rbp3* gene encodes interphotoreceptor retinol binding protein (IRBP), a ~140 kDa glycoprotein that transfers retinol from the RPE to retinal photoreceptors and vice versa for maintenance of the visual cycle (Danciger et al., 1990), though the exact molecular mechanism of transfer between RPE and retina remains unclear. IRBP is expressed in photoreceptors and is secreted into the space between the RPE and the retina. *Rbp3* knockout mice display loss of photoreceptors and abnormal retinal morphology as early as postnatal day 11 (Liou et al., 1998; Ripps et al., 2000). Electroretinographic (ERG) studies of *Rbp3*$^{-/-}$ mice show reduced response amplitude for rods and cones by postnatal day 30. However, *Rbp3* knockout retinas can restore the ability to perceive light indicating IRBP is not required for re-isomerization of the bleached visual chromophore. Further developmental studies indicate an approximate 20% increase in eye size and weight in *Rbp3*$^{-/-}$ eyes with reduced outer nuclear layer

thickness compared to wild-type eyes (Wisard et al., 2011). Despite the presence of retinal and visual phenotypes, no developmental defects consistent with VAD syndrome are observed in *Rbp3*$^{-/-}$ mice.

Rlbp1 is a gene that encodes cellular retinaldehyde binding protein, or CRALBP (Saari et al., 1982). CRALBP is abundant in RPE cells and functions in binding 11-*cis*-retinol for conversion to 11-*cis*-retinaldehyde and transfer to IRBP for eventual photoreceptor uptake (Noy, 2000). A mutation in the human *RLBP1* gene that disrupts CRALBP ligand binding is associated with autosomal recessive non-syndromic retinitis pigmentosa (arRP) (Maw et al., 1997). *Rlbp1* mouse knockout studies show normal photosensitivity; however, rhodopsin regeneration, 11-cis-retinaldehyde isomerization and dark adaptation are all severely impaired (Saari et al., 2001). Unlike in humans with loss-of-function *RLBP1* mutations and *Rbp3*-null mice, *Rlbp1* knockout mice do not show evidence of retinal degeneration even up to one year after birth.

CRABP1 and *CRABP2* encode human gene products with 74% amino acid identity (Giguere et al., 1990; Nilsson et al., 1988). Both CRABPI and CRABPII have high binding affinity for all-*trans*-retinoic acid (Dong et al., 1999), and are considered the primary avenues through which RA is transferred from the cytosol to the nucleus (Gaub et al., 1998; Takase et al., 1986). In the adult stage, CRABPI is ubiquitously expressed (Ong, 1994) whereas CRABPII is restricted to the skin, uterus, ovary and choroid plexus (Wardlaw et al., 1997; Yamamoto et al., 1998; Zheng and Ong, 1998). During gestation, both CRABPI and CRABPII are widely expressed throughout the embryo, but usually without co-localization with one another (Maden, 1994). Both *Crabp1* and *Crabp2* single- and double-knockout mice are essentially normal except for a mild limb defect in

Crabp2$^{-/-}$ mice (Fawcett et al., 1995; Gorry et al., 1994; Lampron et al., 1995). The lack of any phenotype consistent with VAD syndrome indicates that CRABPs are dispensable during development, which raises the possibility of alternative pathways for retinoic acid nuclear translocation to RARs for target gene transcriptional regulation.

Our work has begun examining several of these candidate genes (see Addendum Part II) but thus far has revealed no variants other than in *ALDH1A3*. Nevertheless, it is clear that vitamin A exists in many forms and all are processed by enterocytes, funneled through the chylomicron system and stored in the liver. Many genes contribute to this process, and maternal loss-of-function or dominant mutations may account for a fraction of children born with vitamin A deficiency syndrome.

Consequences of ectopic SOX3 activity in the developing eye

In Chapter III, we investigated the effects of over-expressing two SoxB1 factors (Sox2 and Sox3) in the developing mouse neuroretina using a Chx10 bacterial artificial chromosome (BAC) transgenic system. Sox2 overexpression produced microphthalmia with retinal lamination defects and variably penetrant optic nerve hypoplasia/aplasia in two out of four total lines. The absence of a phenotype in one Chx10>Sox3 line is difficult to interpret. We cannot exclude the possibility that the developing neuroretina is sensitive to Sox2 but not Sox3. Furthermore, it remains to be determined whether ectopic SoxB1 expression in other compartments (e.g. surface ectoderm, RPE, POM) can disrupt eye development as well.

Over the last several decades, a large body of evidence has amassed arguing in favor of all three SoxB1 factors (Sox1, Sox2 and Sox3) sharing significant functional overlap in the CNS (Bylund et al., 2003; Graham et al., 2003). This is supported by our own *in vitro* data. Furthermore, eye size is dependent on proper neuroretinal growth which in turn depends on proper RPE development. RPE development requires repression of SoxB1 genes or else a RPE-to-retina fate switch occurs (Ishii et al., 2009). Based on this requirement, our revised hypothesis states that persistent SOX3 expression in the proband retinal pigment epithelium disrupts its formation, leading to retinal insufficiency and anophthalmia. Therefore, I propose several new experiments that target SoxB1 expression to the developing RPE using a melanocyte-specific driver such as *Tyr*, *Dct* or *Tyrp1* (Mori et al., 2002) BACs or transgenes. Also, because the autosomal translocation in our proband implies a *TRPM3* enhancer adoption mechanism, I also propose to generate Trpm3>Sox2/3-ires-Cre-pA BAC transgenes. If correct, we expect to recapitulate small or absent eyes and possibly a sex reversal phenotype since expression would no longer be limited to the eye.

SOX3 and congenital human diseases

This thesis strengthens the link between *SOX3* regulatory mutations and an ever-expanding list of X-linked congenital diseases that includes XX sex reversal (Sutton et al., 2011), congenital hypertrichosis (Zhu et al., 2011), hypoparathyroidism (Bowl et al., 2005), brachymesomelic dysplasia with Peters anomaly (Bleyl et al., 2007), and hypopituitarism with short stature and mental retardation (Woods et al., 2005). Certainly, the structure of the insertion translocation described in this proband (Chapter III)

suggests that transcriptional dysregulation of *SOX3* may disrupt mammalian eye and testis development. To our knowledge, bilateral clinical anophthalmia with XX sex-reversal represents a new syndrome, as there are no reported human cases that share both hallmark features. The lone mammalian precedent is the *Odsex* mouse that exhibits microphthalmia and XX sex-reversal due to a long-range, *cis*-acting *Sox9* regulatory insertion (Bishop et al., 2000). The *Odsex* mouse phenotype is not surprising, given the importance of SOX genes in development of both organs. Finally, the 180 bp X-linked *SOX3* palindrome now warrants investigation in any as-yet unexplained X-linked genetic disorder. This is especially so now that it is associated with three disease traits that, prior to this study, were considered etiologically distinct.

Concluding remarks

In summary, I have presented seminal findings regarding two new genes in congenital eye disease. My work explores a novel *SOX3* regulatory mutation and its association with a complex human syndrome, and provides further evidence of a genomic “hot spot” that may cause other developmental disorders. My dissertation also presents a completely new dominant-negative disease mechanism for vitamin A deficiency involving plasma retinol binding protein (*RBP4*). Perhaps most important of all, this thesis provides a novel framework for complex non-Mendelian traits from a maternal-fetal perspective where both major genetic and environmental components are strongly implicated by the mutated gene (*RBP4*). The interplay between genes and environment is beautiful but at the same time sobering, because too often this interaction results in human disease. Altogether, this thesis expands our knowledge about human disease mechanisms.

Table 4.1. Embryonic phenotypes of retinoid binding protein knockout mice

Gene knockout	Embryonic phenotype	Reference
Rbp1	Clinically normal but with reduced retinyl ester liver stores, circulating retinol and steady-state RA levels	(Matt et al., 2005)
Rbp2	Clinically normal, but with reduced retinyl ester liver stores. 100% neonatal mortality when born from Rbp2-/- dams on vitamin A deficient diets.	(Xueping et al., 2002)
Rbp3	No embryonic phenotype. Post-natal phenotype: retinal and visual phenotype: loss of photoreceptors and thinning of outer nuclear layer. Impaired isomerization to form 11-cis-retinal and issues with dark adaptation.	(Liou et al., 1998) (Ripps et al., 2000)
Rbp4	No embryonic phenotype under normal maternal dietary vitamin A conditions. Phenotype consistent with VAD syndrome arises under maternal dietary vitamin A deficiency (anophthalmia, cerebral edema, pulmonary agenesis, urogenital and cardiovascular defects).	(Quadro et al., 1999) (Quadro et al., 2005)
Rlbp1	No embryonic phenotype. Post-natal retinal phenotype: impaired rhodopsin regeneration, 11-cis-retinaldehyde isomerization and dark adaptation.	(Saari et al., 2001)
Crabp1	No embryonic phenotype	(Gorry et al., 1994)
Crabp2	Mild limb malformation (extradigital outgrowth).	(Lampron et al., 1995)
Crabp1;Crabp2	Mild limb malformation (extradigital outgrowth). Mild post-natal mortality (9%) prior to 6 weeks of age compared to 2% for wild-type offspring.	(Lampron et al., 1995)

ADDENDUM PART I – Characterization of *ALDH1A3* mutations in autosomal recessive, non-syndromic MAC

Characterization of novel *RALDH3* variants in autosomal recessive MAC

We obtained a large, in-bred Iranian pedigree showing autosomal recessive non-syndromic MAC. Affected individuals suffer from severe or total blindness with no light perception. All other surrounding ocular structures are intact (e.g. bony orbit, eyelids, adnexa). Given the inheritance pattern, we performed autozygosity mapping on eight affected individuals. This revealed a shared 0.8 Mb region of homozygosity on 15q26. Close examination reveals 5 candidate genes, one of which is *RALDH3* (also known as *ALDH1A3* or *ALDH6*), a known retinoid metabolism gene. Subsequent exon-by-exon screening uncovered a novel missense mutation in *RALDH3* exon 4 (G123W) that co-segregates with disease. Subsequent screening of a cohort of 75 unrelated MAC patient DNA samples revealed three additional *RALDH3* variants: G354R, D70N and M386V. One individual was found to possess both G354R and D70N alleles. Subsequent screening of both parents revealed this individual as a compound heterozygote. All variants except M386V affect highly conserved amino acid residues. None are found in any public single nucleotide polymorphism (SNP) databases.

RALDH3 encodes a 512-amino acid peptide (55 kDa subunit) that forms a homo-tetramer (Hsu et al., 1994). RALDH3 catalyzes the irreversible step of retinaldehyde oxidation to retinoic acid (RA), a potent signaling molecule. RA signaling is a critical extrinsic pathway involved throughout early eye development (Molotkov et al., 2006). Based on molecular modeling, all mutations affect residues within the catalytic but not the oligomerization domain (unpublished data, Lev Prasov). I performed two

experiments to functionally test these alleles. The first is a co-transfection luciferase experiment of plasmids encoding RALDH3 wild-type or mutant and a RARE-luciferase reporter in P19 mouse embryonal carcinoma cells (Figure A1-A). After 8 hours exposure to retinoid, I measured renilla-normalized luciferase values as an indirect read-out of retinoic acid synthesis. The results demonstrate RALDH3 G123W and D70N are likely null alleles never exceeded background levels. Subsequent cycloheximide protein stability experiments showed G123W to be a highly unstable protein with a half-life $t_{1/2}$ = 40 min in contrast to wild-type which showed negligible decline over the course of the study (unpublished data, Lev Prasov). RALDH M386V is a non-pathogenic variant, consistently exhibiting equal activity compared to wild-type. RALDH3 G354R appears to be a hypomorphic allele, exhibiting reduced activity compared to wild-type. To better characterize the true severity of the arginine 354 substitution, we repeated the luciferase assay except with a graded level of transfected plasmid (Figure A1-B). Over this range, RALDH3 G354R exhibited 20 – 70% activity which directly correlated to transfection input whereas wild-type levels remained nearly constant at all transfected amounts. Together, these results suggest RALDH3 G354R is capable of forming functional tetramers but with reduced activity, therefore the mutant allele is indeed a hypomorph.

Based on the homo-tetrameric nature of RALDH3, I next tested the ability of RALDH3 G354R to interact in a co-immunoprecipitation assay using the same cell system (Figure A1-C). I co-transfected plasmids encoding myc-tagged WT plus HA-tagged WT in parallel with myc-tagged WT plus HA-tagged G354R. After 8 hr, I immunoprecipitated (IP) with either anti-HA or anti-myc antibodies and performed

parallel HA and myc Western blots for each IP reaction. The results indicate that G354R can form heterotetramers with wild-type, albeit to a lesser extent than pure wild-type homotetramers (Figure A2). Cycloheximide studies indicate the G354R protein is equally stable compared to wild-type; therefore, reduced RARE-luciferase activity most likely stems, in part, from compromised tetramer formation. Enzymatic kinetic studies are necessary to address potential deficiencies in RA synthesis.

My contributions:

1. Aided in *RALDH3* exon PCR screening of MAC patient cohort.
2. Developed, optimized and performed the RARE-luciferase assay.
3. Developed, optimized and performed the co-immunoprecipitation assay.

Addendum I: Methods

Luciferase assay

P19 embryonal carcinoma cells (ATCC, Manassas, VA) were grown to 30% confluency in αMEM supplemented with 7.5% calf serum and 2.5% fetal bovine serum, L-glutamine and pencillin/streptomycin antibiotics. Cells were co-transfected using Fugene 6 (Promega, Madison, WI) in a 3:1 F6:DNA ratio (DNA = 4 µg RALDH3 plasmid, 0.7 µg RARE-Luciferase, 0.3 µg Renilla) with plasmids encoding human wild-type or mutant RALDH3 (pUS2), pGL3-RARE-Luciferase reporter plasmid (Addgene, Cambridge, MA), and a Renilla transfection control plasmid. After 48 hours, cells were switched to retinoid-free media DMEM supplemented with 1% (v/v) insulin-transferrin-selenium liquid solution (ITS; Gibco, Carlsbad, CA), 500 µg/ml AlbuMAX (Gibco), and 100 nM all-*trans*-retinaldehyde for 8 hr. Afterwards, cells were washed twice with 1X PBS and harvested using a dual-luciferase reporter kit (Promega) per the manufacturer protocol and counted on a VICTOR^3 1420 Multilabel counter (Perkin Elmer). All datapoints were collected in triplicate.

RALDH3 co-immunoprecipitation assay

P19 cells were grown and transfected as described above except with 2 µg total plasmid DNA. Cells were treated identically post-transfection. At 56 hr post-transfection, cells were washed twice with 1X PBS and harvested with ice-cold 1X PBS, 1% Triton X-100, 0.1% NP-40 non-denaturing lysate solution (300 µl per 60 mm dish). Cell lysates were briefly sonicated on a Branson 250 sonicator (Branson Ultrasonics, Danbury, CT), and spun to remove the insoluble fraction. One-third of the cell lysate was subjected to

anti-HA IP and an additional third to anti-myc IP (Sigma-Aldrich, St. Louis, MO) overnight at 4^{o}C per the manufacturer's protocol.

Western blot

Eluates were run on denaturing polyacrylamide gel electrophoresis (200V, 40 min) in 1X MES/SDS running buffer (Invitrogen, Carlsbad, CA) and transferred for 2 hours at 120V/200mA at 4^{o}C onto a HyBond ECL nitrocellulose membrane (GE Healthcare). Primary antibodies rat-anti-HA (1:5000, Roche 3F10) or mouse-anti-myc (1:5000, Roche 9E10) were applied overnight at 4^{o}C. Next day, membranes were washed in TBST and exposed to secondary antibodies goat-anti-rat IgG HRP (1:5,000, Amersham) or sheep-anti-mouse (1:5,000, Amersham) for 1 hour at room temperature. Membranes were washed with 1X TBS and applied with chemiluminescent detection substrate (ECL, Amersham) for 5 minutes at room temperature. Membranes were exposed to Biomax MS film (Kodak, Rochester, NY) for 2 to 15 minutes and developed on a Kodak A2000 developer.

Figure A.1. Characterization of novel *RALDH3* (*ALDH1A3*) mutations. (**A**) RALDH3 luciferase assay shows relative activity of each construct in the presence of 100 nM all-*trans*-retinaldehyde substrate (ATRAL). RA, 100 nM all-*trans*-retinoic acid control. Error bars denote standard deviation. (**B**) RALDH3 luciferase titration assay with reduced input relative to (A) shows increasingly reduced relative activity of G354R compared to wild-type. (**C**) RALDH3 co-immunoprecipitation assay of for oligomerization. Transfected constructs are denoted at bottom. Cells underwent anti-myc immunoprecipitation for WT^{myc} and subsequently probed for HA (tetramerization) and myc (loading control). G354R shows reduced oligomerization with wild-type (red box). $G123W^{HA}$, negative control.

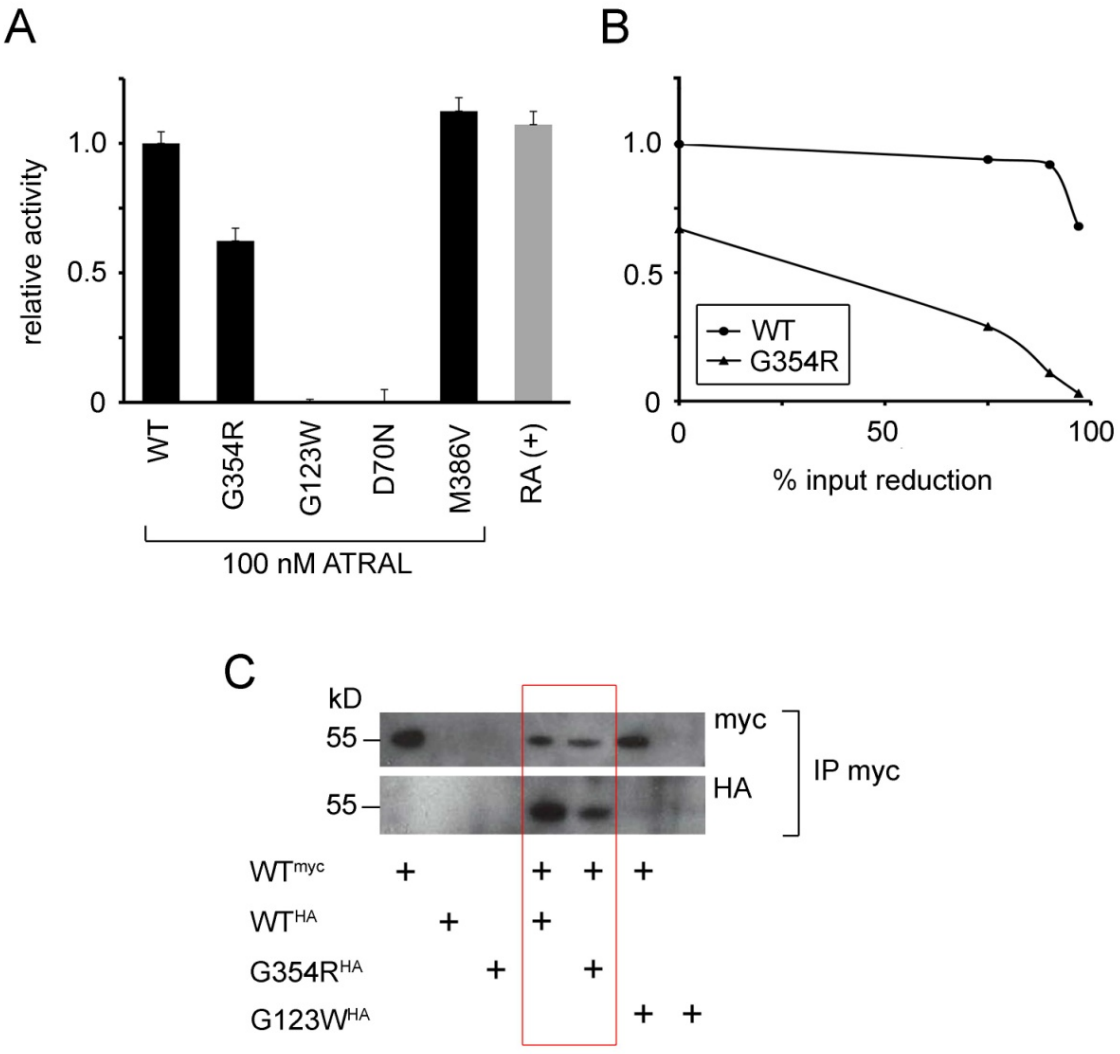
A
relative activity
1.0
0.5
0
WT
G354R
G123W
D70N
M386V
RA (+)
100 nM ATRAL
B
1.0
0.5
0
WT
G354R
0
50
100
% input reduction
C
kD
55
55
myc
HA
IP myc
WT^myc
WT^HA
G354R^HA
G123W^HA

ADDENDUM PART II – Novel retinoid pathway gene variants in MAC patients

Retinoid acid pathway gene screen in MAC

In the pursuit of additional pathogenic mutations in retinoid metabolism genes, I have screened a number of genes in a cohort of 75 unrelated anophthalmia patient samples: *RDH10, RBP1, RBP2, TTR, CYP26A1, CYP26C1* and *LRAT*. This uncovered several novel variants that warrant further investigation.

CYP26C1 (p.Q284fsX128)

I discovered a novel 7 bp microduplication frameshift mutation (p.Q284fsX128) in *CYP26C1* exon 4 in a child with bilateral anophthalmia, trachea-esophageal fistula, esophageal atresia, hydrocephalus and hypospadias (Figure A2-A, B). This allele was paternally-transmitted with no evidence of mutation on the maternal allele. The father is clinically normal. This child does not have a *SOX2* coding mutation.

CYP26C1 is a 522-amino acid monomeric enzyme involved in retinoic acid degradation (Tahayato et al., 2003; Taimi et al., 2004). This frameshift eliminates the important catalytic domains encoded by exons 5 and 6 (Taimi et al., 2004). The DNA surrounding the frameshift site shows 64% GC-content (50 bp window). This allele is not found in any public variant databases. Moreover, the new protein sequence (a.a. 284-411) shares no homology to any known protein (Figure A2-C).

The mouse *Cyp26c1*$^{-/-}$ knockout shows no eye phenotype (Uehara et al., 2007) despite expression of Cyp26c1 in the embryonic eye contained within a wider Cyp26a1 expression domain (Sakai et al., 2004). This is explained by abundant evidence suggesting significant functional overlap of all three CYP26 members *CYP26A1*,

CYP26B1 and *CYP26C1* (Hernandez et al., 2007; Kinkel et al., 2009; Sakai et al., 2004; Uehara et al., 2007). *CYP26A1* and *CYP26C1* are chromosomally linked in mouse and man. Recently, a familial form of autosomal dominant optic nerve hypoplasia/aplasia was reported to be associated with a 363 kb interstitial deletion encompassing *CYP26A1*, *CYP26C1* and *EXOC6* (Meire et al., 2011). Disease pathogenesis has yet to be established. The reported frameshift mutation here is the first known case of a *CYP26C1*-specific mutation associated with human disease. I propose first to screen a large control population to ensure this is not a rare polymorphism. Assuming this allele is restricted to the MAC population, a follow-up experiment would be to perform copy number variation analysis on this index family to look for duplications or deletions that may be present on the maternal allele. In parallel, one could perform cell-based RARE-luciferase assays (see Addendum Part I) as a measure of RA degradation with this frameshift allele, wild-type CYP26C1, wild-type CYP26A1, and corresponding 1:1 mixes (mutant-to-WT) to investigate possible dominant-negative mechanisms. Although no evidence exists to indicate oligomerization, a single constitutively active or stable protein with increased half-life could lead to a localized RA deficiency at the cellular level, depriving neighboring cells of RA needed for signaling.

CYP26A1 **(c.141G>A, p.V33M)**

I discovered a novel *CYP26A1* variant (c.141G>A, p.V33M) in a child with bilateral clinical anophthalmia and a congenital heart malformation (VSD). Subsequent parental screening revealed this allele was maternally inherited; however, the mother does not

show any signs of congenital eye defects. The father is clinically normal as well and PCR exon screening revealed no variants on the paternal allele.

The missense mutation affects the N-terminus prior to the first alpha helix (A) in the predicted CYP26A1 497-amino acid structure (Gomaa et al., 2006). Comparative analysis shows this valine is not highly conserved amongst vertebrate species though generally non-polar amino acids (Val, Leu, Ile, Ala) do occupy this position (UCSC genome browser). The valine-to-methionine substitution maintains non-polarity.

CYP26A1 is located on human chromosome 10q23 (White et al., 1998a) and involved in retinoic acid degradation. Based on *Cyp26a1*$^{-/-}$ mouse knockout studies, this gene is important for establishing anterior-posterior retinoic acid gradients in CNS and axial skeletal development (Abu-Abed et al., 2001; Sakai et al., 2001). *Cyp26a1*$^{-/-}$ mice die *in utero* exhibiting major urogenital and kidney defects, spina bifida, hindbrain abnormalities, caudal truncation, and heart abnormalities. In mouse, Cyp26b1 and Cyp26c1 activities cannot compensate for loss of Cyp26a1, demonstrating the majority of embryonic retinoic acid metabolism depends on the a1 homolog. However, in two independent knock out mouse models, there was no reported eye phenotype, despite its expression in the early embryonic retina (Sakai et al., 2004). Biochemical studies have identified additional human *CYP26A1* missense variants in healthy subjects that show impaired ability to metabolize retinoic acid (Lee et al., 2007).

The methionine substitution may produce a novel translation initiation site that truncates the first 32 amino acids. Upon analysis, though, the newly introduced initiator methionine has a less ideal Kozak sequence compared to the primary translation start site. Nevertheless, cytochrome P450 enzymes, including CYP26 members, are

anchored by the hydrophobic N-terminal signal anchor sequence within the endoplasmic reticulum (ER) membrane to ensure appropriate configuration and enzymatic activity (Ahn et al., 1993; Bar-Nun et al., 1980; Ross and Zolfaghari, 2011; Williams et al., 2000). Elimination of the hydrophobic N-terminal 32 amino acids by translation initiation at M33 may prevent its localization to the ER membrane. While this is predicted to lead to loss-of-function and retinoic acid toxicity, studies in other cytochrome P450 species (e.g. CYP2C5) show that loss of the N-terminus still allows for membrane association, albeit more weakly, due in part to other hydrophobic regions (Johnson et al., 2005; Williams et al., 2000). Should CYP26A1 V33M reach the ER appropriately, it may not establish normal protein-protein interactions with other membrane-associated cofactors, resulting in increased activity and RA deficiency. Indeed, a recent study has shown the hydrophobic N-terminal protein-protein interactions between CYP3A4 and CYP2C9 lead to enzymatic inhibition of CYP2C9 (Subramanian et al., 2010). If this occurs with CYP26A1 and other as-yet unidentified cofactors, the altered N-terminus may allow for increased RA metabolism and a localized cellular RA deficiency, consistent with a vitamin A deficiency model. More work is needed to define the function of the CYP26A1 N-terminus, its requirement for transmembrane anchoring, and in regulation of its overall enzymatic activity. My proposed experimental follow-up to this variant is identical to the *CYP26C1* frameshift variant described above, but with emphasis on cellular organelle localization.

The two CYP26 gene variants described here may represent retinoic acid toxicity susceptibility alleles or rare, clinically insignificant polymorphisms in the population. The animal model studies certainly argue for their importance during embryonic

development, especially *Cyp26a1*; however, the lack of an overt knockout eye phenotype makes this difficult to reconcile with our human cases. The discrepancy may be due to interspecies differences. Additional genetic follow-up experiments and *in vitro* assays can help elucidate the true nature of these two unique variants.

Figure A.2. Novel *CYP26C1* (p.Q284fsX128) frameshift allele. (**A**) Pedigree showing child with bilateral anophthalmia, trachea-esophageal fistula, esophageal atresia and hypospadius with clinically normal carrier father. (**B**) DNA chromatogram of a 7 bp frameshift microduplication at the 3' end of *CYP26C1* exon 4 (red box). Gene exon-intron overlay shown (green bar, exon; green line, exon-intron boundary). This affects the protein sequence starting at amino acid 284. Resulting genomic DNA sequence is shown (top, reference; bottom, frameshift). Forward (5' – TGAGAAGGTTTTCTGGGTAAGTG) and reverse (5' – ATTGGTGTAGGGACCTGCTG) primers amplify a 300 bp product. For thermocycler conditions see Table 2.4. (**C**) Sequence of the 411-amino acid mutant protein encoded by this frameshift allele. Novel amino acids are annotated in red.

A

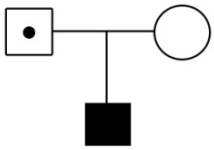

B

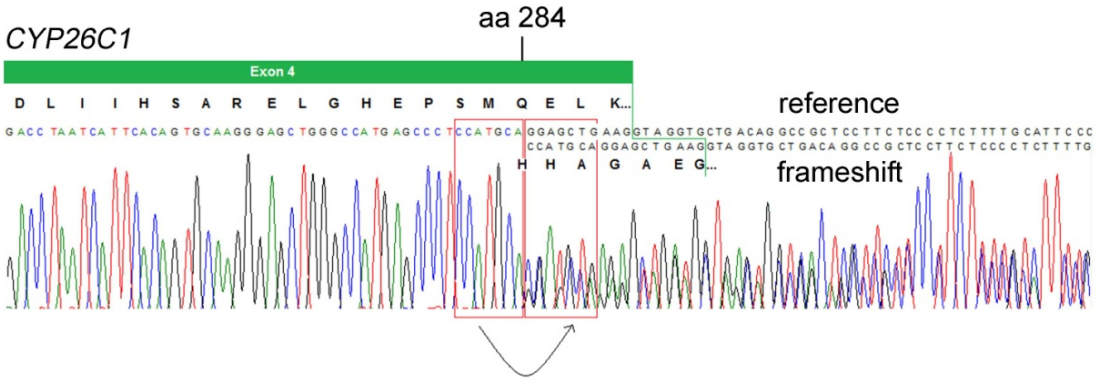

C

```
  1  MFPWGLSCLSVLGAAGTALLCAGLLLSLAQHLWTLRWMLSRDRASTLPLP
 51  KGSMGWPFFGETLHWLVQGSRFHSSRRERYGTVFKTHLLGRPVIRVSGAE
101  NVRTILLGEHRLVRSQWPQSAHILLGSHTLLGAVGEPHRRRRKVLARVFS
151  RAALERYVPRLQGALRHEVRSWCAAGGPVSVYDASKALTFRMAARILLGL
201  RLDEAQCATLARTFEQLVENLFSLPLDVPFSGLRKGIRARDQLHRHLEGA
251  ISEKLHEDKAAEPGDALDLIIHSARELGHEPSMHHAGAEGVGCGAPLRRL
301  LHHGQCQHLARPAATAASGGHRQDSGGAGGAGAGARVRLRARGRWGQRGA
351  PARLRLRARPQPRGAGPSALRRLRGQGGAAPPAASVRGLPHRPAHLRARR
401  LPDPQGLERDV
```

REFERENCES

Exome Variant Server, NHLBI Exome Sequencing Project (ESP), Seattle, WA (URL: http://evs.gs.washington.edu/EVS/) [accessed Mar 11, 2011].

The PyMOL Molecular Graphics System, Version 1.5.0.1 Schrödinger, LLC. (www.pymol.org).

Abecasis, G.R., Cherny, S.S., Cookson, W.O., and Cardon, L.R. (2002). Merlin--rapid analysis of dense genetic maps using sparse gene flow trees. Nat Genet *30*, 97-101.

Abouzeid, H., Boisset, G., Favez, T., Youssef, M., Marzouk, I., Shakankiry, N., Bayoumi, N., Descombes, P., Agosti, C., Munier, F.L.*, et al.* (2011). Mutations in the SPARC-related modular calcium-binding protein 1 gene, SMOC1, cause waardenburg anophthalmia syndrome. Am J Hum Genet *88*, 92-98.

Abouzeid, H., Youssef, M.A., ElShakankiri, N., Hauser, P., Munier, F.L., and Schorderet, D.F. (2009). PAX6 aniridia and interhemispheric brain anomalies. Mol Vis *15*, 2074-2083.

Abu-Abed, S., Dolle, P., Metzger, D., Beckett, B., Chambon, P., and Petkovich, M. (2001). The retinoic acid-metabolizing enzyme, CYP26A1, is essential for normal hindbrain patterning, vertebral identity, and development of posterior structures. Genes Dev *15*, 226-240.

Acampora, D., Mazan, S., Lallemand, Y., Avantaggiato, V., Maury, M., Simeone, A., and Brulet, P. (1995). Forebrain and midbrain regions are deleted in Otx2-/- mutants due to a defective anterior neuroectoderm specification during gastrulation. Development *121*, 3279-3290.

Agadir, A., Nau, H., and Blaner, W.S. (1999). Retinoids : the biochemical and molecular basis of Vitamin A and retinoid action (Berlin ; New York, Springer).

Ahituv, N., Zhu, Y., Visel, A., Holt, A., Afzal, V., Pennacchio, L.A., and Rubin, E.M. (2007). Deletion of ultraconserved elements yields viable mice. PLoS Biol *5*, e234.

Ahn, K., Szczesna-Skorupa, E., and Kemper, B. (1993). The amino-terminal 29 amino acids of cytochrome P450 2C1 are sufficient for retention in the endoplasmic reticulum. J Biol Chem *268*, 18726-18733.

Allenby, G., Bocquel, M.T., Saunders, M., Kazmer, S., Speck, J., Rosenberger, M., Lovey, A., Kastner, P., Grippo, J.F., Chambon, P.*, et al.* (1993). Retinoic acid receptors and retinoid X receptors: interactions with endogenous retinoic acids. Proc Natl Acad Sci U S A *90*, 30-34.

Amengual, J., Golczak, M., Palczewski, K., and von Lintig, J. (2012). Lecithin:retinol acyl transferase is critical for cellular uptake of vitamin A from serum retinol binding protein. J Biol Chem.

Andreazzoli, M., Gestri, G., Angeloni, D., Menna, E., and Barsacchi, G. (1999). Role of Xrx1 in Xenopus eye and anterior brain development. Development *126*, 2451-2460.

Andrews, B.J., Proteau, G.A., Beatty, L.G., and Sadowski, P.D. (1985). The FLP recombinase of the 2 micron circle DNA of yeast: interaction with its target sequences. Cell *40*, 795-803.

Araki, M., and Okada, T.S. (1977). Differentiation of lens and pigment cells in cultures of neural retinal cells of early chick embryos. Dev Biol *60*, 278-286.

Archer, T.C., Jin, J., and Casey, E.S. (2011). Interaction of Sox1, Sox2, Sox3 and Oct4 during primary neurogenesis. Dev Biol *350*, 429-440.

Asai-Coakwell, M., French, C.R., Berry, K.M., Ye, M., Koss, R., Somerville, M., Mueller, R., van Heyningen, V., Waskiewicz, A.J., and Lehmann, O.J. (2007). GDF6, a novel locus for a spectrum of ocular developmental anomalies. Am J Hum Genet *80*, 306-315.

Asai-Coakwell, M., French, C.R., Ye, M., Garcha, K., Bigot, K., Perera, A.G., Staehling-Hampton, K., Mema, S.C., Chanda, B., Mushegian, A.*, et al.* (2009). Incomplete penetrance and phenotypic variability characterize Gdf6-attributable oculo-skeletal phenotypes. Hum Mol Genet *18*, 1110-1121.

Ashkenazi-Hoffnung, L., Lebenthal, Y., Wyatt, A.W., Ragge, N.K., Dateki, S., Fukami, M., Ogata, T., Phillip, M., and Gat-Yablonski, G. (2010). A novel loss-of-function mutation in OTX2 in a patient with anophthalmia and isolated growth hormone deficiency. Hum Genet *127*, 721-729.

Bakrania, P., Robinson, D.O., Bunyan, D.J., Salt, A., Martin, A., Crolla, J.A., Wyatt, A., Fielder, A., Ainsworth, J., Moore, A.*, et al.* (2007). SOX2 anophthalmia syndrome: 12 new cases demonstrating broader phenotype and high frequency of large gene deletions. Br J Ophthalmol *91*, 1471-1476.

Bar-Nun, S., Kreibich, G., Adesnik, M., Alterman, L., Negishi, M., and Sabatini, D.D. (1980). Synthesis and insertion of cytochrome P-450 into endoplasmic reticulum membranes. Proc Natl Acad Sci U S A *77*, 965-969.

Barabino, S.M., Spada, F., Cotelli, F., and Boncinelli, E. (1997). Inactivation of the zebrafish homologue of Chx10 by antisense oligonucleotides causes eye malformations similar to the ocular retardation phenotype. Mech Dev *63*, 133-143.

Bardakjian, T.M., and Schneider, A. (2011). The genetics of anophthalmia and microphthalmia. Curr Opin Ophthalmol *22*, 309-313.

Bates, C.J. (1983). Vitamin A in pregnancy and lactation. Proc Nutr Soc *42*, 65-79.

Baumer, N., Marquardt, T., Stoykova, A., Ashery-Padan, R., Chowdhury, K., and Gruss, P. (2002). Pax6 is required for establishing naso-temporal and dorsal characteristics of the optic vesicle. Development *129*, 4535-4545.

Baumer, N., Marquardt, T., Stoykova, A., Spieler, D., Treichel, D., Ashery-Padan, R., and Gruss, P. (2003). Retinal pigmented epithelium determination requires the redundant activities of Pax2 and Pax6. Development *130*, 2903-2915.

Bavik, C., Ward, S.J., and Chambon, P. (1996). Developmental abnormalities in cultured mouse embryos deprived of retinoic by inhibition of yolk-sac retinol binding protein synthesis. Proc Natl Acad Sci U S A *93*, 3110-3114.

Beby, F., Housset, M., Fossat, N., Le Greneur, C., Flamant, F., Godement, P., and Lamonerie, T. (2010). Otx2 gene deletion in adult mouse retina induces rapid RPE dystrophy and slow photoreceptor degeneration. PLoS One *5*, e11673.

Bellenguez, C., Ober, C., and Bourgain, C. (2009). A multiple splitting approach to linkage analysis in large pedigrees identifies a linkage to asthma on chromosome 12. Genet Epidemiol *33*, 207-216.

Bellovino, D., Lanyau, Y., Garaguso, I., Amicone, L., Cavallari, C., Tripodi, M., and Gaetani, S. (1999). MMH cells: An in vitro model for the study of retinol-binding protein secretion regulated by retinol. J Cell Physiol *181*, 24-32.

Benko, S., Fantes, J.A., Amiel, J., Kleinjan, D.J., Thomas, S., Ramsay, J., Jamshidi, N., Essafi, A., Heaney, S., Gordon, C.T.*, et al.* (2009). Highly conserved non-coding elements on either side of SOX9 associated with Pierre Robin sequence. Nat Genet *41*, 359-364.

Bennett, C.P., Betts, D.R., and Seller, M.J. (1991). Deletion 14q (q22q23) associated with anophthalmia, absent pituitary, and other abnormalities. J Med Genet *28*, 280-281.

Bentley, N.J., Eisen, T., and Goding, C.R. (1994). Melanocyte-specific expression of the human tyrosinase promoter: activation by the microphthalmia gene product and role of the initiator. Mol Cell Biol *14*, 7996-8006.

Bergstrom, D.E., Young, M., Albrecht, K.H., and Eicher, E.M. (2000). Related function of mouse SOX3, SOX9, and SRY HMG domains assayed by male sex determination. Genesis *28*, 111-124.

Berni, R., Stoppini, M., and Zapponi, M.C. (1992). The piscine plasma retinol-binding protein. Purification, partial amino acid sequence and interaction with mammalian transthyretin of rainbow trout (Oncorhynchus mykiss) retinol-binding protein. Eur J Biochem *204*, 99-106.

Bernier, G., Panitz, F., Zhou, X., Hollemann, T., Gruss, P., and Pieler, T. (2000). Expanded retina territory by midbrain transformation upon overexpression of Six6 (Optx2) in Xenopus embryos. Mech Dev *93*, 59-69.

Berry, D.C., Jin, H., Majumdar, A., and Noy, N. (2011). Signaling by vitamin A and retinol-binding protein regulates gene expression to inhibit insulin responses. Proc Natl Acad Sci U S A *108*, 4340-4345.

Biesalski, H.K., Frank, J., Beck, S.C., Heinrich, F., Illek, B., Reifen, R., Gollnick, H., Seeliger, M.W., Wissinger, B., and Zrenner, E. (1999). Biochemical but not clinical vitamin A deficiency results from mutations in the gene for retinol binding protein. Am J Clin Nutr *69*, 931-936.

Bishop, C.E., Whitworth, D.J., Qin, Y., Agoulnik, A.I., Agoulnik, I.U., Harrison, W.R., Behringer, R.R., and Overbeek, P.A. (2000). A transgenic insertion upstream of sox9 is associated with dominant XX sex reversal in the mouse. Nat Genet *26*, 490-494.

Bleyl, S.B., Byrne, J.L., South, S.T., Dries, D.C., Stevenson, D.A., Rope, A.F., Vianna-Morgante, A.M., Schoenwolf, G.C., Kivlin, J.D., Brothman, A.*, et al.* (2007).

Brachymesomelic dysplasia with Peters anomaly of the eye results from disruptions of the X chromosome near the SHOX and SOX3 genes. Am J Med Genet A *143A*, 2785-2795.

Blomhoff, R., Helgerud, P., Rasmussen, M., Berg, T., and Norum, K.R. (1982). In vivo uptake of chylomicron [3H]retinyl ester by rat liver: evidence for retinol transfer from parenchymal to nonparenchymal cells. Proc Natl Acad Sci U S A *79*, 7326-7330.

Bock, C., Reither, S., Mikeska, T., Paulsen, M., Walter, J., and Lengauer, T. (2005). BiQ Analyzer: visualization and quality control for DNA methylation data from bisulfite sequencing. Bioinformatics *21*, 4067-4068.

Borek, C. (1972). Neoplastic transformation in vitro of a clone of adult liver epithelial cells into differentiated hepatoma-like cells under conditions of nutritional stress. Proc Natl Acad Sci U S A *69*, 956-959.

Borek, C., Smith, J.E., and Goodman, D.S. (1980). Liver cells in culture: a model for investigating the regulation of retinol-binding protein metabolism. Ann N Y Acad Sci *349*, 221-227.

Bouillet, P., Sapin, V., Chazaud, C., Messaddeq, N., Decimo, D., Dolle, P., and Chambon, P. (1997). Developmental expression pattern of Stra6, a retinoic acid-responsive gene encoding a new type of membrane protein. Mech Dev *63*, 173-186.

Bowl, M.R., Nesbit, M.A., Harding, B., Levy, E., Jefferson, A., Volpi, E., Rizzoti, K., Lovell-Badge, R., Schlessinger, D., Whyte, M.P.*, et al.* (2005). An interstitial deletion-insertion involving chromosomes 2p25.3 and Xq27.1, near SOX3, causes X-linked recessive hypoparathyroidism. J Clin Invest *115*, 2822-2831.

Bowles, J., Schepers, G., and Koopman, P. (2000). Phylogeny of the SOX family of developmental transcription factors based on sequence and structural indicators. Dev Biol *227*, 239-255.

Brown, K.E., Keller, P.J., Ramialison, M., Rembold, M., Stelzer, E.H., Loosli, F., and Wittbrodt, J. (2010). Nlcam modulates midline convergence during anterior neural plate morphogenesis. Dev Biol *339*, 14-25.

Brunelli, S., Silva Casey, E., Bell, D., Harland, R., and Lovell-Badge, R. (2003). Expression of Sox3 throughout the developing central nervous system is dependent on the combined action of discrete, evolutionarily conserved regulatory elements. Genesis *36*, 12-24.

Bryne, J.C., Valen, E., Tang, M.H., Marstrand, T., Winther, O., da Piedade, I., Krogh, A., Lenhard, B., and Sandelin, A. (2008). JASPAR, the open access database of transcription factor-binding profiles: new content and tools in the 2008 update. Nucleic Acids Res *36*, D102-106.

Bumsted, K.M., and Barnstable, C.J. (2000). Dorsal retinal pigment epithelium differentiates as neural retina in the microphthalmia (mi/mi) mouse. Invest Ophthalmol Vis Sci *41*, 903-908.

Burgoyne, P.S., Buehr, M., Koopman, P., Rossant, J., and McLaren, A. (1988). Cell-autonomous action of the testis-determining gene: Sertoli cells are exclusively XY in XX----XY chimaeric mouse testes. Development *102*, 443-450.

Burkitt Wright, E.M., Perveen, R., Clayton, P.E., Hall, C.M., Costa, T., Procter, A.M., Giblin, C.A., Donnai, D., and Black, G.C. (2009). X-linked isolated growth hormone deficiency: expanding the phenotypic spectrum of SOX3 polyalanine tract expansions. Clin Dysmorphol *18*, 218-221.

Burmeister, M., Novak, J., Liang, M.Y., Basu, S., Ploder, L., Hawes, N.L., Vidgen, D., Hoover, F., Goldman, D., Kalnins, V.I.*, et al.* (1996). Ocular retardation mouse caused by Chx10 homeobox null allele: impaired retinal progenitor proliferation and bipolar cell differentiation. Nat Genet *12*, 376-384.

Burn, J., Brennan, P., Little, J., Holloway, S., Coffey, R., Somerville, J., Dennis, N.R., Allan, L., Arnold, R., Deanfield, J.E.*, et al.* (1998). Recurrence risks in offspring of adults with major heart defects: results from first cohort of British collaborative study. Lancet *351*, 311-316.

Burton, G.J., Watson, A.L., Hempstock, J., Skepper, J.N., and Jauniaux, E. (2002). Uterine glands provide histiotrophic nutrition for the human fetus during the first trimester of pregnancy. J Clin Endocrinol Metab *87*, 2954-2959.

Bylund, M., Andersson, E., Novitch, B.G., and Muhr, J. (2003). Vertebrate neurogenesis is counteracted by Sox1-3 activity. Nat Neurosci *6*, 1162-1168.

Cameron, M.C., Denovan-Wright, E.M., Sharma, M.K., and Wright, J.M. (2002). Cellular retinol-binding protein type II (CRBPII) in adult zebrafish (Danio rerio). cDNA sequence, tissue-specific expression and gene linkage analysis. Eur J Biochem *269*, 4685-4692.

Casey, J., Kawaguchi, R., Morrissey, M., Sun, H., McGettigan, P., Nielsen, J.E., Conroy, J., Regan, R., Kenny, E., Cormican, P.*, et al.* (2011). First implication of STRA6 mutations in isolated anophthalmia, microphthalmia, and coloboma: a new dimension to the STRA6 phenotype. Hum Mutat *32*, 1417-1426.

Cavodeassi, F., Carreira-Barbosa, F., Young, R.M., Concha, M.L., Allende, M.L., Houart, C., Tada, M., and Wilson, S.W. (2005). Early stages of zebrafish eye formation require the coordinated activity of Wnt11, Fz5, and the Wnt/beta-catenin pathway. Neuron *47*, 43-56.

Chassaing, N., Golzio, C., Odent, S., Lequeux, L., Vigouroux, A., Martinovic-Bouriel, J., Tiziano, F.D., Masini, L., Piro, F., Maragliano, G.*, et al.* (2009). Phenotypic spectrum of STRA6 mutations: from Matthew-Wood syndrome to non-lethal anophthalmia. Hum Mutat *30*, E673-681.

Chazaud, C., Bouillet, P., Oulad-Abdelghani, M., and Dolle, P. (1996). Restricted expression of a novel retinoic acid responsive gene during limb bud dorsoventral patterning and endochondral ossification. Dev Genet *19*, 66-73.

Cheli, Y., Ohanna, M., Ballotti, R., and Bertolotto, C. (2010). Fifteen-year quest for microphthalmia-associated transcription factor target genes. Pigment Cell Melanoma Res *23*, 27-40.

Chemical Computing Group, I. (2012). Molecular Operating Environment (MOE), 2010.10.

Cho, S.H., and Cepko, C.L. (2006). Wnt2b/beta-catenin-mediated canonical Wnt signaling determines the peripheral fates of the chick eye. Development *133*, 3167-3177.

Chow, R.L., Altmann, C.R., Lang, R.A., and Hemmati-Brivanlou, A. (1999). Pax6 induces ectopic eyes in a vertebrate. Development *126*, 4213-4222.

Chuang, J.C., and Raymond, P.A. (2001). Zebrafish genes rx1 and rx2 help define the region of forebrain that gives rise to retina. Dev Biol *231*, 13-30.

Clark, A.M., Yun, S., Veien, E.S., Wu, Y.Y., Chow, R.L., Dorsky, R.I., and Levine, E.M. (2008). Negative regulation of Vsx1 by its paralog Chx10/Vsx2 is conserved in the vertebrate retina. Brain Res *1192*, 99-113.

Cogan, U., Kopelman, M., Mokady, S., and Shinitzky, M. (1976). Binding affinities of retinol and related compounds to retinol binding proteins. Eur J Biochem *65*, 71-78.

Collignon, J., Sockanathan, S., Hacker, A., Cohen-Tannoudji, M., Norris, D., Rastan, S., Stevanovic, M., Goodfellow, P.N., and Lovell-Badge, R. (1996). A comparison of the properties of Sox-3 with Sry and two related genes, Sox-1 and Sox-2. Development *122*, 509-520.

Collins, M.D., Tzimas, G., Hummler, H., Burgin, H., and Nau, H. (1994). Comparative teratology and transplacental pharmacokinetics of all-trans-retinoic acid, 13-cis-retinoic acid, and retinyl palmitate following daily administrations in rats. Toxicol Appl Pharmacol *127*, 132-144.

Connolly, H.M., and Warnes, C.A. (1994). Ebstein's anomaly: outcome of pregnancy. J Am Coll Cardiol *23*, 1194-1198.

Coulombre, J.L., and Coulombre, A.J. (1965). Regeneration of neural retina from the pigmented epithelium in the chick embryo. Dev Biol *12*, 79-92.

Cowan, S.W., Newcomer, M.E., and Jones, T.A. (1990). Crystallographic refinement of human serum retinol binding protein at 2A resolution. Proteins *8*, 44-61.

Cowan, S.W., Newcomer, M.E., and Jones, T.A. (1993). Crystallographic studies on a family of cellular lipophilic transport proteins. Refinement of P2 myelin protein and the structure determination and refinement of cellular retinol-binding protein in complex with all-trans-retinol. J Mol Biol *230*, 1225-1246.

Creech Kraft, J., Lofberg, B., Chahoud, I., Bochert, G., and Nau, H. (1989). Teratogenicity and placental transfer of all-trans-, 13-cis-, 4-oxo-all-trans-, and 4-oxo-13-cis-retinoic acid after administration of a low oral dose during organogenesis in mice. Toxicol Appl Pharmacol *100*, 162-176.

Crow, J.A., and Ong, D.E. (1985). Cell-specific immunohistochemical localization of a cellular retinol-binding protein (type two) in the small intestine of rat. Proc Natl Acad Sci U S A *82*, 4707-4711.

D'Ambrosio, D.N., Clugston, R.D., and Blaner, W.S. (2011). Vitamin A metabolism: an update. Nutrients *3*, 63-103.

Danciger, M., Kozak, C.A., Nickerson, J., Redmond, T.M., and Farber, D.B. (1990). Localization of the gene for interphotoreceptor retinoid-binding protein to mouse chromosome 14 near Np-1. Genomics *8*, 727-731.

Dancis, J., Levitz, M., Katz, J., Wilson, D., Blaner, W.S., Piantedosi, R., and Goodman, D.S. (1992). Transfer and metabolism of retinol by the perfused human placenta. Pediatr Res *32*, 195-199.

Dathe, K., Kjaer, K.W., Brehm, A., Meinecke, P., Nurnberg, P., Neto, J.C., Brunoni, D., Tommerup, N., Ott, C.E., Klopocki, E.*, et al.* (2009). Duplications involving a conserved regulatory element downstream of BMP2 are associated with brachydactyly type A2. Am J Hum Genet *84*, 483-492.

David, D., Cardoso, J., Marques, B., Marques, R., Silva, E.D., Santos, H., and Boavida, M.G. (2003). Molecular characterization of a familial translocation implicates disruption of HDAC9 and possible position effect on TGFbeta2 in the pathogenesis of Peters' anomaly. Genomics *81*, 489-503.

Davies, A.F., Mirza, G., Flinter, F., and Ragoussis, J. (1999). An interstitial deletion of 6p24-p25 proximal to the FKHL7 locus and including AP-2alpha that affects anterior eye chamber development. J Med Genet *36*, 708-710.

Davis-Silberman, N., and Ashery-Padan, R. (2008). Iris development in vertebrates; genetic and molecular considerations. Brain Res *1192*, 17-28.

Davis-Silberman, N., Kalich, T., Oron-Karni, V., Marquardt, T., Kroeber, M., Tamm, E.R., and Ashery-Padan, R. (2005). Genetic dissection of Pax6 dosage requirements in the developing mouse eye. Hum Mol Genet *14*, 2265-2276.

De Gobbi, M., Viprakasit, V., Hughes, J.R., Fisher, C., Buckle, V.J., Ayyub, H., Gibbons, R.J., Vernimmen, D., Yoshinaga, Y., de Jong, P.*, et al.* (2006). A regulatory SNP causes a human genetic disease by creating a new transcriptional promoter. Science *312*, 1215-1217.

de Iongh, R.U., Lovicu, F.J., Chamberlain, C.G., and McAvoy, J.W. (1997). Differential expression of fibroblast growth factor receptors during rat lens morphogenesis and growth. Invest Ophthalmol Vis Sci *38*, 1688-1699.

de Iongh, R.U., Lovicu, F.J., Hanneken, A., Baird, A., and McAvoy, J.W. (1996). FGF receptor-1 (flg) expression is correlated with fibre differentiation during rat lens morphogenesis and growth. Dev Dyn *206*, 412-426.

De Leeuw, A.M., Gaur, V.P., Saari, J.C., and Milam, A.H. (1990). Immunolocalization of cellular retinol-, retinaldehyde- and retinoic acid-binding proteins in rat retina during pre- and postnatal development. J Neurocytol *19*, 253-264.

Dee, C.T., Hirst, C.S., Shih, Y.H., Tripathi, V.B., Patient, R.K., and Scotting, P.J. (2008). Sox3 regulates both neural fate and differentiation in the zebrafish ectoderm. Dev Biol *320*, 289-301.

Demmer, L.A., Birkenmeier, E.H., Sweetser, D.A., Levin, M.S., Zollman, S., Sparkes, R.S., Mohandas, T., Lusis, A.J., and Gordon, J.I. (1987). The cellular retinol binding protein II gene. Sequence analysis of the rat gene, chromosomal localization in mice and humans, and documentation of its close linkage to the cellular retinol binding protein gene. J Biol Chem *262*, 2458-2467.

Demura, M., Martin, R.M., Shozu, M., Sebastian, S., Takayama, K., Hsu, W.T., Schultz, R.A., Neely, K., Bryant, M., Mendonca, B.B.*, et al.* (2007). Regional rearrangements in chromosome 15q21 cause formation of cryptic promoters for the CYP19 (aromatase) gene. Hum Mol Genet *16*, 2529-2541.

Deo, M., Yu, J.Y., Chung, K.H., Tippens, M., and Turner, D.L. (2006). Detection of mammalian microRNA expression by in situ hybridization with RNA oligonucleotides. Dev Dyn *235*, 2538-2548.

Diaczok, D., Romero, C., Zunich, J., Marshall, I., and Radovick, S. (2008). A novel dominant negative mutation of OTX2 associated with combined pituitary hormone deficiency. J Clin Endocrinol Metab *93*, 4351-4359.

Dodge, J.A. (1970). Production of duodenal ulcers and hypertrophic pyloric stenosis by administration of pentagastrin to pregnant and newborn dogs. Nature *225*, 284-285.

Dogan, R.I., Getoor, L., Wilbur, W.J., and Mount, S.M. (2007). SplicePort--an interactive splice-site analysis tool. Nucleic Acids Res *35*, W285-291.

Dong, D., Ruuska, S.E., Levinthal, D.J., and Noy, N. (1999). Distinct roles for cellular retinoic acid-binding proteins I and II in regulating signaling by retinoic acid. J Biol Chem *274*, 23695-23698.

Dorval, K.M., Bobechko, B.P., Ahmad, K.F., and Bremner, R. (2005). Transcriptional activity of the paired-like homeodomain proteins CHX10 and VSX1. J Biol Chem *280*, 10100-10108.

Dowling, J.E., and Wald, G. (1958). Vitamin a Deficiency and Night Blindness. Proc Natl Acad Sci U S A *44*, 648-661.

Duester, G. (2000). Families of retinoid dehydrogenases regulating vitamin A function: production of visual pigment and retinoic acid. Eur J Biochem *267*, 4315-4324.

Duester, G. (2008). Retinoic acid synthesis and signaling during early organogenesis. Cell *134*, 921-931.

Duester, G. (2009). Keeping an eye on retinoic acid signaling during eye development. Chem Biol Interact *178*, 178-181.

Dupe, V., Matt, N., Garnier, J.M., Chambon, P., Mark, M., and Ghyselinck, N.B. (2003). A newborn lethal defect due to inactivation of retinaldehyde dehydrogenase type 3 is prevented by maternal retinoic acid treatment. Proc Natl Acad Sci U S A *100*, 14036-14041.

During, A., and Harrison, E.H. (2007). Mechanisms of provitamin A (carotenoid) and vitamin A (retinol) transport into and out of intestinal Caco-2 cells. J Lipid Res *48*, 2283-2294.

Elliott, J., Maltby, E.L., and Reynolds, B. (1993). A case of deletion 14(q22.1-->q22.3) associated with anophthalmia and pituitary abnormalities. J Med Genet *30*, 251-252.

Epstein, C.J., Erickson, R.P., and Wynshaw-Boris, A.J. (2008). Inborn errors of development : the molecular basis of clinical disorders of morphogenesis, 2nd edn (Oxford ; New York, Oxford University Press).

Epstein, J.A., Glaser, T., Cai, J., Jepeal, L., Walton, D.S., and Maas, R.L. (1994). Two independent and interactive DNA-binding subdomains of the Pax6 paired domain are regulated by alternative splicing. Genes Dev *8*, 2022-2034.

Eriksson, U., Das, K., Busch, C., Nordlinder, H., Rask, L., Sundelin, J., Sallstrom, J., and Peterson, P.A. (1984). Cellular retinol-binding protein. Quantitation and distribution. J Biol Chem *259*, 13464-13470.

Evans, A.L., and Gage, P.J. (2005). Expression of the homeobox gene Pitx2 in neural crest is required for optic stalk and ocular anterior segment development. Hum Mol Genet *14*, 3347-3359.

EVS. Exome Variant Server, NHLBI Exome Sequencing Project (ESP), Seattle, WA (URL: http://evs.gs.washington.edu/EVS/) May, 2012.

Fan, X., Molotkov, A., Manabe, S., Donmoyer, C.M., Deltour, L., Foglio, M.H., Cuenca, A.E., Blaner, W.S., Lipton, S.A., and Duester, G. (2003). Targeted disruption of Aldh1a1 (Raldh1) provides evidence for a complex mechanism of retinoic acid synthesis in the developing retina. Mol Cell Biol *23*, 4637-4648.

Fantes, J., Ragge, N.K., Lynch, S.A., McGill, N.I., Collin, J.R., Howard-Peebles, P.N., Hayward, C., Vivian, A.J., Williamson, K., van Heyningen, V.*, et al.* (2003). Mutations in SOX2 cause anophthalmia. Nat Genet *33*, 461-463.

Fantes, J., Redeker, B., Breen, M., Boyle, S., Brown, J., Fletcher, J., Jones, S., Bickmore, W., Fukushima, Y., Mannens, M.*, et al.* (1995). Aniridia-associated cytogenetic rearrangements suggest that a position effect may cause the mutant phenotype. Hum Mol Genet *4*, 415-422.

Farjo, K.M., Moiseyev, G., Nikolaeva, O., Sandell, L.L., Trainor, P.A., and Ma, J.X. (2011). RDH10 is the primary enzyme responsible for the first step of embryonic Vitamin A metabolism and retinoic acid synthesis. Dev Biol *357*, 347-355.

Fawcett, D., Pasceri, P., Fraser, R., Colbert, M., Rossant, J., and Giguere, V. (1995). Postaxial polydactyly in forelimbs of CRABP-II mutant mice. Development *121*, 671-679.

Ferda Percin, E., Ploder, L.A., Yu, J.J., Arici, K., Horsford, D.J., Rutherford, A., Bapat, B., Cox, D.W., Duncan, A.M., Kalnins, V.I.*, et al.* (2000). Human microphthalmia associated with mutations in the retinal homeobox gene CHX10. Nat Genet *25*, 397-401.

Fex, G., Albertsson, P.A., and Hansson, B. (1979). Interaction between prealbumin and retinol-binding protein studied by affinity chromatography, gel filtration and two-phase partition. Eur J Biochem *99*, 353-360.

Flower, D.R. (1996). The lipocalin protein family: structure and function. Biochem J *318 (Pt 1)*, 1-14.

Flower, D.R., North, A.C., and Attwood, T.K. (1993). Structure and sequence relationships in the lipocalins and related proteins. Protein Sci *2*, 753-761.

Folli, C., Viglione, S., Busconi, M., and Berni, R. (2005). Biochemical basis for retinol deficiency induced by the I41N and G75D mutations in human plasma retinol-binding protein. Biochem Biophys Res Commun *336*, 1017-1022.

Forbes, K.P., Pipe, J.G., Bird, C.R., and Heiserman, J.E. (2001). PROPELLER MRI: clinical testing of a novel technique for quantification and compensation of head motion. J Magn Reson Imaging *14*, 215-222.

Forrester, S., Kovach, M.J., Reynolds, N.M., Urban, R., and Kimonis, V. (2001). Manifestations in four males with and an obligate carrier of the Lenz microphthalmia syndrome. Am J Med Genet *98*, 92-100.

Foster, J.W., Dominguez-Steglich, M.A., Guioli, S., Kwok, C., Weller, P.A., Stevanovic, M., Weissenbach, J., Mansour, S., Young, I.D., Goodfellow, P.N.*, et al.* (1994). Campomelic dysplasia and autosomal sex reversal caused by mutations in an SRY-related gene. Nature *372*, 525-530.

Foster, J.W., and Graves, J.A. (1994). An SRY-related sequence on the marsupial X chromosome: implications for the evolution of the mammalian testis-determining gene. Proc Natl Acad Sci U S A *91*, 1927-1931.

Freyer, C., and Renfree, M.B. (2009). The mammalian yolk sac placenta. J Exp Zool B Mol Dev Evol *312*, 545-554.

Fuhrmann, S. (2008). Wnt signaling in eye organogenesis. Organogenesis *4*, 60-67.

Fuhrmann, S. (2010). Eye morphogenesis and patterning of the optic vesicle. Curr Top Dev Biol *93*, 61-84.

Fuhrmann, S., Levine, E.M., and Reh, T.A. (2000). Extraocular mesenchyme patterns the optic vesicle during early eye development in the embryonic chick. Development *127*, 4599-4609.

Furukawa, T., Kozak, C.A., and Cepko, C.L. (1997). rax, a novel paired-type homeobox gene, shows expression in the anterior neural fold and developing retina. Proc Natl Acad Sci U S A *94*, 3088-3093.

Gage, P.J., Rhoades, W., Prucka, S.K., and Hjalt, T. (2005). Fate maps of neural crest and mesoderm in the mammalian eye. Invest Ophthalmol Vis Sci *46*, 4200-4208.

Gaub, M.P., Lutz, Y., Ghyselinck, N.B., Scheuer, I., Pfister, V., Chambon, P., and Rochette-Egly, C. (1998). Nuclear detection of cellular retinoic acid binding proteins I and II with new antibodies. J Histochem Cytochem *46*, 1103-1111.

Ghyselinck, N.B., Bavik, C., Sapin, V., Mark, M., Bonnier, D., Hindelang, C., Dierich, A., Nilsson, C.B., Hakansson, H., Sauvant, P*., et al.* (1999). Cellular retinol-binding protein I is essential for vitamin A homeostasis. EMBO J *18*, 4903-4914.

Ghyselinck, N.B., Dupe, V., Dierich, A., Messaddeq, N., Garnier, J.M., Rochette-Egly, C., Chambon, P., and Mark, M. (1997). Role of the retinoic acid receptor beta (RARbeta) during mouse development. Int J Dev Biol *41*, 425-447.

Giguere, V., Lyn, S., Yip, P., Siu, C.H., and Amin, S. (1990). Molecular cloning of cDNA encoding a second cellular retinoic acid-binding protein. Proc Natl Acad Sci U S A *87*, 6233-6237.

Glaser, T., Jepeal, L., Edwards, J.G., Young, S.R., Favor, J., and Maas, R.L. (1994). PAX6 gene dosage effect in a family with congenital cataracts, aniridia, anophthalmia and central nervous system defects. Nat Genet *7*, 463-471.

Golzio, C., Martinovic-Bouriel, J., Thomas, S., Mougou-Zrelli, S., Grattagliano-Bessieres, B., Bonniere, M., Delahaye, S., Munnich, A., Encha-Razavi, F., Lyonnet, S.,

et al. (2007). Matthew-Wood syndrome is caused by truncating mutations in the retinol-binding protein receptor gene STRA6. Am J Hum Genet *80*, 1179-1187.

Gomaa, M.S., Yee, S.W., Milbourne, C.E., Barbera, M.C., Simons, C., and Brancale, A. (2006). Homology model of human retinoic acid metabolising enzyme cytochrome P450 26A1 (CYP26A1): active site architecture and ligand binding. J Enzyme Inhib Med Chem *21*, 361-369.

Gonzalez-Rodriguez, J., Pelcastre, E.L., Tovilla-Canales, J.L., Garcia-Ortiz, J.E., Amato-Almanza, M., Villanueva-Mendoza, C., Espinosa-Mattar, Z., and Zenteno, J.C. (2010). Mutational screening of CHX10, GDF6, OTX2, RAX and SOX2 genes in 50 unrelated microphthalmia-anophthalmia-coloboma (MAC) spectrum cases. Br J Ophthalmol *94*, 1100-1104.

Goodman, D.S., and Leslie, R.B. (1972). Fluorescence studies of human plasma retinol-binding protein and of the retinol-binding protein-prealbumin complex. Biochim Biophys Acta *260*, 670-678.

Goodman, D.W., Huang, H.S., and Shiratori, T. (1965). Tissue Distribution and Metabolism of Newly Absorbed Vitamin a in the Rat. J Lipid Res *6*, 390-396.

Gorry, P., Lufkin, T., Dierich, A., Rochette-Egly, C., Decimo, D., Dolle, P., Mark, M., Durand, B., and Chambon, P. (1994). The cellular retinoic acid binding protein I is dispensable. Proc Natl Acad Sci U S A *91*, 9032-9036.

Gotter, A.L., Shaikh, T.H., Budarf, M.L., Rhodes, C.H., and Emanuel, B.S. (2004). A palindrome-mediated mechanism distinguishes translocations involving LCR-B of chromosome 22q11.2. Hum Mol Genet *13*, 103-115.

Graham, C.A., Redmond, R.M., and Nevin, N.C. (1991). X-linked clinical anophthalmos. Localization of the gene to Xq27-Xq28. Ophthalmic Paediatr Genet *12*, 43-48.

Graham, V., Khudyakov, J., Ellis, P., and Pevny, L. (2003). SOX2 functions to maintain neural progenitor identity. Neuron *39*, 749-765.

Graves, J.A. (1998). Interactions between SRY and SOX genes in mammalian sex determination. Bioessays *20*, 264-269.

Graw, J. (2003). The genetic and molecular basis of congenital eye defects. Nat Rev Genet *4*, 876-888.

Graw, J. (2010). Eye development. Curr Top Dev Biol *90*, 343-386.

Green, E.S., Stubbs, J.L., and Levine, E.M. (2003). Genetic rescue of cell number in a mouse model of microphthalmia: interactions between Chx10 and G1-phase cell cycle regulators. Development *130*, 539-552.

Grimm, C., Kraft, R., Sauerbruch, S., Schultz, G., and Harteneck, C. (2003). Molecular and functional characterization of the melastatin-related cation channel TRPM3. J Biol Chem *278*, 21493-21501.

Grindley, J.C., Hargett, L.K., Hill, R.E., Ross, A., and Hogan, B.L. (1997). Disruption of PAX6 function in mice homozygous for the Pax6Sey-1Neu mutation produces abnormalities in the early development and regionalization of the diencephalon. Mech Dev *64*, 111-126.

Grun, F., Hirose, Y., Kawauchi, S., Ogura, T., and Umesono, K. (2000). Aldehyde dehydrogenase 6, a cytosolic retinaldehyde dehydrogenase prominently expressed in sensory neuroepithelia during development. J Biol Chem *275*, 41210-41218.

Grzyb, J., Latowski, D., and Strzalka, K. (2006). Lipocalins - a family portrait. J Plant Physiol *163*, 895-915.

Gubbay, J., Collignon, J., Koopman, P., Capel, B., Economou, A., Munsterberg, A., Vivian, N., Goodfellow, P., and Lovell-Badge, R. (1990). A gene mapping to the sex-determining region of the mouse Y chromosome is a member of a novel family of embryonically expressed genes. Nature *346*, 245-250.

Guillemot, F., and Cepko, C.L. (1992). Retinal fate and ganglion cell differentiation are potentiated by acidic FGF in an in vitro assay of early retinal development. Development *114*, 743-754.

Halder, G., Callaerts, P., and Gehring, W.J. (1995). Induction of ectopic eyes by targeted expression of the eyeless gene in Drosophila. Science *267*, 1788-1792.

Hale, F. (1932). The relation of vitamin A to the eye devlepment of pig. The Journal of Heredity, 105-106.

Hale, F. (1935). Pigs born without eyeballs. Journal of Heredity.

Hamel, B.C., Smits, A.P., Otten, B.J., van den Helm, B., Ropers, H.H., and Mariman, E.C. (1996). Familial X-linked mental retardation and isolated growth hormone deficiency: clinical and molecular findings. Am J Med Genet *64*, 35-41.

Harney, J.P., Smith, L.C., Simmen, R.C., Fliss, A.E., and Bazer, F.W. (1994). Retinol-binding protein: immunolocalization of protein and abundance of messenger ribonucleic acid in conceptus and maternal tissues during pregnancy in pigs. Biol Reprod *50*, 1126-1135.

Haustein, J. (1983). On the ultrastructure of the developing and adult mouse corneal stroma. Anat Embryol (Berl) *168*, 291-305.

Heller, J., and Horwitz, J. (1973). Conformational changes following interaction between retinol isomers and human retinol-binding protein and between the retinol-binding protein and prealbumin. J Biol Chem *248*, 6308-6316.

Heller, J., and Horwitz, J. (1974). The binding stoichiometry of human plasma retinol-binding protein to prealbumin. J Biol Chem *249*, 5933-5938.

Hernandez, R.E., Putzke, A.P., Myers, J.P., Margaretha, L., and Moens, C.B. (2007). Cyp26 enzymes generate the retinoic acid response pattern necessary for hindbrain development. Development *134*, 177-187.

Heyman, R.A., Mangelsdorf, D.J., Dyck, J.A., Stein, R.B., Eichele, G., Evans, R.M., and Thaller, C. (1992). 9-cis retinoic acid is a high affinity ligand for the retinoid X receptor. Cell *68*, 397-406.

Hill, R.E., Favor, J., Hogan, B.L., Ton, C.C., Saunders, G.F., Hanson, I.M., Prosser, J., Jordan, T., Hastie, N.D., and van Heyningen, V. (1991). Mouse small eye results from mutations in a paired-like homeobox-containing gene. Nature *354*, 522-525.

Hodgkinson, C.A., Moore, K.J., Nakayama, A., Steingrimsson, E., Copeland, N.G., Jenkins, N.A., and Arnheiter, H. (1993). Mutations at the mouse microphthalmia locus are associated with defects in a gene encoding a novel basic-helix-loop-helix-zipper protein. Cell *74*, 395-404.

Hol, F.A., Schepens, M.T., van Beersum, S.E., Redolfi, E., Affer, M., Vezzoni, P., Hamel, B.C., Karnes, P.S., Mariman, E.C., and Zucchi, I. (2000). Identification and characterization of an Xq26-q27 duplication in a family with spina bifida and panhypopituitarism suggests the involvement of two distinct genes. Genomics *69*, 174-181.

Holtfreter, J. (1939). Gewebeaffinit.t, ein Mittel der embryonalen Formbildung. ArchZellforsch *23*, 169-209.

Hopkins, F.G. (1912). Feeding experiments illustrating the importance of accessory factors in normal dietaries. J Physiol *44*, 425-460.

Hornby, S.J., Gilbert, C.E., Rahi, J.K., Sil, A.K., Xiao, Y., Dandona, L., and Foster, A. (2000). Regional variation in blindness in children due to microphthalmos, anophthalmos and coloboma. Ophthalmic Epidemiol *7*, 127-138.

Hornby, S.J., Ward, S.J., and Gilbert, C.E. (2003). Eye birth defects in humans may be caused by a recessively-inherited genetic predisposition to the effects of maternal vitamin A deficiency during pregnancy. Med Sci Monit *9*, HY23-26.

Horsford, D.J., Nguyen, M.T., Sellar, G.C., Kothary, R., Arnheiter, H., and McInnes, R.R. (2005). Chx10 repression of Mitf is required for the maintenance of mammalian neuroretinal identity. Development *132*, 177-187.

Horwitz, J., and Heller, J. (1973). Interactions of all-trans, 9-, 11-, and 13-cis-retinal, all-trans-retinyl acetate, and retinoic acid with human retinol-binding protein and prealbumin. J Biol Chem *248*, 6317-6324.

Hsu, L.C., Chang, W.C., Hiraoka, L., and Hsieh, C.L. (1994). Molecular cloning, genomic organization, and chromosomal localization of an additional human aldehyde dehydrogenase gene, ALDH6. Genomics *24*, 333-341.

Huang, A.S., and Baltimore, D. (1970). Defective viral particles and viral disease processes. Nature *226*, 325-327.

Huang, H.S., and Goodman, D.S. (1965). Vitamin a and Carotenoids. I. Intestinal Absorption and Metabolism of 14c-Labelled Vitamin a Alcohol and Beta-Carotene in the Rat. J Biol Chem *240*, 2839-2844.

Hughes, M.J., Lingrel, J.B., Krakowsky, J.M., and Anderson, K.P. (1993). A helix-loop-helix transcription factor-like gene is located at the mi locus. J Biol Chem *268*, 20687-20690.

Hyer, J., Kuhlman, J., Afif, E., and Mikawa, T. (2003). Optic cup morphogenesis requires pre-lens ectoderm but not lens differentiation. Dev Biol *259*, 351-363.

Hyer, J., Mima, T., and Mikawa, T. (1998). FGF1 patterns the optic vesicle by directing the placement of the neural retina domain. Development *125*, 869-877.

Inoue, M., Kamachi, Y., Matsunami, H., Imada, K., Uchikawa, M., and Kondoh, H. (2007). PAX6 and SOX2-dependent regulation of the Sox2 enhancer N-3 involved in embryonic visual system development. Genes Cells *12*, 1049-1061.

Inoue, T., Nakamura, S., and Osumi, N. (2000). Fate mapping of the mouse prosencephalic neural plate. Dev Biol *219*, 373-383.

Ishii, Y., Weinberg, K., Oda-Ishii, I., Coughlin, L., and Mikawa, T. (2009). Morphogenesis and cytodifferentiation of the avian retinal pigmented epithelium require downregulation of Group B1 Sox genes. Development *136*, 2579-2589.

Ismadi, S.D., and Olson, J.A. (1975). Vitamin A transport in human fetal blood. Am J Clin Nutr *28*, 967-972.

Jamieson, R.V., Perveen, R., Kerr, B., Carette, M., Yardley, J., Heon, E., Wirth, M.G., van Heyningen, V., Donnai, D., Munier, F.*, et al.* (2002). Domain disruption and

mutation of the bZIP transcription factor, MAF, associated with cataract, ocular anterior segment dysgenesis and coloboma. Hum Mol Genet *11*, 33-42.

Jauniaux, E., Johns, J., Gulbis, B., Spasic-Boskovic, O., and Burton, G.J. (2007). Transfer of folic acid inside the first-trimester gestational sac and the effect of maternal smoking. Am J Obstet Gynecol *197*, 58 e51-56.

Jeong, Y., Leskow, F.C., El-Jaick, K., Roessler, E., Muenke, M., Yocum, A., Dubourg, C., Li, X., Geng, X., Oliver, G.*, et al.* (2008). Regulation of a remote Shh forebrain enhancer by the Six3 homeoprotein. Nat Genet *40*, 1348-1353.

Jiang, W., and Napoli, J.L. (2012). Reorganization of cellular retinol-binding protein type 1 and lecithin:retinol acyltransferase during retinyl ester biosynthesis. Biochim Biophys Acta *1820*, 859-869.

Jiao, Z., Mollaaghababa, R., Pavan, W.J., Antonellis, A., Green, E.D., and Hornyak, T.J. (2004). Direct interaction of Sox10 with the promoter of murine Dopachrome Tautomerase (Dct) and synergistic activation of Dct expression with Mitf. Pigment Cell Res *17*, 352-362.

Johansson, S., Gustafson, A.L., Donovan, M., Eriksson, U., and Dencker, L. (1999). Retinoid binding proteins-expression patterns in the human placenta. Placenta *20*, 459-465.

Johansson, S., Gustafson, A.L., Donovan, M., Romert, A., Eriksson, U., and Dencker, L. (1997). Retinoid binding proteins in mouse yolk sac and chorio-allantoic placentas. Anat Embryol (Berl) *195*, 483-490.

Johnson, D.L., Lewis, B.C., Elliot, D.J., Miners, J.O., and Martin, L.L. (2005). Electrochemical characterisation of the human cytochrome P450 CYP2C9. Biochem Pharmacol *69*, 1533-1541.

Johnston, M.C., Noden, D.M., Hazelton, R.D., Coulombre, J.L., and Coulombre, A.J. (1979). Origins of avian ocular and periocular tissues. Exp Eye Res *29*, 27-43.

Jordan, T., Hanson, I., Zaletayev, D., Hodgson, S., Prosser, J., Seawright, A., Hastie, N., and van Heyningen, V. (1992). The human PAX6 gene is mutated in two patients with aniridia. Nat Genet *1*, 328-332.

Kagiyama, Y., Gotouda, N., Sakagami, K., Yasuda, K., Mochii, M., and Araki, M. (2005). Extraocular dorsal signal affects the developmental fate of the optic vesicle and patterns the optic neuroepithelium. Dev Growth Differ *47*, 523-536.

Kamachi, Y., Uchikawa, M., Collignon, J., Lovell-Badge, R., and Kondoh, H. (1998). Involvement of Sox1, 2 and 3 in the early and subsequent molecular events of lens induction. Development *125*, 2521-2532.

Kamachi, Y., Uchikawa, M., and Kondoh, H. (2000). Pairing SOX off: with partners in the regulation of embryonic development. Trends Genet *16*, 182-187.

Kamachi, Y., Uchikawa, M., Tanouchi, A., Sekido, R., and Kondoh, H. (2001). Pax6 and SOX2 form a co-DNA-binding partner complex that regulates initiation of lens development. Genes Dev *15*, 1272-1286.

Kanai, M., Raz, A., and Goodman, D.S. (1968). Retinol-binding protein: the transport protein for vitamin A in human plasma. J Clin Invest *47*, 2025-2044.

Karali, M., Peluso, I., Marigo, V., and Banfi, S. (2007). Identification and characterization of microRNAs expressed in the mouse eye. Invest Ophthalmol Vis Sci *48*, 509-515.

Kastner, P., Grondona, J.M., Mark, M., Gansmuller, A., LeMeur, M., Decimo, D., Vonesch, J.L., Dolle, P., and Chambon, P. (1994). Genetic analysis of RXR alpha developmental function: convergence of RXR and RAR signaling pathways in heart and eye morphogenesis. Cell *78*, 987-1003.

Kastner, P., Mark, M., Ghyselinck, N., Krezel, W., Dupe, V., Grondona, J.M., and Chambon, P. (1997). Genetic evidence that the retinoid signal is transduced by heterodimeric RXR/RAR functional units during mouse development. Development *124*, 313-326.

Kato, M., Kato, K., and Goodman, D.S. (1984). Immunocytochemical studies on the localization of plasma and of cellular retinol-binding proteins and of transthyretin (prealbumin) in rat liver and kidney. J Cell Biol *98*, 1696-1704.

Kawaguchi, R., and Sun, H. (2010). Techniques to study specific cell-surface receptor-mediated cellular vitamin A uptake. Methods Mol Biol *652*, 341-361.

Kawaguchi, R., Yu, J., Honda, J., Hu, J., Whitelegge, J., Ping, P., Wiita, P., Bok, D., and Sun, H. (2007). A membrane receptor for retinol binding protein mediates cellular uptake of vitamin A. Science *315*, 820-825.

Kawaguchi, R., Yu, J., Ter-Stepanian, M., Zhong, M., Cheng, G., Yuan, Q., Jin, M., Travis, G.H., Ong, D., and Sun, H. (2011). Receptor-mediated cellular uptake mechanism that couples to intracellular storage. ACS Chem Biol *6*, 1041-1051.

Kawaguchi, R., Yu, J., Wiita, P., Honda, J., and Sun, H. (2008a). An essential ligand-binding domain in the membrane receptor for retinol-binding protein revealed by large-scale mutagenesis and a human polymorphism. J Biol Chem *283*, 15160-15168.

Kawaguchi, R., Yu, J., Wiita, P., Ter-Stepanian, M., and Sun, H. (2008b). Mapping the membrane topology and extracellular ligand binding domains of the retinol binding protein receptor. Biochemistry *47*, 5387-5395.

Keagle, M.B. (2005). The principles of clinical cytogenetics, 2nd edn (Totowa, N.J., Humana Press).

Kelberman, D., Rizzoti, K., Avilion, A., Bitner-Glindzicz, M., Cianfarani, S., Collins, J., Chong, W.K., Kirk, J.M., Achermann, J.C., Ross, R.*, et al.* (2006). Mutations within Sox2/SOX2 are associated with abnormalities in the hypothalamo-pituitary-gonadal axis in mice and humans. J Clin Invest *116*, 2442-2455.

Kennedy, B.N., Stearns, G.W., Smyth, V.A., Ramamurthy, V., van Eeden, F., Ankoudinova, I., Raible, D., Hurley, J.B., and Brockerhoff, S.E. (2004). Zebrafish rx3 and mab21l2 are required during eye morphogenesis. Dev Biol *270*, 336-349.

Kidd, K.K., and Spence, M.A. (1976). Genetic analyses of pyloric stenosis suggesting a specific maternal effect. J Med Genet *13*, 290-294.

Kidson, S.H., Kume, T., Deng, K., Winfrey, V., and Hogan, B.L. (1999). The forkhead/winged-helix gene, Mf1, is necessary for the normal development of the cornea and formation of the anterior chamber in the mouse eye. Dev Biol *211*, 306-322.

Kiernan, A.E., Pelling, A.L., Leung, K.K., Tang, A.S., Bell, D.M., Tease, C., Lovell-Badge, R., Steel, K.P., and Cheah, K.S. (2005). Sox2 is required for sensory organ development in the mammalian inner ear. Nature *434*, 1031-1035.

Kinkel, M.D., Sefton, E.M., Kikuchi, Y., Mizoguchi, T., Ward, A.B., and Prince, V.E. (2009). Cyp26 enzymes function in endoderm to regulate pancreatic field size. Proc Natl Acad Sci U S A *106*, 7864-7869.

Kleinjan, D.A., Seawright, A., Schedl, A., Quinlan, R.A., Danes, S., and van Heyningen, V. (2001). Aniridia-associated translocations, DNase hypersensitivity, sequence comparison and transgenic analysis redefine the functional domain of PAX6. Hum Mol Genet *10*, 2049-2059.

Kleinjan, D.J., and Coutinho, P. (2009). Cis-ruption mechanisms: disruption of cis-regulatory control as a cause of human genetic disease. Brief Funct Genomic Proteomic *8*, 317-332.

Kochhar, D.M., Penner, J.D., and Satre, M.A. (1988). Derivation of retinoic acid and metabolites from a teratogenic dose of retinol (vitamin A) in mice. Toxicol Appl Pharmacol *96*, 429-441.

Kondoh, H., and Kamachi, Y. (2010). SOX-partner code for cell specification: Regulatory target selection and underlying molecular mechanisms. Int J Biochem Cell Biol *42*, 391-399.

Koopman, P., Gubbay, J., Vivian, N., Goodfellow, P., and Lovell-Badge, R. (1991). Male development of chromosomally female mice transgenic for Sry. Nature *351*, 117-121.

Kopelman, M., Cogan, U., Mokady, S., and Shinitzky, M. (1976). The interaction between retinol-binding proteins and prealbumins studied by fluorescence polarization. Biochim Biophys Acta *439*, 449-460.

Koster, R.W., Kuhnlein, R.P., and Wittbrodt, J. (2000). Ectopic Sox3 activity elicits sensory placode formation. Mech Dev *95*, 175-187.

Kraft, J.C., Shepard, T., and Juchau, M.R. (1993). Tissue levels of retinoids in human embryos/fetuses. Reprod Toxicol *7*, 11-15.

Krogh, C., Fischer, T.K., Skotte, L., Biggar, R.J., Oyen, N., Skytthe, A., Goertz, S., Christensen, K., Wohlfahrt, J., and Melbye, M. (2010). Familial aggregation and heritability of pyloric stenosis. JAMA *303*, 2393-2399.

Kurahashi, H., and Emanuel, B.S. (2001). Long AT-rich palindromes and the constitutional t(11;22) breakpoint. Hum Mol Genet *10*, 2605-2617.

Kurose, H., Okamoto, M., Shimizu, M., Bito, T., Marcelle, C., Noji, S., and Ohuchi, H. (2005). FGF19-FGFR4 signaling elaborates lens induction with the FGF8-L-Maf cascade in the chick embryo. Dev Growth Differ *47*, 213-223.

Kurth, I., Klopocki, E., Stricker, S., van Oosterwijk, J., Vanek, S., Altmann, J., Santos, H.G., van Harssel, J.J., de Ravel, T., Wilkie, A.O.*, et al.* (2009). Duplications of noncoding elements 5' of SOX9 are associated with brachydactyly-anonychia. Nat Genet *41*, 862-863.

Lagerstrom-Fermer, M., Sundvall, M., Johnsen, E., Warne, G.L., Forrest, S.M., Zajac, J.D., Rickards, A., Ravine, D., Landegren, U., and Pettersson, U. (1997). X-linked recessive panhypopituitarism associated with a regional duplication in Xq25-q26. Am J Hum Genet *60*, 910-916.

Lagutin, O.V., Zhu, C.C., Kobayashi, D., Topczewski, J., Shimamura, K., Puelles, L., Russell, H.R., McKinnon, P.J., Solnica-Krezel, L., and Oliver, G. (2003). Six3 repression of Wnt signaling in the anterior neuroectoderm is essential for vertebrate forebrain development. Genes Dev *17*, 368-379.

Lakich, D., Kazazian, H.H., Jr., Antonarakis, S.E., and Gitschier, J. (1993). Inversions disrupting the factor VIII gene are a common cause of severe haemophilia A. Nat Genet *5*, 236-241.

Lammer, E.J., Chen, D.T., Hoar, R.M., Agnish, N.D., Benke, P.J., Braun, J.T., Curry, C.J., Fernhoff, P.M., Grix, A.W., Jr., Lott, I.T.*, et al.* (1985). Retinoic acid embryopathy. N Engl J Med *313*, 837-841.

Lampron, C., Rochette-Egly, C., Gorry, P., Dolle, P., Mark, M., Lufkin, T., LeMeur, M., and Chambon, P. (1995). Mice deficient in cellular retinoic acid binding protein II (CRABPII) or in both CRABPI and CRABPII are essentially normal. Development *121*, 539-548.

Laronda, M.M., and Jameson, J.L. (2011). Sox3 functions in a cell-autonomous manner to regulate spermatogonial differentiation in mice. Endocrinology *152*, 1606-1615.

Lauderdale, J.D., Wilensky, J.S., Oliver, E.R., Walton, D.S., and Glaser, T. (2000). 3' deletions cause aniridia by preventing PAX6 gene expression. Proc Natl Acad Sci U S A *97*, 13755-13759.

Laumonnier, F., Ronce, N., Hamel, B.C., Thomas, P., Lespinasse, J., Raynaud, M., Paringaux, C., Van Bokhoven, H., Kalscheuer, V., Fryns, J.P.*, et al.* (2002). Transcription factor SOX3 is involved in X-linked mental retardation with growth hormone deficiency. Am J Hum Genet *71*, 1450-1455.

Le Lievre, C.S., and Le Douarin, N.M. (1975). Mesenchymal derivatives of the neural crest: analysis of chimaeric quail and chick embryos. J Embryol Exp Morphol *34*, 125-154.

Lee, E.C., Yu, D., Martinez de Velasco, J., Tessarollo, L., Swing, D.A., Court, D.L., Jenkins, N.A., and Copeland, N.G. (2001). A highly efficient Escherichia coli-based chromosome engineering system adapted for recombinogenic targeting and subcloning of BAC DNA. Genomics *73*, 56-65.

Lee, H.S., Bong, Y.S., Moore, K.B., Soria, K., Moody, S.A., and Daar, I.O. (2006). Dishevelled mediates ephrinB1 signalling in the eye field through the planar cell polarity pathway. Nat Cell Biol *8*, 55-63.

Lee, K., Tan, J., Morris, M.B., Rizzoti, K., Hughes, J., Cheah, P.S., Felquer, F., Liu, X., Piltz, S., Lovell-Badge, R.*, et al.* (2012). Congenital hydrocephalus and abnormal subcommissural organ development in Sox3 transgenic mice. PLoS One *7*, e29041.

Lee, N., Chen, J., Sun, L., Wu, S., Gray, K.R., Rich, A., Huang, M., Lin, J.H., Feder, J.N., Janovitz, E.B.*, et al.* (2003). Expression and characterization of human transient receptor potential melastatin 3 (hTRPM3). J Biol Chem *278*, 20890-20897.

Lee, S.J., Perera, L., Coulter, S.J., Mohrenweiser, H.W., Jetten, A., and Goldstein, J.A. (2007). The discovery of new coding alleles of human CYP26A1 that are potentially defective in the metabolism of all-trans retinoic acid and their assessment in a recombinant cDNA expression system. Pharmacogenet Genomics *17*, 169-180.

Lemyre, E., Lemieux, N., Decarie, J.C., and Lambert, M. (1998). Del(14)(q22.1q23.2) in a patient with anophthalmia and pituitary hypoplasia. Am J Med Genet *77*, 162-165.

Lequeux, L., Rio, M., Vigouroux, A., Titeux, M., Etchevers, H., Malecaze, F., Chassaing, N., and Calvas, P. (2008). Confirmation of RAX gene involvement in human anophthalmia. Clin Genet *74*, 392-395.

Lettice, L.A., Daniels, S., Sweeney, E., Venkataraman, S., Devenney, P.S., Gautier, P., Morrison, H., Fantes, J., Hill, R.E., and FitzPatrick, D.R. (2011). Enhancer-adoption as a mechanism of human developmental disease. Hum Mutat *32*, 1492-1499.

Leung, W.C., Hessel, S., Meplan, C., Flint, J., Oberhauser, V., Tourniaire, F., Hesketh, J.E., von Lintig, J., and Lietz, G. (2009). Two common single nucleotide polymorphisms in the gene encoding beta-carotene 15,15'-monoxygenase alter beta-carotene metabolism in female volunteers. FASEB J *23*, 1041-1053.

Levin, A.A., Sturzenbecker, L.J., Kazmer, S., Bosakowski, T., Huselton, C., Allenby, G., Speck, J., Kratzeisen, C., Rosenberger, M., Lovey, A.*, et al.* (1992). 9-cis retinoic acid stereoisomer binds and activates the nuclear receptor RXR alpha. Nature *355*, 359-361.

Li, E., and Norris, A.W. (1996). Structure/function of cytoplasmic vitamin A-binding proteins. Annu Rev Nutr *16*, 205-234.

Li, H., Wagner, E., McCaffery, P., Smith, D., Andreadis, A., and Drager, U.C. (2000). A retinoic acid synthesizing enzyme in ventral retina and telencephalon of the embryonic mouse. Mech Dev *95*, 283-289.

Li, L.C., and Dahiya, R. (2002). MethPrimer: designing primers for methylation PCRs. Bioinformatics *18*, 1427-1431.

Li, X., Perissi, V., Liu, F., Rose, D.W., and Rosenfeld, M.G. (2002). Tissue-specific regulation of retinal and pituitary precursor cell proliferation. Science *297*, 1180-1183.

Lietz, G., Oxley, A., Leung, W., and Hesketh, J. (2012). Single nucleotide polymorphisms upstream from the beta-carotene 15,15'-monoxygenase gene influence provitamin A conversion efficiency in female volunteers. J Nutr *142*, 161S-165S.

Ligtenberg, M.J., Kuiper, R.P., Chan, T.L., Goossens, M., Hebeda, K.M., Voorendt, M., Lee, T.Y., Bodmer, D., Hoenselaar, E., Hendriks-Cornelissen, S.J.*, et al.* (2009).

Heritable somatic methylation and inactivation of MSH2 in families with Lynch syndrome due to deletion of the 3' exons of TACSTD1. Nat Genet *41*, 112-117.

Lindqvist, A., Sharvill, J., Sharvill, D.E., and Andersson, S. (2007). Loss-of-function mutation in carotenoid 15,15'-monooxygenase identified in a patient with hypercarotenemia and hypovitaminosis A. J Nutr *137*, 2346-2350.

Liou, G.I., Fei, Y., Peachey, N.S., Matragoon, S., Wei, S., Blaner, W.S., Wang, Y., Liu, C., Gottesman, M.E., and Ripps, H. (1998). Early onset photoreceptor abnormalities induced by targeted disruption of the interphotoreceptor retinoid-binding protein gene. J Neurosci *18*, 4511-4520.

Liu, H., Mohamed, O., Dufort, D., and Wallace, V.A. (2003). Characterization of Wnt signaling components and activation of the Wnt canonical pathway in the murine retina. Dev Dyn *227*, 323-334.

Liu, H., and Naismith, J.H. (2008). An efficient one-step site-directed deletion, insertion, single and multiple-site plasmid mutagenesis protocol. BMC Biotechnol *8*, 91.

Liu, H., Thurig, S., Mohamed, O., Dufort, D., and Wallace, V.A. (2006). Mapping canonical Wnt signaling in the developing and adult retina. Invest Ophthalmol Vis Sci *47*, 5088-5097.

Liu, H., Xu, S., Wang, Y., Mazerolle, C., Thurig, S., Coles, B.L., Ren, J.C., Taketo, M.M., van der Kooy, D., and Wallace, V.A. (2007). Ciliary margin transdifferentiation from neural retina is controlled by canonical Wnt signaling. Dev Biol *308*, 54-67.

Liu, I.S., Chen, J.D., Ploder, L., Vidgen, D., van der Kooy, D., Kalnins, V.I., and McInnes, R.R. (1994). Developmental expression of a novel murine homeobox gene (Chx10): evidence for roles in determination of the neuroretina and inner nuclear layer. Neuron *13*, 377-393.

Liu, K.H., Brewton, R.G., Baumbach, G.A., and Godkin, J.D. (1991). Characterization of protein production by ovine placental membranes: identification of a placental retinol-binding protein. Endocrinology *129*, 126-132.

Liu, R.Z., Denovan-Wright, E.M., Degrave, A., Thisse, C., Thisse, B., and Wright, J.M. (2004). Spatio-temporal distribution of cellular retinol-binding protein gene transcripts (CRBPI and CRBPII) in the developing and adult zebrafish (Danio rerio). Eur J Biochem *271*, 339-348.

Liu, R.Z., Sun, Q., Thisse, C., Thisse, B., Wright, J.M., and Denovan-Wright, E.M. (2005). The cellular retinol-binding protein genes are duplicated and differentially transcribed in the developing and adult zebrafish (Danio rerio). Mol Biol Evol *22*, 469-477.

Liu, W., Lagutin, O., Swindell, E., Jamrich, M., and Oliver, G. (2010). Neuroretina specification in mouse embryos requires Six3-mediated suppression of Wnt8b in the anterior neural plate. J Clin Invest *120*, 3568-3577.

Lobo, G.P., Hessel, S., Eichinger, A., Noy, N., Moise, A.R., Wyss, A., Palczewski, K., and von Lintig, J. (2010). ISX is a retinoic acid-sensitive gatekeeper that controls

intestinal beta,beta-carotene absorption and vitamin A production. FASEB J *24*, 1656-1666.

Lohnes, D., Kastner, P., Dierich, A., Mark, M., LeMeur, M., and Chambon, P. (1993). Function of retinoic acid receptor gamma in the mouse. Cell *73*, 643-658.

Lohnes, D., Mark, M., Mendelsohn, C., Dolle, P., Dierich, A., Gorry, P., Gansmuller, A., and Chambon, P. (1994). Function of the retinoic acid receptors (RARs) during development (I). Craniofacial and skeletal abnormalities in RAR double mutants. Development *120*, 2723-2748.

Loosli, F., Staub, W., Finger-Baier, K.C., Ober, E.A., Verkade, H., Wittbrodt, J., and Baier, H. (2003). Loss of eyes in zebrafish caused by mutation of chokh/rx3. EMBO Rep *4*, 894-899.

Loosli, F., Winkler, S., and Wittbrodt, J. (1999). Six3 overexpression initiates the formation of ectopic retina. Genes Dev *13*, 649-654.

Lopriore, E., Oepkes, D., and Walther, F.J. (2011). Neonatal morbidity in twin-twin transfusion syndrome. Early Hum Dev *87*, 595-599.

Lorente, C.A., and Miller, S.A. (1977). Fetal and maternal vitamin A levels in tissues of hypervitaminotic A rats and rabbits. J Nutr *107*, 1816-1821.

Lufkin, T., Lohnes, D., Mark, M., Dierich, A., Gorry, P., Gaub, M.P., LeMeur, M., and Chambon, P. (1993). High postnatal lethality and testis degeneration in retinoic acid receptor alpha mutant mice. Proc Natl Acad Sci U S A *90*, 7225-7229.

MacDonald, P.N., and Ong, D.E. (1987). Binding specificities of cellular retinol-binding protein and cellular retinol-binding protein, type II. J Biol Chem *262*, 10550-10556.

MacDonald, P.N., and Ong, D.E. (1988). Evidence for a lecithin-retinol acyltransferase activity in the rat small intestine. J Biol Chem *263*, 12478-12482.

Maden, M. (1994). In Vitamin A in Health and Disease, R. Blomhoff, ed. (New York, NY, Marcel Dekker), pp. 289-322.

Majumdar, A., Vainio, S., Kispert, A., McMahon, J., and McMahon, A.P. (2003). Wnt11 and Ret/Gdnf pathways cooperate in regulating ureteric branching during metanephric kidney development. Development *130*, 3175-3185.

Mamede, A.C., Tavares, S.D., Abrantes, A.M., Trindade, J., Maia, J.M., and Botelho, M.F. (2011). The role of vitamins in cancer: a review. Nutr Cancer *63*, 479-494.

Marinari, L., Lenich, C.M., and Ross, A.C. (1987). Production and secretion of retinol-binding protein by a human hepatoma cell line, HepG2. J Lipid Res *28*, 941-948.

Marquardt, T., Ashery-Padan, R., Andrejewski, N., Scardigli, R., Guillemot, F., and Gruss, P. (2001). Pax6 is required for the multipotent state of retinal progenitor cells. Cell *105*, 43-55.

Martinez-Morales, J.R., Dolez, V., Rodrigo, I., Zaccarini, R., Leconte, L., Bovolenta, P., and Saule, S. (2003). OTX2 activates the molecular network underlying retina pigment epithelium differentiation. J Biol Chem *278*, 21721-21731.

Martinez-Morales, J.R., Rodrigo, I., and Bovolenta, P. (2004). Eye development: a view from the retina pigmented epithelium. Bioessays *26*, 766-777.

Martinez-Morales, J.R., Signore, M., Acampora, D., Simeone, A., and Bovolenta, P. (2001). Otx genes are required for tissue specification in the developing eye. Development *128*, 2019-2030.

Mathers, P.H., Grinberg, A., Mahon, K.A., and Jamrich, M. (1997). The Rx homeobox gene is essential for vertebrate eye development. Nature *387*, 603-607.

Matsuo, I., Kuratani, S., Kimura, C., Takeda, N., and Aizawa, S. (1995). Mouse Otx2 functions in the formation and patterning of rostral head. Genes Dev *9*, 2646-2658.

Matsushima, D., Heavner, W., and Pevny, L.H. (2011). Combinatorial regulation of optic cup progenitor cell fate by SOX2 and PAX6. Development *138*, 443-454.

Matt, N., Schmidt, C.K., Dupe, V., Dennefeld, C., Nau, H., Chambon, P., Mark, M., and Ghyselinck, N.B. (2005). Contribution of cellular retinol-binding protein type 1 to retinol metabolism during mouse development. Dev Dyn *233*, 167-176.

Maurus, D., Heligon, C., Burger-Schwarzler, A., Brandli, A.W., and Kuhl, M. (2005). Noncanonical Wnt-4 signaling and EAF2 are required for eye development in Xenopus laevis. EMBO J *24*, 1181-1191.

Maw, M.A., Kennedy, B., Knight, A., Bridges, R., Roth, K.E., Mani, E.J., Mukkadan, J.K., Nancarrow, D., Crabb, J.W., and Denton, M.J. (1997). Mutation of the gene encoding cellular retinaldehyde-binding protein in autosomal recessive retinitis pigmentosa. Nat Genet *17*, 198-200.

McCollum, E.D.M. (1913). The necessity of certain lipids in the diet during growth. Journal of Biological Chemistry *15*, 167-175.

McCollum, E.D.M. (1915). The essential factors in diet during growth. Journal of Biological Chemistry *23*, 231-254.

Mears, A.J., Jordan, T., Mirzayans, F., Dubois, S., Kume, T., Parlee, M., Ritch, R., Koop, B., Kuo, W.L., Collins, C.*, et al.* (1998). Mutations of the forkhead/winged-helix

gene, FKHL7, in patients with Axenfeld-Rieger anomaly. Am J Hum Genet *63*, 1316-1328.

Medina-Martinez, O., Amaya-Manzanares, F., Liu, C., Mendoza, M., Shah, R., Zhang, L., Behringer, R.R., Mahon, K.A., and Jamrich, M. (2009). Cell-autonomous requirement for rx function in the mammalian retina and posterior pituitary. PLoS One *4*, e4513.

Meire, F., Delpierre, I., Brachet, C., Roulez, F., Van Nechel, C., Depasse, F., Christophe, C., Menten, B., and De Baere, E. (2011). Nonsyndromic bilateral and unilateral optic nerve aplasia: first familial occurrence and potential implication of CYP26A1 and CYP26C1 genes. Mol Vis *17*, 2072-2079.

Melhus, H., Laurent, B., Rask, L., and Peterson, P.A. (1992). Ligand-dependent secretion of rat retinol-binding protein expressed in HeLa cells. J Biol Chem *267*, 12036-12041.

Melhus, H., Nilsson, T., Peterson, P.A., and Rask, L. (1991). Retinol-binding protein and transthyretin expressed in HeLa cells form a complex in the endoplasmic reticulum in both the absence and the presence of retinol. Exp Cell Res *197*, 119-124.

Mendelsohn, C., Ruberte, E., LeMeur, M., Morriss-Kay, G., and Chambon, P. (1991). Developmental analysis of the retinoic acid-inducible RAR-beta 2 promoter in transgenic animals. Development *113*, 723-734.

Mic, F.A., Haselbeck, R.J., Cuenca, A.E., and Duester, G. (2002). Novel retinoic acid generating activities in the neural tube and heart identified by conditional rescue of Raldh2 null mutant mice. Development *129*, 2271-2282.

Mic, F.A., Molotkov, A., Benbrook, D.M., and Duester, G. (2003). Retinoid activation of retinoic acid receptor but not retinoid X receptor is sufficient to rescue lethal defect in retinoic acid synthesis. Proc Natl Acad Sci U S A *100*, 7135-7140.

Mitchell, T.N., Free, S.L., Williamson, K.A., Stevens, J.M., Churchill, A.J., Hanson, I.M., Shorvon, S.D., Moore, A.T., van Heyningen, V., and Sisodiya, S.M. (2003). Polymicrogyria and absence of pineal gland due to PAX6 mutation. Ann Neurol *53*, 658-663.

Miyagi, S., Nishimoto, M., Saito, T., Ninomiya, M., Sawamoto, K., Okano, H., Muramatsu, M., Oguro, H., Iwama, A., and Okuda, A. (2006). The Sox2 regulatory region 2 functions as a neural stem cell-specific enhancer in the telencephalon. J Biol Chem *281*, 13374-13381.

Miyagi, S., Saito, T., Mizutani, K., Masuyama, N., Gotoh, Y., Iwama, A., Nakauchi, H., Masui, S., Niwa, H., Nishimoto, M*., et al.* (2004). The Sox-2 regulatory regions display their activities in two distinct types of multipotent stem cells. Mol Cell Biol *24*, 4207-4220.

Mochii, M., Mazaki, Y., Mizuno, N., Hayashi, H., and Eguchi, G. (1998). Role of Mitf in differentiation and transdifferentiation of chicken pigmented epithelial cell. Dev Biol *193*, 47-62.

Mollard, R., Viville, S., Ward, S.J., Decimo, D., Chambon, P., and Dolle, P. (2000). Tissue-specific expression of retinoic acid receptor isoform transcripts in the mouse embryo. Mech Dev *94*, 223-232.

Molotkov, A., Fan, X., Deltour, L., Foglio, M.H., Martras, S., Farres, J., Pares, X., and Duester, G. (2002). Stimulation of retinoic acid production and growth by ubiquitously expressed alcohol dehydrogenase Adh3. Proc Natl Acad Sci U S A *99*, 5337-5342.

Molotkov, A., Molotkova, N., and Duester, G. (2006). Retinoic acid guides eye morphogenetic movements via paracrine signaling but is unnecessary for retinal dorsoventral patterning. Development *133*, 1901-1910.

Monaco, H.L., Rizzi, M., and Coda, A. (1995). Structure of a complex of two plasma proteins: transthyretin and retinol-binding protein. Science *268*, 1039-1041.

Moore, T. (1971). Vitamin A transfer from mother to offspring in mice and rats. Int J Vitam Nutr Res *41*, 301-306.

Mori, M., Ghyselinck, N.B., Chambon, P., and Mark, M. (2001). Systematic immunolocalization of retinoid receptors in developing and adult mouse eyes. Invest Ophthalmol Vis Sci *42*, 1312-1318.

Mori, M., Metzger, D., Garnier, J.M., Chambon, P., and Mark, M. (2002). Site-specific somatic mutagenesis in the retinal pigment epithelium. Invest Ophthalmol Vis Sci *43*, 1384-1388.

Morrison, D., FitzPatrick, D., Hanson, I., Williamson, K., van Heyningen, V., Fleck, B., Jones, I., Chalmers, J., and Campbell, H. (2002). National study of microphthalmia, anophthalmia, and coloboma (MAC) in Scotland: investigation of genetic aetiology. J Med Genet *39*, 16-22.

Muller, F., Rohrer, H., and Vogel-Hopker, A. (2007). Bone morphogenetic proteins specify the retinal pigment epithelium in the chick embryo. Development *134*, 3483-3493.

Munro, S., and Pelham, H.R. (1987). A C-terminal signal prevents secretion of luminal ER proteins. Cell *48*, 899-907.

Muto, Y., Smith, J.E., Milch, P.O., and Goodman, D.S. (1972). Regulation of retinol-binding protein metabolism by vitamin A status in the rat. J Biol Chem *247*, 2542-2550.

Navab, M., Smith, J.E., and Goodman, D.S. (1977). Rat plasma prealbumin. Metabolic studies on effects of vitamin A status and on tissue distribution. J Biol Chem *252*, 5107-5114.

Navratilova, P., Fredman, D., Hawkins, T.A., Turner, K., Lenhard, B., and Becker, T.S. (2009). Systematic human/zebrafish comparative identification of cis-regulatory activity around vertebrate developmental transcription factor genes. Dev Biol *327*, 526-540.

Naylor, H.M., and Newcomer, M.E. (1999). The structure of human retinol-binding protein (RBP) with its carrier protein transthyretin reveals an interaction with the carboxy terminus of RBP. Biochemistry *38*, 2647-2653.

Newcomer, M.E., Jones, T.A., Aqvist, J., Sundelin, J., Eriksson, U., Rask, L., and Peterson, P.A. (1984). The three-dimensional structure of retinol-binding protein. EMBO J *3*, 1451-1454.

Ng, D., Thakker, N., Corcoran, C.M., Donnai, D., Perveen, R., Schneider, A., Hadley, D.W., Tifft, C., Zhang, L., Wilkie, A.O*., et al.* (2004). Oculofaciocardiodental and Lenz microphthalmia syndromes result from distinct classes of mutations in BCOR. Nat Genet *36*, 411-416.

Nguyen, M., and Arnheiter, H. (2000). Signaling and transcriptional regulation in early mammalian eye development: a link between FGF and MITF. Development *127*, 3581-3591.

Niederreither, K., and Dolle, P. (2008). Retinoic acid in development: towards an integrated view. Nat Rev Genet *9*, 541-553.

Niederreither, K., Subbarayan, V., Dolle, P., and Chambon, P. (1999). Embryonic retinoic acid synthesis is essential for early mouse post-implantation development. Nat Genet *21*, 444-448.

Nilsson, M.H., Spurr, N.K., Saksena, P., Busch, C., Nordlinder, H., Peterson, P.A., Rask, L., and Sundelin, J. (1988). Isolation and characterization of a cDNA clone corresponding to bovine cellular retinoic-acid-binding protein and chromosomal localization of the corresponding human gene. Eur J Biochem *173*, 45-51.

Nora, J.J., and Nora, A.H. (1987). Maternal transmission of congenital heart diseases: new recurrence risk figures and the questions of cytoplasmic inheritance and vulnerability to teratogens. Am J Cardiol *59*, 459-463.

Nordstrom, U., Jessell, T.M., and Edlund, T. (2002). Progressive induction of caudal neural character by graded Wnt signaling. Nat Neurosci *5*, 525-532.

Nowakowska, B.A., de Leeuw, N., Ruivenkamp, C.A., Sikkema-Raddatz, B., Crolla, J.A., Thoelen, R., Koopmans, M., den Hollander, N., van Haeringen, A., van der Kevie-

Kersemaekers, A.M.*, et al.* (2012). Parental insertional balanced translocations are an important cause of apparently de novo CNVs in patients with developmental anomalies. Eur J Hum Genet *20*, 166-170.

Noy, N. (2000). Retinoid-binding proteins: mediators of retinoid action. Biochem J *348 Pt 3*, 481-495.

O'Byrne, S.M., Wongsiriroj, N., Libien, J., Vogel, S., Goldberg, I.J., Baehr, W., Palczewski, K., and Blaner, W.S. (2005). Retinoid absorption and storage is impaired in mice lacking lecithin:retinol acyltransferase (LRAT). J Biol Chem *280*, 35647-35657.

Oberwinkler, J., Lis, A., Giehl, K.M., Flockerzi, V., and Philipp, S.E. (2005). Alternative splicing switches the divalent cation selectivity of TRPM3 channels. J Biol Chem *280*, 22540-22548.

Okada, I., Hamanoue, H., Terada, K., Tohma, T., Megarbane, A., Chouery, E., Abou-Ghoch, J., Jalkh, N., Cogulu, O., Ozkinay, F.*, et al.* (2011). SMOC1 is essential for ocular and limb development in humans and mice. Am J Hum Genet *88*, 30-41.

Oliver, G., Loosli, F., Koster, R., Wittbrodt, J., and Gruss, P. (1996). Ectopic lens induction in fish in response to the murine homeobox gene Six3. Mech Dev *60*, 233-239.

Ong, D., Newcomer, M., Chytil, F. (1994). Cellular retinoid binding proteins. In The Retinoids, Biology, Chemistry and Medicine, R.A. Sporn MB, Goodman DS, ed. (New York, NY, Raven), pp. 283-318.

Ong, D.E., Kakkad, B., and MacDonald, P.N. (1987). Acyl-CoA-independent esterification of retinol bound to cellular retinol-binding protein (type II) by microsomes from rat small intestine. J Biol Chem *262*, 2729-2736.

Ong, D.E., and Page, D.L. (1987). Cellular retinol-binding protein (type two) is abundant in human small intestine. J Lipid Res *28*, 739-745.

Onwochei, B.C., Simon, J.W., Bateman, J.B., Couture, K.C., and Mir, E. (2000). Ocular colobomata. Surv Ophthalmol *45*, 175-194.

Opas, M., Davies, J.R., Zhou, Y., and Dziak, E. (2001). Formation of retinal pigment epithelium in vitro by transdifferentiation of neural retina cells. Int J Dev Biol *45*, 633-642.

Osborne, T.M.L. (1914a). The influence of butter-fat on growth. Journal of Biological Chemistry *16*, 423-437.

Osborne, T.M.L. (1914b). The influence of cod liver oil and some other fats on growth. Journal of Biological Chemistry *16*, 423-437.

Ottaviani, A., Rival-Gervier, S., Boussouar, A., Foerster, A.M., Rondier, D., Sacconi, S., Desnuelle, C., Gilson, E., and Magdinier, F. (2009). The D4Z4 macrosatellite repeat acts as a CTCF and A-type lamins-dependent insulator in facio-scapulo-humeral dystrophy. PLoS Genet *5*, e1000394.

Pagnamenta, A.T., Holt, R., Yusuf, M., Pinto, D., Wing, K., Betancur, C., Scherer, S.W., Volpi, E.V., and Monaco, A.P. (2011). A family with autism and rare copy number variants disrupting the Duchenne/Becker muscular dystrophy gene DMD and TRPM3. J Neurodev Disord *3*, 124-131.

Parma, P., Radi, O., Vidal, V., Chaboissier, M.C., Dellambra, E., Valentini, S., Guerra, L., Schedl, A., and Camerino, G. (2006). R-spondin1 is essential in sex determination, skin differentiation and malignancy. Nat Genet *38*, 1304-1309.

Pasutto, F., Sticht, H., Hammersen, G., Gillessen-Kaesbach, G., Fitzpatrick, D.R., Nurnberg, G., Brasch, F., Schirmer-Zimmermann, H., Tolmie, J.L., Chitayat, D.*, et al.* (2007). Mutations in STRA6 cause a broad spectrum of malformations including anophthalmia, congenital heart defects, diaphragmatic hernia, alveolar capillary dysplasia, lung hypoplasia, and mental retardation. Am J Hum Genet *80*, 550-560.

Peterson, P.A. (1971). Demonstration in serum of two physiological forms of the human retinol binding protein. Eur J Clin Invest *1*, 437-444.

Peterson, P.A., Rask, L., Ostberg, L., Andersson, L., Kamwendo, F., and Pertoft, H. (1973). Studies on the transport and cellular distribution of vitamin A in normal and vitamin A-deficient rats with special reference to the vitamin A-binding plasma protein. J Biol Chem *248*, 4009-4022.

Pevny, L.H., Sockanathan, S., Placzek, M., and Lovell-Badge, R. (1998). A role for SOX1 in neural determination. Development *125*, 1967-1978.

Polanco, J.C., Wilhelm, D., Davidson, T.L., Knight, D., and Koopman, P. (2010). Sox10 gain-of-function causes XX sex reversal in mice: implications for human 22q-linked disorders of sex development. Hum Mol Genet *19*, 506-516.

Popova, B.C., Tada, T., Takagi, N., Brockdorff, N., and Nesterova, T.B. (2006). Attenuated spread of X-inactivation in an X;autosome translocation. Proc Natl Acad Sci U S A *103*, 7706-7711.

Porter, F.D., Drago, J., Xu, Y., Cheema, S.S., Wassif, C., Huang, S.P., Lee, E., Grinberg, A., Massalas, J.S., Bodine, D.*, et al.* (1997). Lhx2, a LIM homeobox gene, is required for eye, forebrain, and definitive erythrocyte development. Development *124*, 2935-2944.

Prakash, S.K., Cormier, T.A., McCall, A.E., Garcia, J.J., Sierra, R., Haupt, B., Zoghbi, H.Y., and Van Den Veyver, I.B. (2002). Loss of holocytochrome c-type synthetase causes the male lethality of X-linked dominant microphthalmia with linear skin defects (MLS) syndrome. Hum Mol Genet *11*, 3237-3248.

Prasad, R., Basu, B., Mishra, O.P., Singh, U.K., and Singh, M.K. (2009). The co-existence of CHARGE and myelodysplastic syndrome in a child. BMJ Case Rep *2009*.

Qin, Y., Kong, L.K., Poirier, C., Truong, C., Overbeek, P.A., and Bishop, C.E. (2004). Long-range activation of Sox9 in Odd Sex (Ods) mice. Hum Mol Genet *13*, 1213-1218.

Quadro, L., Blaner, W.S., Hamberger, L., Novikoff, P.M., Vogel, S., Piantedosi, R., Gottesman, M.E., and Colantuoni, V. (2004a). The role of extrahepatic retinol binding protein in the mobilization of retinoid stores. J Lipid Res *45*, 1975-1982.

Quadro, L., Blaner, W.S., Salchow, D.J., Vogel, S., Piantedosi, R., Gouras, P., Freeman, S., Cosma, M.P., Colantuoni, V., and Gottesman, M.E. (1999). Impaired retinal function and vitamin A availability in mice lacking retinol-binding protein. EMBO J *18*, 4633-4644.

Quadro, L., Hamberger, L., Gottesman, M.E., Colantuoni, V., Ramakrishnan, R., and Blaner, W.S. (2004b). Transplacental delivery of retinoid: the role of retinol-binding protein and lipoprotein retinyl ester. Am J Physiol Endocrinol Metab *286*, E844-851.

Quadro, L., Hamberger, L., Gottesman, M.E., Wang, F., Colantuoni, V., Blaner, W.S., and Mendelsohn, C.L. (2005). Pathways of vitamin A delivery to the embryo: insights from a new tunable model of embryonic vitamin A deficiency. Endocrinology *146*, 4479-4490.

Ragge, N.K., Brown, A.G., Poloschek, C.M., Lorenz, B., Henderson, R.A., Clarke, M.P., Russell-Eggitt, I., Fielder, A., Gerrelli, D., Martinez-Barbera, J.P.*, et al.* (2005a). Heterozygous mutations of OTX2 cause severe ocular malformations. Am J Hum Genet *76*, 1008-1022.

Ragge, N.K., Lorenz, B., Schneider, A., Bushby, K., de Sanctis, L., de Sanctis, U., Salt, A., Collin, J.R., Vivian, A.J., Free, S.L.*, et al.* (2005b). SOX2 anophthalmia syndrome. Am J Med Genet A *135*, 1-7; discussion 8.

Ragge, N.K., Subak-Sharpe, I.D., and Collin, J.R. (2007). A practical guide to the management of anophthalmia and microphthalmia. Eye (Lond) *21*, 1290-1300.

Raghu, P., Ravinder, P., and Sivakumar, B. (2003). A new method for purification of human plasma retinol-binding protein and transthyretin. Biotechnol Appl Biochem *38*, 19-24.

Rainger, J., van Beusekom, E., Ramsay, J.K., McKie, L., Al-Gazali, L., Pallotta, R., Saponari, A., Branney, P., Fisher, M., Morrison, H.*, et al.* (2011). Loss of the BMP antagonist, SMOC-1, causes Ophthalmo-acromelic (Waardenburg Anophthalmia) syndrome in humans and mice. PLoS Genet *7*, e1002114.

Rask, L., Valtersson, C., Anundi, H., Kvist, S., Eriksson, U., Dallner, G., and Peterson, P.A. (1983). Subcellular localization in normal and vitamin A-deficient rat liver of vitamin A serum transport proteins, albumin, ceruloplasmin and class I major histocompatibility antigens. Exp Cell Res *143*, 91-102.

Raverot, G., Weiss, J., Park, S.Y., Hurley, L., and Jameson, J.L. (2005). Sox3 expression in undifferentiated spermatogonia is required for the progression of spermatogenesis. Dev Biol *283*, 215-225.

Raymond, S.M., and Jackson, I.J. (1995). The retinal pigmented epithelium is required for development and maintenance of the mouse neural retina. Curr Biol *5*, 1286-1295.

Raz, A., Shiratori, T., and Goodman, D.S. (1970). Studies on the protein-protein and protein-ligand interactions involved in retinol transport in plasma. J Biol Chem *245*, 1903-1912.

Redondo, C., Vouropoulou, M., Evans, J., and Findlay, J.B. (2008). Identification of the retinol-binding protein (RBP) interaction site and functional state of RBPs for the membrane receptor. FASEB J *22*, 1043-1054.

Reh, T.A., and Pittack, C. (1995). Transdifferentiation and retinal regeneration. Semin Cell Biol *6*, 137-142.

Reis, L.M., Tyler, R.C., Schilter, K.F., Abdul-Rahman, O., Innis, J.W., Kozel, B.A., Schneider, A.S., Bardakjian, T.M., Lose, E.J., Martin, D.M.*, et al.* (2011). BMP4 loss-of-function mutations in developmental eye disorders including SHORT syndrome. Hum Genet *130*, 495-504.

Reneker, L.W., Silversides, D.W., Xu, L., and Overbeek, P.A. (2000). Formation of corneal endothelium is essential for anterior segment development - a transgenic mouse model of anterior segment dysgenesis. Development *127*, 533-542.

Rex, M., Orme, A., Uwanogho, D., Tointon, K., Wigmore, P.M., Sharpe, P.T., and Scotting, P.J. (1997). Dynamic expression of chicken Sox2 and Sox3 genes in ectoderm induced to form neural tissue. Dev Dyn *209*, 323-332.

Ripps, H., Peachey, N.S., Xu, X., Nozell, S.E., Smith, S.B., and Liou, G.I. (2000). The rhodopsin cycle is preserved in IRBP "knockout" mice despite abnormalities in retinal structure and function. Vis Neurosci *17*, 97-105.

Rizzoti, K., Brunelli, S., Carmignac, D., Thomas, P.Q., Robinson, I.C., and Lovell-Badge, R. (2004). SOX3 is required during the formation of the hypothalamo-pituitary axis. Nat Genet *36*, 247-255.

Rizzoti, K., and Lovell-Badge, R. (2007). SOX3 activity during pharyngeal segmentation is required for craniofacial morphogenesis. Development *134*, 3437-3448.

Rocchi, M., Covone, A., Romeo, G., Faraonio, R., and Colantuoni, V. (1989). Regional mapping of RBP4 to 10q23----q24 and RBP1 to 3q21----q22 in man. Somat Cell Mol Genet *15*, 185-190.

Ross, A.C. (1982). Retinol esterification by rat liver microsomes. Evidence for a fatty acyl coenzyme A: retinol acyltransferase. J Biol Chem *257*, 2453-2459.

Ross, A.C., and Gardner, E.M. (1994). The function of vitamin A in cellular growth and differentiation, and its roles during pregnancy and lactation. Adv Exp Med Biol *352*, 187-200.

Ross, A.C., and Zolfaghari, R. (2011). Cytochrome P450s in the regulation of cellular retinoic acid metabolism. Annu Rev Nutr *31*, 65-87.

Rossant, J., Zirngibl, R., Cado, D., Shago, M., and Giguere, V. (1991). Expression of a retinoic acid response element-hsplacZ transgene defines specific domains of transcriptional activity during mouse embryogenesis. Genes Dev *5*, 1333-1344.

Rothman, K.J., Moore, L.L., Singer, M.R., Nguyen, U.S., Mannino, S., and Milunsky, A. (1995). Teratogenicity of high vitamin A intake. N Engl J Med *333*, 1369-1373.

Rozen, R. (1996). Molecular genetics of methylenetetrahydrofolate reductase deficiency. J Inherit Metab Dis *19*, 589-594.

Ruiz, A., Mark, M., Jacobs, H., Klopfenstein, M., Hu, J., Lloyd, M., Habib, S., Tosha, C., Radu, R.A., Ghyselinck, N.B.*, et al.* (2012). Retinoid content, visual responses and ocular morphology are compromised in the retinas of mice lacking the retinol-binding protein receptor, STRA6. Invest Ophthalmol Vis Sci.

Saari, J.C., Bredberg, L., and Garwin, G.G. (1982). Identification of the endogenous retinoids associated with three cellular retinoid-binding proteins from bovine retina and retinal pigment epithelium. J Biol Chem *257*, 13329-13333.

Saari, J.C., Nawrot, M., Kennedy, B.N., Garwin, G.G., Hurley, J.B., Huang, J., Possin, D.E., and Crabb, J.W. (2001). Visual cycle impairment in cellular retinaldehyde binding protein (CRALBP) knockout mice results in delayed dark adaptation. Neuron *29*, 739-748.

Saigou, Y., Kamimura, Y., Inoue, M., Kondoh, H., and Uchikawa, M. (2010). Regulation of Sox2 in the pre-placodal cephalic ectoderm and central nervous system by enhancer N-4. Dev Growth Differ *52*, 397-408.

Sakai, Y., Luo, T., McCaffery, P., Hamada, H., and Drager, U.C. (2004). CYP26A1 and CYP26C1 cooperate in degrading retinoic acid within the equatorial retina during later eye development. Dev Biol *276*, 143-157.

Sakai, Y., Meno, C., Fujii, H., Nishino, J., Shiratori, H., Saijoh, Y., Rossant, J., and Hamada, H. (2001). The retinoic acid-inactivating enzyme CYP26 is essential for establishing an uneven distribution of retinoic acid along the anterio-posterior axis within the mouse embryo. Genes Dev *15*, 213-225.

Sandell, L.L., Lynn, M.L., Inman, K.E., McDowell, W., and Trainor, P.A. (2012). RDH10 oxidation of Vitamin A is a critical control step in synthesis of retinoic acid during mouse embryogenesis. PLoS One *7*, e30698.

Sandell, L.L., Sanderson, B.W., Moiseyev, G., Johnson, T., Mushegian, A., Young, K., Rey, J.P., Ma, J.X., Staehling-Hampton, K., and Trainor, P.A. (2007). RDH10 is essential for synthesis of embryonic retinoic acid and is required for limb, craniofacial, and organ development. Genes Dev *21*, 1113-1124.

Sapin, V., Bouillet, P., Oulad-Abdelghani, M., Dastugue, B., Chambon, P., and Dolle, P. (2000a). Differential expression of retinoic acid-inducible (Stra) genes during mouse placentation. Mech Dev *92*, 295-299.

Sapin, V., Chaib, S., Blanchon, L., Alexandre-Gouabau, M.C., Lemery, D., Charbonne, F., Gallot, D., Jacquetin, B., Dastugue, B., and Azais-Braesco, V. (2000b). Esterification of vitamin A by the human placenta involves villous mesenchymal fibroblasts. Pediatr Res *48*, 565-572.

Sapin, V., Ward, S.J., Bronner, S., Chambon, P., and Dolle, P. (1997). Differential expression of transcripts encoding retinoid binding proteins and retinoic acid receptors during placentation of the mouse. Dev Dyn *208*, 199-210.

Satoh, K., Kasai, M., Ishidao, T., Tago, K., Ohwada, S., Hasegawa, Y., Senda, T., Takada, S., Nada, S., Nakamura, T.*, et al.* (2004). Anteriorization of neural fate by inhibitor of beta-catenin and T cell factor (ICAT), a negative regulator of Wnt signaling. Proc Natl Acad Sci U S A *101*, 8017-8021.

Satre, M.A., Ugen, K.E., and Kochhar, D.M. (1992). Developmental changes in endogenous retinoids during pregnancy and embryogenesis in the mouse. Biol Reprod *46*, 802-810.

Sax, L. (2002). How common is intersex? a response to Anne Fausto-Sterling. J Sex Res *39*, 174-178.

Schilter, K.F., Schneider, A., Bardakjian, T., Soucy, J.F., Tyler, R.C., Reis, L.M., and Semina, E.V. (2011). OTX2 microphthalmia syndrome: four novel mutations and delineation of a phenotype. Clin Genet *79*, 158-168.

Schimmenti, L.A., de la Cruz, J., Lewis, R.A., Karkera, J.D., Manligas, G.S., Roessler, E., and Muenke, M. (2003). Novel mutation in sonic hedgehog in non-syndromic colobomatous microphthalmia. Am J Med Genet A *116A*, 215-221.

Schneider, A., Bardakjian, T., Reis, L.M., Tyler, R.C., and Semina, E.V. (2009). Novel SOX2 mutations and genotype-phenotype correlation in anophthalmia and microphthalmia. Am J Med Genet A *149A*, 2706-2715.

Seino, Y., Miki, T., Kiyonari, H., Abe, T., Fujimoto, W., Kimura, K., Takeuchi, A., Takahashi, Y., Oiso, Y., Iwanaga, T.*, et al.* (2008). Isx participates in the maintenance of vitamin A metabolism by regulation of beta-carotene 15,15'-monooxygenase (Bcmo1) expression. J Biol Chem *283*, 4905-4911.

Sekido, R., and Lovell-Badge, R. (2008). Sex determination involves synergistic action of SRY and SF1 on a specific Sox9 enhancer. Nature *453*, 930-934.

Sekido, R., and Lovell-Badge, R. (2009). Sex determination and SRY: down to a wink and a nudge? Trends Genet *25*, 19-29.

Seller, M.J., Davis, T.B., Fear, C.N., Flinter, F.A., Ellis, I., and Gibson, A.G. (1996). Two sibs with anophthalmia and pulmonary hypoplasia (the Matthew-Wood syndrome). Am J Med Genet *62*, 227-229.

Semina, E.V., Ferrell, R.E., Mintz-Hittner, H.A., Bitoun, P., Alward, W.L., Reiter, R.S., Funkhauser, C., Daack-Hirsch, S., and Murray, J.C. (1998). A novel homeobox gene PITX3 is mutated in families with autosomal-dominant cataracts and ASMD. Nat Genet *19*, 167-170.

Semina, E.V., Reiter, R., Leysens, N.J., Alward, W.L., Small, K.W., Datson, N.A., Siegel-Bartelt, J., Bierke-Nelson, D., Bitoun, P., Zabel, B.U.*, et al.* (1996). Cloning and characterization of a novel bicoid-related homeobox transcription factor gene, RIEG, involved in Rieger syndrome. Nat Genet *14*, 392-399.

Sharp, A.J., Spotswood, H.T., Robinson, D.O., Turner, B.M., and Jacobs, P.A. (2002). Molecular and cytogenetic analysis of the spreading of X inactivation in X;autosome translocations. Hum Mol Genet *11*, 3145-3156.

Shenefelt, R.E. (1972). Morphogenesis of malformations in hamsters caused by retinoic acid: relation to dose and stage at treatment. Teratology *5*, 103-118.

Shevchenko, A., Wilm, M., Vorm, O., and Mann, M. (1996). Mass spectrometric sequencing of proteins silver-stained polyacrylamide gels. Anal Chem *68*, 850-858.

Sigulinsky, C.L., Green, E.S., Clark, A.M., and Levine, E.M. (2008). Vsx2/Chx10 ensures the correct timing and magnitude of Hedgehog signaling in the mouse retina. Dev Biol *317*, 560-575.

Simeone, A., Acampora, D., Mallamaci, A., Stornaiuolo, A., D'Apice, M.R., Nigro, V., and Boncinelli, E. (1993). A vertebrate gene related to orthodenticle contains a homeodomain of the bicoid class and demarcates anterior neuroectoderm in the gastrulating mouse embryo. EMBO J *12*, 2735-2747.

Sisodiya, S.M., Free, S.L., Williamson, K.A., Mitchell, T.N., Willis, C., Stevens, J.M., Kendall, B.E., Shorvon, S.D., Hanson, I.M., Moore, A.T.*, et al.* (2001). PAX6 haploinsufficiency causes cerebral malformation and olfactory dysfunction in humans. Nat Genet *28*, 214-216.

Sivaprasadarao, A., Boudjelal, M., and Findlay, J.B. (1994). Solubilization and purification of the retinol-binding protein receptor from human placental membranes. Biochem J *302 (Pt 1)*, 245-251.

Sivaprasadarao, A., and Findlay, J.B. (1994). Structure-function studies on human retinol-binding protein using site-directed mutagenesis. Biochem J *300 (Pt 2)*, 437-442.

Sklan, D., and Ross, A.C. (1987). Synthesis of retinol-binding protein and transthyretin in yolk sac and fetus in the rat. J Nutr *117*, 436-442.

Sklan, D., Shalit, I., Lasebnik, N., Spirer, Z., and Weisman, Y. (1985). Retinol transport proteins and concentrations in human amniotic fluid, placenta, and fetal and maternal sera. Br J Nutr *54*, 577-583.

Slavotinek, A., Lee, S.S., and Hamilton, S.P. (2005). A family with X-linked anophthalmia: exclusion of SOX3 as a candidate gene. Am J Med Genet A *138A*, 89-94.

Slavotinek, A.M. (2011). Eye development genes and known syndromes. Mol Genet Metab *104*, 448-456.

Smith, A.N., Miller, L.A., Radice, G., Ashery-Padan, R., and Lang, R.A. (2009). Stage-dependent modes of Pax6-Sox2 epistasis regulate lens development and eye morphogenesis. Development *136*, 2977-2985.

Smith, A.N., Radice, G., and Lang, R.A. (2010). Which FGF ligands are involved in lens induction? Dev Biol *337*, 195-198.

Smith, F.R., and Goodman, D.S. (1971). The effects of diseases of the liver, thyroid, and kidneys on the transport of vitamin A in human plasma. J Clin Invest *50*, 2426-2436.

Smith, J.E., Borek, C., and Goodman, D.S. (1978). Regulation of retinol-binding protein metabolism in cultured rat liver cell lines. Cell *15*, 865-873.

Smith, J.E., DeMoor, L.M., Handler, C.E., Green, E.L., and Ritter, S.J. (1998). The complex between retinol and retinol-binding protein is formed in the rough microsomes of liver following repletion of vitamin A-depleted rats. Biochim Biophys Acta *1380*, 10-20.

Sommer, A. (2008). Vitamin a deficiency and clinical disease: an historical overview. J Nutr *138*, 1835-1839.

Soprano, D.R., Blaner WS (1994). Plasma retinol-binding protein. In The Retinoids: Biology, Chemistry, and Medicine, R.A. Sporn MB, Goodman DS, ed. (New York, Raven Press), pp. 257-282.

Soprano, D.R., Pickett, C.B., Smith, J.E., and Goodman, D.S. (1981). Biosynthesis of plasma retinol-binding protein in liver as a larger molecular weight precursor. J Biol Chem *256*, 8256-8258.

Soprano, D.R., Smith, J.E., and Goodman, D.S. (1982). Effect of retinol status on retinol-binding protein biosynthesis rate and translatable messenger RNA level in rat liver. J Biol Chem *257*, 7693-7697.

Soprano, D.R., Soprano, K.J., and Goodman, D.S. (1986a). Retinol-binding protein and transthyretin mRNA levels in visceral yolk sac and liver during fetal development in the rat. Proc Natl Acad Sci U S A *83*, 7330-7334.

Soprano, D.R., Soprano, K.J., and Goodman, D.S. (1986b). Retinol-binding protein messenger RNA levels in the liver and in extrahepatic tissues of the rat. J Lipid Res *27*, 166-171.

Soprano, D.R., Wyatt, M.L., Dixon, J.L., Soprano, K.J., and Goodman, D.S. (1988). Retinol-binding protein synthesis and secretion by the rat visceral yolk sac. Effect of retinol status. J Biol Chem *263*, 2934-2938.

Sparrow, D.B., Chapman, G., Smith, A.J., Mattar, M.Z., Major, J.A., O'Reilly, V.C., Saga, Y., Zackai, E.H., Dormans, J.P., Alman, B.A.*, et al.* (2012). A mechanism for gene-environment interaction in the etiology of congenital scoliosis. Cell *149*, 295-306.

Spemann, H. (1924). Über organisatoren in der tierischen entwicklung. Naturwissenschaften *48*, 1092-1094.

Spiegler, E., Kim, Y.K., Wassef, L., Shete, V., and Quadro, L. (2012). Maternal-fetal transfer and metabolism of vitamin A and its precursor beta-carotene in the developing tissues. Biochim Biophys Acta *1821*, 88-98.

Sporn, M.B., Roberts, A.B., and Goodman, D.S. (1994). The Retinoids : biology, chemistry, and medicine, 2nd edn (New York, Raven Press).

Stark, K., Vainio, S., Vassileva, G., and McMahon, A.P. (1994). Epithelial transformation of metanephric mesenchyme in the developing kidney regulated by Wnt-4. Nature *372*, 679-683.

Stevanovic, M., Lovell-Badge, R., Collignon, J., and Goodfellow, P.N. (1993). SOX3 is an X-linked gene related to SRY. Hum Mol Genet *2*, 2013-2018.

Stevanovic, M., Zuffardi, O., Collignon, J., Lovell-Badge, R., and Goodfellow, P. (1994). The cDNA sequence and chromosomal location of the human SOX2 gene. Mamm Genome *5*, 640-642.

Stigloher, C., Ninkovic, J., Laplante, M., Geling, A., Tannhauser, B., Topp, S., Kikuta, H., Becker, T.S., Houart, C., and Bally-Cuif, L. (2006). Segregation of telencephalic and eye-field identities inside the zebrafish forebrain territory is controlled by Rx3. Development *133*, 2925-2935.

Strauss, O. (2005). The retinal pigment epithelium in visual function. Physiol Rev *85*, 845-881.

Subramanian, M., Tam, H., Zheng, H., and Tracy, T.S. (2010). CYP2C9-CYP3A4 protein-protein interactions: role of the hydrophobic N terminus. Drug Metab Dispos *38*, 1003-1009.

Sucov, H.M., Dyson, E., Gumeringer, C.L., Price, J., Chien, K.R., and Evans, R.M. (1994). RXR alpha mutant mice establish a genetic basis for vitamin A signaling in heart morphogenesis. Genes Dev *8*, 1007-1018.

Sutton, E., Hughes, J., White, S., Sekido, R., Tan, J., Arboleda, V., Rogers, N., Knower, K., Rowley, L., Eyre, H.*, et al.* (2011). Identification of SOX3 as an XX male sex reversal gene in mice and humans. J Clin Invest *121*, 328-341.

Tahayato, A., Dolle, P., and Petkovich, M. (2003). Cyp26C1 encodes a novel retinoic acid-metabolizing enzyme expressed in the hindbrain, inner ear, first branchial arch and tooth buds during murine development. Gene Expr Patterns *3*, 449-454.

Taimi, M., Helvig, C., Wisniewski, J., Ramshaw, H., White, J., Amad, M., Korczak, B., and Petkovich, M. (2004). A novel human cytochrome P450, CYP26C1, involved in metabolism of 9-cis and all-trans isomers of retinoic acid. J Biol Chem *279*, 77-85.

Tajima, T., Ohtake, A., Hoshino, M., Amemiya, S., Sasaki, N., Ishizu, K., and Fujieda, K. (2009). OTX2 loss of function mutation causes anophthalmia and combined pituitary hormone deficiency with a small anterior and ectopic posterior pituitary. J Clin Endocrinol Metab *94*, 314-319.

Takahashi, Y.I., Smith, J.E., and Goodman, D.S. (1977). Vitamin A and retinol-binding protein metabolism during fetal development in the rat. Am J Physiol *233*, E263-272.

Takase, S., Ong, D.E., and Chytil, F. (1986). Transfer of retinoic acid from its complex with cellular retinoic acid-binding protein to the nucleus. Arch Biochem Biophys *247*, 328-334.

Tanaka, H., Bergstrom, D.A., Yao, M.C., and Tapscott, S.J. (2005). Widespread and nonrandom distribution of DNA palindromes in cancer cells provides a structural platform for subsequent gene amplification. Nat Genet *37*, 320-327.

Taranova, O.V., Magness, S.T., Fagan, B.M., Wu, Y., Surzenko, N., Hutton, S.R., and Pevny, L.H. (2006). SOX2 is a dose-dependent regulator of retinal neural progenitor competence. Genes Dev *20*, 1187-1202.

Theodosiou, M., Laudet, V., and Schubert, M. (2010). From carrot to clinic: an overview of the retinoic acid signaling pathway. Cell Mol Life Sci *67*, 1423-1445.

Thomas, T., Southwell, B.R., Schreiber, G., and Jaworowski, A. (1990). Plasma protein synthesis and secretion in the visceral yolk sac of the fetal rat: gene expression, protein synthesis and secretion. Placenta *11*, 413-430.

Torma, H., and Vahlquist, A. (1986). Uptake of vitamin A and retinol-binding protein by human placenta in vitro. Placenta *7*, 295-305.

Tosetti, F., Ferrari, N., Pfeffer, U., Brigati, C., and Vidali, G. (1992). Regulation of plasma retinol binding protein secretion in human HepG2 cells. Exp Cell Res *200*, 467-472.

Trembath, D.G., Semina, E.V., Jones, D.H., Patil, S.R., Qian, Q., Amendt, B.A., Russo, A.F., and Murray, J.C. (2004). Analysis of two translocation breakpoints and identification of a negative regulatory element in patients with Rieger's syndrome. Birth Defects Res A Clin Mol Teratol *70*, 82-91.

Tucker, P., Laemle, L., Munson, A., Kanekar, S., Oliver, E.R., Brown, N., Schlecht, H., Vetter, M., and Glaser, T. (2001). The eyeless mouse mutation (ey1) removes an alternative start codon from the Rx/rax homeobox gene. Genesis *31*, 43-53.

Tufarelli, C., Stanley, J.A., Garrick, D., Sharpe, J.A., Ayyub, H., Wood, W.G., and Higgs, D.R. (2003). Transcription of antisense RNA leading to gene silencing and methylation as a novel cause of human genetic disease. Nat Genet *34*, 157-165.

Uchikawa, M., Ishida, Y., Takemoto, T., Kamachi, Y., and Kondoh, H. (2003). Functional analysis of chicken Sox2 enhancers highlights an array of diverse regulatory elements that are conserved in mammals. Dev Cell *4*, 509-519.

Uehara, M., Yashiro, K., Mamiya, S., Nishino, J., Chambon, P., Dolle, P., and Sakai, Y. (2007). CYP26A1 and CYP26C1 cooperatively regulate anterior-posterior patterning of the developing brain and the production of migratory cranial neural crest cells in the mouse. Dev Biol *302*, 399-411.

Uhlenhaut, N.H., Jakob, S., Anlag, K., Eisenberger, T., Sekido, R., Kress, J., Treier, A.C., Klugmann, C., Klasen, C., Holter, N.I.*, et al.* (2009). Somatic sex reprogramming of adult ovaries to testes by FOXL2 ablation. Cell *139*, 1130-1142.

Uwanogho, D., Rex, M., Cartwright, E.J., Pearl, G., Healy, C., Scotting, P.J., and Sharpe, P.T. (1995). Embryonic expression of the chicken Sox2, Sox3 and Sox11 genes suggests an interactive role in neuronal development. Mech Dev *49*, 23-36.

Vahlquist, A., and Nilsson, S. (1984). Vitamin A transfer to the fetus and to the amniotic fluid in rhesus monkey (Macaca mulatta). Ann Nutr Metab *28*, 321-333.

van Bennekum, A., Werder, M., Thuahnai, S.T., Han, C.H., Duong, P., Williams, D.L., Wettstein, P., Schulthess, G., Phillips, M.C., and Hauser, H. (2005). Class B scavenger receptor-mediated intestinal absorption of dietary beta-carotene and cholesterol. Biochemistry *44*, 4517-4525.

van Bennekum, A.M., Fisher, E.A., Blaner, W.S., and Harrison, E.H. (2000). Hydrolysis of retinyl esters by pancreatic triglyceride lipase. Biochemistry *39*, 4900-4906.

van Bennekum, A.M., Wei, S., Gamble, M.V., Vogel, S., Piantedosi, R., Gottesman, M., Episkopou, V., and Blaner, W.S. (2001). Biochemical basis for depressed serum retinol levels in transthyretin-deficient mice. J Biol Chem *276*, 1107-1113.

Van Hemel, J.O., and Eussen, H.J. (2000). Interchromosomal insertions. Identification of five cases and a review. Hum Genet *107*, 415-432.

Van Heyningen, V., and Yeyati, P.L. (2004). Mechanisms of non-Mendelian inheritance in genetic disease. Hum Mol Genet *13 Spec No 2*, R225-233.

Van Raay, T.J., Moore, K.B., Iordanova, I., Steele, M., Jamrich, M., Harris, W.A., and Vetter, M.L. (2005). Frizzled 5 signaling governs the neural potential of progenitors in the developing Xenopus retina. Neuron *46*, 23-36.

Verma, A.S., and Fitzpatrick, D.R. (2007). Anophthalmia and microphthalmia. Orphanet J Rare Dis *2*, 47.

Visel, A., Minovitsky, S., Dubchak, I., and Pennacchio, L.A. (2007). VISTA Enhancer Browser--a database of tissue-specific human enhancers. Nucleic Acids Res *35*, D88-92.

Voronina, V.A., Kozhemyakina, E.A., O'Kernick, C.M., Kahn, N.D., Wenger, S.L., Linberg, J.V., Schneider, A.S., and Mathers, P.H. (2004). Mutations in the human RAX homeobox gene in a patient with anophthalmia and sclerocornea. Hum Mol Genet *13*, 315-322.

Vriens, J., Owsianik, G., Hofmann, T., Philipp, S.E., Stab, J., Chen, X., Benoit, M., Xue, F., Janssens, A., Kerselaers, S.*, et al.* (2011). TRPM3 is a nociceptor channel involved in the detection of noxious heat. Neuron *70*, 482-494.

Wagner, E., McCaffery, P., and Drager, U.C. (2000). Retinoic acid in the formation of the dorsoventral retina and its central projections. Dev Biol *222*, 460-470.

Wald, G. (1968). The molecular basis of visual excitation. Nature *219*, 800-807.

Wang, Y., Thekdi, N., Smallwood, P.M., Macke, J.P., and Nathans, J. (2002). Frizzled-3 is required for the development of major fiber tracts in the rostral CNS. J Neurosci *22*, 8563-8573.

Warburton, P.E., Giordano, J., Cheung, F., Gelfand, Y., and Benson, G. (2004). Inverted repeat structure of the human genome: the X-chromosome contains a preponderance of large, highly homologous inverted repeats that contain testes genes. Genome Res *14*, 1861-1869.

Wardlaw, S.A., Bucco, R.A., Zheng, W.L., and Ong, D.E. (1997). Variable expression of cellular retinol- and cellular retinoic acid-binding proteins in the rat uterus and ovary during the estrous cycle. Biol Reprod *56*, 125-132.

Warkany, J., and Schraffenberger, E. (1946). Congenital malformations induced in rats by maternal vitamin A deficiency; defects of the eye. Arch Ophthal *35*, 150-169.

Warming, S., Costantino, N., Court, D.L., Jenkins, N.A., and Copeland, N.G. (2005). Simple and highly efficient BAC recombineering using galK selection. Nucleic Acids Res *33*, e36.

Warnecke, P.M., Stirzaker, C., Song, J., Grunau, C., Melki, J.R., and Clark, S.J. (2002). Identification and resolution of artifacts in bisulfite sequencing. Methods *27*, 101-107.

Webster, M.K., and Donoghue, D.J. (1996). Constitutive activation of fibroblast growth factor receptor 3 by the transmembrane domain point mutation found in achondroplasia. EMBO J *15*, 520-527.

Wegner, M., and Stolt, C.C. (2005). From stem cells to neurons and glia: a Soxist's view of neural development. Trends Neurosci *28*, 583-588.

Weiss, J., Meeks, J.J., Hurley, L., Raverot, G., Frassetto, A., and Jameson, J.L. (2003). Sox3 is required for gonadal function, but not sex determination, in males and females. Mol Cell Biol *23*, 8084-8091.

Westenskow, P., Piccolo, S., and Fuhrmann, S. (2009). Beta-catenin controls differentiation of the retinal pigment epithelium in the mouse optic cup by regulating Mitf and Otx2 expression. Development *136*, 2505-2510.

Westfall, T.A., Brimeyer, R., Twedt, J., Gladon, J., Olberding, A., Furutani-Seiki, M., and Slusarski, D.C. (2003). Wnt-5/pipetail functions in vertebrate axis formation as a negative regulator of Wnt/beta-catenin activity. J Cell Biol *162*, 889-898.

White, J.A., Beckett, B., Scherer, S.W., Herbrick, J.A., and Petkovich, M. (1998a). P450RAI (CYP26A1) maps to human chromosome 10q23-q24 and mouse chromosome 19C2-3. Genomics *48*, 270-272.

White, W.M., Willard, H.F., Van Dyke, D.L., and Wolff, D.J. (1998b). The spreading of X inactivation into autosomal material of an x;autosome translocation: evidence for a difference between autosomal and X-chromosomal DNA. Am J Hum Genet *63*, 20-28.

Williams, P.A., Cosme, J., Sridhar, V., Johnson, E.F., and McRee, D.E. (2000). Mammalian microsomal cytochrome P450 monooxygenase: structural adaptations for membrane binding and functional diversity. Mol Cell *5*, 121-131.

Wilson, J.G., Roth, C.B., and Warkany, J. (1953). An analysis of the syndrome of malformations induced by maternal vitamin A deficiency. Effects of restoration of vitamin A at various times during gestation. Am J Anat *92*, 189-217.

Wimplinger, I., Shaw, G.M., and Kutsche, K. (2007). HCCS loss-of-function missense mutation in a female with bilateral microphthalmia and sclerocornea: a novel gene for severe ocular malformations? Mol Vis *13*, 1475-1482.

Winkler, S., Loosli, F., Henrich, T., Wakamatsu, Y., and Wittbrodt, J. (2000). The conditional medaka mutation eyeless uncouples patterning and morphogenesis of the eye. Development *127*, 1911-1919.

Winter, N.S., Bratt, J.M., and Banaszak, L.J. (1993). Crystal structures of holo and apo-cellular retinol-binding protein II. J Mol Biol *230*, 1247-1259.

Wisard, J., Faulkner, A., Chrenek, M.A., Waxweiler, T., Waxweiler, W., Donmoyer, C., Liou, G.I., Craft, C.M., Schmid, G.F., Boatright, J.H.*, et al.* (2011). Exaggerated eye growth in IRBP-deficient mice in early development. Invest Ophthalmol Vis Sci *52*, 5804-5811.

Wolf, G. (1996). A history of vitamin A and retinoids. FASEB J *10*, 1102-1107.

Wongsiriroj, N., Piantedosi, R., Palczewski, K., Goldberg, I.J., Johnston, T.P., Li, E., and Blaner, W.S. (2008). The molecular basis of retinoid absorption: a genetic dissection. J Biol Chem *283*, 13510-13519.

Wood, H.B., and Episkopou, V. (1999). Comparative expression of the mouse Sox1, Sox2 and Sox3 genes from pre-gastrulation to early somite stages. Mech Dev *86*, 197-201.

Woods, K.S., Cundall, M., Turton, J., Rizotti, K., Mehta, A., Palmer, R., Wong, J., Chong, W.K., Al-Zyoud, M., El-Ali, M.*, et al.* (2005). Over- and underdosage of SOX3 is associated with infundibular hypoplasia and hypopituitarism. Am J Hum Genet *76*, 833-849.

Wyatt, A., Bakrania, P., Bunyan, D.J., Osborne, R.J., Crolla, J.A., Salt, A., Ayuso, C., Newbury-Ecob, R., Abou-Rayyah, Y., Collin, J.R.*, et al.* (2008). Novel heterozygous OTX2 mutations and whole gene deletions in anophthalmia, microphthalmia and coloboma. Hum Mutat *29*, E278-283.

Xueping, X., Zhang, L., Lu, J., Tso, P., Blaner, W.S., Levin, M.S., and Li, E. (2002). Increased neonatal mortality in mice lacking cellular retinol-binding protein II. J Biol Chem *277*, 36617-36623.

Yamada, M., Blaner, W.S., Soprano, D.R., Dixon, J.L., Kjeldbye, H.M., and Goodman, D.S. (1987). Biochemical characteristics of isolated rat liver stellate cells. Hepatology *7*, 1224-1229.

Yamamoto, M., Drager, U.C., Ong, D.E., and McCaffery, P. (1998). Retinoid-binding proteins in the cerebellum and choroid plexus and their relationship to regionalized retinoic acid synthesis and degradation. Eur J Biochem *257*, 344-350.

Yang, Q., Graham, T.E., Mody, N., Preitner, F., Peroni, O.D., Zabolotny, J.M., Kotani, K., Quadro, L., and Kahn, B.B. (2005). Serum retinol binding protein 4 contributes to insulin resistance in obesity and type 2 diabetes. Nature *436*, 356-362.

Yashiro, K., Zhao, X., Uehara, M., Yamashita, K., Nishijima, M., Nishino, J., Saijoh, Y., Sakai, Y., and Hamada, H. (2004). Regulation of retinoic acid distribution is required for proximodistal patterning and outgrowth of the developing mouse limb. Dev Cell *6*, 411-422.

Yasumoto, K., Yokoyama, K., Shibata, K., Tomita, Y., and Shibahara, S. (1994). Microphthalmia-associated transcription factor as a regulator for melanocyte-specific transcription of the human tyrosinase gene. Mol Cell Biol *14*, 8058-8070.

Yavuzer, U., Keenan, E., Lowings, P., Vachtenheim, J., Currie, G., and Goding, C.R. (1995). The Microphthalmia gene product interacts with the retinoblastoma protein in vitro and is a target for deregulation of melanocyte-specific transcription. Oncogene *10*, 123-134.

Zanotti, G., Ottonello, S., Berni, R., and Monaco, H.L. (1993). Crystal structure of the trigonal form of human plasma retinol-binding protein at 2.5 A resolution. J Mol Biol *230*, 613-624.

Zetterstrom, R.H., Simon, A., Giacobini, M.M., Eriksson, U., and Olson, L. (1994). Localization of cellular retinoid-binding proteins suggests specific roles for retinoids in the adult central nervous system. Neuroscience *62*, 899-918.

Zhang, M., Hu, P., Krois, C.R., Kane, M.A., and Napoli, J.L. (2007). Altered vitamin A homeostasis and increased size and adiposity in the rdh1-null mouse. FASEB J *21*, 2886-2896.

Zhao, H., Yang, T., Madakashira, B.P., Thiels, C.A., Bechtle, C.A., Garcia, C.M., Zhang, H., Yu, K., Ornitz, D.M., Beebe, D.C.*, et al.* (2008). Fibroblast growth factor receptor signaling is essential for lens fiber cell differentiation. Dev Biol *318*, 276-288.

Zhao, S., Nichols, J., Smith, A.G., and Li, M. (2004). SoxB transcription factors specify neuroectodermal lineage choice in ES cells. Mol Cell Neurosci *27*, 332-342.

Zheng, W.L., and Ong, D.E. (1998). Spatial and temporal patterns of expression of cellular retinol-binding protein and cellular retinoic acid-binding proteins in rat uterus during early pregnancy. Biol Reprod *58*, 963-970.

Zhu, H., Shang, D., Sun, M., Choi, S., Liu, Q., Hao, J., Figuera, L.E., Zhang, F., Choy, K.W., Ao, Y.*, et al.* (2011). X-linked congenital hypertrichosis syndrome is associated with interchromosomal insertions mediated by a human-specific palindrome near SOX3. Am J Hum Genet *88*, 819-826.